Novel Polyaromatics for Organic Electronics and Graphene Exfoliation: Synthetic Approaches Utilising Regioselective Aromatic C-H Borylation

A thesis submitted to the University of Manchester for the degree of Doctor of Philosophy in the Faculty of Engineering and Physical Sciences.

2016

Kane W. J. Heard

School of Chemistry

Table of Contents

Final word count: 57,567.

List of Figures

List of Tables

Glossary of Abbreviations

abs	Absorbance
AFM	Atomic force microscopy
APCI	Atmospheric pressure chemical ionisation
APPI	Atmospheric pressure photoionisation
ASAP	Atmospheric solids acquisition probe
B_2pin_2	*Bis*(pinacolato)diboron
Bcat	Catecholboronate ester
Bpin	Pinacolboronate ester
bpy	2,2′-Bipyridyl
BTBT	Benzothieno[3,2-*b*][1]benzothiophene
CCDC	Cambridge crystallographic data centre
CHCA	α-Cyano-4-hydroxycinnamic acid
CMOS	Complementary metal-oxide-semiconductor
COD	1,5-Cyclooctadiene
COE	Cyclooctene
CV	Cyclic voltammetry
CVD	Chemical vapour deposition
dba	Dibenzylideneacetone
DCM	Dichloromethane
DCTB	*trans*-2-[3-(4-*tert*-Butylphenyl)-2-methyl-2-propenylidene]malononitrile
DFT	Density functional theory
DME	Dimethoxyethane
DMF	Dimethylformamide
dmpe	1,2-*Bis*(dimethylphosphino)ethane
DMSO	Dimethyl sulfoxide
DNTT	Dinaphtho[2,3-*b*:2′,3′-*f*]thieno[3,2-*b*]thiophene
DNT-V	Dinaphtho[2,3-*b*:2′,3′-*d*]thiophene
dppe	1,2-*Bis*(diphenylphosphino)ethane
DPPT-TT	Diketopyrrolopyrrole-thieno[3,2-*b*]thiophene
dtbpy	4,4′-Di-*tert*-butyl-2,2′-dipyridyl
ε	Extinction coefficient

E_g	Band gap
EG	Expanded graphite
EI	Electron ionisation
eq	Equivalents
ESI	Electrospray ionisation
EtOH	Ethanol
Fc	Ferrocene
FET	Field-effect transistor
fluor	Fluorescence
GC	Gas chromatography
GPC	Gel permeation chromatography
h	Hours
HESI	Heated electrospray ionisation
HG	Graphene prepared by the arc evaporation of graphite electrodes in a hydrogen atmosphere
HOMO	Highest occupied molecular orbital
HPLC	High performance liquid chromatography
HR	High resolution
HSQC	Heteronuclear single quantum coherence
ICT	Intramolecular charge-transfer
J	Coupling constant
LED	Light-emitting diode
LUMO	Lowest unoccupied molecular orbital
MALDI	Matrix assisted laser desorption/ionisation
MeOH	Methanol
MO	Molecular orbital
MOSFET	Metal-oxide-semiconductor field-effect transistor
MS	Mass spectrometry
MWI	Microwave irradiation
NBS	N-Bromosuccinimide
NMP	N-Methyl-2-pyrrolidone
NMR	Nuclear magnetic resonance
OTf	Trifluoromethanesulfonate

PAH	Polyaromatic hydrocarbon
PBI	Perylene bisimide
PEG	Polyethylene glycol
PEPPSI-IPr	[1,3-*Bis*(2,6-diisopropylphenyl)imidazol-2-ylidene](3-chloropyridyl)palladium(II) dichloride
PMF	Potential of mean force
ppm	Parts per million
PV	Photovoltaic
RBF	Round bottomed flask
rpm	Revolutions per minute
RT	Room temperature
SAM	Self-assembled monolayer
SPhos	2-Dicyclohexylphosphino-2′,6′-dimethoxybiphenyl
TBAF	Tetra-*n*-butylammonium fluoride
TBHP	*tert*-Butyl hydroperoxide
TBS	*tert*-Butyldimethylsilyl
TCNQ	Tetracyanoquinodimethane
TD	Time dependent
TEM	Transmission electron microscopy
TES	Triethylsilyl
THF	Tetrahydrofuran
TIPS	Triisopropylsilyl
TLC	Thin-layer chromatography
TOF	Time-of-flight
UoM	University of Manchester
UV	Ultraviolet
vis	Visible
XPS	X-ray photoelectron spectroscopy
δ	Chemical shift relative to tetramethylsilane
λ_{edge}	High wavelength absorption onset
λ_{max}	Wavelength of greatest absorbance/fluorescence
μ	Hole/electron mobility ($cm^2\ V^{-1}\ S^{-1}$)

Abstract

Projects were undertaken investigating the functionalisation of polyaromatic cores (chrysene, pyrene and perylene) for use in organic electronics and aqueous graphene stabilisation. In each case an iridium-catalysed aromatic C-H borylation formed a key synthetic step, allowing access to unique substitution patterns.

The development of strategies for the orthogonal and asymmetric functionalisation of polyaromatic hydrocarbons was explored. In a key synthetic step 4,10-dichlorochrysene was regioselectively borylated in high yields at the 2,8-positions though C-H activation chemistry. The subsequent application of sequential palladium-catalysed Suzuki and Kumada coupling reactions to this intermediate enabled the synthesis of a series of chrysene derivatives with a unique orthogonal "A_2B_2" 2,8- and 4,10-substitution pattern. In addition the application of a trifluoromethylation at the borylated 2,8-positions enabled the synthesis of a donor-acceptor chrysene derivative. The effect of these substitution patterns on the photophysical and electrochemical properties of these derivatives was investigated and their potential use as organic semiconducting materials evaluated. In particular the synthesised chrysene derivatives displayed broadened UV-vis absorption spectra, redshifted fluorescence spectra, increased HOMO levels and decreased band gaps.

In an extension of these aromatic substitution methodologies, pyrene and perylene aromatic cores were functionalised to perform as stabilisers for aqueous graphene dispersions, investigating asymmetric motifs that may maximise performance. A series of amphiphilic pyrene- and perylene-based alkylsulfonic acid salts were synthesised *via* their intermediate hydroxyalkyl derivatives. In addition the application of the previously explored aromatic C-H borylation allowed access to 7- and 5,8,11- asymmetrically substituted pyrene and perylene derivatives. Through collaboration, initial steps have been undertaken to compare and evaluate these novel stabilisers for their ability exfoliate graphite to graphene in aqueous solution.

The University of Manchester, March 2016
Kane W. J. Heard

Degree Title: Doctor of Philosophy
Thesis Title: Novel Polyaromatics for Organic Electronics and Graphene Exfoliation: Synthetic Approaches Utilising Regioselective Aromatic C-H Borylation.

Declaration

Work undertaken in collaboration with other researchers has been attributed in the text. Work undertaken in the synthesis and evaluation of chrysene derivative **133** included herein (section 2.1-1.3 and 2.1-2) was also included in the MChem report (University of Manchester) of supervised student Chi Him Lo.[1] Preliminary graphene exfoliation results included in brief herein (section 2.2-3) will be included in full in the MSci thesis (University of Manchester) of supervised student Junru Zhang. Computational DFT studies of chrysene derivatives included herein (sections 2.1-1.1 and 2.1-3) will also be included in the PhD thesis (University of Manchester) of Laura Weston (McDouall group). No other portion of the work referred to in the thesis has been submitted in support of an application for another degree or qualification of this or any other university or other institute of learning.

Investigations into the synthesis and properties of "A_2B_2" tetrasubstituted chrysene derivatives (section 2.1) was the focus of a publication in chemical communications.[2]

Copyright Statement

i. The author of this thesis (including any appendices and/or schedules to this thesis) owns certain copyright or related rights in it (the "Copyright") and s/he has given The University of Manchester certain rights to use such Copyright, including for administrative purposes.

ii. Copies of this thesis, either in full or in extracts and whether in hard or electronic copy, may be made **only** in accordance with the Copyright, Designs and Patents Act 1988 (as amended) and regulations issued under it or, where appropriate, in accordance with licensing agreements which the University has from time to time. This page must form part of any such copies made.

iii. The ownership of certain Copyright, patents, designs, trade marks and other intellectual property (the "Intellectual Property") and any reproductions of copyright works in the thesis, for example graphs and tables ("Reproductions"), which may be described in this thesis, may not be owned by the author and may be owned by third parties. Such Intellectual Property and Reproductions cannot and must not be made available for use without the prior written permission of the owner(s) of the relevant Intellectual Property and/or Reproductions.

iv. Further information on the conditions under which disclosure, publication and commercialisation of this thesis, the Copyright and any Intellectual Property University IP Policy (see http://documents.manchester.ac.uk/display.aspx?DocID=24420), in any relevant Thesis restriction declarations deposited in the University Library, the University Library's regulations (see http://www.library.manchester.ac.uk/about/regulations/) and in the University's policy on Presentation of Theses.

Acknowledgements

First and foremost I must thank must supervisors Professor Stephen Yeates and Dr Peter Quayle for giving me the opportunity to undertake these PhD studies and for their impeccable support and supervision throughout.

I owe special thanks to Dr John Morrison for his coaching, advice and assistance though each year and Dr Mark Little for his support and tips in the synthesis of chrysene derivatives. I would also like to take this opportunity to thank my computational collaborators Laura Weston (DFT studies) and Dr Chris Williams (molecular dynamics simulations). I thank my Master's students Junru Zhang (initial experimental graphite exfoliation studies) and Chi Lo (assistance in the synthesis and evaluation of chrysene derivative **133**) for working with me during their projects and for their contributions to this work. I would also like to thank Dr James Raftery (crystallographic data) and Gareth Smith (mass spectrometry) for their help in the characterisation of these compounds.

I would like to thank everyone in OMIC for a fantastic 3.5 years and making this a great place to work. There are too many people to mention adequately here, but needless to say it has been a thoroughly enjoyable experience that would have been much harder without such good friends and colleagues.

Finally I thank my friends and family for their endless support and encouragement throughout.

This work was supported by the Engineering and Physical Sciences Research Council, who I gratefully acknowledge for the provision of my DTA studentship.

Nomenclature of Polyaromatic Hydrocarbon Cores

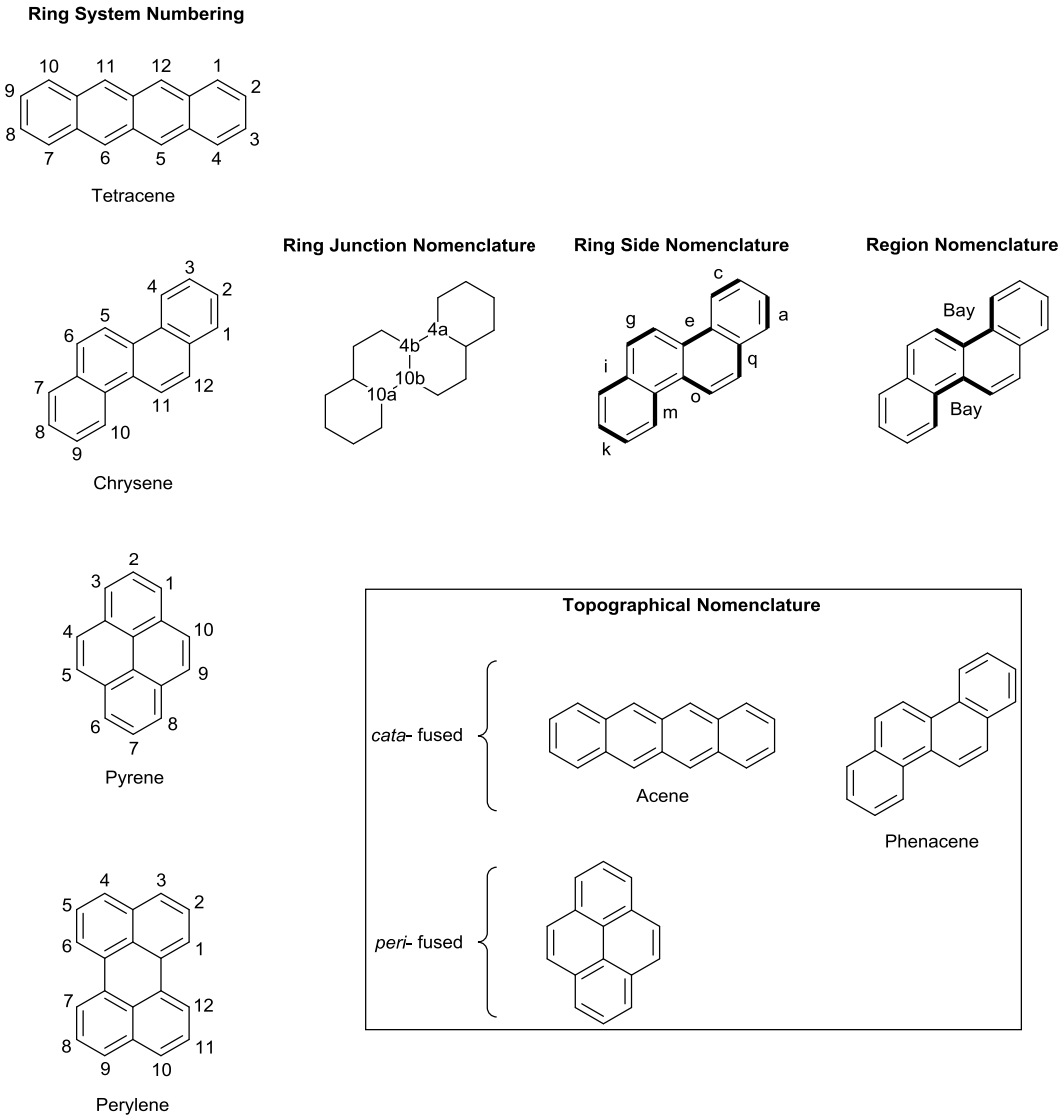

Figure 1 – Summary of key nomenclature of polyaromatic hydrocarbon cores[3, 4]

1 Introduction

This section consists of three constituent parts. Section 1.1 covers the field of organic electronics, including its applications; classes of organic semiconductors and their morphologies and how these apply to phenacenes such as chrysene. Section 1.2 briefly reviews the literature surrounding the iridium-catalysed aromatic C-H borylation which became a key reaction throughout this thesis and focuses on its development, mechanism and use in the functionalisation of polyaromatic systems. Finally, section 1.3 covers graphene and its production, in particular the liquid phase exfoliation of graphene; amphiphilic graphene stabilisers that have been investigated in the literature and the desirable structural motifs of these stabilisers.

1.1 Organic Electronics

Processors have become a major component of modern life, with millions occupying personal computers and other electronic devices. These processors largely utilise metal-oxide-semiconductor field-effect transistors (MOSFETs) and almost all of these MOSFETs use silicon as the active layer and owe their ubiquity in modern life to the improvements made in handling silicon over many years.[5] The production of silicon-based electronics however has expensive setup costs, while research into organic electronics derives from the possibility of the commercial production of cheap, light, flexible and large area devices.[6] Such devices could also be applicable to printable electronics, low cost sensors and single-use electronics[5] in a way silicon-based materials are not. Given recent advances in organic electronics, such devices are becoming a realistic possibility as organic field-effect transistors (OFETs) are beginning to rival and surpass the mobilities of amorphous silicon (~ 1 cm^2 V^{-1} S^{-1}) such as that used in commercial flat panel displays.[7] In recent years the field of organic electronics has matured with publications including the fabrication of electronic circuits that "can be crumpled like paper" (being as light as 3 g m^{-2} and only 2 μm in thickness)[8] and the development of solar cells with 4.2% power conversion efficiency which have a total device thickness less than a typical thread of spider silk (specific weight value of 10 W g^{-1}).[9] Despite these impressive advances challenges still remain in the field of organic electronics, including their sensitivity to oxidation and the requirement to improve device stability;[10] the movement of device fabrication to the large production-scale once it has been proven in the laboratory[11] and the synthesis of new higher performance organic semiconducting materials to compete with the currently superior silicon-based devices.[12]

1.1-1 Applications/Context of Organic Semiconductors

There are three major applications in which organic semiconductors have potential to replace their inorganic counterparts: field-effect transistors (FETs), light-emitting diodes (LEDs) and photovoltaics (PVs). The two most widely reported architectures of an OFET are shown in figure 2.

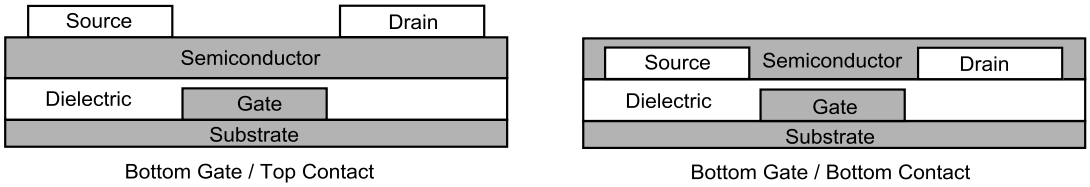

Figure 2 – Top and bottom contact architectures of an OFET[13]

Each device geometry has different advantages. The top contact architecture is advantageous as it tends to reduce contact resistance between the semiconductor and the electrodes while bottom contact architecture is advantageous as it can be smaller and tends to lend itself more to low-cost industrial manufacture.[13]

In the "off" state (when no voltage is applied to the gate) the semiconductor essentially acts as an insulator,[14] however in the "on" state (figure 3) a bias is applied to the gate, generating an electric field at the boundary between the semiconductor and the dielectric. This process forms a conductive channel of holes or electrons (depending on the gate bias) which allows a current to flow from the source to drain electrodes modulated by the gate voltage.[13]

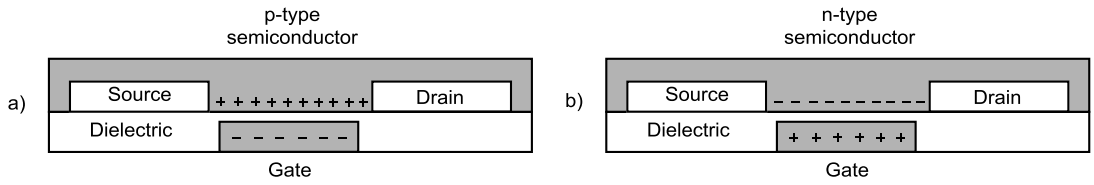

Figure 3 – The conducting channel of holes (a) or electrons (b) formed in a bottom contact OFET when the corresponding bias is applied to the gate[14]

Two other major applications of organic semiconductors include organic light-emitting diodes (OLEDs) and organic photovoltaics (OPVs). While early devices often utilised a single organic semiconductor and balanced charge injection by alteration of the work function of the anode and cathode,[15] more contemporary devices typically utilise a heterojunction structure. Figure 4 summarises the electronics of simple OLED and OPV heterojunction devices and the importance of the positioning of the highest occupied molecular orbital (HOMO) and lowest unoccupied molecular orbital (LUMO) of each p- (hole conducting) and n- (electron conducing) type material for successful operation. Simply put (and ignoring any

intermediate states) the operation of an OLED can be described by charge injection producing holes in the p-type material and electrons in the n-type material. The charges then migrate to the centre of the device and undergo recombination at the heterojunction where the two materials meet resulting in a photon being emitted. The reverse is true in OPVs in which the absorption of photons generates exciton states which diffuse to the heterojunction. At this point the exciton states dissociate to form charge separated states. Diffusion of these separated charge carriers away from the heterojunction and collection by the top and bottom contacts leads to the generation of current.[16]

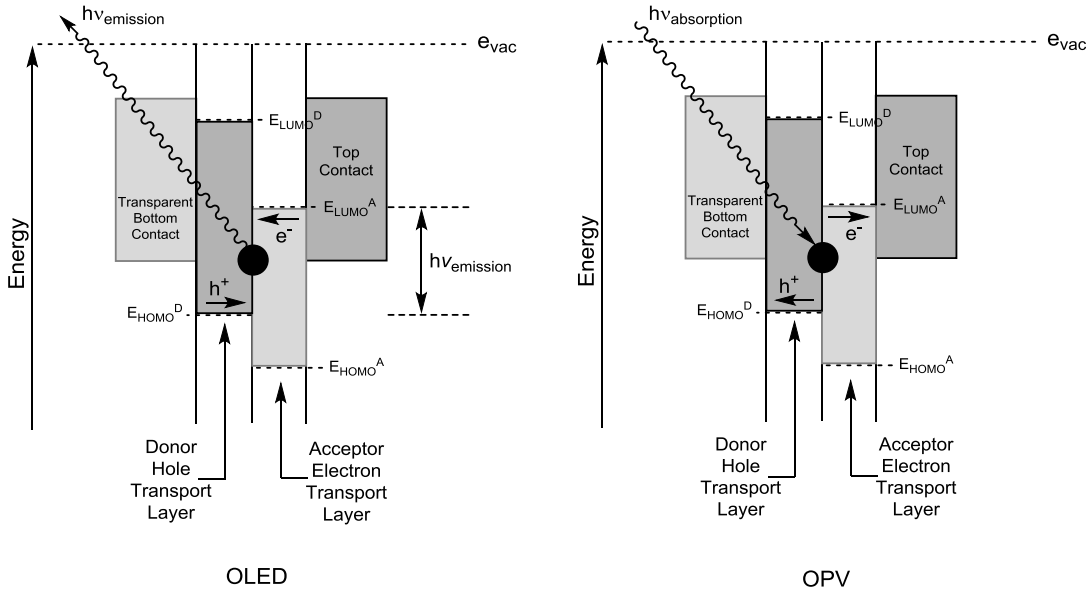

Figure 4 – Summary of the mechanism OLED and OPV heterojunction devices[16]

1.1-2 Classes of Organic Electronics

Organic electronic molecules can be either polymers or small molecules. While polymers are more processable and are generally considered more suitable for mass production,[17] they tend to be amorphous with microcrystalline regions. Small molecules meanwhile generally produce higher mobilities[18] and tend to form more ordered crystalline thin films.[17] Small molecules feature several other advantageous traits compared to polymers; they are monodisperse, possess a precisely defined chemical structure and they are more synthetically reproducible.[19] This project focuses on the synthesis of small molecule semiconductors, which will be the focus of this review.

Figure 5 (a) illustrates the key difference between a conductor and a semiconductor. That is the presence of a band gap (E_g) between valence and conduction bands. In an insulator this gap is large enough that there is essentially no conduction, while in a semiconductor the E_g is small enough that there is appreciable thermal population of the conduction band at room temperature.[5]

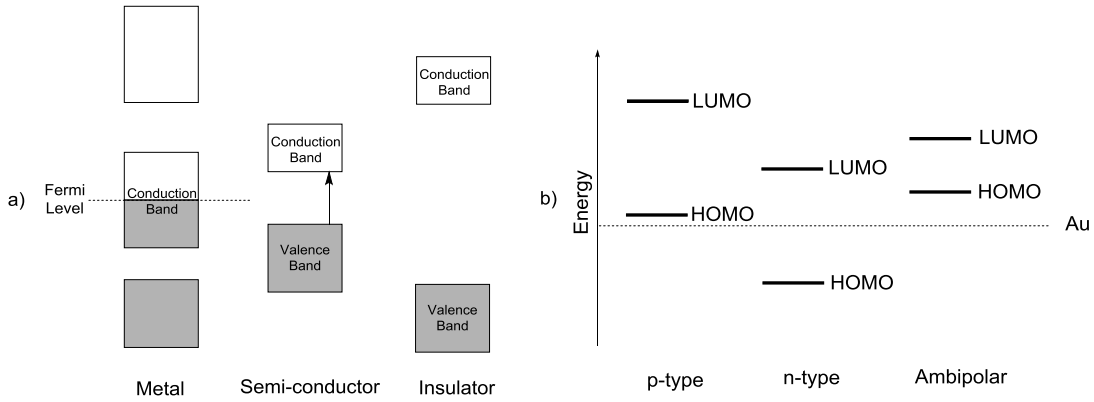

Figure 5 – The band structure of a metallic conductor, a semiconductor and an insulator (a) and the representation of the energy levels of a p-type, n-type and ambipolar semiconductor relative to the work function of gold (b)[5]

A major factor governing whether the semiconductor will be useful in terms of p- or n-type transport properties is the energy of the HOMO and LUMO in relation to the electrode. For example figure 5, b shows a representation of the respective energies of the HOMO and LUMO levels of a p-type, n-type and ambipolar semiconductor relative to the work function of gold. P-type semiconductors generally feature efficient hole injection due to a close match in energy between their HOMO and the work function of the electrode. Conversely n-type semiconductors feature lower LUMO levels to allow more efficient electron injection.[5] A third class are ambipolar semiconductors (discussed in section 1.1-3.2) which feature smaller E_g values and allow the injection of both holes and electrons.

1.1-2.1 Hole Transporting (P-Type) Semiconductors

Figure 6 shows examples of various p-type semiconductors and their highest recorded hole mobilities (μ in $cm^2\ V^{-1}\ S^{-1}$). Mobility is defined as the "the drift velocity of carriers under unit electric field".[20] P-type semiconductors form the bulk

of the organic semiconducting literature and frequently form near ohmic contact with high work function metals (e.g. gold and platinum).[13]

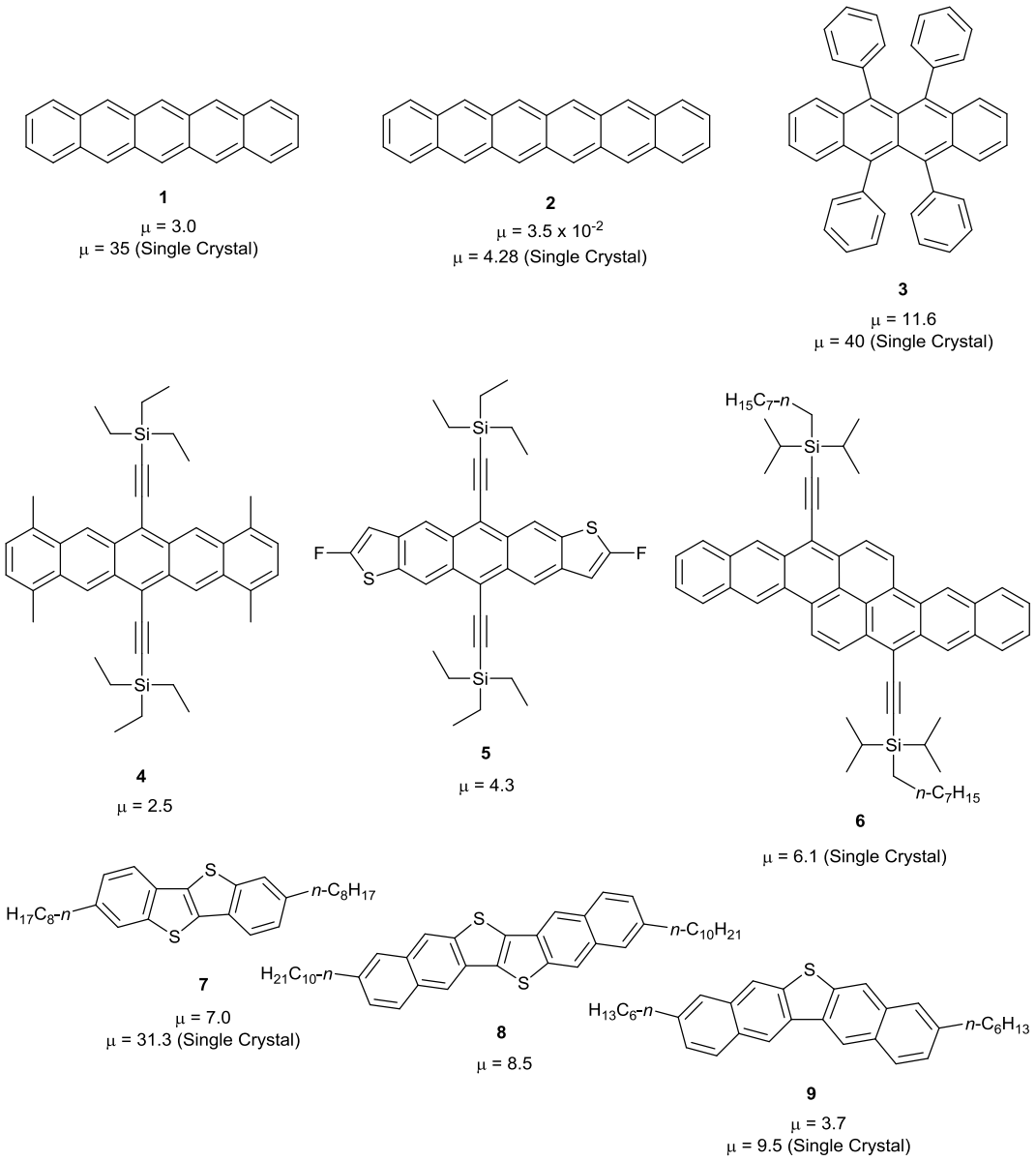

Figure 6 – Selected examples of p-type semiconductors and their thin film hole mobilities (unless otherwise noted)

References: **1**,[21, 22] **2**,[23, 24] **3**,[25, 26] **4**,[27] **5**,[28] **6**,[29] **7**,[30, 31] **8**,[32] **9**[33]

Pentacene (**1**, figure 6) has been a molecule of keen interest for many years. As early as 2002 thin film mobilities as large as 3.0 cm^2 V^{-1} S^{-1} were achieved using a polymeric dielectric[21] and pentacene OFETs have been reported to approach mobilities of up to 5 cm^2 V^{-1} S^{-1}.[20] Pentacene is however non-ideal as it is known to be unstable towards oxygen and light. Furthermore, it has extremely low solubility

(even in hot aromatic solvents)[34] requiring the use of vacuum sublimation with a temperature gradient to effectively purify pentacene from its oxidation product (6,13-pentacenequinone) and produce the single crystals capable of mobilities as high as 35 cm^2 V^{-1} S^{-1} under vacuum.[22] Given these disadvantages, pentacene derivatives are often functionalised in the 6,13-positions with triisopropylsilyl (TIPS) or triethylsilyl (TES) groups *via* an ethynyl linker. Such groups are designed to both increase solubility and enhance face-to-face stacking[35] as in **4**[27] and the related thienoacene **5**.[28] Due to the excellent properties exhibited by **1** higher acenes up to derivatised nonacene have been investigated[36] although hexacene (**2**) is the highest unsubstituted acene successfully tested in transistors. Chow *et al*[23, 24] produced and tested OFET thin films and single crystals of **2**, in each case heating a precursor molecule to produce **2** in the state required. Rubrene (**3**) is a curiosity as it features a phenomenal single crystal mobility of up to 40 cm^2 V^{-1} S^{-1}.[26] Yet its applications in organic electronics have been severely limited by its quite poor quality amorphous thin films, usually with mobilities orders of magnitude lower than single crystal devices. Only recently have high mobilities (up to 11.6 cm^2 V^{-1} S^{-1}) been achieved though weak epitaxial growth of rubrene thin films.[25] **3** is however limited in its practical applications, as even with high mobility thin films, it has a particularly strong affinity for oxidation.[37]

A relatively recently investigated air stable polyacene is bistetracene (**6**), with its departure from a purely linear core it gains an additional Clar sextet (further discussed in section 1.1-5) which aids in in its observed stability. Two derivatives of bistetracene were synthesised, one featuring TIPS groups the other with *n*-octyldiisopropylsilyl groups (**6**), each *via* an ethynyl linker. The latter featured by far the greater mobility in a single crystal with the highest observed mobility reaching an impressive 6.1 cm^2 V^{-1} S^{-1}.[29] Also shown in figure 6 are thienoacenes **5**, **7**, **8** and **9**. Oligothienoacenes and thienoacenes themselves are some of the most studied molecules in organic electronics in large part due to their relative stability and favourable charge transport properties, courtesy of short range S-S intermolecular interactions.[34] Thienoacene **7** (known as C_8-BTBT) achieved mobilities of up to 7.0 cm^2 V^{-1} S^{-1} using vacuum-deposited thin films measured under vacuum with chemical doping at the charge injection interface.[30] Meanwhile inkjet printed single crystals of **7** achieved mobilities of up to 31.3 cm^2 V^{-1} S^{-1} (16.4 cm^2 V^{-1} S^{-1} on

average) when measured under an argon atmosphere.[31] Furthermore using off-centre spin coating, thin films cast from a blended solution of **7** and polystyrene resulted in stunning mobilities of up to 43 $cm^2 V^{-1} S^{-1}$ (average of 25 $cm^2 V^{-1} S^{-1}$) attributed to phase separation of the mixture and the formation of a highly aligned meta-stable crystalline film of **7**.[38]

Of particular note is **8** (known as C_{10}-DNTT), as whilst showing extremely high vacuum-deposited thin film mobilities of 8.5 $cm^2 V^{-1} S^{-1}$,[32] devices with mobilities as high as 11 $cm^2 V^{-1} S^{-1}$ have been fabricated from highly ordered solution-crystallised thin films.[39] DNTT is also a remarkably stable aromatic core, with thin film devices of unalkylated DNTT remaining functional (with no drop in mobility) when stored in ambient conditions over 9 months.[40] A related structure with high motilities is DNT-V, the *n*-hexyl substituted derivative of which (**9**) is shown in figure 6. This V shaped thiophene derivative is a departure from the pseudolinear structures of **7** and **8** and exhibits improved solubility (due to internal dipole moments).[33]

1.1-2.2 Electron Transporting (N-Type) Semiconductors

N-type materials are generally electron deficient and as previously described, feature low lying LUMOs which allow charge transport by electron injection.[41] In addition to their possible application in complementary metal-oxide-semiconductor (CMOS) circuits, n-type semiconductors are vitally important in p-n junction devices such as OPVs and OLEDs.[42] A major issue with n-type semiconductors however, is their sensitivity to moisture and oxygen.[5] This is a particularly pressing problem as often n-type semiconductors are not intrinsically unstable to ambient conditions, but when in operation the charge carriers are particularly prone to trapping by moisture and oxygen which significantly degrades mobility.[43]

There are several techniques for lowering the LUMO to produce an n-type semiconductor, for example adding electron withdrawing groups and incorporating electronegative heteroatoms into the aromatic system.[41]

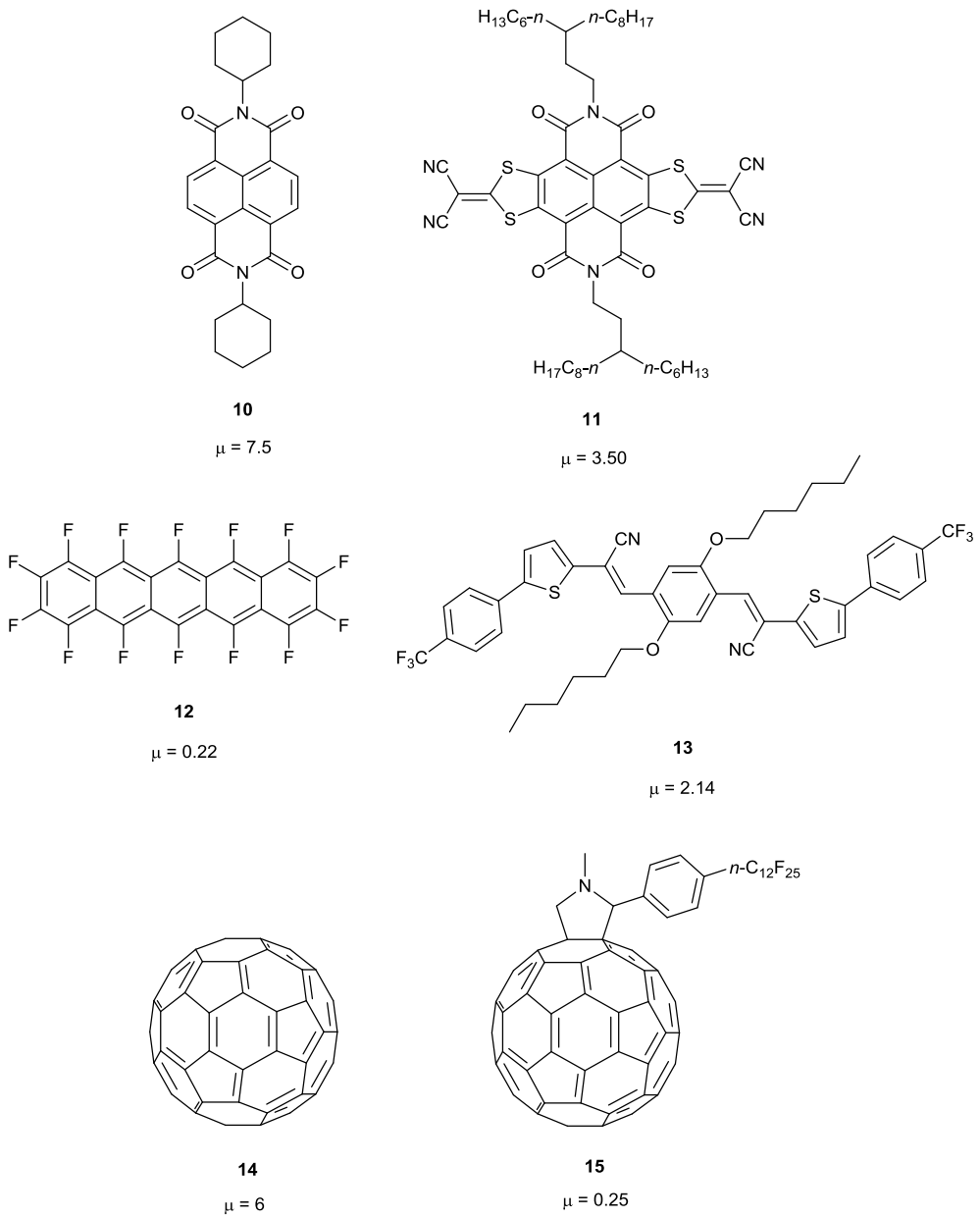

Figure 7 – Selected examples of n-type semiconductors and their thin film electron mobilities (unless otherwise noted)

References: **10**,[44] **11**,[45] **12**,[46] **13**,[47] **14**,[48] **15**[42]

Naphthalene and perylene bisimides feature electron deficiency as two sets of electron withdrawing imide groups are conjugated to a single aromatic system.[41] These materials can feature very high thin film electron mobilities, for example with naphthalene bisimide **10** mobilities as high as 7.5 cm^2 V^{-1} S^{-1} have been achieved (with the device tested in low humidity under argon).[44] Meanwhile air stable example **11** has achieved mobilities of up to 3.50 cm^2 V^{-1} S^{-1} with similar performance both under N_2 and ambient conditions.[45] N-type behaviour can also be

imparted to polyacenes by perfluorinating them, as in perfluoropentacene (**12**) thin films of which achieved electron mobilities as high as 0.22 $cm^2 V^{-1} S^{-1}$ (measured under vacuum).[46] An excellent example of imparting n-type behaviour though the use of electron withdrawing groups is **13**. In this instance, a combination of electron withdrawing trifluoromethyl and cyano groups were added to lower the LUMO and also induce high crystallinity in the solid structure. This approach proved successful as under N_2 evaporated thin film OFETs of **13** achieved a maximum electron mobility of 2.14 $cm^2 V^{-1} S^{-1}$.[47]

Fullerene (**14**) and its derivatives have also been extensively investigated as n-type semiconducting materials.[41] Films of **14** have achieved impressive electron mobilities of up to 6 $cm^2 V^{-1} S^{-1}$ although fullerene devices are highly air sensitive[48] and **14** is poorly soluble. In an attempt to address solubility issues and enable the tuning of electronic properties many different derivatives of fullerene have also been synthesised.[41] For example, **15** which in addition to a maximum electron mobility of 0.25 $cm^2 V^{-1} S^{-1}$ in a vacuum, also features electron mobilities of up to 0.078 $cm^2 V^{-1} S^{-1}$ in air. It is hypothesised that the relative air stability of **15** is likely due to the tightly packed fluorinated chains preventing the diffusion of oxygen and water into the channel region.[42]

1.1-3 Donor-Acceptor Semiconductors

Of particular interest in the fabrication of electro-optic materials (for applications such as OPVs, OLEDs and flexible displays) and ambipolar materials (section 1.1-3.2) are compounds featuring donor and acceptor moieties. Importantly, control of E_g is possible by tailoring the donor and acceptor groups used.[49] In general, the stronger the acceptor the lower the LUMO and the stronger the donor the higher the HOMO, hence with a strong donor and acceptor combination low E_g values can be achieved.[50] Furthermore, the presence of donor and acceptor groups generally improves intramolecular charge-transfer (ICT) resulting in a broadening of the absorption spectrum.[49] This is important as a broad absorption spectrum (along with a high extinction coefficient) leads to greater light harvesting efficiency, which contributes to a higher photogenerated current in OPVs.[51]

1.1-3.1 Donor-Acceptor Architectures

One of the simplest donor-acceptor architectures is a donor (D) and acceptor (A) separated by a π bridge (D-π-A). An excellent example is **16** (figure 8) in which triphenylamine was used as the donor and tetrathiophene with alkylated units as the π bridge substituted with a variety of acceptor units that could be used to tune the resulting electronic properties of the system. It was found that the greater the strength of the electron acceptor, the greater the extinction coefficient, the more redshifted the absorption maxima and the lower the optical E_g (as measured from thin films) of the molecule. In fact thin films of **16-b** and **16-c** were panchromatic, absorbing across the visible spectrum (although only **16-c** had measureable hole mobilities, which were themselves very low).[49]

Another example of a D-π-A architecture is **17**, this time incorporating benzothiazole as the acceptor unit and triphenylamine (**17-a**) or ferrocene (**17-b**) as donor units. To enhance the observed photophysical properties **17-a** and **17-b** were then modified to a unique D-A_2-A_1 architecture though a [2+2] cycloaddition-retroelectrocyclisation reaction with tetracyanoquinodimethane (TCNQ), to form compounds **18-a** and **18-b** in 60% and 68% yields respectively. This modification resulted in strong ICT and significantly reduced optical E_g values in both examples (an E_g reduction of >1 eV) owing to the increased acceptor strength. Computational analysis of the HOMO and LUMO levels on moving from **17** to **18** showed the effect was primarily to lower the LUMO, which was mainly localised over the newly incorporated acceptor unit, with the HOMO localised mainly over the donor unit.[52]

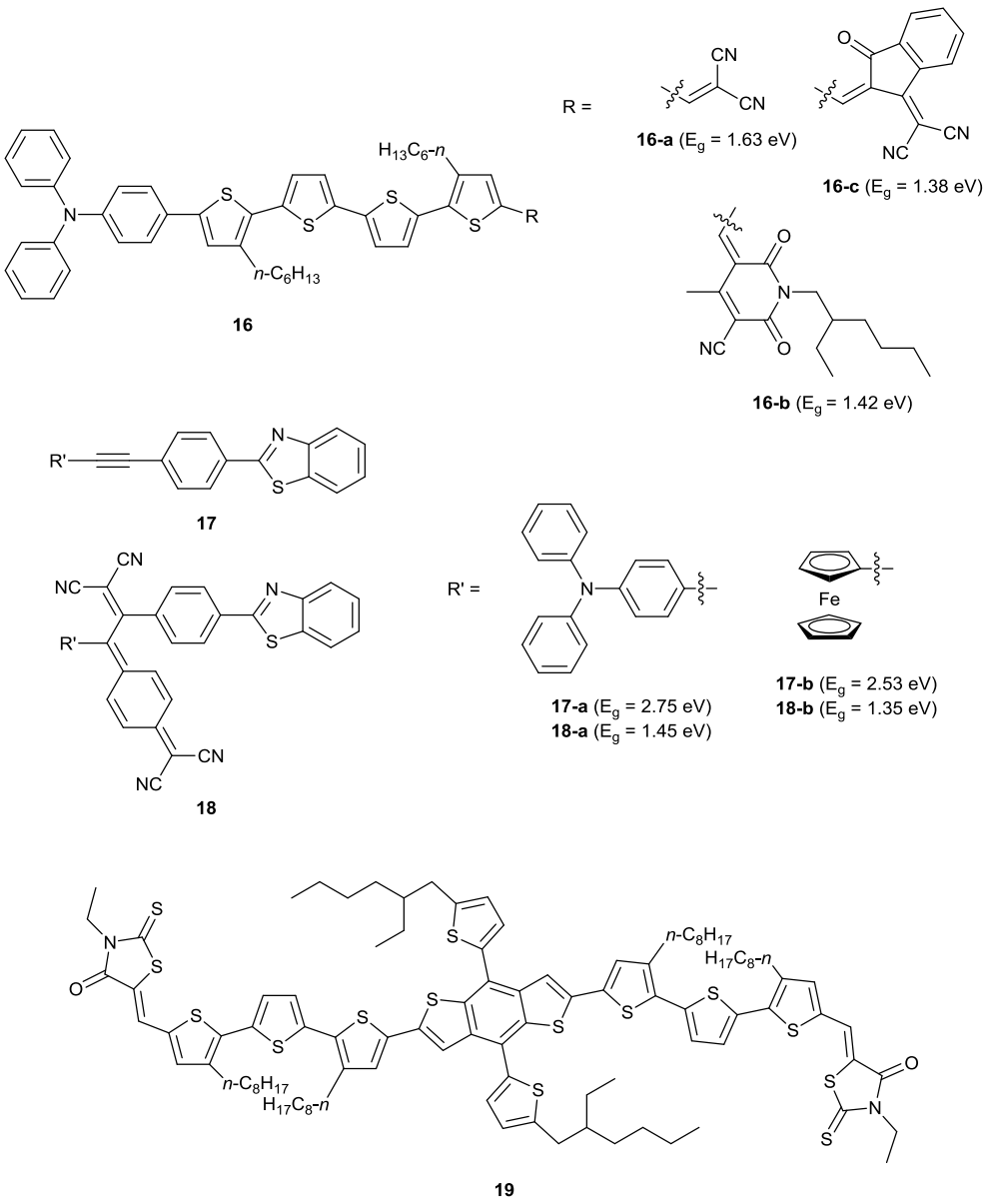

Figure 8 – Selected examples of different donor-acceptor architectures

References: **16**,[49] **17**, **18**,[52] **19**[53]

Also depicted in figure 8 is **19**, an example of a high performance small molecule for use in OPVs which features an A-π-D-π-A architecture deliberately chosen to provide broadened absorption spectra and strong ICT. The central benzodithiophene unit behaves as the donor with rhodanine units behaving as the acceptors and when utilised in optimised bulk heterojunction OPVs a high power conversion efficiency of 8.12% was obtained.[53]

1.1-3.2 Ambipolar Charge Transport Semiconductors

Reconsidering p- and n-type transport materials, there is also significant interest in ambipolar semiconducting materials that can exhibit both p- and n-type channels. In particular, they may provide a method of mimicking CMOS circuits that can be more powerful and cost effective. Although not as common in the literature as p- and n-type materials a significant number of ambipolar materials have been reported,[54] selected examples of which are shown in figure 9. Many appear as semiconducting copolymers with a donor-acceptor structure[54] such as ambipolar donor-acceptor copolymer **20** (DPPT-TT) (figure 9) featuring remarkable electron and hole mobilities of up to 1.86 $cm^2 V^{-1} S^{-1}$ and 1.18 $cm^2 V^{-1} S^{-1}$ respectively (under N_2, after thermal annealing at 320 °C in a device utilising solvent cleaned gold electrodes).[55]

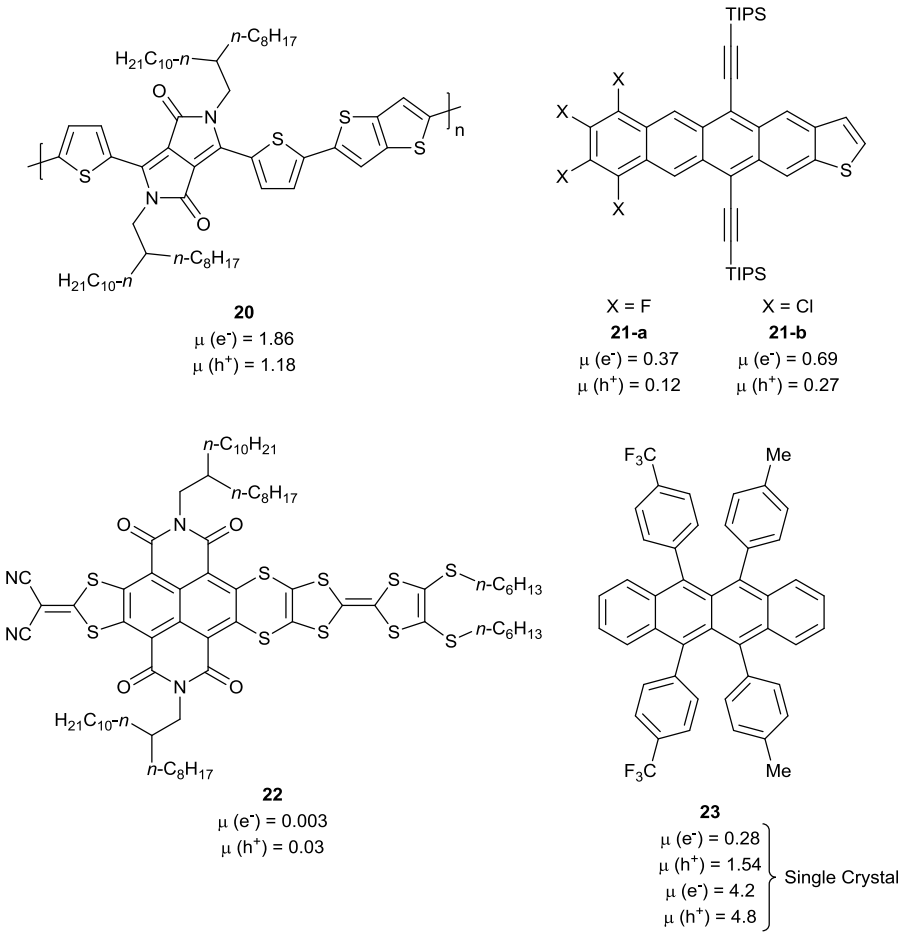

Figure 9 – Selected examples of ambipolar semiconductors and their thin film mobilities

References: **20**,[55] **21-a**,[56] **21-b**,[57] **22**,[58] **23**[59, 60]

An excellent example of an ambipolar small molecule with donor-acceptor functionality is **21-a**. This compound features an electron mobility as high as 0.37 $cm^2 V^{-1} S^{-1}$ under N_2, a hole mobility as high as 0.12 $cm^2 V^{-1} S^{-1}$ in air and is both solution processable and stable.[56] Meanwhile the chlorinated derivative **21-b** features even more impressive mobilities, as high as 0.69 $cm^2 V^{-1} S^{-1}$ and 0.27 $cm^2 V^{-1} S^{-1}$ for electrons and holes respectively in a dry N_2 atmosphere.[57] Another example of an ambipolar small molecule is **22** with which electron and hole mobilities of 0.003 and 0.03 $cm^2 V^{-1} S^{-1}$ respectively were achieved (after annealing at 160 °C). This is notable as these OFETs were measured in air.[58] Molecule **23** is based on high performance p-type material rubrene (**3**, figure 6) but is functionalised with 4-trifluoromethylphenyl and 4-methylphenyl groups. Initial single crystal devices yielded promising mobilities of 0.28 $cm^2 V^{-1} S^{-1}$ and 1.54 $cm^2 V^{-1} S^{-1}$ for electrons and holes respectively under N_2.[59] These mobilities were however lower than expected and it was hypothesised that this novel functionalisation resulted in deeper HOMO and LUMO levels than observed in **3**, making charge injection inefficient from gold electrodes. This was overcome by modifying the gold electrodes with single walled carbon nanotubes at the charge injection interface. This significantly reduced the contact resistance of the electrodes resulting in exceptional single crystal mobilities of 4.2 $cm^2 V^{-1} S^{-1}$ and 4.8 $cm^2 V^{-1} S^{-1}$ for electrons and holes respectively under N_2.[60]

1.1-4 The Morphology of Organic Semiconductors

The room temperature movement of charges though small molecule organic semiconductors can be described as a hopping transport process. This process is fastest (*i.e.* the highest mobilities are obtained) when the transfer integral (electronic coupling between neighbouring molecules) is maximised[61] and the reorganisation energy (the energy associated with the movement of the molecule from a neutral to a charged state geometry and *vice versa*) is minimised.[62] Both of these parameters are dependent on the crystalline packing structure of the semiconducting molecules. Four common motifs are herring bone with face-to-edge stacking (a), herring bone with face-to-face packing (also called slipped π-stacking) (b), 1D lamellar packing (c) and 2D lamellar packing (d) as shown in figure 10.

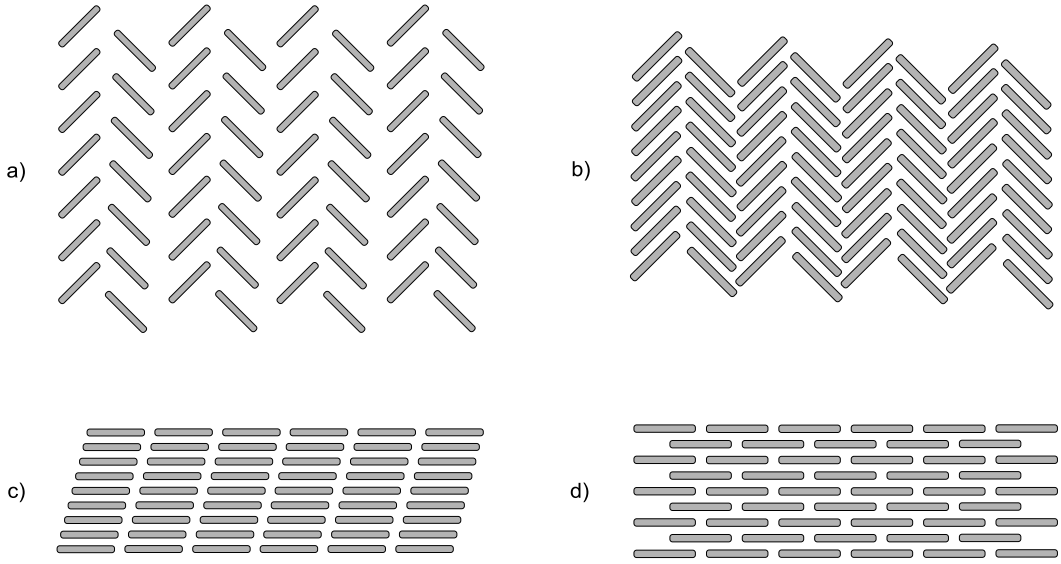

Figure 10 – The four common crystalline packing motifs among small molecule organic semiconductors[20]

Face-to-face stacking is far more desirable than edge-to-face as it allows π-π overlap (leading to a greater transfer integral), with 2D lamellar packing generally considered the most desirable as charge carriers can travel in a straight line though the motif, minimising distance.[20] It is inherently difficult to predict the packing motif that organic semiconductors will assume on crystallisation[17] however there are several techniques designed to encourage organic semiconductors to adopt a 2D lamellar packing motif, for example substitution at the *peri*-position (side position) of acenes and increasing the C/H ratio (to reduce the opportunity for edge-to-face interactions).[20]

Further to these crystalline packing motifs, one must also consider the morphology of the thin film of the semiconductor on preparation for OFET applications as heterogeneities (such as defects or misalignment in the crystalline regions formed) can degrade performance.[63] The surface of the substrate is extremely important to the quality of the semiconductor thin film cast, as both its roughness and surface energy must be considered. It is therefore common to modify the dielectric surface to improve the quality of the thin film of an organic semiconductor that is subsequently deposited, for example by the use of a self-assembled monolayer (SAM) or polymer buffer layer.[64] It is also common to thermally anneal the cast film in order to increase

its crystallinity after deposition, for example the mobility of pentacene OFETs can be increased from 0.19 to 0.49 $cm^2 V^{-1} S^{-1}$ through this process.[63]

The method of deposition of the organic semiconductor is also important in determining the quality of the thin film formed. Thermal evaporation under vacuum (vacuum-deposition) is particularly useful for low solubility organic molecules and control of both the deposition rate and substrate temperature can be used to increase average grain size.[64] A key advantage of organic semiconductors however is being able to cast thin films from solution and a variety of methods exist to do this aside from simply drop casting. Notable examples include: spin coating (the solution is placed on a spinning substrate and a uniform thin film is rapidly formed due to centrifugal forces);[65] dip coating (by slowly removing a substrate from the solution, a crystalline thin film that is aligned in the direction of removal is formed on the surface);[66, 67] tilt coating (drop casting onto a tilted substrate to form crystallites with the stacking axis orientated along the substrate);[68] zone casting (a solution of the semiconductor is deposited onto a moving substrate from a fixed nozzle)[69] and solution sheering (a shearing plate is dragged across the surface of a heated substrate keeping the bulk of the solution between the plate and the substrate while leaving a propagating thin film behind).[70] In particular, solution shearing has recently produced impressive results; by using a micropillar-patterned shearing blade and controlled nucleation on the substrate (by patterning it with wetting and non-wetting regions) single crystalline thin films of TIPS-pentacene (pentacene, **1** substituted with triisopropylsilylethynyl groups in the 6,13- positions) with exceptional mobilities of up to 11 $cm^2 V^{-1} S^{-1}$ and average mobilities of 8.1 ± 1.2 $cm^2 V^{-1} S^{-1}$ have been produced.[71] In summary, not only the semiconductor film, but also the manner in which it was cast is crucial to the performance of the transistor.

1.1-5 Chrysene: A Phenacene Isomer of Tetracene

As shown in figure 11 "*cata*"-fused acenes have two key isomeric topologies. Tetracene (**24**), pentacene (**1**) and hexacene (**2**) are examples of linearly fused "acenes" while chrysene (**25**), picene (**26**) and [6]phenacene (**27**) are corresponding examples of zig-zag-fused "phenacenes".[72]

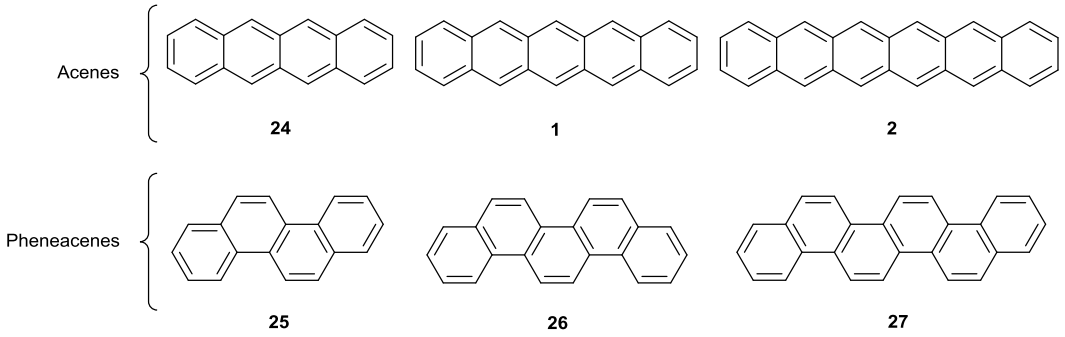

Figure 11 – Tetracene (**24**), pentacene (**1**), hexacene (**1**), chrysene (**25**), picene (**26**) and [6]phenacene (**27**). Linear acenes and their non-linear phenacene isomers[72]

In organic electronic applications tetracene (**24**, figure 11) has received considerable attention, along with anthracene and pentacene (**1**), as a potentially useful oligoacene semiconductor.[20] The non-linear phene-type tetracene isomer chrysene (**25**) has been far less studied despite investigations into other isomers of **24** (e.g. pyrene[73] and triphenylene[74]). In the initial project of this thesis (section 2.1) **25** acts as a central fused aromatic core from which derivatives can be formed.

Chrysene is of particular interest as an aromatic core for organic electronic applications due to the greater stability that can be expected from such non-linear pheneacene structures. For example chrysene has a HOMO level of -5.9 eV,[75] while tetracene has a HOMO level of -5.4 eV[76] hence chrysene is less prone to oxidation on exposure to atmospheric conditions due to its lower HOMO (*i.e.* higher oxidation potential).[77] In particular, in phenacenes such as chrysene, additional fused benzene rings do not destabilise the HOMO in the same manner as linear acenes.[78] Considering the extension of the aromatic system of chrysene in the initial project of this thesis, a lower initial HOMO level can be expected to be advantageous in end-product molecules.

Despite their lower HOMO and larger E_g, pheneacenes have been shown in the literature to have excellent device performances. For instance thin films of [6]pheneacene (**27**, figure 11) have produced hole mobilities[79] as high as 7.4 $cm^2\ V^{-1}\ S^{-1}$ and despite its smaller ring system, previous studies on disubstituted chrysene derivatives have concluded that it shows significant potential as a planar aromatic

core that can be functionalised to generate OFET materials[80, 81, 82, 83] (section 1.1-6.1).

The stability of chrysene and other phene-type aromatics can be very simply (but quite elegantly) explained in terms of Clar's aromatic sextet theory[84, 85] which aims to describe the given aromaticity of a polyaromatic hydrocarbon (PAH) system. In this theory six π electrons in a single benzene ring make up a sextet, which is represented by a circle. Formal C-C bonds then separate a sextet from adjacent rings,[86] thus circles cannot be drawn in adjacent rings. As many circles as possible are drawn throughout the PAH system wherever sextets are found until the rings left are either empty or contain a Kekulé structure.[84] The application of these rules to tetracene, pentacene and chrysene results in the Clar structures shown in figure 12.[87]

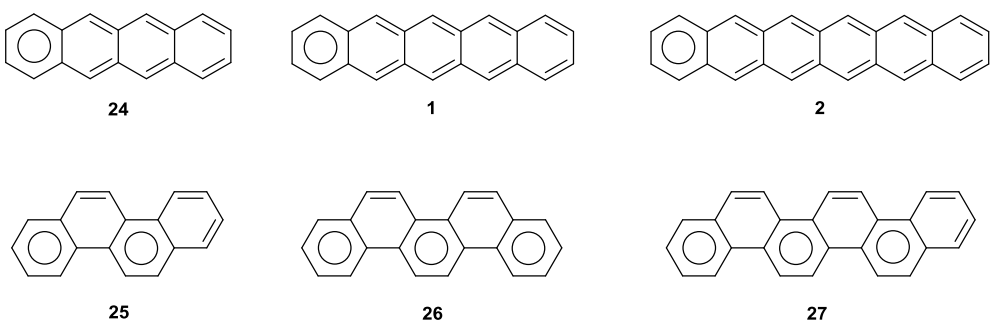

Figure 12 - Clar structures of tetracene (**24**), pentacene (**1**), hexacene (**2**), chrysene (**25**), picene (**26**) and [6]pheneacene (**27**)[87]

In the linear acenes, as the number of fused aromatic rings increases (exemplified by the movement from tetracene to pentacene) the number of aromatic sextets remains the same resulting in a gradual loss of aromatic character as one sextet is shared by an increasing number of rings. However in phenacenes the addition of each alternate angular ring adds an additional sextet, serving to "top up" aromatic character as the size of the system increases.[85] This is why [n]phenacenes are less reactive than their linear counterparts.[88] In other words, the isomer with the larger Clar number will have the larger E_g (lower HOMO and higher LUMO) which confers greater stability.[87]

1.1-6 4,10-Dichlorochrysene: A Versatile Substituted PAH Core

In this project, 4,10-dichlorochrysene (**32**, figure 13) acts as the starting point from which a series of chrysene derivatives can be synthesised. First reported[89] in 2007, **32** can be relatively simply synthesised in an 21% overall yield from 1,5-dihydroxynapthalene (**28**) as illustrated in figure 13.[90]

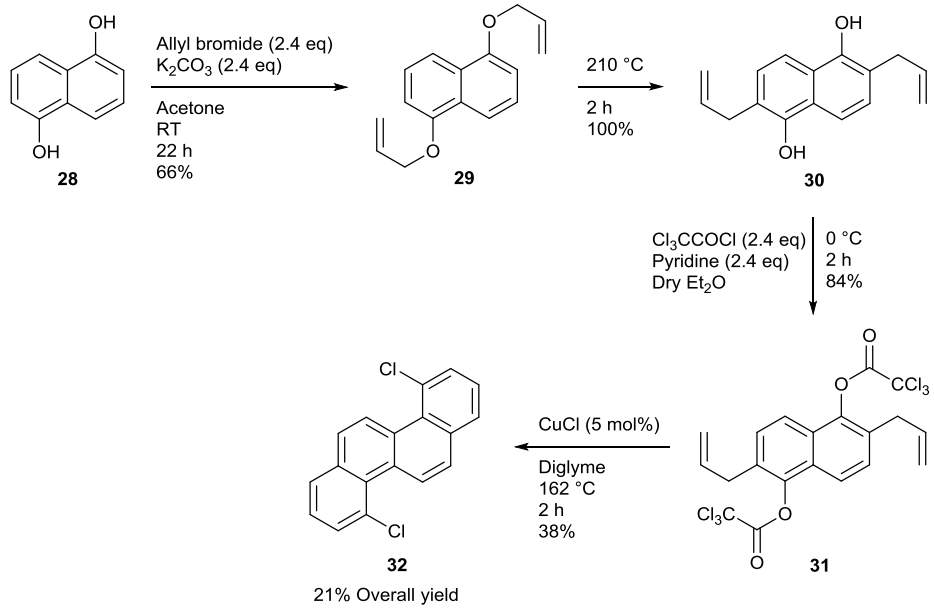

Figure 13 – Synthetic route to 4,10-dichlorochrysene (**32**)[90]

29 is formed *via* a Williamson ether synthesis from **28**. A thermal Claisen rearrangement then leads to the formation of **30** and a subsequent trichloroacetylation yields the acetylated intermediate product **31**. Thermolysis of **31** in the presence of Cu(I) then results in a benzannulation *via* an atom transfer radical cyclisation (the Bull-Hutchings-Quayle reaction)[89] to yield 4,10-dichlorochrysene (**32**).[90]

1.1-6.1 Disubstituted Derivatives of Chrysene in the Literature

Various derivatives of chrysene have been previously synthesised in the literature, particularly at the 6,12-positions (for example **33** *via* nitration)[91] (figure 14) and at the 4,5-positions (for example **34** *via* lithiation).[92] A common method to access disubstituted chrysenes at the 6,12-positions is to brominate chrysene using Br_2.[93, 94] Most notably the 3-carbazole substituted derivative **35** was synthesised *via* this method and showed potential as a blue emissive material for OLEDs. **35** was

considered particularly suitable for OLED applications due to its high thermal stability and twisted structure to prevent crystallisation and hence lower fluorescence self-quenching.[94]

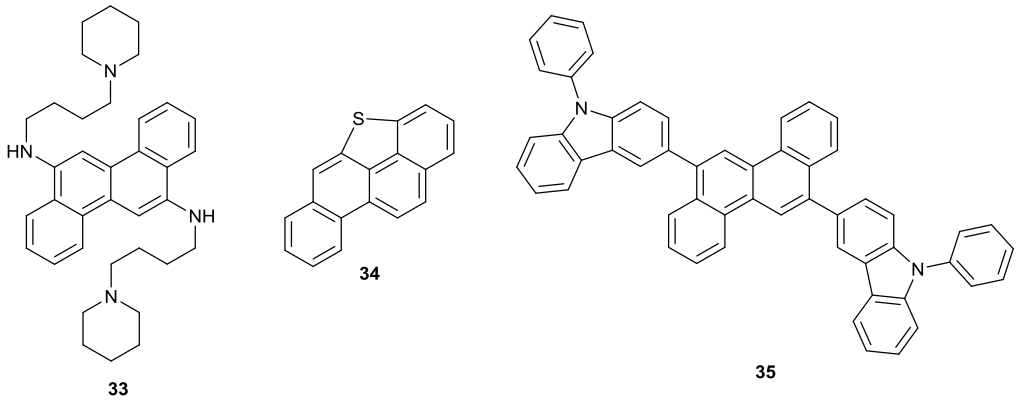

Figure 14 – Examples of 6,12- and 4,5-substituted chrysene derivatives

References: **33**,[91] **34**,[92] **35**[94]

Many 2,8-substituted chrysenes have appeared in the literature previously with the 2,8-derivatives shown in figure 15 being applied in organic electronic applications by Okamoto *et al*.[80, 81, 82, 83] In this work the 2,8-positions were accessed *via* nitration of a partially oxidised chrysene followed by reductive aromatization.[95]

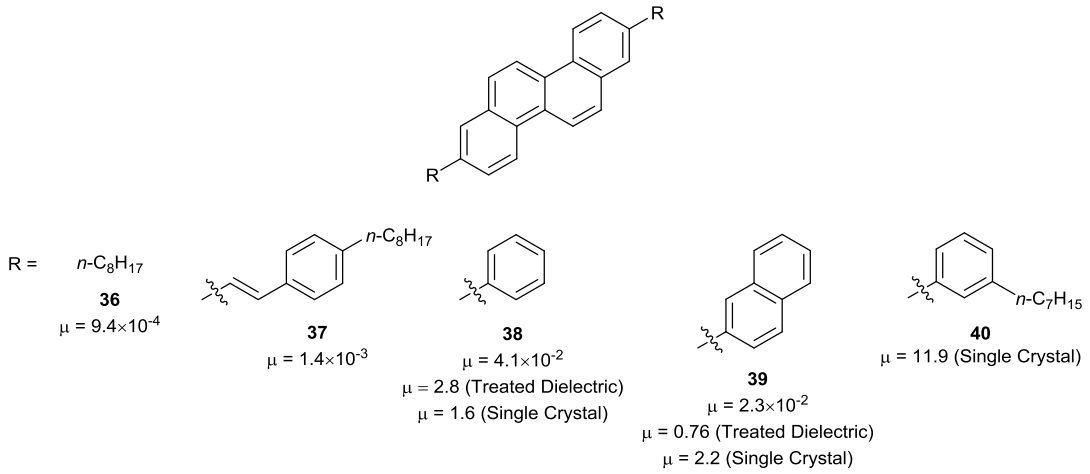

Figure 15 – Examples of 2,8-substituted chrysene derivatives and their thin film hole mobilities (unless otherwise noted) investigated by Okamoto *et al*[80, 81, 82, 83]

The materials were shown to be p-type with the best thin film mobility achieved using 2,8-diphenylchrysene (**38**, figure 15) reaching a mobility of 4.1×10^{-2} cm^2 V^{-1}

S^{-1}.[80] Grain size and molecular ordering were both shown to have a strong effect on the performance of the devices however[81] and when polymer treated SiO_2 was used as the dielectric layer, mobilities as high as 2.8 cm^2 V^{-1} S^{-1} were achieved with **38**.[82] Additional investigations by the same research group also produced single crystal devices of the phenyl (**38**) and naphthyl (**39**) derivatives to better probe their intrinsic charge transport properties[81] but single crystal studies of **40** (grown though solution processing rather than vapour transport as with **38** and **39**) yielded the most impressive mobilities of 11.9 cm^2 V^{-1} S^{-1}, showcasing the intrinsic potential of chrysene-based materials to perform as p-type semiconductors.[83]

1.1-6.2 Tetrasubstituted Derivatives of Chrysene in the Literature

The first "A_4" tetrasubstituted chrysene derivative was reported in 2008. Under forceful conditions (Br_2 in trimethylphosphate at 100 °C for three days) chrysene was tetrabrominated at the 3,6,9,12-positions. Subsequent Suzuki coupling to *tert*-butylphenylboronic acid produced **41-a** (figure 16) which showed a blue photoluminescence and was used as the emissive material in an OLED device.[96]

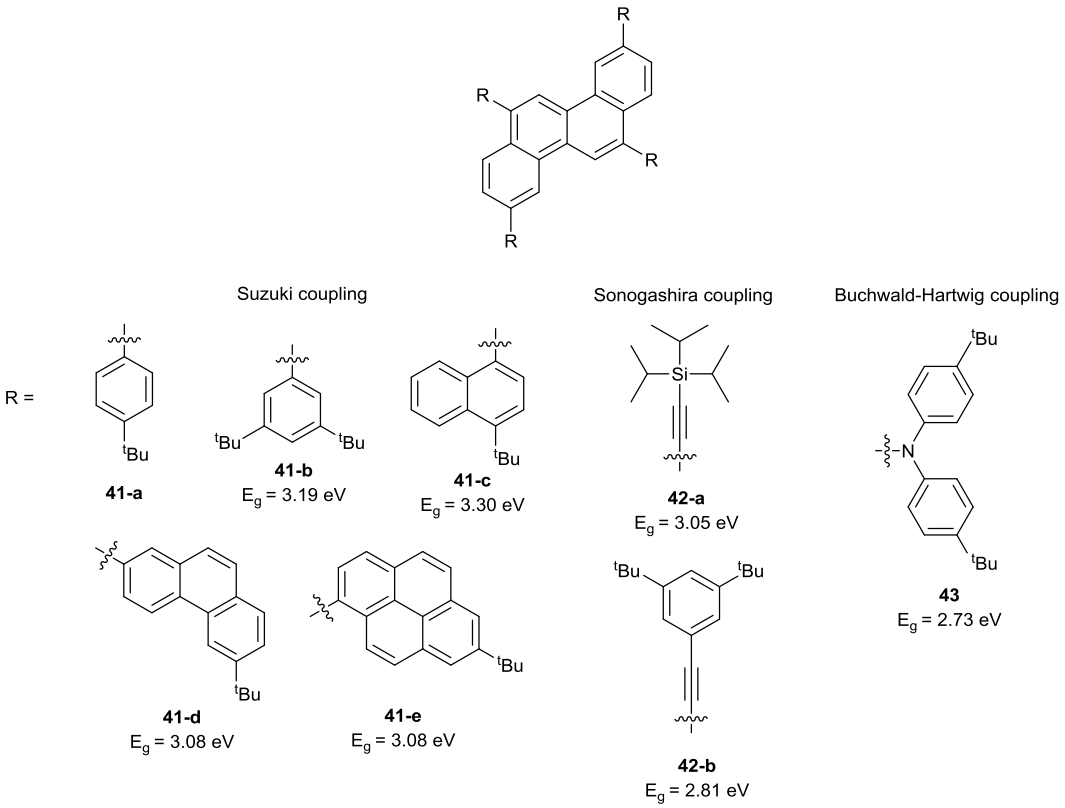

Figure 16 – "A_4" tetrasubstituted chrysene derivatives

References: **41-a,**[96] **41-b - 43**[97]

In a continuation of this work by a different group, 3,6,9,12-tetrabromochrysene was Suzuki coupled to a variety of additional aromatics (**41-b** - **e**); Sonogashira coupled to both a TIPS acetylene group (**42-a**) and an acetylenic aromatic (**42-b**) and Buchwald−Hartwig coupled to *bis*(4-*tert*-butylphenyl)amine (**43**). Significant bathochomatic shifts were observed in both the absorption and emission spectra of these derivatives compared to the parent chrysene and optical E_g values were significantly reduced. Derivative **43** bearing strongly electron donating *bis*(4-*tert*-butylphenyl)amine groups showed the largest bathochomatic shift and lowest E_g and was used to fabricate a blue fluorescent OLED with an excellent external quantum efficiency of 6.31%.[97]

A limited number of "A_2B_2" substituted chrysenes also appear in the literature associated with Isobe *et al*[98, 99, 100] who first published a synthesis of 6,12-dialkyl chrysenes bearing a halogen at the 3,9- or 2,8-positions in 2009. The starting material **44** (figure 17) was exposed to acidic conditions to generate (along with the expected product **45**) the "A_2B_2" substituted chrysene derivative **46**, with **45** behaving as an intermediate that underwent both a skeletal rearrangement and a dehydrogenation (although the precise mechanism of this rearrangement is unclear). Interestingly when single crystals of each derivative of **46** were analysed it was found the halogenation seemed to induce π-π stacking with the positions of the halogens resulting in variations in the type of stacking observed.[98]

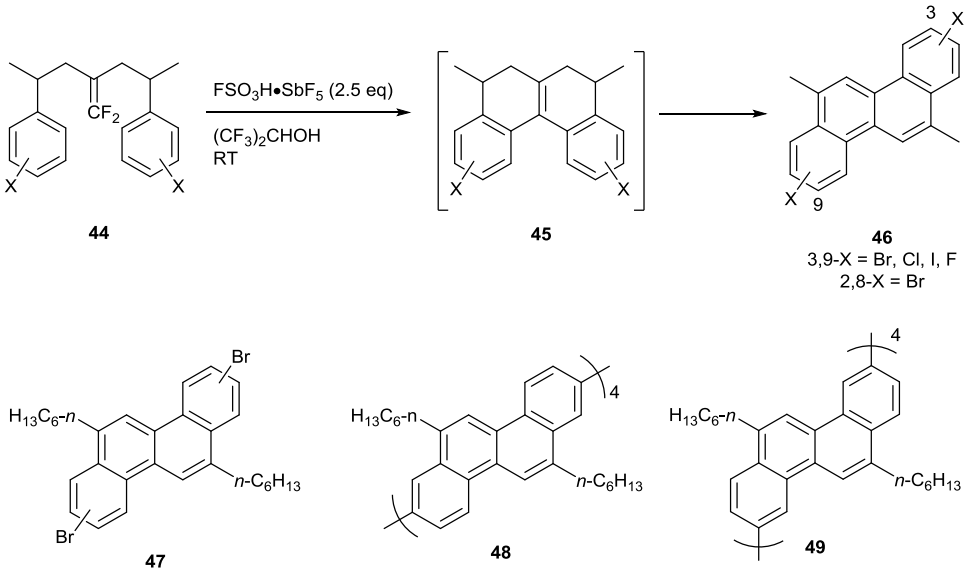

Figure 17 – "A_2B_2" tetrasubstituted chrysene derivatives

References: **44**-**46**,[98] **47**,[99, 100] **48**,[99] **49**[100]

Using the methodology discussed above, Isobe *et al* then synthesised **47** bearing *n*-hexyl chains at the 6,12-positions and bromines at either the 2,8- or the 3,9-positions as desired.[99, 100] These derivatives were then applied in the synthesis of hoop shaped aromatic systems forming essentially a four membered chrysene macrocycle first though the 2,8-positions[99] and then though the 3,9-positions.[100] These hoop shaped chrysene derivatives **48** and **49** were then used as finite models for helical and zig-zag single walled carbon nanotubes respectively.[99, 100]

1.1-6.3 Previous Derivatisations of 4,10-Dichlorochrysene

In previous work within our group 4,10-dichlorochrysene (**32**, figure 13) was shown to have favourable π-π stacking with an interlamellar distance of 3.78 Å and a minimum C-C bond distance of 3.48 Å,[90] however its E_g (3.26 eV)[4] is too large for it to be suitable in an OFET. It was therefore hoped that other 4,10-derivatives of chrysene, accessible though coupling at the chlorinated positions, would show superior properties. With this aim, several derivatives of **32** were produced, as shown in figure 18 along with the coupling method used in their synthesis.[90]

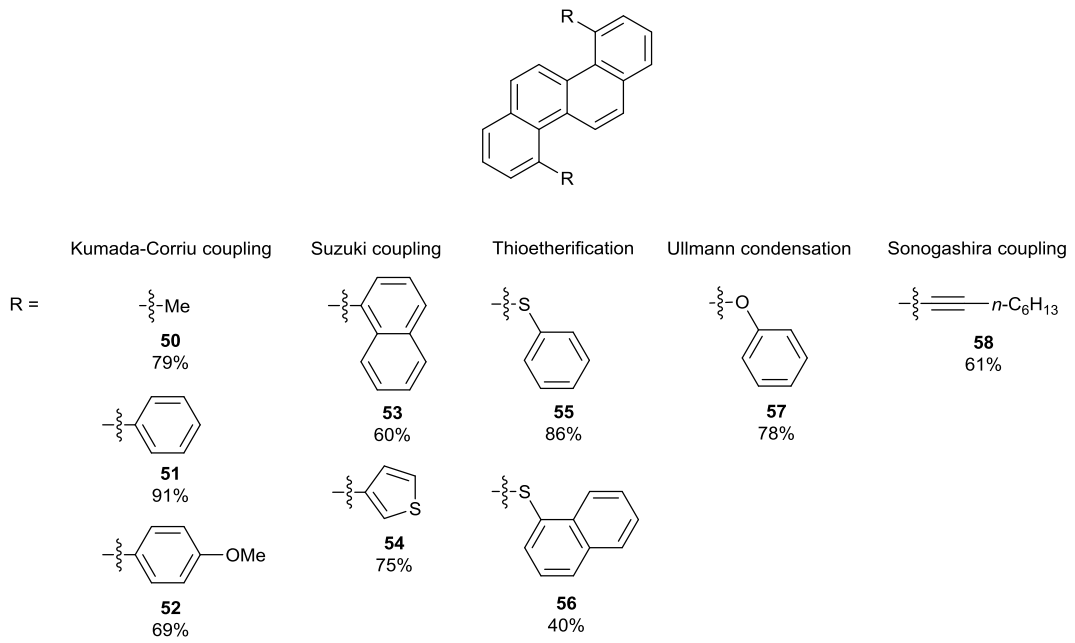

Figure 18 – Derivatives of 4,10-dichlorochrysene (**32**) and their isolated yields[90]

Many of the reactions in figure 18 proved to be surprisingly effective considering the low reactivity generally associated with aryl chlorides. It has however been shown by X-ray crystallography that the chloro substituents of **32** are twisted out-of-plane with an average bay region torsion 22.48 ° and this may account for their enhanced reactivity.[90]

Substitution of the 4,10-positions had a profound effect on the crystal packing structure observed. Substitution with a phenyl group (**51**) was unfavourable as H-π interactions came to dominate and π-π stacking was disrupted, while **54** and **55** featured herringbone stacking with **55** incorporating π-π stacking down to 3.33 Å. Density functional theory (DFT) calculations suggest that there was no significant delocalisation from the 4,10-positions to the chrysene core except in **55** and **56** however the HOMO level (as determined by cyclic voltammetry) was increased from -5.99 eV in **32** to -5.78 eV in **55** and -5.77 eV in **50**. The UV-vis absorption spectra of these compounds were redshifted compared to chrysene with lower intensity absorptions generally from 300-350 nm, although **55** and **56** featured low intensity absorptions up to almost 400 nm.[90]

The above work (figure 18) demonstrates the large chemical space that can be directly accessed from the 4,10-dichloro positions of **32**. The surprising reactivity of

the 4,10-positions of **32** in a variety of coupling techniques, with a range of coupling partners, made it an ideal starting point for further synthesis.

1.1-7 Aims and Objectives 1 – Synthesis and Evaluation of "A_2B_2" Tetrasubstituted Chrysene Derivatives

In this project the reactivity of 4,10-dichlorochrysene (**32**) was reinvestigated, not only at the 4,10-positions but also at the 2,8-positions of the chrysene core *via* a regioselective, iridium-catalysed aromatic C-H borylation (described in detail in section 1.2) of **32**. In this project the small molecule synthesis of a variety of 2,8- and 4,10-substituted chrysenes in an orthogonal "A_2B_2" format was investigated.

In summary, the project had the following aims:

1. The formation of a generic methodology for the orthogonal coupling of the 2,8- and 4,10-positions of the chrysene core following the regioselective C-H activated 2,8-diborylation of **32**.
2. The substitution of aromatic, donor and acceptor moieties in the two sets of positions in an "A_2B_2" substitution pattern (as shown in figure 19) enabling the synthesis of a small library of chrysene derivatives.
3. Investigation of the effects of these substitution patterns on the UV-vis absorption/fluorescence spectrum; single crystal packing structure and HOMO/LUMO levels of the potential organic semiconductors synthesised to evaluate their suitability for organic electronic applications.

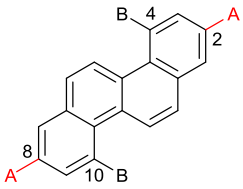

Figure 19 – The proposed "A_2B_2" substitution of the chrysene core. Substitution at positions accessed *via* C-H borylation shown in red

1.2 Iridium-Catalysed Aromatic C-H Borylation

Throughout this thesis, extensive use is made of the iridium-catalysed aromatic C-H borylation primarily developed by Smith, Hartwig, Ishiyama and Miyaura.[101] It proved a key reaction in the sterically directed functionalisation of a variety of polyaromatic intermediates including derivatives of chrysene, pyrene and perylene. As such, the development, mechanism and application of this borylation to polyaromatic systems is briefly reviewed here.

1.2-1 Development

In 1995 Hartwig *et al*[102] studied one of the earliest instances of C-H borylation using catecholborane (Bcat) substituted manganese, ruthenium and iron (**59**, figure 20) complexes which lead to the borylation of arenes and alkenes under irradiation. These photochemical reactions used stoichiometric amounts of the metal complex and were reacted neat with the arene and alkenes used. The complex **59** proved particularly effective, forming Ph-Bcat in an 80-90% yield.[102]

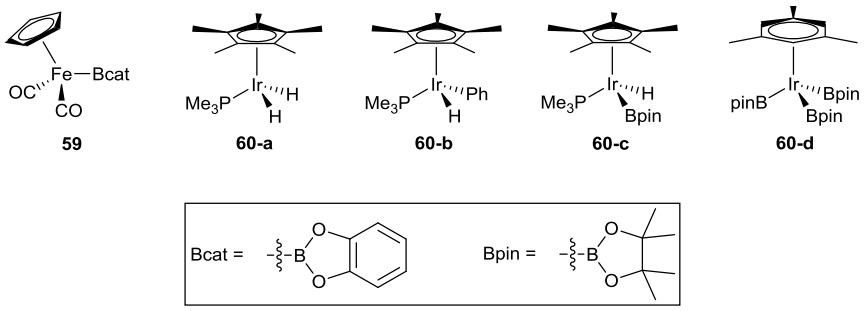

Figure 20 – Early aryl C-H borylation catalysts developed by Hartwig *et al*[102] and Smith *et al*[103, 104, 105]

In 1999 Smith *et al*[103] explored aromatic C-H borylations using iridium complexes known to engage in C-H activation chemistry. Initially the hydrogen substituted iridium complex (**60-a**) was dissolved in a benzene solution with HBpin, before photolysis then promoted C-H activation of the benzene solvent and the formation of phenyl substituted iridium complex (**60-b**). Thermal heating then allowed conversion of the iridium complex to the boronate substituted derivative **60-c** producing the borylated phenyl derivative as a product. This process of photolysis and thermal heating was then repeated two further times, allowing full conversion of the added

HBpin to Ph-Bpin. Interestingly, the presence of a thermal catalytic process was noted in this work and in a later study, 17 mol% of **60-a** mixed with HBpin in a benzene solvent system allowed generation of Ph-Bpin in a 53% yield (relative to HBpin) simply by heating at 150 °C for 120 h with no irradiation necessary.[103] This paper marked the first reported example of the transition metal-catalysed C-H borylation of aromatic systems.[106] Using this thermal catalytic method a later paper by Smith *et al*[104] then explored the functional group tolerance and directing effects of this borylation, noting its tolerance of heteroatom substituents (including esters and amides) and the nature of steric effects on regioselectively.[104]

Smith *et al*[105] elaborated on this work further in 2002 noting that the presence of phosphine ligands enabled iridium complex **60-d** to catalyse aromatic C-H borylations at 150 °C, with dmpe (1,2-*bis*(dimethylphosphino)ethane) and particularly dppe (1,2-*bis*(diphenylphosphino)ethane) proving to be promising ligands. It was also identified that effective catalysts could be generated *in situ* from the commercially available complex $[IrCl(COD)]_2$ (**61-a**, figure 21) and that cyclohexane could be used as an inert solvent.[105] Concurrently with this piece of work Hartwig and Miyaura *et al*[107] noted that **61-a** with a 2,2′-bipyridyl (bpy) ligand (**62-a**) could catalyse the borylation of neat benzene by *bis*(pinacolato)diboron (B_2pin_2) in an exceptional 95% yield (relative to B_2pin_2) after 16 h at 80 °C. The further elaboration of this reaction with a variety of neat arenes highlighted the sterically directed nature of this borylation. It was found that substituents generally block *ortho*- borylation due to steric effects and that 1,3-disubsituted arenes generally produce isomerically pure products due to the common *meta*-position, even with two distinct substituents at the 1- and 3-positions. It was additionally noted that aromatic C-H bonds were selectively borylated over aromatic C-Cl and C-Br bonds despite the thermodynamically favoured formation of haloboranes. Remarkably, when reactions were conducted with $[IrCl(COE)_2]_2$, as the cyclooctadiene (COD) ligand was found to be reduced to cyclooctene (COE) in the initial stages of the reaction, no induction period was observed. Furthermore when $[IrCl(COE)_2]_2$ was used with a 4,4'-di-*tert*-butyl-2,2'-byipyridine (dtbpy) ligand (**62-b**) (which produces a more soluble catalyst system) Ph-Bpin was produced in an 83% yield (relative to B_2pin_2) in 4.5 hours at room temperature.[107]

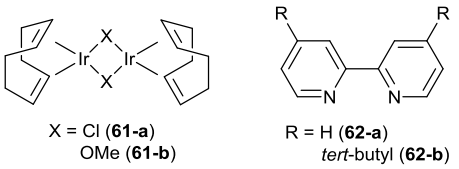

Figure 21 – Later, air stable and commercially available iridium catalyst and ligand systems including **61-b** and **62-b** used in this project[107, 108]

In a key paper later that year Hartwig and Miyaura *et al*[108] further disclosed the $[Ir(OMe)(COD)]_2$ (**61-b**)/dtbpy (**62-b**) catalyst system (as used throughout section 2 of this thesis) utilising hexane as a solvent, allowing the borylation of arenes in solution with a stoichiometric amount of B_2pin_2. It was found that the air stable iridium complexes featuring OH, OPh or OMe ligands even catalysed borylations at room temperature, with these ligands likely aiding the formation of the boryl iridium complexes. Reactions were found to be fastest in non-polar solvents with the order of reactivity being hexane > DME > DMF. This borylation was applied to a variety of substituted arenes and also benzofused heteroarenes (in which borylation occurred at the activated 2-position) and was found to be tolerant of a variety of functionalities including: OMe, CO_2Me, CN, CF_3, Cl, Br and I.[108] This methodology was later additionally extended to include HPin rather than B_2pin_2 as the boryl source.[109] The synthetic utility of this borylation reaction has continued to develop over time with subsequent high-throughput studies expanding available methodologies, in particular highlighting alternative ligands and polar solvent systems (e.g. THF) that may be used.[110]

Of significant interest in this aromatic C-H borylation reaction are the steric, rather than electronic effects, which dominate its observed regioselectively. Smith *et al*[111] studied the borylation of 4-substituted benzonitriles and 1,3- dicyano and difluoro benzenes in a THF solvent system at room temperature. The results clearly pointed to sterically directed regioselectively overriding directed *ortho*- metalation selectivity that might have been observed.[111] Meanwhile Steel *et al*[112] observed that when borylating sterically equivalent but electronically different sites in aromatic carbocycles, while underlying electronic directing effects are present at room temperature, at elevated temperatures steric regioselectivities predominate resulting in the formation of statistical mixtures of products.[112]

1.2-2 Mechanism of Borylation

Concerning the mechanism of this iridium-catalysed borylation, the triboryl complex [Ir(dtbpy)(COE)(Bpin)$_3$] (**63**, figure 22) has been identified as a likely catalytic intermediate. It has been isolated from the reaction, identified by ^{1}H NMR and shown to catalyse aromatic C-H borylations at room temperature. It is noteworthy that in the formation of intermediate **63**, the COD ligand is reduced to COE, explaining the induction period to the reaction when using **61-a** as a starting material. Indeed, when [IrCl(COE)$_2$]$_2$ is utilised as a precursor, no induction period is observed. However the exact nature of this hydrogenation is unknown and while studies have shown the protons to be abstracted from the arene, no homocoupling is observed, and the fate of the phenyl groups generated is unknown.[107] This same induction period was also observed with the **61-b**/**62-b** catalyst system and was similarly absent when the [Ir(dtbpy)(COE)(Bpin)$_3$] (**63**) complex was directly utilised in the reaction, this together with the exceptional reactivity of **63** made it a starting point for extensive mechanistic studies published in 2005 by Miyaura and Hartwig *et al*[113] in which the catalytic cycle depicted in figure 22 was proposed.

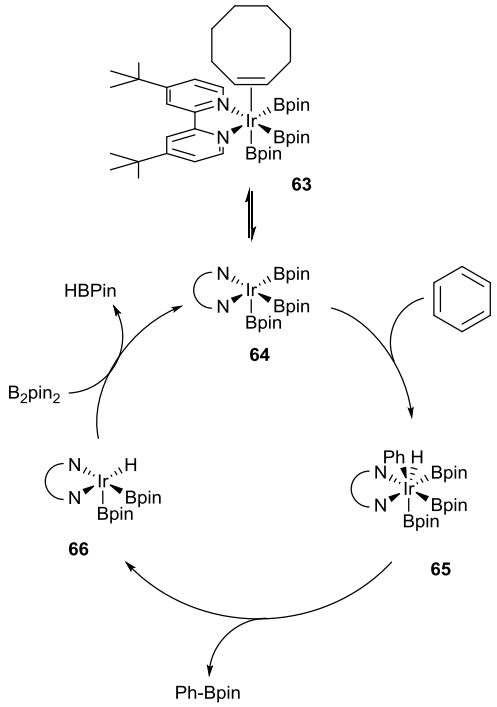

Figure 22 – Proposed catalytic cycle of the iridium-catalysed borylation of arenes[113]

This cycle begins with the previously identified key intermediate **63**. Kinetic and NMR data then indicates the dissociation of the cyclooctene ligand to give the triboryl 16 electron complex **64** which would then engage in C-H bond insertion with the arene in the turn over limiting step. The catalytic cycle may then go through a 7 coordinate intermediate such as **65** before generating the diboryl hydride complex **66** and the borylated arene product. The initial complex **64** could then be regenerated by the reaction of **66** with B_2pin_2. The C-H bond insertion is likely to be the turn over limiting step as kinetic data indicates that the reaction is first order in relation to the arene and zero order in relation to B_2pin_2.

It is proposed that the mechanism of C-H bond cleavage proceeds though an η^2-arene complex. When compared to their electron neutral counterparts, **63** reacts fastest with arenes that are electron poor and 5 membered hetroarenes that are electron rich. In each of these instances an intermediate η^2 complex would exhibit the greatest stability, rationalising these results.

Three computationally evaluated mechanisms for the C-H bond cleavage of the arene by iridium complex **64** are shown below in figure 23. Pathway A features oxidative addition of the complex into the C-H bond followed by reductive elimination to generate the C-B bond. Pathway B involves the σ-bond metathesis of the C-H bond forming the C-B bond at the same time in a single transition state. Pathway C involves the formation of an intermediate borane complex in the σ-bond metathesis, which if necessary, would undergo a rearrangement to positon the carbon and boron components *cis* to one another before C-B bond formation occurs.

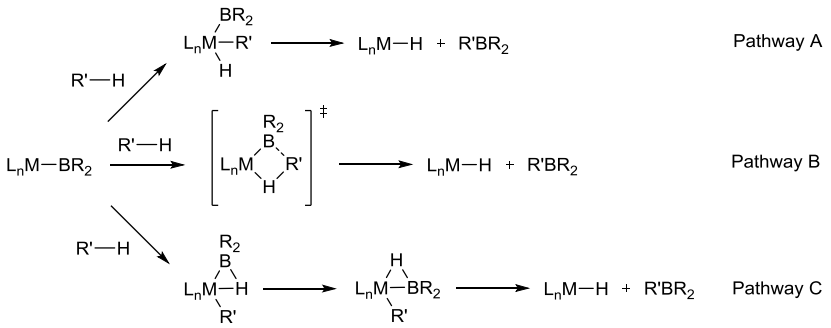

Figure 23 – Proposed mechanisms of C-H bond cleavage by iridium complex **64**[113]

The precise mechanism of C-H bond cleavage is still the subject of debate in the literature. Pathway B appears to be the least likely as computational studies have shown it to have a higher activation energy than pathway C. Past computational studies meanwhile have determined pathway A to be the most probable, although it is notable that the energy difference between pathway A and pathway C is likely to be very small.[113] Subsequent experimental and computational studies have however indicated pathway C to be the most likely method of C-H bond cleavage. Investigations into the reactivity of phosphine ligated boryl iridium complexes analogous to **64** (featuring an open coordination site) alongside bipyridyl ligated complexes have suggested that changes in the boryl group or acene that promote proton transfer to the boryl group result in lower activation energies.[114] Results suggest a basic boryl group can "deprotonate" the iridium complexed arene, thus accounting for the importance of C-H acidity in regioselectivity of room temperature borylations using **61-b**/**62-b**.[112] It is further suggested the greater reactivity of boryl pinacolate complexes over their corresponding catechol analogues is due to C-H bond cleavage being assisted by a more nucleophilic boryl group,[114] providing additional experimental as well as computational evidence for pathway C.

1.2-3 Iridium-Catalysed C-H Borylation of Polyaromatic Systems

An initial investigation into the borylation of polyaromatics was conducted by Perutz *et al*[115] in 2005. This study investigated the borylation of naphthalene, pyrene and perylene using "standard" reaction conditions with the **61-b**/**62-b** (figure 21) catalyst/ligand system with B_2pin_2 using cyclohexane as a solvent, as in figure 24.

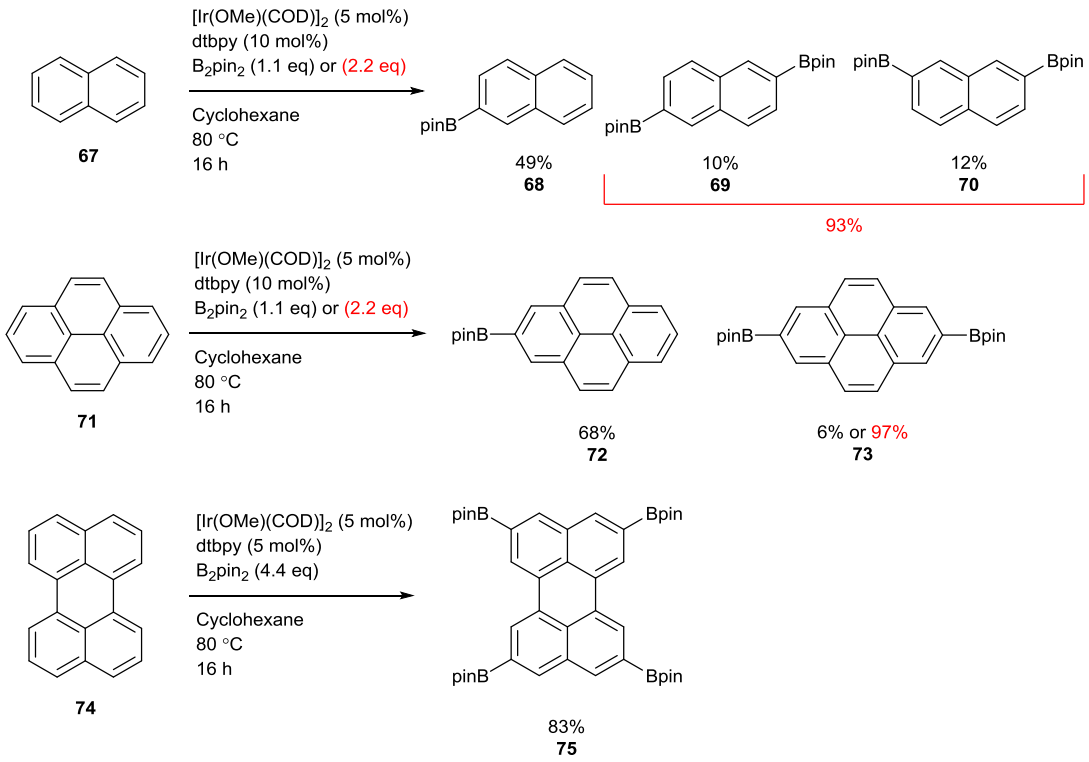

Figure 24 – Iridium-catalysed borylation of naphthalene (**67**), pyrene (**71**) and perylene (**74**)[115]

Of particular importance in this work, was the noted borylation of compounds *meta*- to a ring junction in PAHs, as ring junctions just like other R groups, block *ortho*-borylation when other more accessible sites are available due to the steric bulk of the active catalyst. Also notable in this work was the mono-, di- and tetra-borylation of compounds controlled by the number of equivalents of B_2pin_2 added.[115]

Based on the above work, the borylation of pyrene in particular has attracted significant interest allowing efficient access to the 2,7-positions *vs* electrophilic aromatic substitution which usually occurs at the 1,3,6,8-positions. Marder *et al*[116] investigated the application of this selective borylation synthesising mono- and di-borylated 2- and 2,7- pyrenes which could be converted to the corresponding OTf, Br, BF_3K or $B(OH)_2$ derivatives which were then reacted in Sonogashira, Negishi, Buchwald-Hartwig and Suzuki cross coupling reactions.[116] In a later expansion of this work Marder *et al*[117] utilised the sequential iridium borylation of pyrene to synthesise asymmetric 2,7- donor-acceptor pyrene **78** as in figure 25. The photophysical properties of donor-acceptor **78** were investigated, however

computational DFT calculations revealed the cyano functionally to be a relatively poor acceptor at the 2-position of the pyrene core resulting in limited impact on the photophysical properties of **78**.[117]

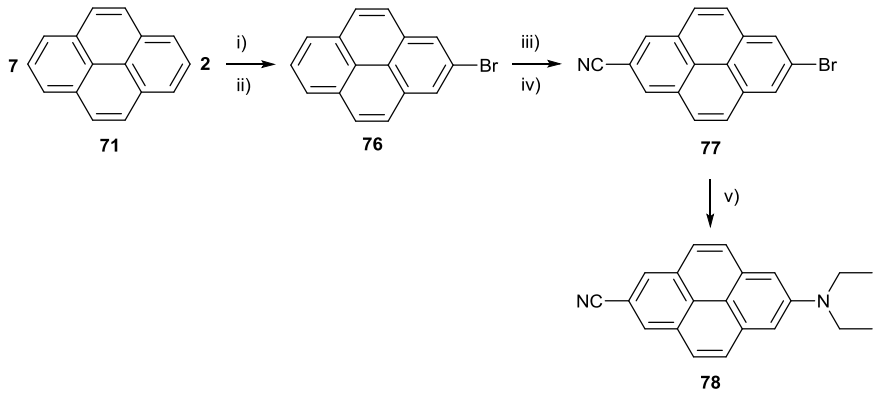

Figure 25 – Sequential iridium-catalysed borylations in the synthesis of 2,7-substituted donor-acceptor pyrene **78**[116, 117]

Conditions: i) $[Ir(OMe)(COD)]_2$ (1 mol%), dtbpy (2 mol%), B_2pin_2 (1.1 eq), hexane, 80 °C, 16 h, 65%; ii) $CuBr_2$ (3 eq), MeOH/H_2O (1:1), 90 °C, 16 h, 83%; iii) $[Ir(OMe)(COD)]_2$ (0.5 mol%), dtbpy (1 mol%), B_2pin_2 (1.2 eq), THF, 80 °C, overnight; iv) $Cu(NO_3)_2 \cdot 3H_2O$ (2.3 eq), $ZnCN_2$ (3.5 eq), CsF (1.2 eq), THF/H_2O/MeOH, 100 °C, overnight, 30% over two steps; v) $HNEt_2$ (6.1 eq), NaO^tBu (3.6 eq), $Pd_2(dba)_3$ (1 mol%), SPhos (3 mol%), toluene, 120 °C, 2 h, 36%.

Again using the **61-b**/**62-b** catalyst/ligand system, this iridium-catalysed C-H borylation has also been applied to larger PAH systems, for example hexabenzocoronenes **79-81** in figure 26 (borylated previously C-H sites indicated in red).[118, 119]

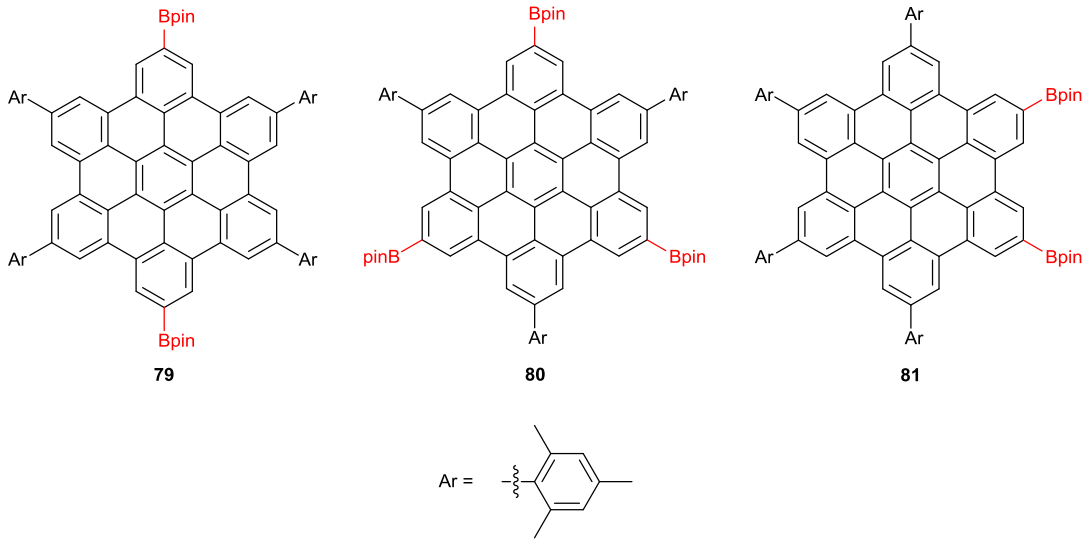

Figure 26 – Iridium-catalysed borylation of hexabenzocoronene derivatives.[118, 119] Borylated previously C-H sites indicated in red

Further notable examples of the application of this C-H borylation to PAH systems are shown in figure 27. Using the **61-b**/**62-b** catalyst/ligand system, the C-H diborylation products of anthracene (**82**) and tetracene (**83**) are produced in isomeric 1:1 mixtures in 88 and 80% yields respectively, with the isomers eventually separated by recrystallisation.[120, 121] An early example of a largely regioselective monoborylation is that of azulene producing **84**. This example was performed with the chloro iridium complex **61-a** and bpy ligand **62-a** allowing the product to be obtained in a 70% yield *via* column chromatography; it wasn't totally regioselective however, with a 10% yield of the other isomer borylated in the 1-positon, also isolated.[122] Using the "standard" **61-b**/**62-b** catalyst/ligand system there are examples of regioselective diborylations in the literature. 6,12-Substituted anthanthrene was regioselectively diborylated to produce **85**, however in addition to column chromatography, gel permeation chromatography (GPC) had to be used to obtain pure material.[123] Notably 2,7-substituted naphthodithiophene was regioselectively diborylated to form **86** in a quantitative yield with relatively simple purification by column chromatography.[124]

Perylene bisimides have also been the subject of C-H borylations, for instance the tetraborylation of an N,N'-*bis*(1-hexylheptyl) substituted perylene bisimide to form **87**, obtained in an 78% yield after column chromatography and a subsequent

recrystallisation. Notably this reaction used **61-b** in conjunction with a *tris*(pentafluorophenyl)phosphine ligand.[125] Figure 27 also depicts the C-H borylation of corannulene by Scott *et al*[126] to furnish the 1,3,5,7,9- pentasubstituted derivative **88**. This is of some interest, as under standard conditions (*i.e.* those of Perutz *et al*[115] depicted in figure 24) this compound is produced as a minor product in competition with two tetrasubstituted isomers, as borylation can sterically block further substitution at the *peri*-position of the adjacent ring, preventing the pentasubstituted derivatives formation. When the reaction is run under altered conditions however, with excess B_2pin_2; high catalyst loadings of **61-b** (20 mol%); a 4,4'-dimethylbipyridyl ligand; a catalytic amount of base (10 mol% potassium *t*-butoxide or sodium methoxide); in a concentrated THF solvent system at 85 °C in a pressure vessel for long periods of time (4 days); the reaction can be driven essentially completely to the pentasubstituted derivative. Monitoring the reaction, it is observed that the undesired tetrasubstituted isomers are formed, but then slowly disappear over the course of the reaction in preference to the pentasubstituted derivative. This suggests a kinetic deborylation pathway allowing a redistribution of products favouring the "saturated" pentasubstituted derivative *via* a deborylation/reborylation process.[126] It is noteworthy however that Marder *et al*[127] question the scope of this reversible borylation process and found that pyrene substrates did not undergo a reversible borylation under these conditions, pointing out that Scott *et al* failed to identify an alternative tetraborylated pyrene isomer in the crude product in their investigaitons.[127]

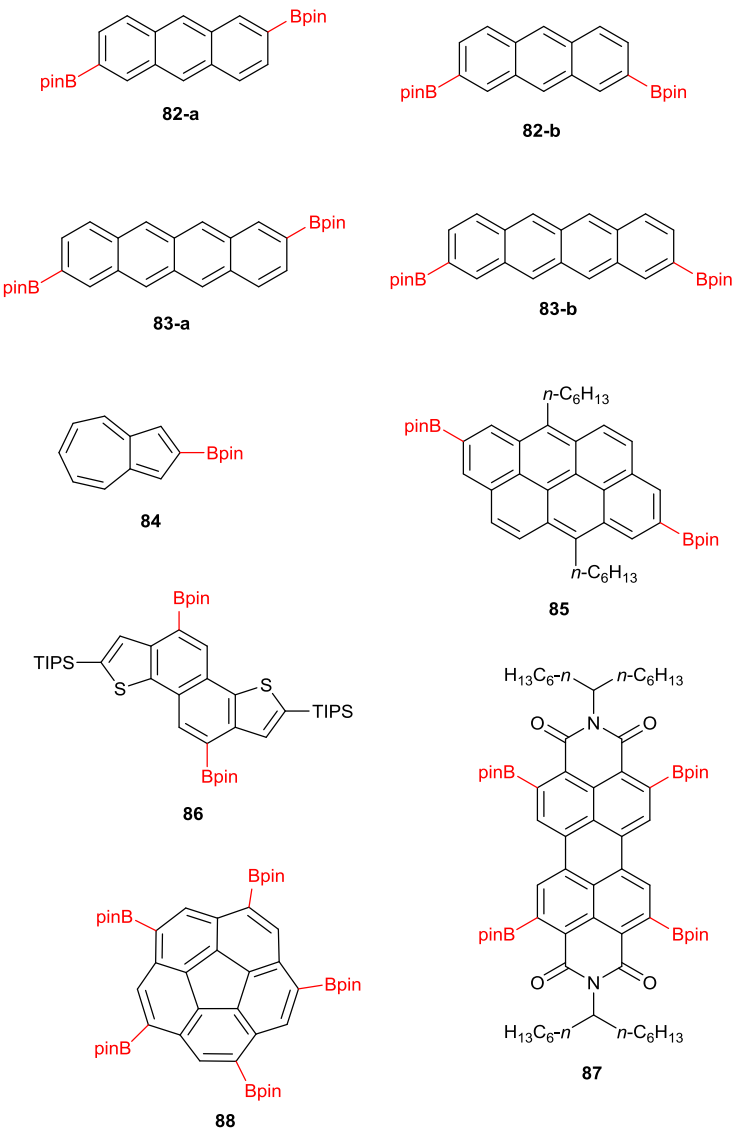

Figure 27 – Additional notable examples of the iridium-catalysed borylation of PAH systems. Borylated previously C-H sites indicated in red

References: **82**,[120] **83**,[121] **84**,[122] **85**,[123] **86**,[124] **87**,[125] **88**[126]

1.2-3.1 Iridium-Catalysed Aromatic C-H Borylation of Phenacenes

Our group became interested in iridium-catalysed aromatic C-H borylations due to the work of Isobe *et al*[123, 128] and their report concerning the direct borylation of PAH phenacenes chrysene (**25**), pheneathrene (**92**) and picene (**107**) (figure 28).

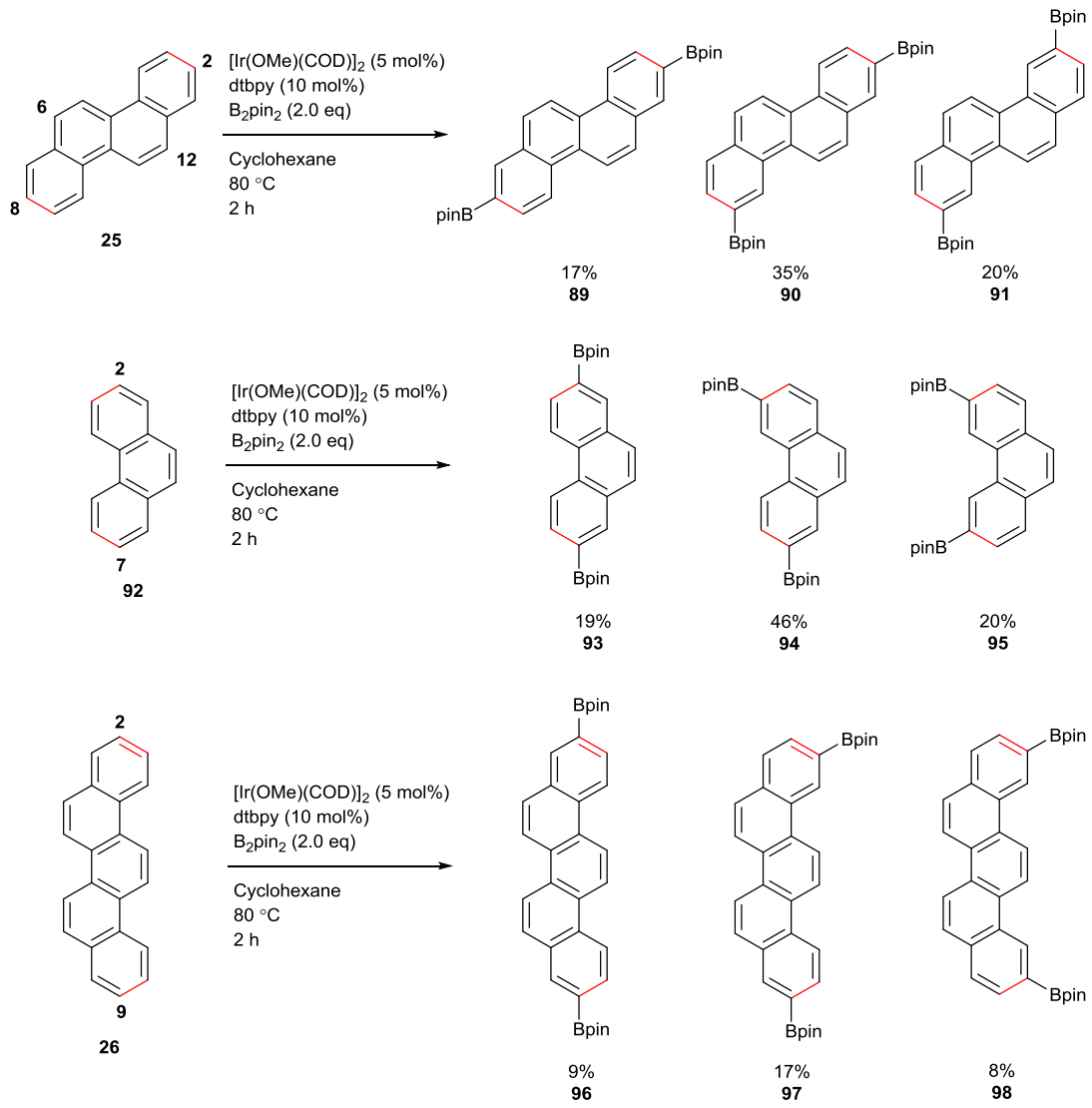

Figure 28 – Iridium-catalysed borylation of phenacenes: chrysene (**25**), phenanthrene (**92**) and picene (**26**). "Edge positons" indicated in red[128]

As would be expected phenacenes **25**, **92** and **26** were functionalised *meta*- to ring junctions first, resulting in isomers borylated at the sterically similar edge positions (indicated in red in figure 28). It is noteworthy however that when chrysene was reacted with 10 equivalents of B_2pin_2 additional functionalisation was observed at the 6,12-positons, presumably as these were the next least sterically hindered sites after the edge positons had been diborylated. The borylations of **25**, **92** and **26** depicted in figure 28 resulted in difficult to separate isomeric mixtures of diborylated compounds that were ultimately separated by preparative high performance liquid chromatography (HPLC) as the edge positions were sterically so similar that there was little selectivity as to which site was borylated.[128] The subsequent application of

this borylation process to the substituted pheneacene 4,10-dichlorochrysene (**32**, figure 13) (and the effect of this 4,10-dichloro substitution on regioselectively) is the subject of section 2.1-1.1.

1.3 Graphene and its Production

Graphene is reported to be the thinnest and strongest known material; it is highly conductive, ductile and impermeable to gases.[129] It consists of a honeycomb lattice of carbon atoms in single 2D sheet and its mechanical thermal and electrical properties have been the subject of enormous interest in the last decade.[130]

When monolayer graphene was reported in 2004 it was produced *via* mechanical exfoliation, with repeated pealing of graphite flakes using scotch tape.[131] The number of layers the exfoliated flakes consisted of could then be determined though elastic and inelastic light scattering along with Raman spectroscopy which can also be used to quickly analyse defects that may be present in the graphene sample. This makes it an excellent method to produce small quantities of high quality graphene. For many years graphene produced by this method has been the favourite among those wishing to analyse its intrinsic properties and build prototype devices.[132]

1.3-1 "Bottom Up" Production of Graphene

While micromechanical cleavage can produce micrometre sized flakes for laboratory testing, the large scale production of graphene would require a more scalable method. One answer to this problem is chemical vapour deposition (CVD) in which vapour phase carbon is precipitated onto a nickel or copper surface which is then removed with an etchant.[133] Using CVD predominantly monolayer graphene sheets have been produced up to 30 inches in size (measured diagonally).[134] However such CVD films are usually polycrystalline, with single-crystalline grains growing from uncontrolled locations and coalescing into a polycrystalline film.[135] While CVD at first appears suitable for the large scale production of graphene it features some intrinsic disadvantages, including the intricate setup required and the high costs associated with the temperatures (~ 1000 °C)[133, 134, 135] and pressures (depending on method) which must be maintained. Furthermore, the transfer of the produced graphene sheets between substrates is a significant problem in this process.[136] Alternatively the growth of graphene sheets on the surface of silicon carbide (SiC) is an additional method considered for large scale high quality production. Graphene sheets can be grown on the SiC surface as it thermally decomposes at high

temperatures (> 1000 °C). The great advantage of this technique is that SiC is an insulator, so that the produced graphene does not need to be transferred to an insulating substrate before it can be used in electronic applications. As with CVD however, the growth of uniform single layer graphene over large length scales is limited. Morphological changes in the SiC surface as it is heated result in small-grain structure and the decomposition of SiC is not self-limiting, resulting in the formation of areas of multilayer graphene.[137]

An alternative "bottom up" strategy that has been explored in the production of graphene is the organic synthesis of large fused aromatic systems. These come in the form of molecular nanographenes[138] such as graphene quantum dots[139] and graphene nanoribbons (of particular interest as the geometric confinement of graphene to <10 nm wide strips produces a non-zero E_g semiconductor).[140] The advantage of the organic synthesis of these graphenes includes their defined chemical structure; their processability and the scalability this approach offers. The synthesis of nanographenes often begins with dendritic polyphenylenes (e.g **99**, figure 29, a) which can then undergo oxidative cyclodehydrogenation and planarization when reacted with $FeCl_3$ to form the desired nanographene structures.[138] One of the simplest examples this being the synthesis of hexabenzocoronene (**100**, figure 29, a). Importantly however, such cyclodehydrogenation reactions can also be applied to much larger dendritic structures enabling the synthesis of a variety of graphene topologies such as graphene quantum dots (e.g. **101**, figure 29, b) and graphene nanoribbons (e.g **102**, figure 29, c). As early as 2002 Müllen *et al* reported the synthesis of a 222 "carbon graphite sheet" using this cyclodehydrogenation method.[141]

However the "bottom up" synthesis of such graphenes is not without challenges. Firstly as these graphene structures become increasingly large, they become increasingly difficult to solubilise, particularly when forming nanographenes tending towards graphene sheets. Even with solubilising side chains, as the graphene core becomes ever larger aggregation becomes increasingly difficult to prevent by simply placing solubilising chains at the perimeter of the sheet, requiring more specialised solubilising techniques such as a 3D "cage" as used in the synthesis of **101**.[139] Secondly, reactions and cyclodehydrogenations in solution on increasingly large

substrates is problematic, leading to only partial cyclodehydrogenation or unexpected reactivity which can disrupt regioselectively. Thirdly, one of the key advantages of this bottom-up synthetic approach is the precision with which such molecules can be made, however as these graphene structures become increasingly large, so to their precise characterisation becomes ever more difficult.[142] For instance, in the synthesis of the graphene nanoribbon **102**, despite its solution processability, its structural characterisation was significantly limited and while a model trimer of the nanoribbon could be characterised by high resolution matrix assisted laser desorption/ionisation-time-of-flight (MALDI-TOF) mass spectrometry, liquid state ^{1}H NMR data of the trimer could not be obtained even at 170 °C in 1,2-dichlorobenzene-d_4.[143]

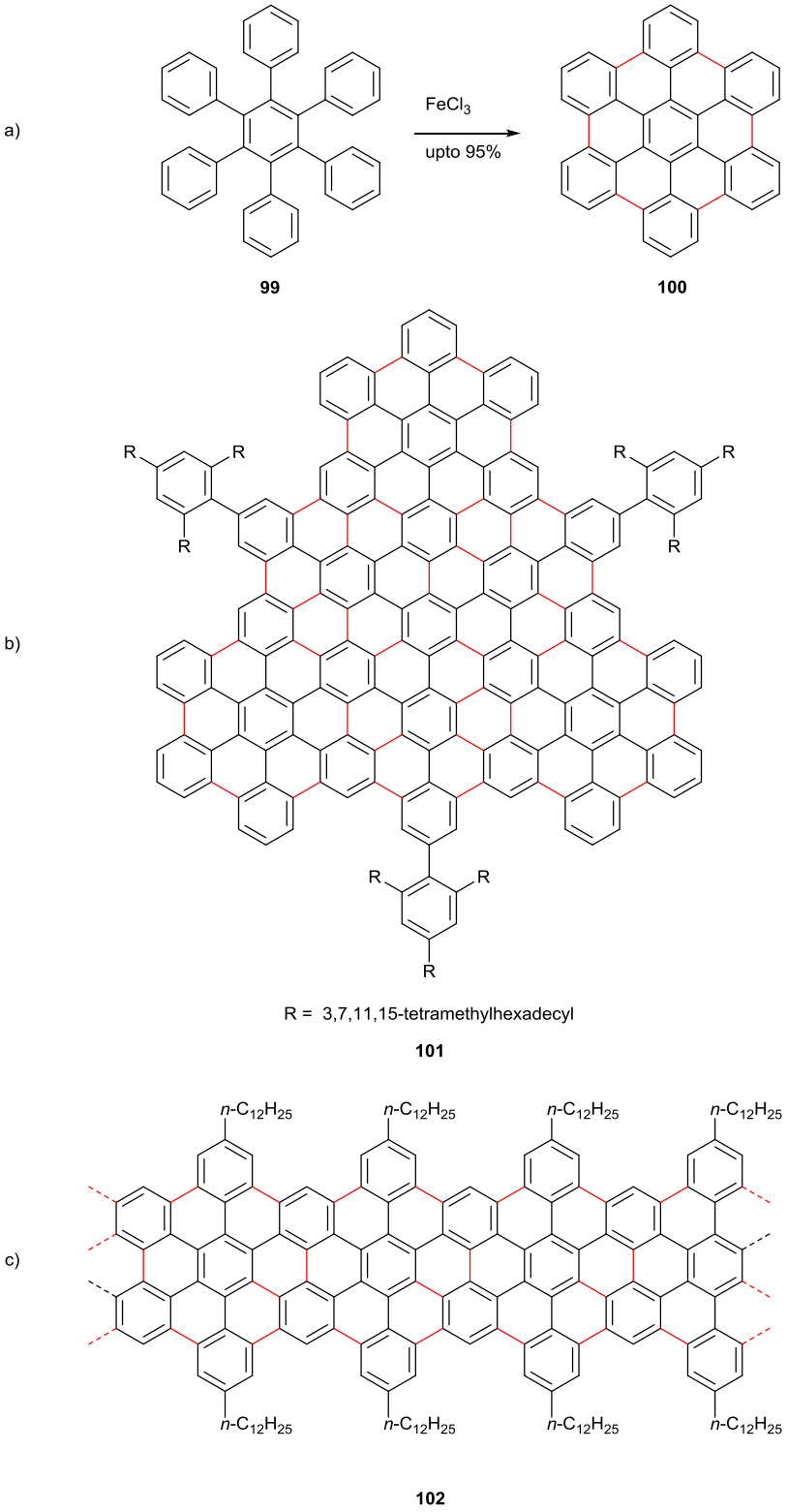

Figure 29 – Examples of molecular graphenes synthesised *via* cyclodehydrogenation. a) Synthesis of hexabenzocoronene[138] b) synthesised graphene quantum dot[139] c) synthesised solution processable graphene nanoribbon.[143]
(bonds formed during cyclodehydrogenation are indicated in red)

1.3-2 Liquid Phase Exfoliation of Graphene – A "Top Down" Production Method

Alternative to the "bottom up" formation of graphene using methods such as organic synthesis or CVD is the "top down" production method, taking graphite (composed of stacked graphene sheets) and exfoliating it to graphene. One stand out method in the "top down" production of graphene from graphite is liquid phase exfoliation. It has been shown to be both scalable and versatile with extensive potential applications in polymer composites, conductive thin films, aerogels, inkjet printing[144] and solar cells (in which graphene can behave as an electron acceptor material).[145] Graphene can be exfoliated from graphite in solution though sonication, which results in cavitation and shear forces that break the graphite apart into single and few layers. This is generally performed in relatively low surface tension ($\gamma \sim 40$ mJ m^{-2}) solvents such as DMF, NMP and dichlorobenzene. However, these solvents are toxic irritants with very high boiling points which makes them less than ideal for large scale exfoliation. A cheaper and non-toxic alternative is water, in which an amphiphilic stabiliser is added to enable the dispersion of the hydrophobic graphene in aqueous media.[130] Other "top down" methods in the production of graphene include anodic bonding (applying a voltage across a Pyrex/graphite interface causing few and single layer graphene to stick to the Pyrex surface when the bulk graphite is cleaved off)[146] and photoexfoliation (generation of few and single layer graphene from the laser ablation/exfoliation of multi-layered graphene samples).[147] This thesis however focuses on the exfoliation and stabilisation of graphene in aqueous media though the use of aromatic amphiphilic stabilisers, thus the remainder of this review will be limited to this process, which has shown itself to be cheap, scalable and non-toxic.[148]

Graphene can be stabilised in aqueous solution by surfactants, polymers and aromatic stabilisers. The latter operate though non-covalent π-π interactions with the graphene surface and this surface absorption prevents the re-aggregation of the dispersed graphene in solution and reduces the surface free energy of the dispersed graphene though π-π interactions[144] as illustrated in figure 30.

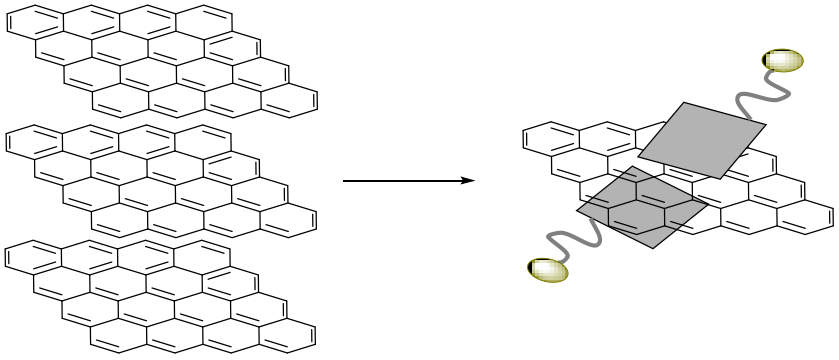

Figure 30 – Illustration of dispersion of graphene by a stabiliser in aqueous media[148]

The π-π stacking mechanism exploited by aromatic stabilisers is favourable as it does not disrupt the sp^2 network of the graphene, retaining its intrinsic quality. When dealing with aqueous dispersions it is important that such stabiliser molecules are amphiphilic *i.e.* possess a non-polar aromatic group (similar in structure to graphene itself enabling strong non-covalent π-π interactions) and a polar hydrophilic group. Upon sonication to break up the graphite, exposed graphene layers become non-covalently functionalised by these aromatic groups with dangling hydrophilic groups, allowing single and few layer graphene to be dispersed in water. Performing this process in water can also enable graphene stabiliser interactions, as the hydrophobic interactions of the aromatic segment of the stabiliser provide a driving force to engage in π-π interactions with the graphene surface in order to minimize interactions with the extremely polar aqueous solvent.[149]

1.3-2.1 Pyrene-Based Amphiphilic Graphene Stabilisers

Amphiphilic pyrenes have played a key role in the dispersion chemistry of both carbon nanotubes and graphene in recent years. Pyrene-based probes were used to non-covalently functionalise carbon nanotubes as early as 2001[150] and amphiphilic pyrenes were used to disperse them in aqueous solution in 2002,[151] while 1-pyrenecarboxylic acid (**105**, figure 31) has been used to disperse both carbon nanotubes[152] and graphene[149] in aqueous solution. It is noteworthy that a lot of the dispersion chemistry of graphene is analogous to that initially developed for carbon nanotubes (which are conceptually rolled up graphene sheets).[131] However it is also important to note key differences in nanotube *vs* graphene dispersions as one features a 1D curved surface, the other a 2D flat surface. Carbon nanotubes for instance can

be stabilised by micelle formation preventing re-aggregation[153] a principle that is reported to be less applicable to graphene dispersions.[148]

Green *et al*[144] systematically investigated amphiphilic pyrene derivatives and their ability to exfoliate graphite to graphene in aqueous solution at optimum concentrations. The key pyrene derivatives investigated in this study alongside other literature examples are shown in figure 31.

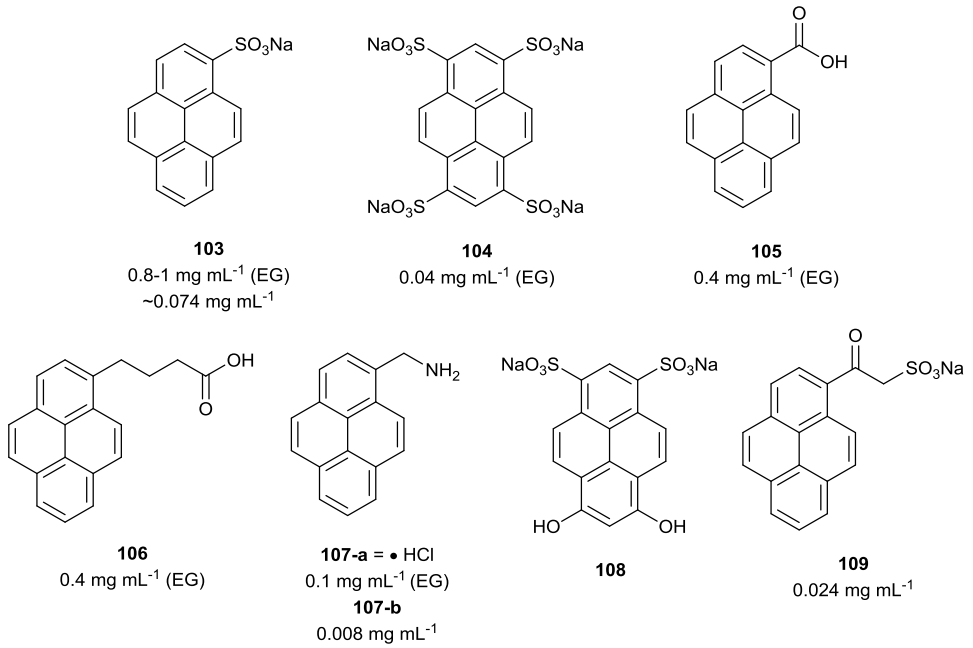

Figure 31 - Key pyrene derivatives used as stabilisers and where applicable, the reported graphene concentrations produced. EG denotes the use of expanded graphite in the production of the dispersion

References: **103**,[144, 154, 155] **104**, **105**, **106**, **107-a**,[144] **104**, **108**,[154] **107-b**, **109**[156]

Of the derivatives studied by Green *et al*[144] it was found that at optimum concentration sodium pyrene-1-sulfonate (**103**) produced the highest graphene concentrations of 0.8-1 mg mL^{-1} after sonication in aqueous media, using expanded graphite (EG) and centrifuging at 5000 rpm. This can be compared to its tetrasubstituted analogue **104** in order to understand the differences additional sulfonic acid functionalities make. Under the same conditions and at optimum concentration **104** produces graphene concentrations of just 0.04 mg mL^{-1}. It is suggested that the symmetrical arrangement of functional groups may sterically

hinder the adsorption of the aromatic pyrene functionality onto the graphene surface and the tetrafunctionalisation of the molecule may also increase the localised concentration of SO_3Na groups, reducing the favourability of complete dissociation in aqueous solution at higher concentrations.[144]

1-Pyrenecarboxylic acid (**105**) could also be compared and contrasted with 1-pyrenebutryic acid (**106**) to provide insight into the effects of alkyl spacers between the amphiphilic functionalities. Both **105** and **106** feature the same hydrophilic carboxylic acid functionality, but in **106** it is separated by a *n*-C_3H_6 carbon chain. Although both produced similar optimum graphene concentrations (0.4 mg mL^{-1}), it was found that **106** performed better at higher concentrations than **105**. A plausible explanation for this is that as **105** adsorbs onto the surface of the graphene, charge from the dissociated carboxylic acid functionality hinders the attachment of additional stabilisers as they must be spaced out across the graphene surface to avoid the build-up of localised charge. Conversely, in **106** that charge is separated from the pyrene, thus avoiding the excessive build-up of charge on the surface of the graphene and allowing greater density in the packing of the pyrene groups. It is suggested that **104** would be an excellent candidate for this style of charge separation as it seems to perform particularly poorly at higher concentrations, likely due to the build-up of charge at the graphene surface.[144]

The study by Green *et al* also allows the comparison of hydrophilic groups attached to the pyrene core and the relative concentration of the graphene dispersions produced. It was found that at low stabiliser concentrations **103** (and its corresponding sulfonic acid hydrate) were the most effective, followed by the carboxylic acid derivatives **105** and **106** while the amine derivatives (such as pyrenemethylamine hydrochloride **107-a**) performed the worst (at optimum concentration **107-a** produced a graphene concentration of just 0.1 mg mL^{-1}). They correlate this performance with the relative electronegativity of those groups, with the sulfonic acid groups being the most electron withdrawing and therefore enabling a stronger charger-transfer π-π interaction from the relatively electron deficient pyrene core to the more electron rich graphene.[144] It should be noted however that this assessment makes no comment on the insulating *n*-C_3H_6 and CH_2 chains of **106** and **107-a** whilst including them in the described trend and it is likely the

effectiveness of different hydrophilic groups will also be affected by additional, more complex solvent interactions than simply electronegativity.

Green *et al* also compare **103** with its corresponding sulfonic acid hydrate to gain insight into counter ion effect. It was found that the sulfonic acid sodium salt forms more stable dispersions than the sulfonic acid hydrate. It is hypothesised that the sodium counterion, being larger and having greater ionic strength than the proton counter ion aids in the stabilisation of the negatively charged graphene sheets by forming a protective layer of counterions at a distance around the sheets providing electrostatic stabilisation forces and helping to prevent re-aggregation.[144]

Palermo *et al*[154] also studied the behaviour of pyrene derivatives in the exfoliation of graphene from graphite powder, looking at **103**, **104** and additionally **108** (figure 31). Similarly to the study by Green *et al*[144] it was found in their exfoliation studies that **104** exfoliated the lowest concentration of graphene, while **108** outperformed **103**. These observations were made on the basis of relative UV-vis absorption spectra after sonication with no concentrations of suspended graphene calculated. The authors inferred a correlation between the quantity of material solubilized and the graphene adsorption energy of the stabiliser (as predicted computationally from molecular dynamic simulations) but there also appears to be a relationship between the amount of material solubilised and the dipole moment of the molecule predicted by DFT calculations. Potential of mean force (PMF) curves calculated though molecular dynamic simulations of the stabiliser approaching the graphene surface indicate that **103** and **108** have a single global minimum in free energy (face-face stacking on the graphene surface). **104** meanwhile shows additional minima (kinetic traps) on approaching the graphene surface, in particular as the molecule tilts from an initial edge-on interaction to a fully adsorbed face-face interaction. It was shown that **108** approaches the graphene surface OH first (SO_3^- groups pointing away from the surface into solution) before "sliding" into a face-face interaction. The authors propose that the presence of an asymmetric polarity across the molecule facilitates the adsorption of the pyrene onto the surface of the graphene by enabling this "sliding" effect, allowing the molecule to more easily displace the final layer of water molecules between the graphene and the stabiliser.[154] These results suggest **104** performs so poorly as not only do the bulky SO_3^- groups disrupt π-π stacking

due to adverse steric interactions (as suggested by Green *et al*)[144] but because its symmetrical substitution means it has no significant dipole to facilitate a "sliding" effect on its final approach into a face-face interaction on the graphene surface.[154] In addition to these results, when the contributions of the different functionalities (SO_3^-, OH, pyrene) to the graphene adsorption energy were analysed it was found that the presence of OH groups in **108** decreases its interaction with the solvent while the presence of additional SO_3^- groups in **104** increases its interaction with the aqueous solvent. It is suggested that **104** is essentially too water soluble, reducing the favourability of its interaction with graphene.[154]

In an additional study by Lukkari *et al*[156] the performance of pyrene-based stabilisers **107-b** and **109** (figure 31) was also explored. This study investigated the exfoliation of natural graphite though a sheer-assisted exfoliation technique in which natural graphite and the stabiliser molecules were mechanically ground together with a small amount of water before sonication in aqueous media, with centrifugation at 3000 rpm, followed by dialysis to remove excess stabiliser. This technique produces relatively low dispersed graphene concentrations of 0.024 and 0.008 mg mL^{-1} for **109** and **107-b** respectively (based on their absorption at 660 nm in UV-vis analysis). Detailed spectroscopic analysis revealed that these pyrene derivatives are generally aggregated in aqueous solution even down to submicromolar concentrations, suggesting graphene sheets are in fact solubilised by partially aggregated stabilisers. In any case, the most aggregated derivatives (such as **109**) produce some of the highest concentration dispersions, although they appear to be more multilayered than graphene flakes produced with less aggregated derivatives (such as **107-b**).[156]

While those graphene dispersion concentrations reported by Lukkari *et al*[156] are low, it should be noted that the concentration of the final graphene dispersion produced is highly dependent on the process by which the exfoliation process was conducted. For example the study by Green *et al*[144] reports very high graphene concentrations (0.8-1 mg mL^{-1}) with stabiliser **103** through the use of expanded graphite with no post-exfoliation "washing" procedures to remove excess stabiliser.[144] In contrast a study by Casiraghi *et al*[155] reported far lower graphene concentrations of ~0.074 mg mL^{-1} when using **103**. This is because the sonication was conducted in low

concentrations, with natural graphite, while using extensive "washing" procedures to remove the excess stabiliser from the solution.[155]

1.3-2.2 Electron Deficient Amphiphilic Graphene Stabilisers

Graphene stabilisers need not necessarily be pyrene-based, with many examples in the literature of stabilisers based around other aromatic motifs, for instance the electron deficient examples depicted in figure 32.

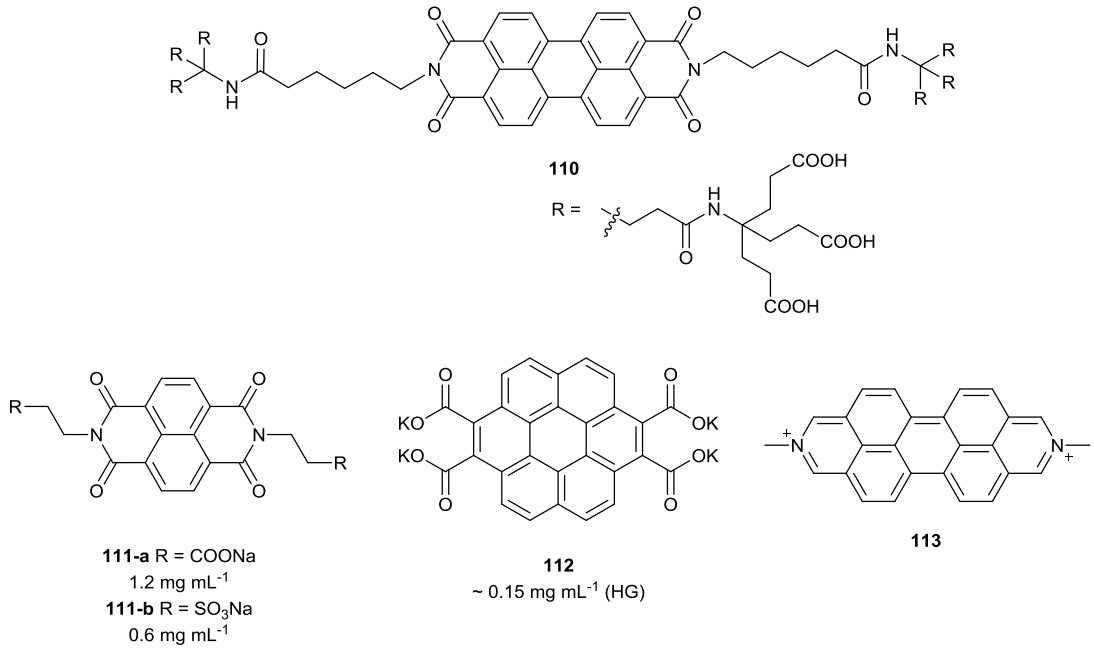

Figure 32 – Electron deficient stabilisers and where applicable, the reported graphene concentrations produced. HG denotes the use of graphene prepared by the arc evaporation of graphite in a hydrogen atmosphere in the production of the dispersion

References: **110**,[157] **111**,[148] **112**,[158] **113**[159]

Stabilisers incorporating electron withdrawing groups (such as those in figure 32) have proven popular in the literature. Electron deficient polyaromatics generally feature superior π-π interactions with graphene as they can engage in charge-transfer interactions. Such interactions were exploited by Hirsch *et al*[157] in the perylene bisimide-based dendrimeric graphene stabiliser **110**,[157] which was synthesized from the perylene dianhydride initially with *tert*-butyl protected carboxylic acids which could be removed post-purification with formic acid.[160] The stabiliser was sonicated

with graphite powder in buffered pH 7 water solutions and the presence of single layer and few layer graphene was confirmed by Raman spectroscopy and atomic force microscopy (AFM) analysis, although exact graphene concentrations were not investigated.[157]

Similar naphthalene bisimide-based graphene stabilisers (**111**) were investigated by Wang *et al*[148]. With stabilisers **111-a** and **111-b** graphene concentrations as high as 1.2 and 0.6 mg mL^{-1} respectively were produced by sonicating with graphite powder, followed by centrifugation at 5000 rpm. The highest concentration (1.2 mg mL^{-1}) was produced by the carboxylic acid sodium salt derivative **111-a** with the authors suggesting this is due to the lower solubility of the sulfonic acid salt derivative in water. Important in the molecular design of these stabilisers are the alkyl spacers separating the aromatic core from the sulfonic acid and carboxylic acid sodium salt functionalities. This design was important as it allowed the two functionalities of the molecule to behave independently, allowing the best interactions with both the solvent and the graphene surface to enable the effective dispersion of graphene. It is also proposed the high adsorption free energy calculated for compounds **111** is also aided by reduced steric interaction of the graphene with the bulky hydrophilic functionalities which are removed from the graphene surface *via* the alkyl spacers.[148]

Another example of an electron deficient stabiliser designed to interact with graphene though charge-transfer interactions is coroene tetracarboxylic acid (**112**). In this study, graphene samples were prepared by the arc evaporation of graphite in a hydrogen atmosphere (HG) and the thermal exfoliation of graphite oxide. These few layer graphene samples were then dispersed in aqueous media, heating in the presence of the stabiliser before additional sonication and centrifugation. The stabiliser was most effective in solubilising HG producing graphene concentrations of ~0.15 mg mL^{-1}. Notably in this particular example Raman spectroscopy confirmed the charge-transfer interactions occurring between the electron rich graphene and electron deficient coroene stabiliser.[158]

Stoddart *et al*[159] investigated diazaperopyrene-based stabiliser **113** which was found to exfoliate graphite powder to graphene (although the concentrations of the exfoliated graphene produced were not investigated). In this instance π-π charge-

transfer interactions of the stabiliser with the graphene surface were evidenced by the 90% quenching of the fluorescence of the stabiliser in the presence of graphene. Interestingly when **113** was contrasted with a diazapyrene-based stabiliser (the latter having 58% less aromatic surface) the diazapyrene stabiliser was found to be unable to exfoliate graphite to graphene, highlighting the importance of sufficient aromatic surface area in the effective stabilisation of graphene when using these types of aromatic stabilisers.[159]

1.3-2.3 Macromolecular Amphiphilic Graphene Stabilisers

While many graphene stabilisers are based on the motifs discussed above, having a large aromatic area is important to ensure sufficient π-π stacking occurs to enable a strong graphene-stabiliser interaction. Two particularly large aromatic area graphene stabilisers are shown in figure 33.

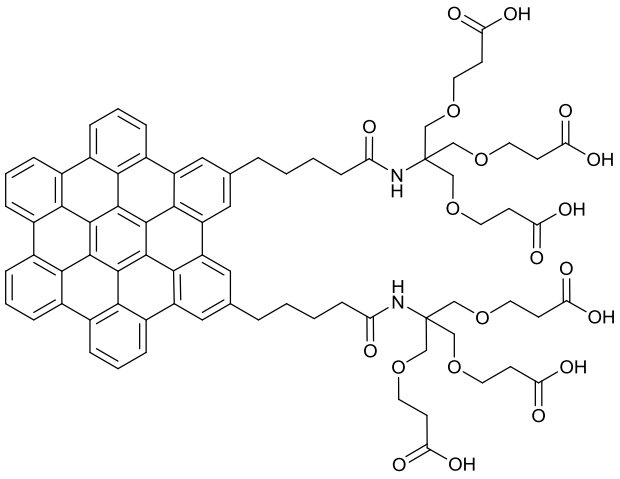

114
1.1 mg mL^{-1} (Methanol)

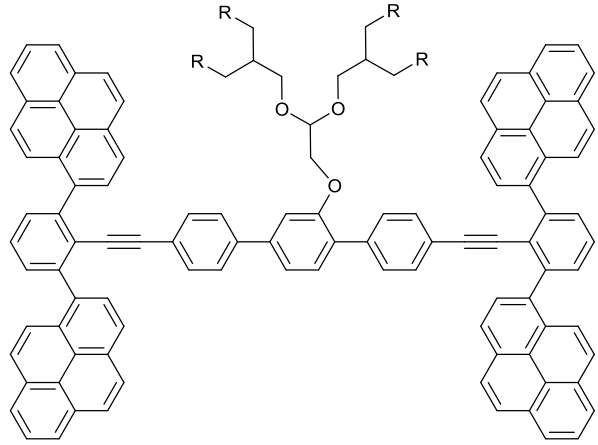

115
R = Hexaethylene glycol monomethyl ether
1.5 mg mL^{-1}

Figure 33 – Macromolecular aromatic stabilisers and the reported graphene concentrations produced. NB: Graphene exfoliation with **114** conducted in methanol
References: **114**,[161] **115**[162]

Studies based on larger PAH cores include hexabenzocoronene-based stabiliser **114**.[161] This example is of particular note as not only does it feature a large aromatic core, but it is also asymmetrically functionalised with hydrophilic functionalities separated from the core by alkyl chains. Graphene dispersions with concentrations as high as 1.1 mg mL^{-1} were achieved in methanol by sonication of the stabiliser with graphite powder, followed by centrifugation at 1000 rpm. This resulted in a suspension of multilayer (2-6) graphene sheets with a monolayer of stabiliser on each side. It is important to note however that this large aromatic core demonstrated

a propensity to stack with itself in the absence of graphene, as when a methanolic solution of **114** was spin coated onto SiO_2 and annealed, AFM images of distinct nanofibers were observed, in which the material had self-assembled into columnar stacks with the hydrophilic groups exposed on the outside. Such strong π-π interactions with itself might suggest an upper limit to the desired size of the stabiliser aromatic core as such competing interactions may be unfavourable in graphene exfoliation processes.

It is interesting to note that when utilising **114**, the highest concentration graphene dispersions were produced in methanol not water.[161] This is rather unusual as the study by Green *et al*[144] discussed above found that the presence of ethanol can lead to the desorption of the stabiliser from the graphene surface. It was found that graphene dispersions were severely destabilised in methanol, ethanol and acetone solvent systems with complete aggregation of graphene sheets above 60 vol% ethanol in water after centrifugation. Green *et al* propose the addition of ethanol, methanol and acetone lower the surface energy and polarity of the solvent, disrupting the driving force for adsorption of the stabiliser onto the graphene surface as the interactions between the aromatic core of the stabiliser and the aqueous solvent become less unfavourable compared to pure water.[144]

An alternative graphene stabiliser design is **115** depicted in figure 33. **115** features four pyrene "feet" grafted to central polyethylene glycol (PEG) based hydrophilic dendrimer, on the principal that the pyrene components will π-π stack on the graphene surface while the large hydrophilic component is directed away from the surface into solution. This stabiliser was able to produce graphene dispersions with concentrations as high as 1.5 mg mL^{-1} after sonicating graphite powder in a 7:3 water:methanol solvent system followed by centrifugation at 1300 rpm. Interestingly while many graphene stabilisers are borrowed from techniques used to disperse carbon nanotubes, this example does not disperse carbon nanotubes under the same conditions used to disperse graphene. This is due to this stabilisers flat aromatic "feet" segments with which it is readily able to π-π stack on the 2D graphene surface but cannot stack effectively with the curved surface of carbon nanotubes.[162]

1.3-2.4 Favourable Non π-π Interactions with Graphene

Each of the graphene stabiliser examples discussed previously in this section rely on aromatic π-π stacking interactions with graphene to enable its effective dispersion. Aside from surfactants which rely on simple hydrophobic interactions, there are limited examples of stabilisers which can produce graphene dispersions though non π-π interactions. Most remarkably, graphene has been successfully exfoliated with urea (**116**, figure 34) producing a dispersion with a graphene concentration as high as 0.15 mg mL^{-1} after sonication with graphite powder followed by centrifugation at 3000 rpm. The authors of this study propose an attractive interaction between the graphene surface and the NH_2 functionality (as investigated computationally) while the other NH_2 moiety may react with dissolved CO_2 in solution forming a carbamic acid functionality which can ionise and negatively charge the graphene surface, enabling an electrostatically stabilised dispersion. This mechanism is evidenced by additional experiments which measure increases in conductivity in CO_2 fed solutions of urea due to the formation of an ionisable group. The authors propose that a primary amine, which can form an ionisable group *in situ* in this manner, may be useful in future strategies in the liquid phase exfoliation of graphene.[163] This proposal must be tempered however by the observation that pyrene-based stabilisers featuring primary amine groups generally underperform compared to more readily ionisable groups, as observed both by Green *et al*[144] who investigated **107-a** and Lukkari *et al*[156] who investigated **107-b** (figure 31).

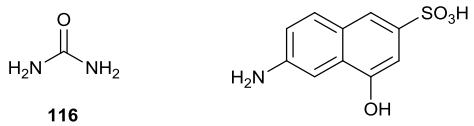

116
0.15 mg mL^{-1}

117
0.020 mg mL^{-1}

Figure 34 – Non π-π stacking stabilisers and the reported graphene concentrations produced
References: **116**,[163] **117**[156]

Another non π-π stacking stabiliser was naphthalene derivative **117** (figure 34) investigated by Lukkari *et al*.[156] Compared to other derivatives investigated in this manner (**107-b** and **109**, figure 31) the effectiveness of **117** in this study was unexpected, resulting in a graphene concentration of 0.020 mg mL^{-1}. It's aromatic

system is generally too small to engage in significant π-π interactions but its luminescence behaviour suggested partial electron donation from graphene to the hydroxyl group, allowing it to interact with graphene in a presumably edge-on manner though a graphene-OH interaction. This edge-on interaction may be additionally favourable as it would partially eliminate the need to laterally displace the final layer of water molecules on the graphene surface,[156] a process described by Palermo *et al*[154] when computationally investigating the behaviour of pyrene derivative **108** (figure 31). Interestingly, while Palermo *et al* suggests the presence of a dipole across **108** enables this "sliding" effect, the results of Lukkari *et al* may also suggest a graphene-OH interaction as a precursor to the "sliding" that was computationally observed.

1.3-3 Summary of Desirable Properties of Amphiphilic Graphene Stabilisers

Given the literature reviewed above, the potential desirable properties of aromatic stabilisers for use in the generation of aqueous graphene dispersions can be summarised as follows:

1. The stabiliser should be amphiphilic, possessing a non-polar aromatic group to enable π-π interactions and a polar hydrophilic group.[149] It is important that the aromatic group is large enough to engage in strong π-π interactions with graphene surface,[159] although not so large that it may engage excessive self-aggregation.[161]
2. When using charged hydrophilic functionalities, counter ions may well be important in the formation of stable dispersions, in particular the sulfonic acid sodium salt is superior to the sulfonic acid hydrate.[144]
3. Ideally the stabiliser should be asymmetrically functionalised with the hydrophilic functionality on one side of the molecule[161] and should possess a dipole moment across the molecule to enable the "sliding" of the molecule into a face-face interaction displacing the final layer of water molecules between the graphene surface and the stabiliser.[154]
4. Hydrophilic groups should be isolated away from the aromatic core, possibly by alkyl spacers, in order to allow the amphiphilic functionalities to behave independently from one another, reduce steric hindrance to adsorption onto

the graphene surface and reduce the localised concentration of charged groups.[144, 148, 161]

5. An electron deficient aromatic group may enable stronger charge-transfer π-π interactions with graphene.[148, 157, 158]

1.3-4 Aims and Objectives 2 – Synthesis and Evaluation of Pyrene- and Perylene-Based Amphiphilic Graphene Stabilisers

In this project pyrene and perylene cores were functionalised to behave as amphiphilic graphene stabilisers. The pyrene and perylene cores could be first functionalised though electrophilic aromatic substitution at the 1- and 3-positions respectively, before applying a sterically directed aromatic C-H borylation to access the 7-position in pyrene and the 5,8,11-positions in perylene to add additional functionality.

In summary the project had the following aims:

1. Synthesise pyrene- and perylene-based amphiphilic graphene stabilisers, substituted with hydrophilic SO_3Na groups separated from the aromatic core by a range of alkyl spacers of differing lengths.
2. Explore the use of a sterically directed regioselective aromatic C-H borylation to install electron withdrawing nitrile functionalities and/or OH functionalities at additional positons in the synthesised stabilisers (as in figure 35).
3. Begin to investigate the relative effectiveness of these stabilisers when sonicated in aqueous solution with graphitic material, analysing the quantity and quality of dispersed graphene produced.

Additional aims that were to be achieved though collaboration were:

4. Computationally analyse the performance of the stabilisers synthesised to enable further investigation of their intrinsic properties and enable the identification of trends to inform future synthesis.

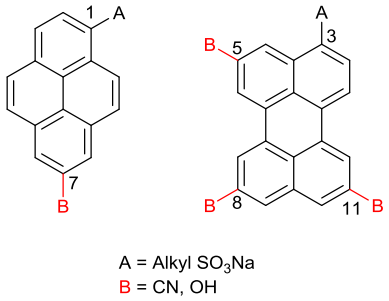

Figure 35 – Proposed substitution of pyrene and perylene cores. Substitution at positions accessed *via* C-H borylation shown in red

2 Results and Discussion

Section 2.1 covers the synthesis of "A_2B_2" tetrasubstituted chrysene derivatives, accessed *via* an iridium-catalysed aromatic C-H borylation, for potential applications in organic electronics. In addition to the synthesis that was undertaken, the determined properties of these compounds will also be discussed, including analysis by UV-vis absorption/fluorescence spectroscopy, cyclic voltammetry (CV) and X-ray crystallography. Computational studies of these derivatives (as provided by collaborators) will also be briefly described. This work was the focus of a publication in chemical communications.[2]

Section 2.2 covers the synthesis and analysis of pyrene and perylene derivatives for use as amphiphilic graphene stabilisers. The synthesis of the initial target stabilisers is described along with the additional functionalisation that was achieved *via* the application of the previously explored iridium-catalysed aromatic C-H borylation to these substituted cores. In addition, computational analysis of the interactions of these stabilisers with the graphene surface in aqueous solution (as investigated by collaborators) and the initial application of the simplest synthesised stabiliser to the generation of aqueous graphene dispersions are also briefly described.

2.1 Synthesis and Properties of "A_2B_2" Tetrasubstituted Chrysene Derivatives

2.1-1 Synthesis of "A_2B_2" Tetrasubstituted Chrysene Derivatives

As identified in section 1.1-6, chrysene is a versatile PAH core, derivatives of which have significant potential for applications in organic electronics, both as a p-type materials[80, 81, 82, 83] and as emissive materials for OLED applications.[94, 96, 97] In addition the core chrysene unit can be expected to maintain an inherent stability due to its phene-type angular ring fusion leading to an increased number of Clar sextets[87] (section 1.1-5). Given the previously developed synthesis of 4,10-dichlorochrysene (**32**)[89, 90] it was hoped further derivatisation of the chrysene core would enable the enhancement of its photophysical and electrochemical properties (increasing the HOMO level and decreasing the E_g) making it more suitable for organic electronic applications. Previous work has explored the derivatisation of **32** at the chlorinated 4,10-positions[90] (section 1.1-6.3) and while this proved an effective synthetic strategy, the overall effect of this substitution on the photophysical and electrochemical properties of the derivatives produced was not as pronounced as originally hoped. Considering the iridium-catalysed aromatic C-H borylation described in section 1.2 and its previous application to phenacenes[128] (section 1.2-3.1) it was hopped that the application of this borylation to **32** may open up the opportunity for the tetrafunctionalisation of the chrysene core and that these "A_2B_2" derivatives may have significantly enhanced photophysical and electrochemical properties over and above those of previously synthesised chrysene derivatives in the literature.

2.1-1.1 Synthesis of 4,10-Dichlorochrysene and the Application of an Iridium-Catalysed Aromatic C-H Borylation

The first stage of this project was the replication of the literature[90] synthesis of 4,10-dichlorochrysene (**32**) from the commercially available starting material 1,5-dihydroxynapthalene (**28**) (figure 36) as previously described in section 1.1-6.

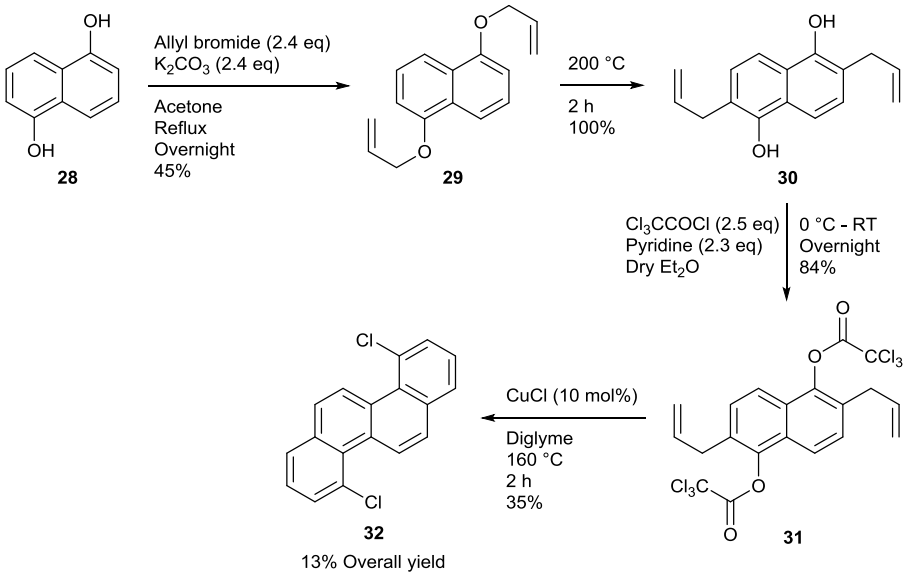

Figure 36 – Synthesis of 4,10-dichlorochrysene (**32**) from 1,5-dihydroxynapthalene (**28**)

One modification made in this synthesis compared to that previously described was to perform the Williamson ether synthesis of **29** at reflux (as described in related literature procedures),[164] rather than stir at room temperature, enabling the simplified purification of **29**. This synthesis allowed the isolation of 4,10-dichlorochrysene (**32**) in a 13% overall yield in four steps.

Based on the work of Isobe *et al*[128] and their report regarding the borylation of phenacenes (section 1.2-3.1), **32** was then subjected to similar reaction conditions using the "standard" procedure described by Pertuz *et al*[115] (as shown in figure 37) in the hope that the aryl chloride functionality (known to be tolerant of this catalyst/ligand system)[108, 165] installed at the 4,10-postions of **32** would help control the regioselectivity of the diborylation.

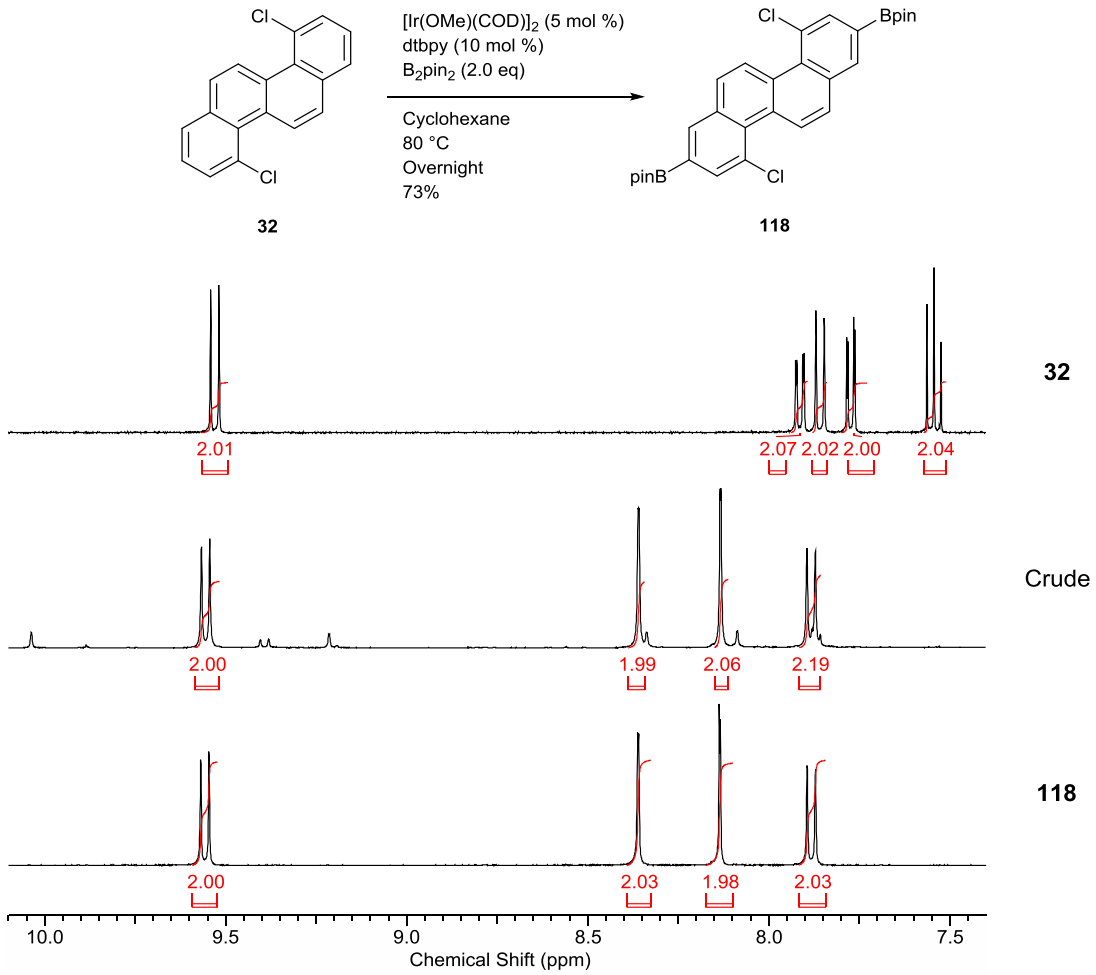

Figure 37 – Regioselective aromatic C-H diborylation of **32** and the associated ^{1}H NMR data (aromatic region) of the corresponding compounds and crude reaction mixture

Pleasingly this reaction proceeded with excellent regioselectivity and high conversion to the desired product, the crude ^{1}H NMR spectrum (figure 37) indicating consumption of the starting material together with only minor side product formation. With this favourable reactivity the purified target compound **118** could be isolated in a 73% yield through direct recrystallisation of the crude reaction mixture, avoiding intensive purification procedures such as HPLC,[128] GPC[123] or repetitive recrystallisation processes[120] as described in previous literature examples of this borylation. Comparison of these results to the C-H borylation of unsubstituted phenacenes by Isobe *et al*[128] is marked. When unsubstituted chrysene was borylated under similar conditions, a 72% overall yield of a mixture of the 2,8- 2,9- and 3,9-isomers was obtained in a 1:2.1:1.2 ratio (**89**, **90**, **91**, figure 28, section 1.2-3.1). In

the borylation of **32** however, the chlorine functionality at the 4,10-positions acted at a steric directing group, hindering unwanted *ortho*- borylation at the 3,9-positions. In addition, without forcing conditions (e.g. excess B_2pin_2) these reactions typically do not proceed *ortho*- to ring junctions,[115] hindering the 5,6,11,12-positions, leaving the observed 2,8-positons of **32** as the favoured borylation site, allowing easy isolation of **118**.

As briefly observed in section 1.2-1, Steel *et al*[112] noted that when run at room temperature these iridium-catalysed borylations tend to be more subject to underlying electronic effects, while at elevated temperatures sterics tend to dominate. In this work a correlation was found between computationally calculated C-H acidities (pK_a values) and the preferred site of borylation in reactions run at room temperature.[112] Given these observations, DFT calculations were performed by our collaborators (Dr Joseph McDouall *et al* at the University of Manchester)[2] using the method of Guo *et al*[166] (as used by Steel *et al*) to investigate the C-H acidities of **32** in an attempt to understand what contribution (if any) underlying electronic effects may have on the observed regioselective diborylation. These results are displayed in figure 38.

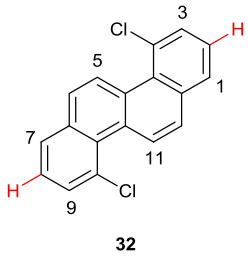

32

Hydrogen	pK_a
3,9-	33.36
1,7-	39.24
6,12-	39.43
5,11-	39.83
2,8-	42.28

Figure 38 – Computationally calculated (DFT) C-H acidities of **32**. 2,8-Positions borylated in the subsequent aromatic C-H activation step shown in red

As can be observed in figure 38 the 2,8-positons of **32** are in fact calculated to be the least acidic in the molecule, further confirming the hypothesis that at elevated temperatures sterics are the dominant factor in the regioselectivity of this aromatic C-H borylation process, proceeding essentially irrespective of underlying C-H acidity.

In a further development of this borylation methodology, heating *via* microwave irradiation (MWI) was also briefly investigated. It was observed by Steel *et al*[167] that heating *via* MWI significantly enhances the rate of this aromatic C-H borylation compared to conventional heating. Combined with observations by those such as Smith *et al*[110] that dry THF may be a superior solvent system to hexanes, the adaptation of a literature procedure[168] allowed the borylation of **32** as in figure 39, utilising a THF solvent system with heating *via* MWI.

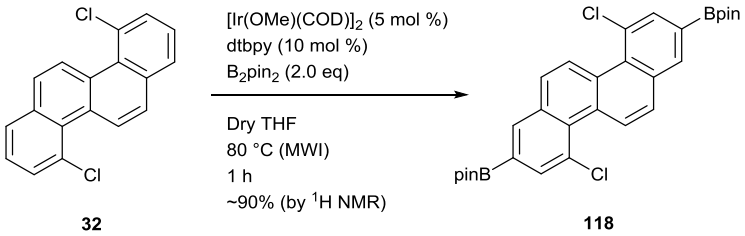

32 **118**

Figure 39 – Aromatic C-H diborylation of **32** *via* MWI

These results obtained under MWI mirror those in figure 37, with the crude ^{1}H NMR indicating the desired diborylation to **118** in high yield (~90% by ^{1}H NMR) with excellent regioselectivity. In addition this reaction was completed in just 1 hour under MWI and utilised a more versatile THF solvent system. It is noteworthy however that these microwave reactions were concentration sensitive and when performed at lower concentrations (0.05 M rather than 0.4 M) significant starting material was evident in the crude ^{1}H NMR spectrum after 1 hour MWI, with only slight additional conversion after 2 hours MWI.

Chrysene **118** was seen as a key intermediate in this project allowing access to "A_2B_2" 2,8- and 4,10-orthogonally substituted chrysene derivatives as in figure 40. The formation of a donor-acceptor chrysene from this intermediate also became a key objective as this synthesis progressed in order to fully exploit the available substitution pattern.

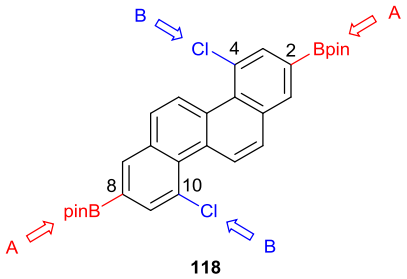

Figure 40 – Proposed "A_2B_2" orthogonal coupling pattern of key intermediate **118**

2.1-1.2 Substitution of the Borylated 2,8-Positons of the Chrysene Core

Utilising key intermediate **118** a variety of functionalisations were undertaken at the 2,8-positons of the chrysene core. Initial substitutions were conducted *via* the Suzuki coupling of a variety of aryl halides with the newly formed diboryl chrysene. An immediate concern in this reaction process however was preservation of the chlorine functionality in the product, with dehalogenation or coupling of the 4,10-dichloro functionalities being potential side processes in this reaction. It was for these reasons the more reactive aryl iodides were chosen as coupling reagents in this process. Pleasingly, with such reagents the dicoupling of **118** was successfully performed with a variety of partners, in reasonable yields, with preservation of the 4,10-dichloro functionality, as shown in figure 41.

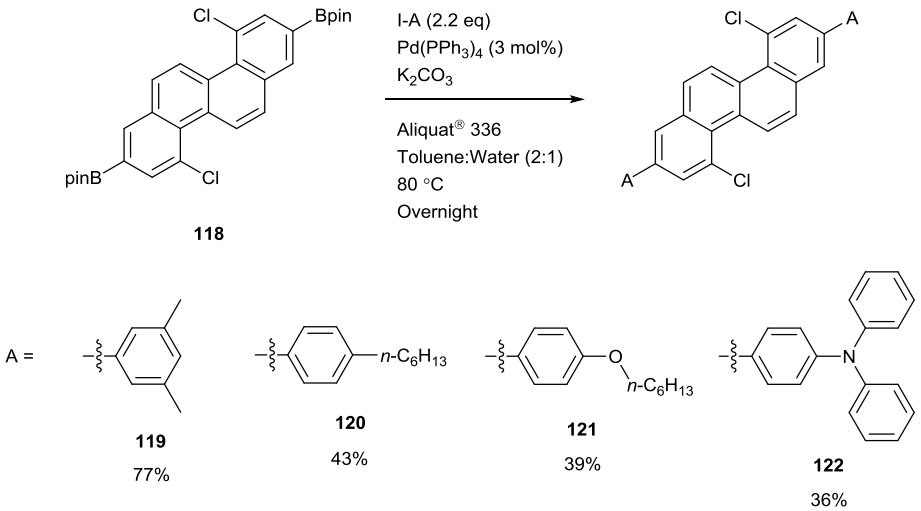

Figure 41 – Suzuki coupling of the 2,8-positons of **118**

The first coupling regent chosen in this process was 1-iodo-2,5-dimethylbenzene due to the simplicity of the ^{1}H NMR the product (**119**) would generate, however **119** in

particular featured extremely low solubility in common organic solvents, preventing ^{13}C NMR analysis and forcing purification to be achieved *via* gradient sublimation. For this reason future syntheses of **120** and **121** utilised substituents bearing solubilising *n*-hexyl chains. Notable in this synthesis was the use of progressively stronger electron donating groups from **120**, a simple extension of the aromatic system, to the *para*- positioned electron donating oxygen present in **121** and finally the *para*- positioned nitrogen in **122**, representing a stronger still electron donating group. The effect of these substituents on the electronics of the chrysene core is the subject of section 2.1-2.

The use of aryl iodides as coupling partners proved successful, however this necessitated the synthesis of 4-(*n*-hexyloxy)iodobenzene (**125**) and 4-iodo-N,N-diphenylaniline (**128**) used in the synthesis of **121** and **122** respectively. These syntheses were undertaken according to literature procedures[169, 170, 171] from 4-bromophenol (**123**) and triphenylamine (**126**) respectively as in figure 42.

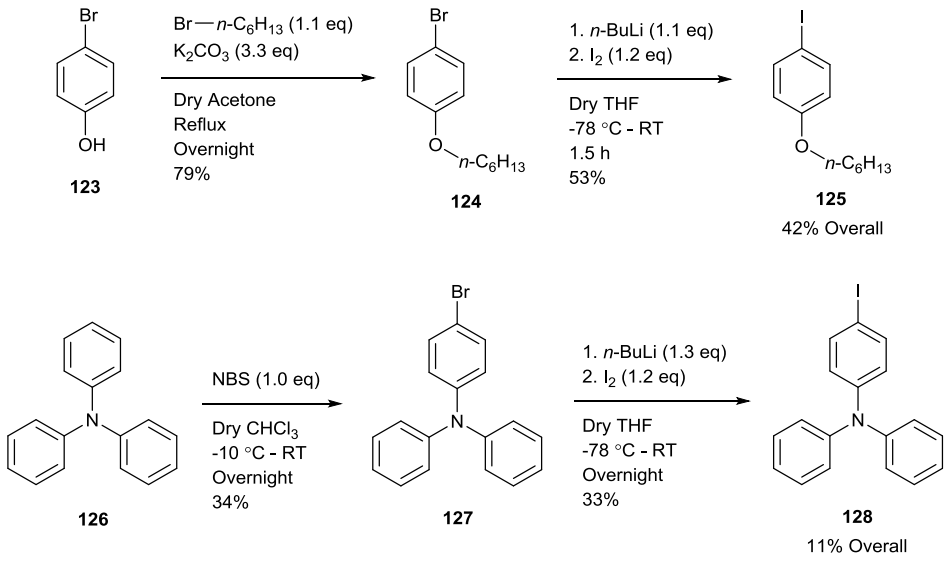

Figure 42 – Preparation of aryl iodide coupling partners for use in the synthesis of **121** and **122**

In addition to Suzuki coupling progressively stronger electron donating groups, an electron withdrawing CF_3 group was also installed at the 2,8-positions of **118**. Following a procedure described by Hartwig *et al*[172] the boronic ester groups of **118**

were hydrolysed to the corresponding boronic acid **129**, using $NaIO_4$ as an oxidising agent to drive the hydrolysis reaction (figure 43). Characterisation of **129** was completed using DMSO-d_6 as the appropriate NMR solvent however characterisation by mass spectrometry (MALDI-TCNQ) proved problematic. Exposure of **129** to methanol during mass measurement resulted in the methyl ester of the corresponding acid (in various stages of derivatisation, from mono- to tetra-substituted) being a significant component in the mass spectrum. Due to additional difficulty obtaining a high resolution mass spectrum, the boronic acid was derivatised *in situ* with ethylene glycol to the corresponding dioxaborolane prior to mass measurement in order to provide a clear molecular ion.

Following the successful formation of boronic acid **129** a trifluoromethylation procedure as developed by Sanford *et al*[173] was then applied, utilising *tert*-butylhydroperoxide (TBHP) as the radical initiator, sodium triflinate ($NaSO_2CF_3$) as the trifluoromethyl source and CuCl as the coupling mediator (figure 43). To our knowledge this is the only example of a *bis* trifluoromethylation *via* this methodology and allowed the synthesis of this 2,8-*bis*(trifluoromethyl) derivative (**130**) in a 27% overall yield from diboryl chrysene **118**.

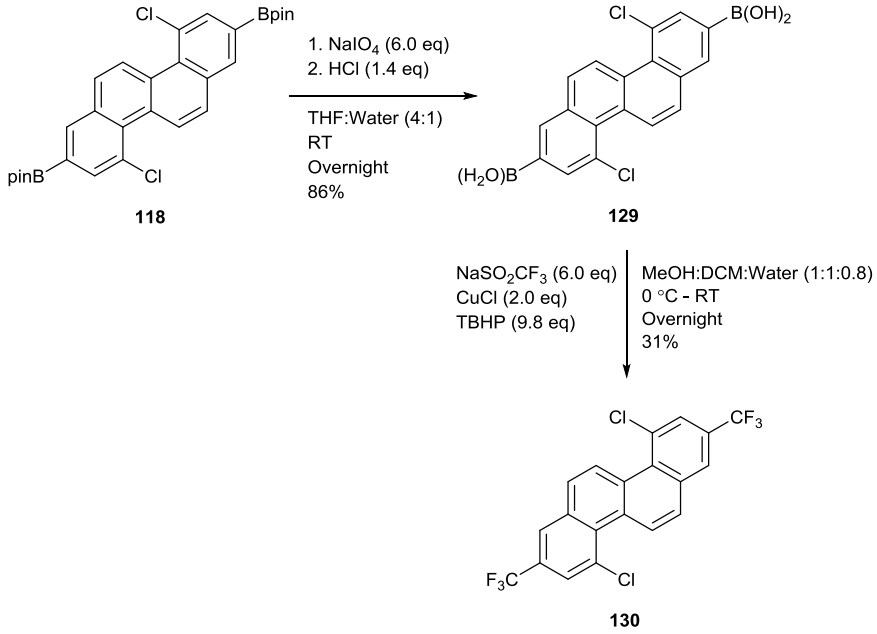

Figure 43 – Trifluoromethylation of **118**

In an additional experiment the chemical space accessible *via* diboryl chrysene **118** was further elaborated through the conversion of the boronic pinacol ester groups to the corresponding diol as in figure 44 below.

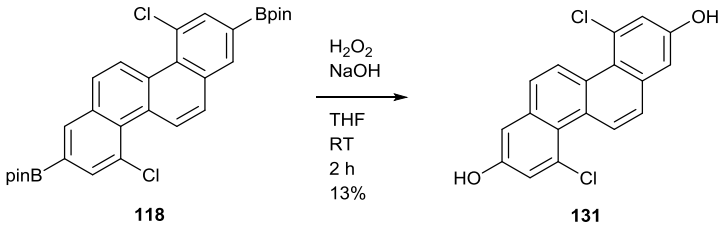

Figure 44 – Oxidation of chrysene **118** to the corresponding diol **131**

The initial crude ^{1}H NMR spectrum of this transformation indicated excellent conversion to the desired product **131** however purification was unsuccessful by both trituration and recrystallisation, necessitating purification by column chromatography. This proved extremely challenging and low yielding however, requiring a solvent system as polar as 0.5-1.5% methanol in DCM and resulted in a relatively poor 13% isolated yield, most likely due to the relatively polar hydroxyl groups of **131**.

2.1-1.3 Substitution of the 4,10-Positons of the Chrysene Core – Formation of "A_2B_2" Derivatives

Following the successful formation of 2,8-substiuted chrysenes **119-122**, **130** and **131** attention was then turned to functionalising the residual chlorinated 4,10-positons of these derivatives. Given its favourable solubility **120** was chosen as an initial substrate for further functionalisation. A problem in these further substitutions however was the lower reactivity associated with aryl chlorides, which are generally less reactive than their bromide or iodide equivalents. Based on the previous functionalisations of 4,10-dichlorochrysene (**32**) that had been conducted (section 1.1-6.3) it was proposed that the PEPPSI-IPr catalyst (containing an N-heterocyclic carbene ligand to promote catalytic activity) may prove the most suitable for the coupling of the 4,10-dichloro positions, in particular when used in Kumada coupling reactions.[90, 174] Literature procedures[90] for the Kumada coupling of **32** were therefore adapted as in figure 45 in order to install phenyl and (with input from a supervised

student)[2] thienyl substituents at the 4,10-positions of **120**, through the generation of their corresponding Grignard reagents from the commercially available bromide.

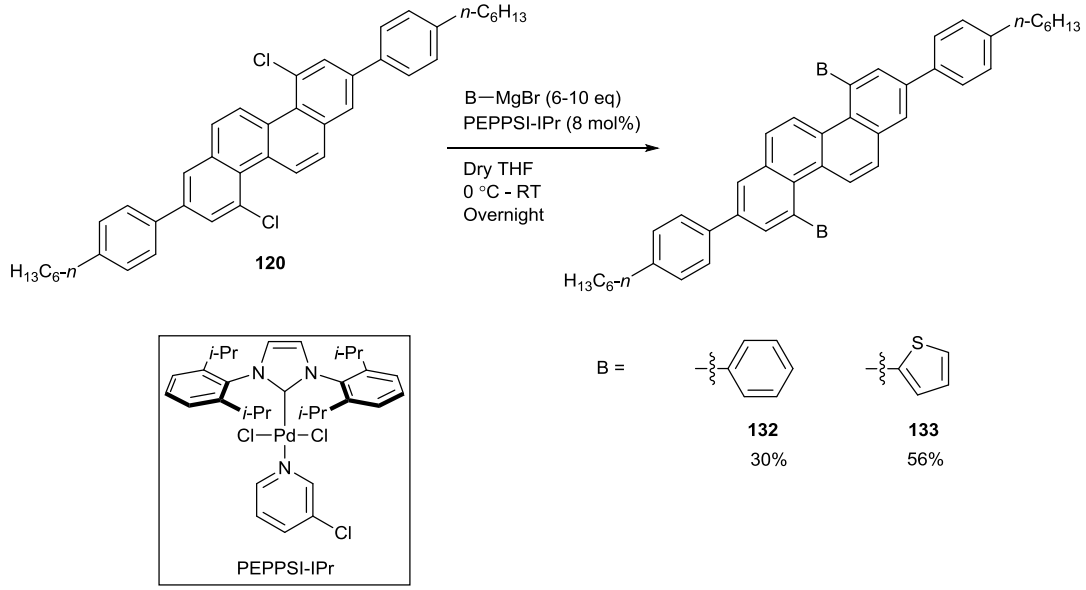

Figure 45 – Kumada coupling of 4,10-positions of **120** to form **132** and **133**

This Kumada coupling step was successful in installing a further phenyl as in **132** and an electron rich thienyl as in **133**. Not only were these derivatives interesting due to their potential photophysical and electrochemical properties but their successful formation also validated our synthetic route to orthogonal "A_2B_2" substituted chrysenes. Overall yields however were poor, 1% and 2% for **132** and **133** respectively over seven synthetic steps from 1,5-dihydroxynapthalene (**28**) but this must be tempered by the fact this includes benzannulation (step 4), C-H activation (step 5), chemoselective Suzuki coupling (step 6) and aryl chloride Kumada coupling (step 7) processes.

Following the synthesis of these first "A_2B_2" derivatives as in figure 45, the synthesis of an "A_2B_2" donor-acceptor chrysene was identified as a synthetic target that would exploit this substitution pattern and produce derivatives with the most marked improvement in photophysical and electrochemical properties. 4-Nitrophenyl and 4-cyanophenyl substituents were identified as suitable electron withdrawing moieties that may be installed at the 4,10-positions of previously synthesised electron rich chrysenes **121** and **122** (figure 41). Such electron withdrawing moieties

however precluded the use of a Kumada coupling reaction (previously used to functionalise the chlorinated 4,10-positions as in figure 45) as suitable literature methods for the preparation of electron deficient 4-nitrophenyl and 4-cyanophenyl Grignard reagents proved elusive. This necessitated a switch from Kumada couplings to more tolerant Suzuki couplings of which 4-nitro and 4-cyano phenylboronic acids were commercially available. Test coupling reactions of these substituents with **32** were conducted (figure 46) and although yields were low, the reaction proved promising.

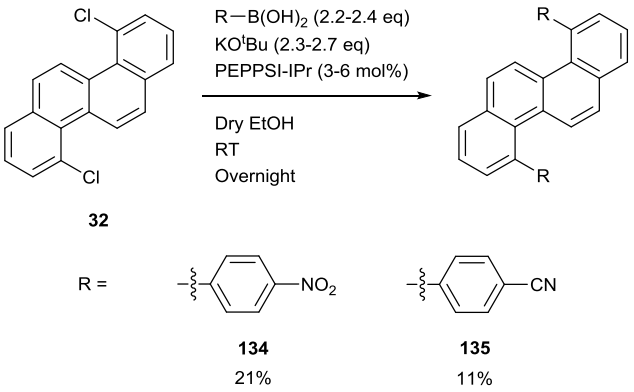

Figure 46 – Test Suzuki couplings of **32** with electron withdrawing group functionalised aryl boronic acids

As in in previous Suzuki couplings of **32** the reactions completed in figure 46 were performed in dry ethanol,[90] however when these conditions were applied to **121** (figure 41) in order to synthesise a donor-acceptor chrysene, no reaction was observed. This is likely due to the observation that 2,8-substituted chrysene derivatives proved essentially insoluble in ethanol.

At this point alternative preparations and solvent systems were investigated, in which the synthesised 2,8-substituted chrysene derivatives may be soluble. In a series of test reactions the Suzuki coupling of **32** with an unsubstituted phenylboronic acid/pinacol ester partner was attempted. These reactions were heated at 60 °C overnight with both THF and dioxane investigated as potential solvents. A variety of bases were investigated (Cs_2CO_3, K_2CO_3, KOH and KO^{t}Bu), as was pre-activation of the catalyst though stirring at room temperature with the chosen base prior to the addition of coupling substrates, however in each instance insufficient

reactivity was observed to isolate the desired product. Seemingly the requisite reactivity was only observed when reactions were performed in ethanol and indeed literature observations of the performance of the PEPPSI-IPr catalyst indicated Suzuki couplings of aryl chlorides proceed with significantly greater yields when performed in a simple alcoholic solvent (isopropanol) at room temperature than in an ethereal solvent (dioxane) at 60 °C.[174] Based on these observations a mixed dioxane:ethanol (5:1) solvent system was also investigated, but again reactivity provided insufficient to isolate the desired product.

While the PEPPSI-IPr catalyst was effective in Suzuki couplings performed in ethanol at room temperature with a KO^tBu base, it proved remarkably capricious under alternative conditions. In one attempted Suzuki coupling of **32** for instance, a toluene:methanol (1:1) solvent system was utilised, with Cs_2CO_3 as the base and heating at 90 °C overnight in adaptation of an existing literature procedure.[175] Remarkably however this resulted in dehalogenation of the starting material, resulting in the formation of unsubstituted chrysene in a 75% yield. Dehalogenation in the presence of alcoholic solvents in particular appeared to be a temperature dependent process. When using the standard Suzuki coupling conditions explored in figure 46 (ethanol solvent, KO^tBu base) simply heating the reaction to 60 °C for 1 hour resulted in significant dehalogenation of the starting material.

Given the intense difficulty associated with the Suzuki coupling of the chlorinated 4,10-positions of the 2,8-substituted chrysenes synthesised, attention was instead turned to the substitution of an electron rich substituent at the 4,10-positions of electron deficient chrysene **130**. While still generating a donor-acceptor chrysene, the installation of an electron rich substituent at these positions allowed the use of the previously successful (figure 45) Kumada coupling procedure, as the necessary Grignard reagent could be accessed by standard methods. In this instance 4-(diphenylamino)phenyl was once again chosen as a suitable strong electron donating group and its corresponding Grignard reagent could be quickly generated from its readily synthesised brominated derivative (**127**, figure 42). This approach finally allowed the successful synthesis of an "A_2B_2" donor-acceptor chrysene (**137**) to be completed as in figure 47.

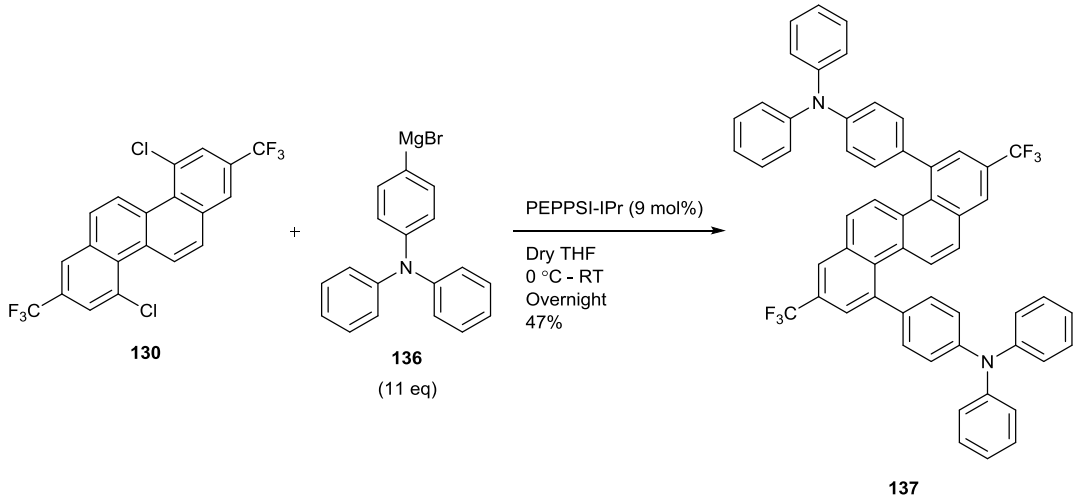

Figure 47 – Synthesis of donor-acceptor "A_2B_2" chrysene **137** *via* Kumada coupling of the 4,10-positions of **130**

The use of a PEPPSI-IPr catalysed Kumada coupling procedure in this final step allowed **137** to be isolated in 47% yield from **130**. The final synthesis an "A_2B_2" donor-acceptor chrysene required switching the order of donor-acceptor substitution that was originally envisioned as it proved so exceptionally difficult to install an electron deficient aromatic at the chlorinated 4,10-positions. It was hoped however that the successful synthesis of donor-acceptor derivative **137** would validate our "A_2B_2" substitution approach. To our knowledge **137** is the first donor-acceptor chrysene derivative to be reported and featuring a unique "A_2B_2" substitution pattern demonstrated great potential among those chrysene derivatives investigated to exhibit markedly different photophysical and electrochemical properties compared to the parent chrysene (**32**).

2.1-2 Properties of Chrysene Derivatives Synthesised

Following the successful synthesis of the above chrysene derivatives their photophysical and electrochemical properties were investigated in order to estimate their respective E_g, HOMO and LUMO levels. Where possible additional analysis was also conducted by X-ray crystallography and in conjunction with collaborators key derivatives were also subjected to computational DFT analysis. Derivatives **119** (figure 41) and **131** (figure 44) were not analysed due to their relative insolubility and low yielding synthesis respectively. Derivative **133** was analysed by UV-vis absorbance spectroscopy and CV with input from a supervised student.[2]

2.1-2.1 UV-vis Absorption and Fluorescence Spectra

In order to analyse the photophysical properties of the derivatives synthesised, UV-vis absorption and fluorescence spectra in dilute DCM solution were obtained of the parent chrysene **32**, each of the 2,8-substituted derivatives (**120**-**122** and **130**) and the three "A_2B_2" derivatives synthesised **132**, **133** and **137** to gain a stepwise insight into electronic changes which occur with each substitution. The normalised absorption (a) and fluorescence (b) spectra of derivatives **32**, **120**-**122** and **130** are shown in figure 48.

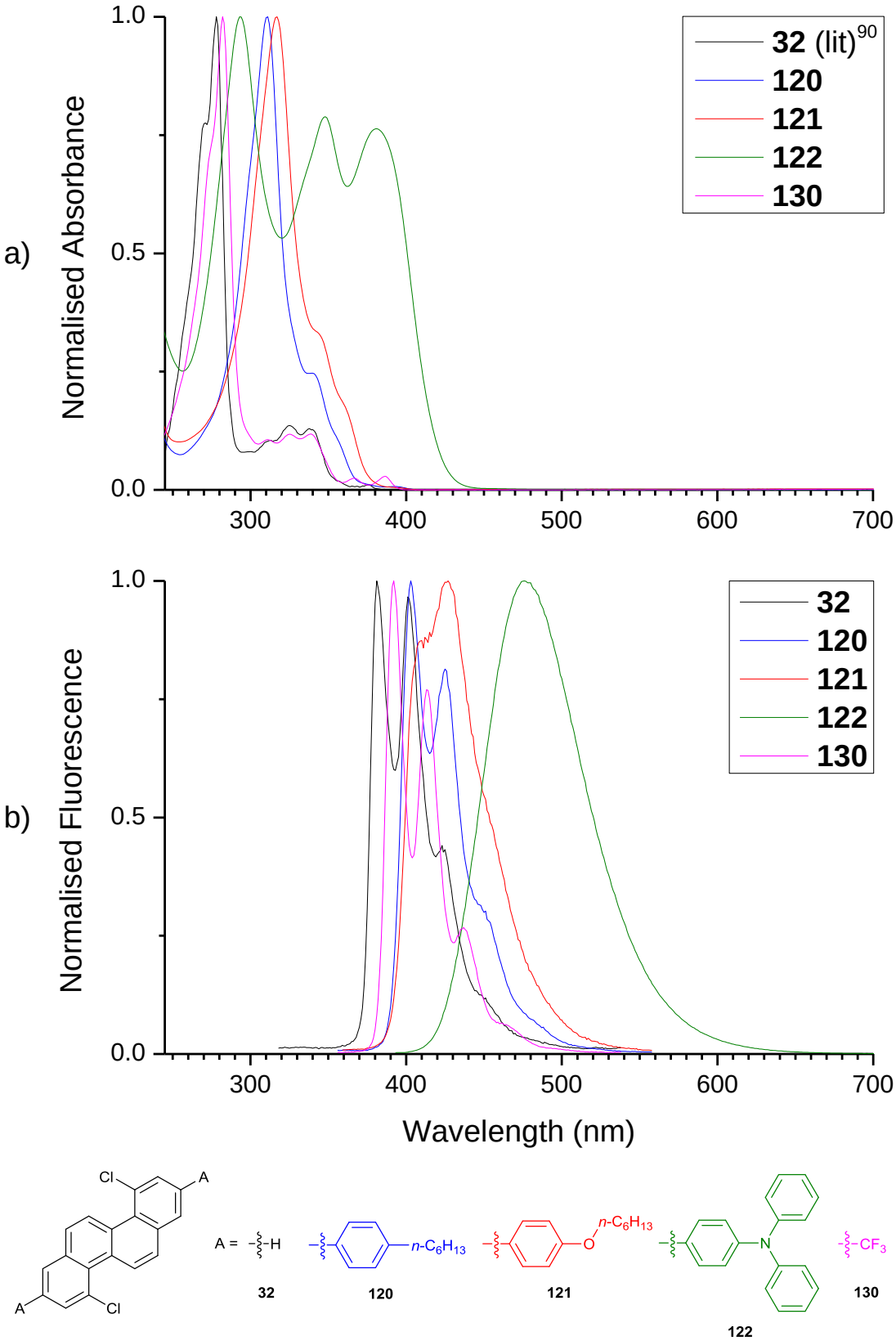

Figure 48 – Normalised UV-vis absorption (a) and fluorescence (b) spectra of parent chrysene (**32**) and 2,8-substituted chrysenes **120**-**122** and **130** recorded in DCM

The spectra in figure 48 are presented for ready comparison between the absorption (a) and fluorescence (b) spectra and for comparison with the UV-vis absorption/fluorescence spectra of later derivatives (figures 49 and 50). For clarity, larger representations of these spectra are presented in the appendix (section 6.1).

In the previous substitution of chrysene at the 4,10-positions alone, only a small bathochromic shift in the λ_{max}^{abs} compared to **32** was observed (up to 14 nm).[90] Meanwhile as can be observed in figure 48, the substitution of the 2,8-positions even with a simple 4-*n*-hexylphenyl substituent (**120**) results in a significant bathochromic shift in λ_{max}^{abs} of 33 nm, that is increased to 39 nm with the use of a 4-*n*-hexyloxyphenyl substituent as in **121**. Meanwhile substitution with 4-(diphenylamino)phenyl substituents (**122**) results in a significant departure from the band structure previously observed and while the λ_{max}^{abs} is only shifted 15 nm relative to **32**, significant lower energy transitions at 348 and 381 nm become apparent. Substitution with trifluoromethyl functionalities (**130**) results in a much smaller shift in λ_{max}^{abs} compared to other derivatives investigated (4 nm) and a very similar band structure compared to the parent compound **32** is observed, most likely as there is no extension of the aromatic system in this derivative. Comparing fluorescence, we again see bathochromic shifts compared to the parent chrysene (**32**) as the 2,8-substituents become increasingly electron releasing. Compared to **32** the installation of 4-*n*-hexylphenyl substituents (**120**) results in a shift in λ_{max}^{fluor} of 22 nm and with the installation 4-*n*-hexyloxyphenyl substituents (**121**) it is shifted 46 nm. Outstandingly, the λ_{max}^{fluor} of **122** is shifted 95 nm compared to **32** in a single broadened emission.

The UV-vis absorption (a) and fluorescence (b) spectra of "A_2B_2" chrysene derivatives **132** and **133** can be contrasted with their parent structure **120** as in figure 49.

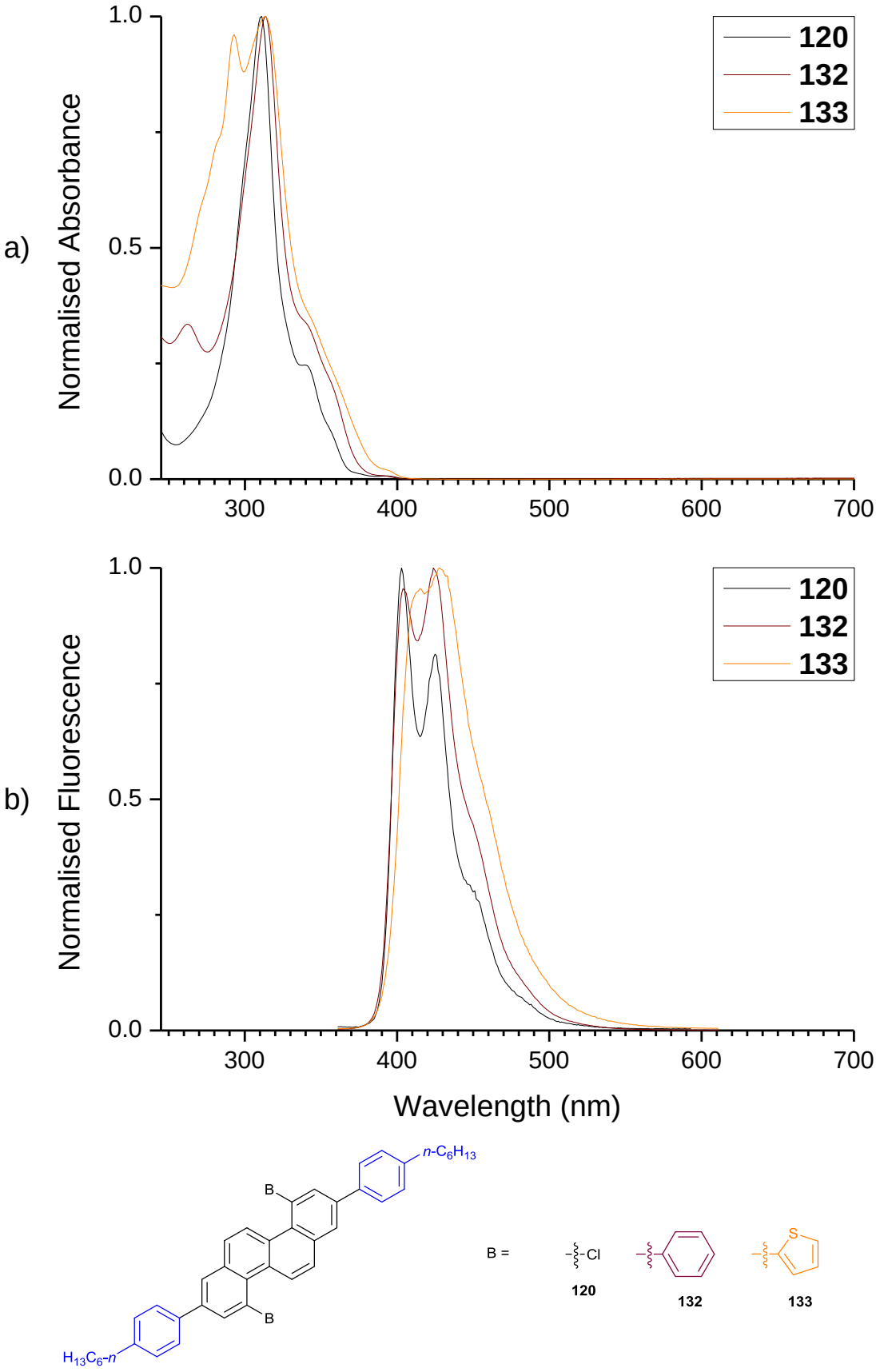

Figure 49 – Normalised UV-vis absorption (a) and fluorescence (b) spectra of **120** and "A_2B_2" chrysenes **132** and **133** recorded in DCM

On analysis of figure 49 it can be observed in the absorption spectra (a) that the additional substitution of the 4,10-positions of **120** with phenyl (**132**) and thienyl (**133**) substituents results in a much smaller bathochromic shift than previously observed when substituting the 2,8-positions. In fact the λ_{max}^{abs} of **132** and **133** is identical despite the more electron rich nature of the thienyl substituent and their λ_{max}^{abs} is redshifted only 2 nm relative to **120**. When considering the fluorescence spectra (b) of **132** and **133** it can be observed that while the redshift in the λ_{max}^{fluor} is a reasonable 21 and 25 nm respectively, the installation of an electron rich thienyl substituent (**133**) only results in an increase of 4 nm in the λ_{max}^{fluor} compared to the installation of simple phenyl substituent (**132**). Additionally while an increase in the λ_{max}^{fluor} is noted for **132** and **133** compared to **120**, it is notable that the onset of the emission and band structure of these compounds is very similar, once again suggesting a lack of electronic communication between the 4,10-substituents and the chrysene core.

Finally, the absorption (a) and fluorescence (b) spectra of "A_2B_2" donor-acceptor compound **137** can be compared with its parent compound **130** as in figure 50.

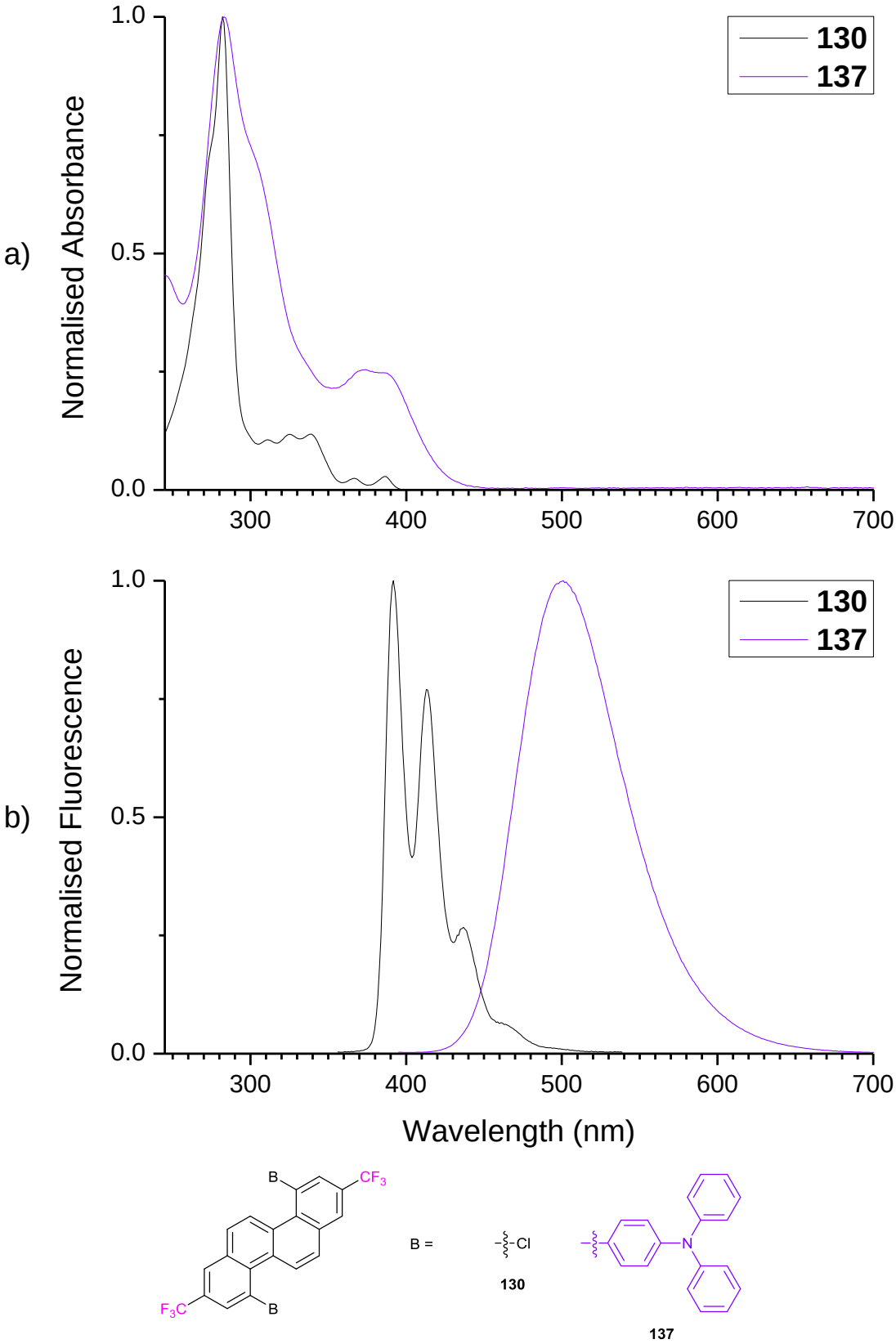

Figure 50 – Normalised UV-vis absorption (a) and fluorescence (b) spectra of **130** and "A_2B_2" donor-acceptor chrysene **137** recorded in DCM

The absorption and emission spectra presented in figure 50 reveal a critical insight into the effectiveness of the "A_2B_2" donor-acceptor strategy adopted in the synthesis of **137**. Considering absorption spectra (a) of **137** compared to **130**, it can be observed that the installation of 4-(diphenylamino)phenyl groups at the 4,10-positions results in only a meagre shift in the λ_{max}^{abs} of 1 nm, although promising new and significant lower energy transitions at 374 and 385 nm become apparent. Comparison of fluorescence spectra (b) of these compounds indicates a significant 109 nm bathochromic shift in the λ_{max}^{fluor} of **137** compared to the parent **130**, producing a single broad emission with λ_{max}^{fluor} at 501 nm.

An important feature of UV-vis absorption spectra when analysing photophysical properties is that it can be used to determine the optical E_g of a compound. The optical E_g corresponds to the λ_{edge} (high wavelength absorption onset) which was estimated by taking the tangent of the lowest energy transition in the UV-vis absorption spectrum.[176] For many of the chrysene derivatives analysed, this lowest energy transition was of very low intensity, requiring each spectrum to be expanded before that transition became apparent (figure 51, a). The most redshifted derivatives however (**122**, **137**) featured clear and defined low energy transitions (figure 51, b), making the estimation of the λ_{edge} less ambiguous. For clarity each of the lowest energy transitions in figure 51 is indicated with a *.

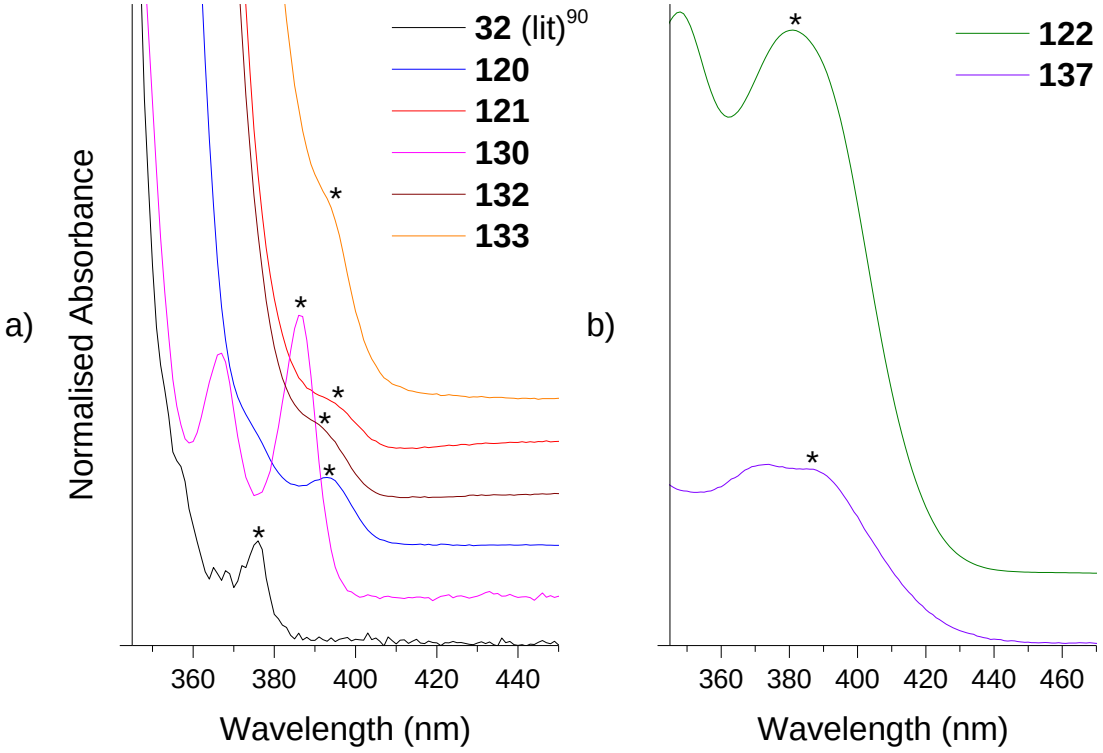

Figure 51 – Normalised UV-vis absorption spectra in DCM indicating the lowest energy transitions of **32** (lit)[90], **120**, **121**, **130**, **132** and **133** (a) and **122** and **137** (b). Spectra are vertically offset for clarity, * indicates the lowest energy transition used in the determination of λ_{edge}

The overall electronic properties of the spectra presented above, along with the determined λ_{edge} and corresponding optical E_g (in eV) of each derivative investigated are presented in table 1.

Derivative	λ_{max}^{abs} (nm)	λ_{max}^{fluor} (nm)	λ_{edge} (nm)	Optical E_g (eV)
32	278	381	380	3.26
120	311	403	404	3.07
121	317	427	405	3.06
122	293	476	419	2.96
130	282	392	394	3.15
132	313	424	403	3.08
133	313	428	404	3.07
137	283	501	424	2.92

Table 1 – Summary of UV-vis absorption and fluorescence data of the chrysene derivatives synthesised

Notably it can be observed from the λ_{edge} determinations in table 1 that with the installation of 4-*n*-hexylphenyl (**120**) or 4-*n*-hexyloxyphenyl (**121**) substituents at the 2,8-positions a significant decrease in E_g (0.19 and 0.20 eV respectively) is observed in comparison to the parent chrysene **32**. Meanwhile subsequent functionalisation of **120** with of phenyl (**132**) and thienyl (**133**) substituents at the 4,10-positions had essentially no effect on the E_g observed (actually increasing by 0.01 eV in **132**). It is therefore notable that in donor-acceptor derivative **137** substitution of the 4,10-positions resulted in an E_g decrease of 0.23 eV relative to **130**, producing the lowest recorded E_g (2.92 eV) followed closely by 2,8-[*bis*(4-(diphenylamino)phenyl] substituted derivative **122** (2.96 eV). The results obtained above are the subject of further discussion in section 2.1-2.3 when interpreted in light of additional data collected by electrochemical analysis, which can help provide a more complete interpretation of the observed E_g with respect to the energies of the HOMO and LUMO levels of each derivative.

Qualitatively the UV-vis absorption and fluorescence changes presented above can be observed by eye when inspecting these chrysene derivatives in solution (figure 52). 4-(Diphenylamino)phenyl derivatives **122** and **137** in particular present a green hue in solution and exhibit a strong florescence when placed under a 365 nm UV light.

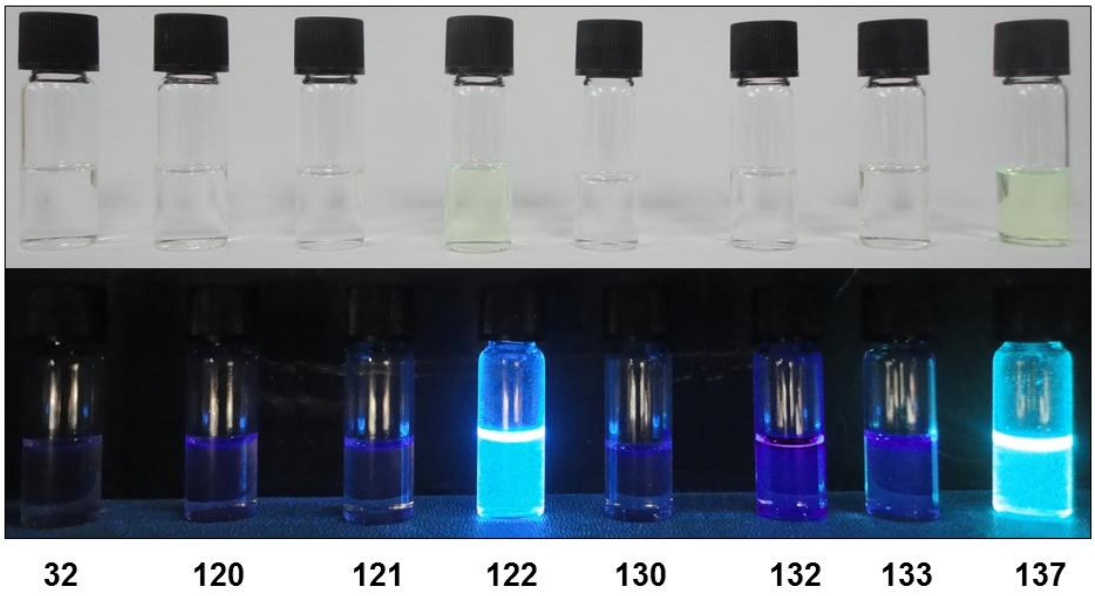

Figure 52 – ~1 mg mL^{-1} DCM solutions of the chrysene derivatives investigated qualitatively indicating the colour and fluorescence changes observed under ambient light (top) and 365 nm UV light (bottom)

It is of note that the most substantial photophysical changes are observed in those chrysenes bearing triphenylamine moieties (**122** and **137**). Triphenylamine-based materials have been the subject of intense interest in organic electronics, particularly as hole-transport materials in OLED devices[177] and triphenylamine moieties have been reported extensively in the literature as effective electron donating substituents in donor-acceptor materials. For example triphenylamine substituents feature in donor-acceptor materials **16**,[49] **19a** and **20a**[52] (figure 8, section 1.1-3.1) and have been shown to be effective in broadening the UV-vis absorption spectra of organic electronic materials, for instance in perylene monoimide-based compounds for use in dye sensitised solar cells.[178] It should be noted however that while triphenylamine is the strongest electron donating moiety used in these studies, the broadening of the observed absorption spectra in **122** is quite exceptional in comparison to similar literature precedents. For instance the substitution of an anthradithiophene core (the PAH core of **5**, figure 6, section 1.1-2.1) with triphenylamine moieties while resulting in a redshift of the lowest energy transition[179] did not produce the stark kind of change in band structure observed in the absorption spectrum of **122**.

2.1-2.2 Single Crystal X-ray Crystallography

Throughout this project, growth of singe crystals suitable for analysis by X-ray crystallography was attempted for each derivative investigated. Due to a mixture of poor solubility (e.g. **122** and **137**) and lack of crystallinity in the sample (e.g. **121** due to the flexibility of the *n*-hexyloxy substituents) only crystal structures of **120**, **130** and **132** were obtained. The crystal structures of **120** and **132** can be compared as in figure 53.

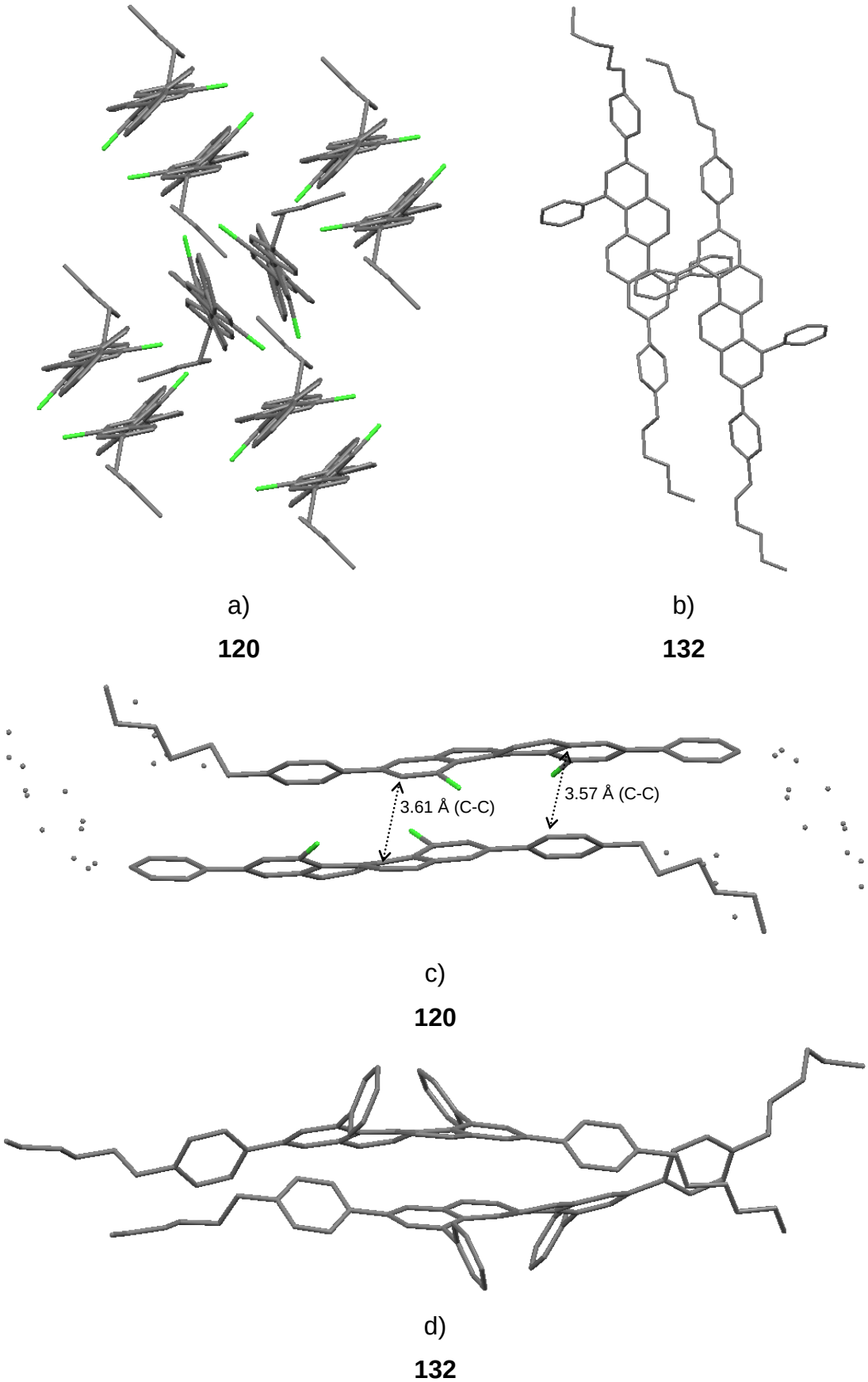

Figure 53 – Crystal structures of **120** and **132**. Alternative *n*-hexyl conformations are indicated by residual carbon atoms in c. For clarity, these have been removed in a

Considering the crystal structure of **120** it should be noted that while the chrysene core and its phenyl substituents are well resolved, the *n*-hexyl chains can take one of two conformations leading to a certain amount of disorder, as shown in figure 53, c. One *n*-hexyl chain features a dominant conformation and this is shown in full while alternative conformations are indicated by residual carbon atoms. For clarity, these alternative conformations have been removed in figure 53, a.

On crystallisation 4,10-dichlorochrysene (**32**) has been shown to adopt a 2D lamellar stack with a minimum C-C distance of 3.48 Å.[90] In comparison **120** adopts a dimeric herringbone structure (also known as a sandwich-herringbone motif)[180] (figure 53, a) with each dimer consisting of a slipped π-π stacking interaction (figure 53, c) with a minimum C-C distance between chrysene cores of 3.61 Å (although a closer C-C distance of 3.57 Å can be observed between the chrysene core and the phenyl substituent). Considering the crystal structure of **132** it can be observed that the installation of phenyl substituents at the 4,10-positions results in a complete disruption of π-π stacking, the crystal structure being dominated by dimers with prevalent H-π interactions between the out-of-plane 4,10-diphenyl substituents and the chrysene core of its partner (figure 53, b and d).

At this point the crystal structure 2,8-*bis*(trifluoromethyl) substituted chrysene **130**, which was additionally determined by single crystal X-ray crystallography, can also be considered.

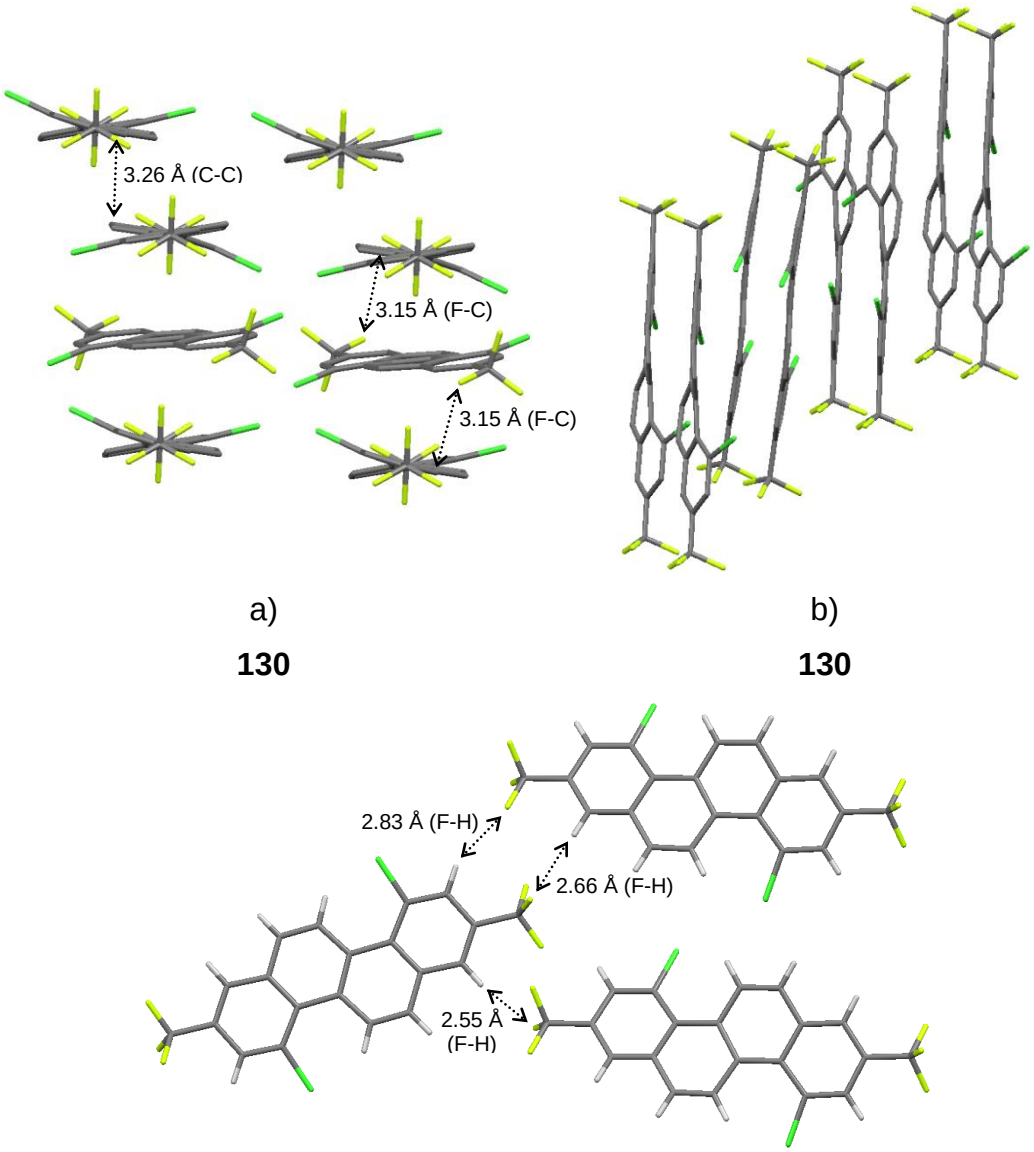

Figure 54 – Crystal structure of **130**

The crystal structure of **130** (figure 54) is particularly curious among those chrysene derivatives previously analysed by X-ray crystallography. This crystal structure presents a trimeric stack of a central rotationally off centre, almost planar chrysene (average bay region torsion of just 5.7 °) sandwiched between two chrysenes with significant bay region torsion (20.5 °) (figure 54, a). This crystal structure furthermore also features significant slipped π-π stacking in two dimensions, with each trimeric stack slipped from the next (figure 54, a) and significant slipped stacking appearing within each trimeric stack (figure 54, b) presumably to maximise

F-C interactions. The crystal structure of **130** also features some of the smallest C-C π-π stacking distances observed, containing C-C distances as low as 3.26 Å (figure 54, a).

Particularly notable in the crystal structure of **130** are the unique interactions which take place due to the fluorinated substituents of the molecule. For instance each planar chrysene (central in each trimeric stack) engages in a C-F interaction (3.15 Å) with each of its stacking partners (figure 54, a), these interactions are further favoured by a tilt in the molecule relative to its stacking partners (most clearly seen in figure 54, b) and may explain its unusual planar structure. Most remarkable in the structure of **130** however are the interactions between columnar stacks as shown in figure 54, c. Here there is some indication of weak fluorophilic[181] F-F interactions (3.31 and 3.24 Å) between trifluoromethyl groups, but more importantly we observe F-H hydrogen bonds as short as 2.55 Å which mesh together neighbouring stacks. Each planar chrysene is observed to engage in three F-H hydrogen bonds with its neighbours at each end of the molecule. It is this strong interaction that explains the off centre twist of the central planar chrysene (most clearly observed in figure 54, a) as it attempts to maximise these F-H hydrogen bonds. In comparison to the literature, these interactions are comparable to those observed in the crystal structures of other trifluoromethyl substituted PAHs. 6,13-*Bis*(trifluoromethyl)pentacene for instance is known to engage in similar length F-H hydrogen bonds between stacks.[182]

Key data from the crystal structures disclosed in figures 53 and 54 can be summarised as the table 2 below.

Derivative	Average bay region torsion[a] (°)	Average torsion of 2,8-substituents[b] (°)	Average torsion of 4,10-substituents (°)	Minimum chrysene C-C π-π stacking distance (Å)
32 (lit)[90]	22.5	-	-	3.48
120	23.1	32.4	-	3.61
130	5.7/20.5	-	-	3.26
132	20.0[c]	35.0[c]	58.8[c]	-

Table 2 – Summary of crystallographic data obtained for **120**, **130** and **132**. [a] averaged from torsion of C4-C4a-C4b-C5 and C10-C10a-C10b-C11. [b] averaged from torsion of substituent with C2-C1, C2-C3, C8-C7 and C8-C9. [c] averaged from torsion of substituent with C4-C3, C4-C4a, C10-C9 and C10-C10a across two chrysene molecules present in the unit cell

The UV-vis absorbance and fluorescence changes observed across these derivatives (figures 48, 49 and 50, section 2.1-2.1) can be informed by information gleamed from X-ray crystallographic structures obtained for derivatives **120**, **130** and **132** above. It is immediately apparent from UV-vis analysis that substitution at the 2,8-positions has a far greater effect on the UV-vis spectra and electronic properties of these derivatives than does substitution at the 4,10-positions. For instance substitution of **32** with 4-*n*-hexylphenyl groups at the 2,8-positions (**120**) resulted in a bathochromic shift in the λ_{max}^{abs} of 33 nm while subsequent additional substitution with phenyl groups at the 4,10-positions (**132**) resulted in a shift in λ_{max}^{abs} of just 2 nm. It can be hypothesised that the starkly different influence of these two almost identical substituents is due to the greater twist observed in those substituents at the 4,10-positons compared to those at the 2,8-positions (59 *vs* 35 °) presumably due to increased sterics in the bay region. It can be suggested that the larger twist experienced by those substituents at the 4,10-positons disrupts orbital overlap and communication with the chrysene core, limiting their impact on the overall electronics of the system compared to the less twisted 2,8-postions. One exception to this observation however is donor-acceptor chrysene **137** which in spite of its presumably out-of-plane twisted electron donating groups at the 4,10-positons still

experiences a significant change in its absorption and fluorescence spectra. As will be discussed in section 2.1-3, computational DFT studies of **137** further highlight the surprising levels of communication observed between the out-of-plane 4,10-positons and the chrysene core in this donor-acceptor derivative.

2.1-2.3 Electrochemical Cyclic Voltammetry Studies

In order to evaluate the HOMO level of the various chrysene derivatives synthesised CV measurements were conducted in DCM at a scan speed of 100 mV S^{-1} using ferrocene (Fc) as a reference. Tetrabutylammoniumhexafluorophosphate (0.1 M) was used as the supporting electrolyte with the chrysene derivative in a 1.0 mg mL^{-1} concentration. The CV measurements for each derivative investigated are displayed as in figures 55 and 56 below.

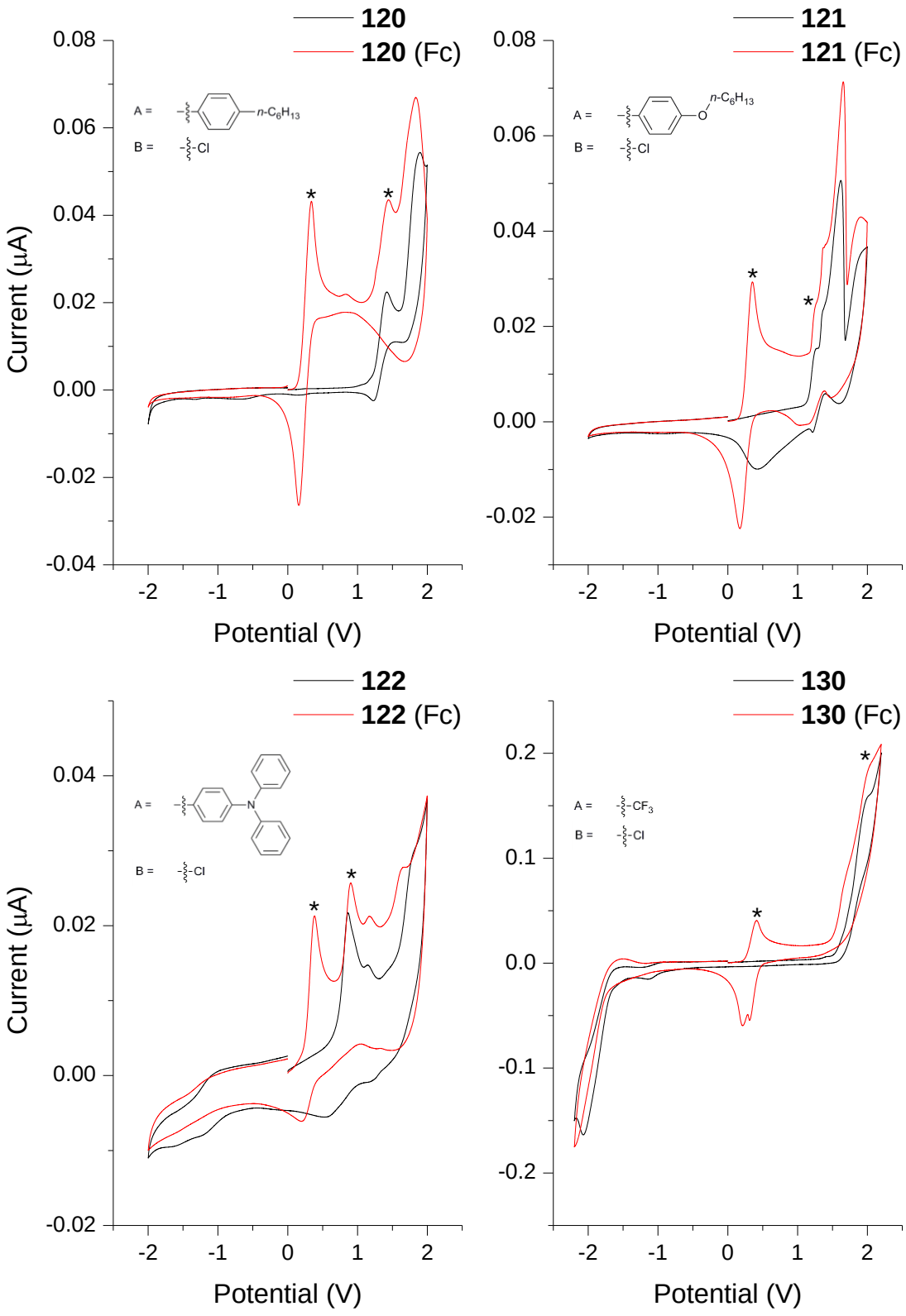

Figure 55 – Cyclic voltammograms of 2,8-substituted chrysene derivatives recorded in DCM at a scan speed of 100 mV S^{-1}. * indicates the current maxima of the ferrocene oxidation potential and the first oxidation potential of the chrysene derivative investigated

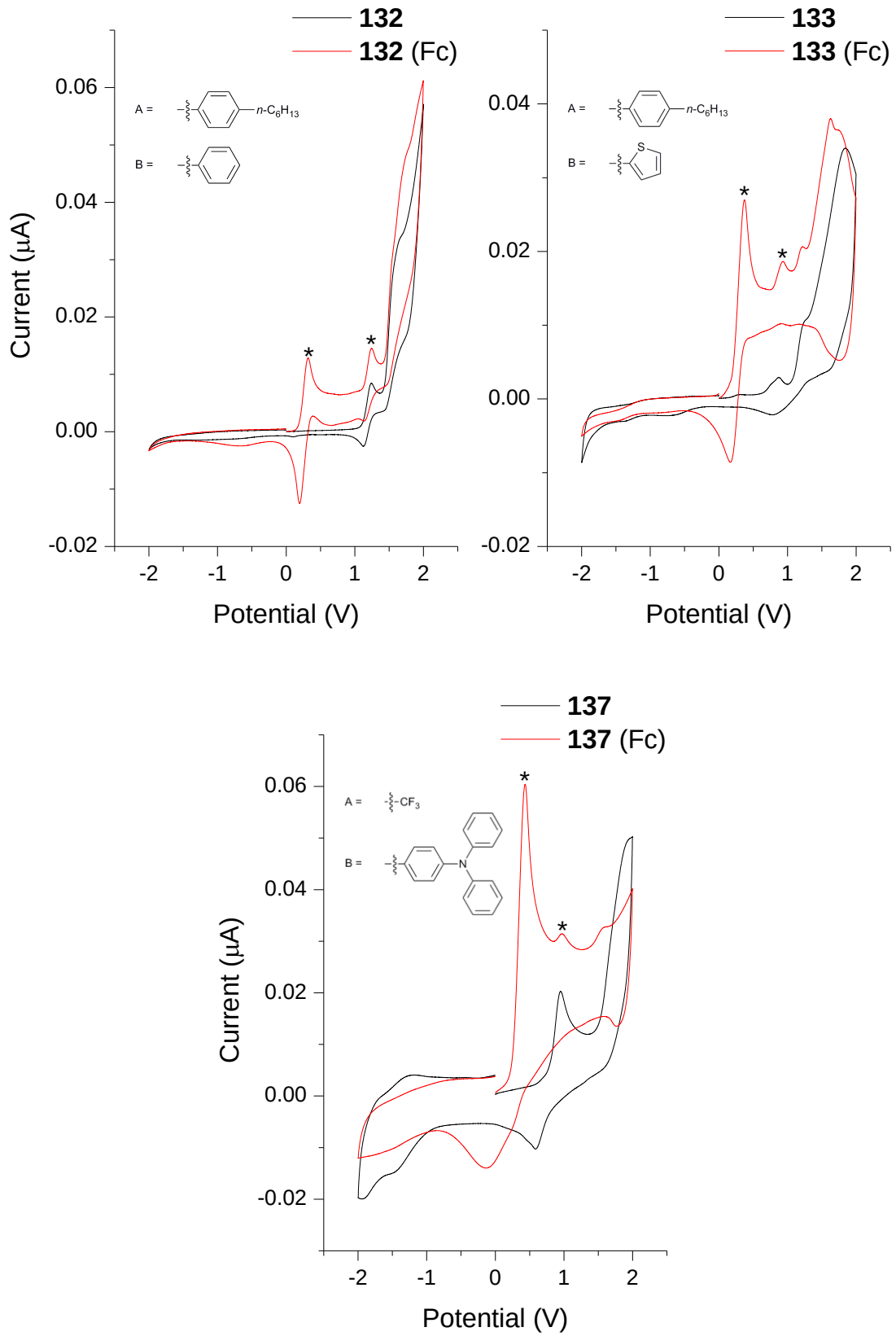

Figure 56 – Cyclic voltammograms of "A_2B_2" substituted chrysene derivatives recorded in DCM at a scan speed of 100 mV S^{-1}. * indicates the current maxima of the ferrocene oxidation potential and the first oxidation potential of the chrysene derivative investigated

It can be observed in figures 55 and 56 that the oxidation of these chrysene derivatives was often irreversible as previously noted by our group in the electrochemical study of chrysene derivatives.[90] It is likely such irreversibility is due to decomposition[183] or possible insolubility of the oxidised product. Even in those examples where reversibility of oxidation was noted (**120**, **132**, figures 55 and 56) the oxidised product was observed to react with the ferrocene reference, resulting in a loss of reversibility. For these reasons, while it is usual to report the oxidation potential as the mean of the of the oxidation and corresponding reduction potential,[184] in this instance the first oxidation potential of the chrysene derivative (V_{Ox}) and that of the ferrocene Fc/Fc^+ couple $\left(V_{Fc/Fc^+}\right)$ was taken from their anodic current maxima in the ferrocene spiked run, marked with a * in figures 55 and 56.

In these studies the Fc/Fc^+ couple was taken to have an energy of -4.8 eV (corresponding to the HOMO of ferrocene)[184, 185] allowing the estimation of the HOMO level of each chrysene derivative using equation 1 below.

$$HOMO = -4.8 - \left(V_{Ox} - V_{Fc/Fc^+}\right) \qquad [1]^{184}$$

The CV data presented in figures 55 and 56 can be summarised in table 3 below along with the estimated HOMO levels of the various chrysene derivatives investigated.

Derivative	Fc/Fc^+ potential (V_{Fc/Fc^+}) (V)	Analyte first oxidation potential (V_{Ox}) (V)	Estimated HOMO level (eV)
120	0.339	1.44	-5.90
121	0.352	1.26	-5.71
122	0.384	0.902	-5.32
130	0.414	2.04	-6.43
132	0.320	1.24	-5.72
133	0.372	0.934	-5.36
137	0.435	0.973	-5.34

Table 3 – Summary of key CV data and estimated HOMO levels of the chrysenes investigated

A significant drawback of the electrochemical analysis of these chrysene derivatives by this method is that their reduction potential frequently lay beyond -2.0 V, nearing the limit of the electrochemical window of DCM, preventing its measurement.[186] Given this the LUMO level of each derivative was estimated using its previously determined optical E_g as in equation 2 below.

$$LUMO = HOMO + E_g \qquad [2]^{176}$$

Using the above equation, the estimated LUMO along with the estimated HOMO and E_g of each derivative investigated is presented in table 5 and figure 57 below for comparison (for clarity, a key to the substitution pattern of each derivative is presented in table 4). It should be noted at this point that these values are an estimate, useful for internal comparison but not necessarily suitable for quantitative comparison with compounds where HOMO and LUMO levels have been evaluated by different methods.

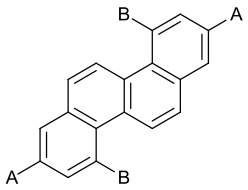

Derivative	A	B
32		
120	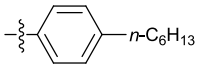	
121	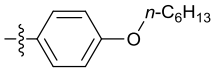	
122	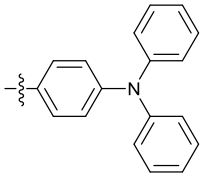	
130		
132	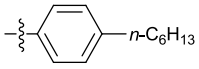	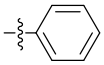
133	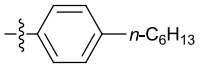	
137		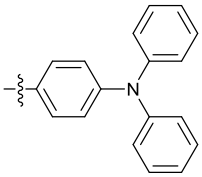

Table 4 – Substitution pattern key for each chrysene derivative investigated

Derivative	Optical E_g (eV)	Estimated HOMO level (eV)	Estimated LUMO level (eV)
32 (lit)[4]	3.26	-6.05	-2.79
120	3.07	-5.90	-2.83
121	3.06	-5.71	-2.65
122	2.96	-5.32	-2.36
130	3.15	-6.43	-3.28
132	3.08	-5.72	-2.64
133	3.07	-5.36	-2.29
137	2.92	-5.34	-2.42

Table 5 – Summary of the electronic properties of the chrysene derivatives analysed determined by UV-vis absorption spectroscopy and CV

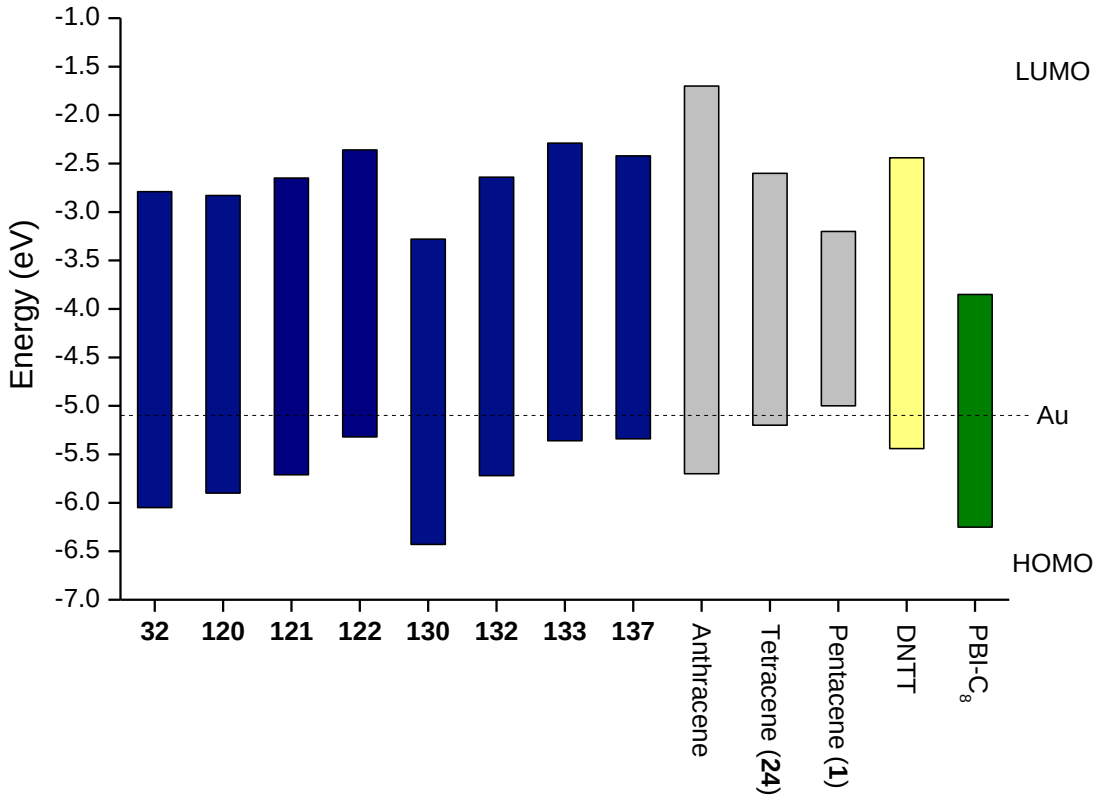

Figure 57 – Graphical representation of the estimated HOMO and LUMO levels of **32** (lit)[4], the chrysene derivatives investigated (blue) compared with those of acenes (grey),[187, 188, 189] p-type material DNTT (yellow),[190] n-type material *n*-C_8H_{17} substituted perylene bisimide (PBI-C_8) (green)[191, 192] and the work function of gold (-5.1 eV)[193]

In review of the data presented in table 5 and figure 57, it can be observed that **120** has a slightly reduced E_g when compared with its parent compound **32** and features a higher HOMO and lower LUMO, likely due to increased conjugation upon the installation of 4-*n*-hexylphenyl substituents at the 2,8-positions of the chrysene core. The observed HOMO and LUMO levels are steadily increased in **121** and **122** as increasingly electron releasing substituents are added. **122** in particular features a significant reduction in E_g due to the installation of very strongly electron donating 4-(diphenylamino)phenyl groups. Compared with its parent compound **120**, the additional substitution of a phenyl group at the 4,10-positions in **132** results in higher HOMO and LUMO levels while the E_g is largely unchanged. This effect is even more pronounced in **133** owing to use of the more electron rich thiophene moiety. In **130** the installation of strongly electron withdrawing trifluoromethyl moieties results in a large decrease in the HOMO and LUMO although the observed E_g (while smaller than **32**) is still large.

Donor-acceptor chrysene **137** exhibits the smallest E_g among the chrysene derivatives investigated with a dramatically increased HOMO relative to **130** in spite of the presumably out-of-plane positioning of the 4,10-substituted 4-(diphenylamino)phenyl substituents. Owing to its donor-acceptor structure **137** also features a relatively deep LUMO, lower than either **122** or **133**. In particular chrysenes **122**, **133** and **137** compare well with bench-mark literature materials such as tetracene or DNTT with comparable HOMO and LUMO levels, suggesting possible applications as p-type materials. This is dependent however on their crystal structures allowing charge transport, which may be doubtful for **133** and **137** considering the out-of-plane twisting of the 4,10-substituents of **132** and the consequent break up of π-π stacking in its crystal structure. **137** may however show promise as an emissive material suitable for OLED applications due to its expected contorted structure which may prevent fluorescence self-quenching.[94, 97] In addition the broad, redshifted fluorescence of **137** $\left(\lambda_{max}^{fluor} = 501 \text{ nm}\right)$ is similar in nature to related *tetrakis*(diphenylamino) chrysene **43** (figure 16, section 1.1-6.2) $\left(\lambda_{max}^{fluor} = 471 \text{ nm}\right)$ which showed promise in the literature as a blue fluorescent emitter when utilised in an OLED device.[97]

2.1-3 Computational Analysis of Chrysene Derivatives

In conjunction with collaborators (Dr Joseph McDouall *et al* at the University of Manchester)[2] the investigated chrysene derivatives were further analysed computationally. Of particular interest in the analysis of these compounds were the results obtained for *bis*[4-(diphenylamino)phenyl] substituted chrysene **122** and donor-acceptor chrysene **137**. Using time-dependent (TD) DFT calculations predicted gas-phase UV-vis absorption spectra of **122** and **137** could be produced for comparison with their experimentally determined spectra as in figure 58.

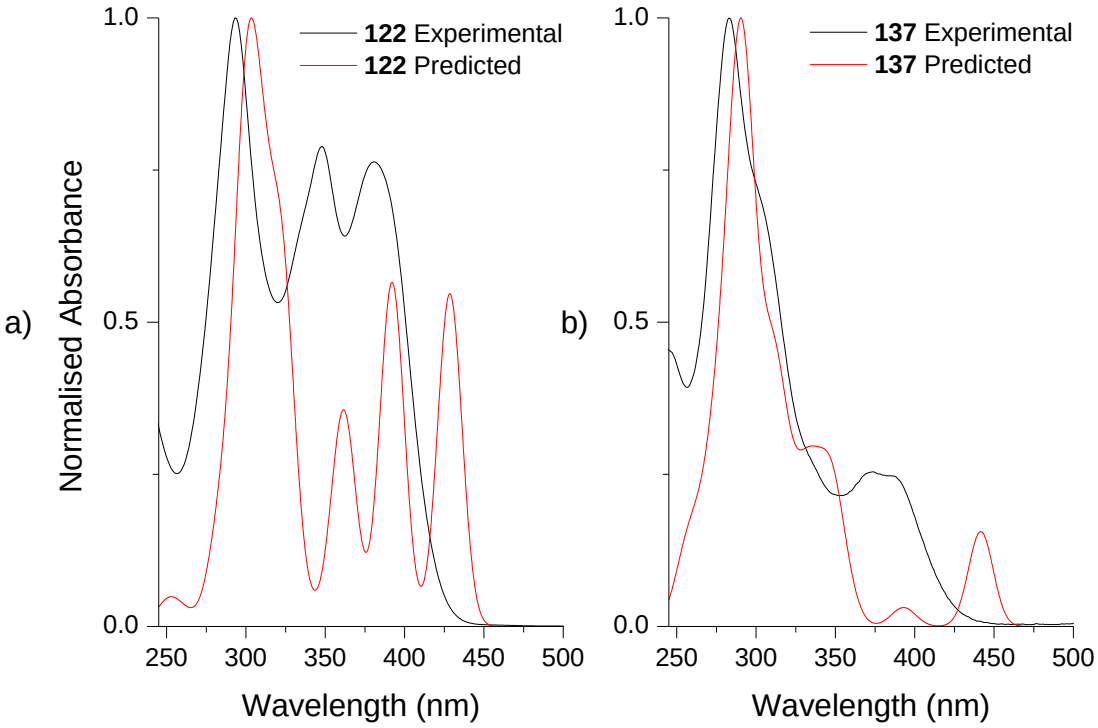

Figure 58 – Comparison of experimental and computationally predicted UV-vis absorption spectra of **122** (a) and **137** (b)

The predicted UV-vis absorption spectra produced were broadly comparable to their corresponding experimental spectra although there were some systematic errors, for instance the lowest energy transition was often too low, usually by 40-50 nm (exemplified in figure 58). The λ_{max}^{abs} however was usually very close to that of the experimental spectrum and is suggested to comprise mainly of HOMO – 1 to LUMO and HOMO to LUMO + 1 transitions.

Importantly this computational analysis allows an insight into the molecular orbital (MO) arrangements of the HOMO and LUMO levels of these compounds. This is of particular interest in **122** and donor-acceptor **137** which exhibit exceptional electronic characteristics compared to the other derivatives investigated. The computationally predicted HOMO and LUMO arrangements of **122** and **137** are displayed in figure 59.

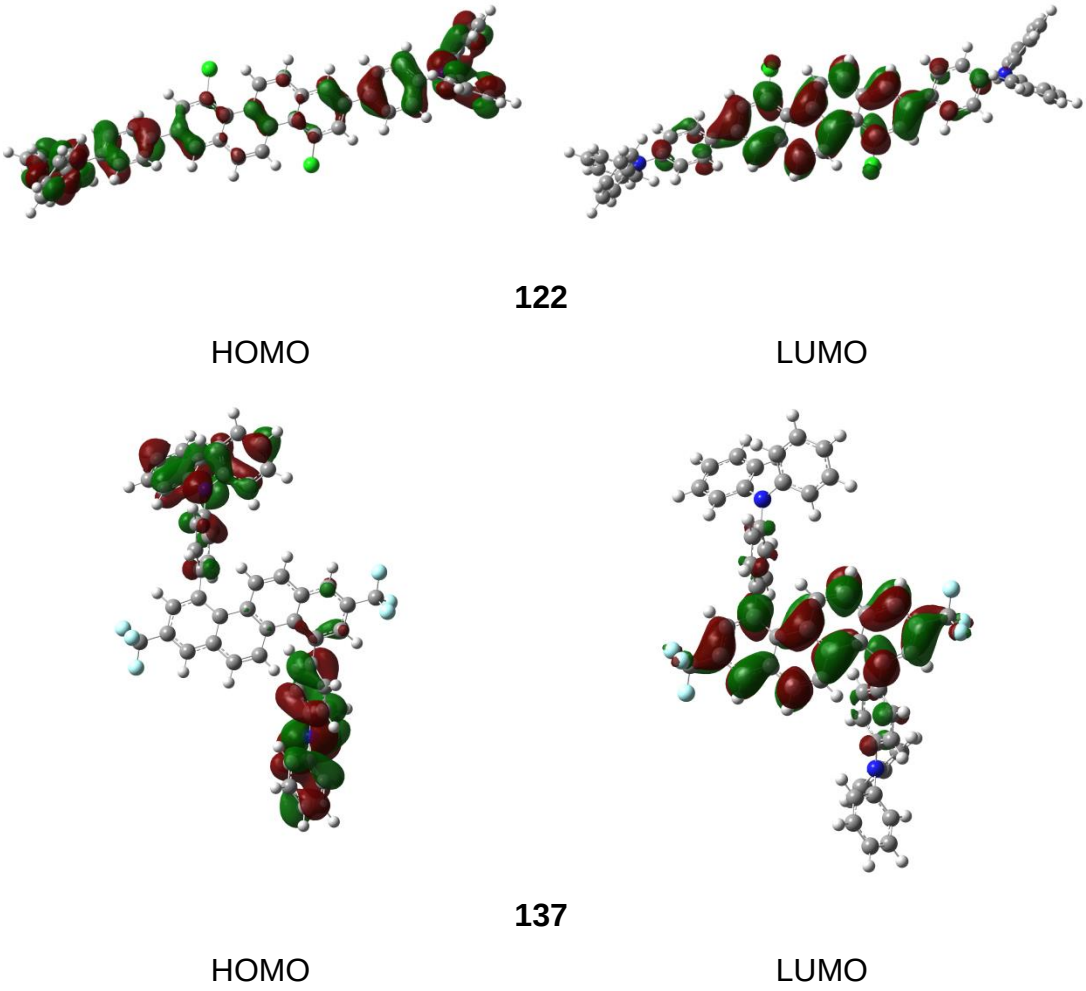

Figure 59 – Predicted HOMO and LUMO molecular orbitals of **122** and **137**

It is of note in the MOs displayed in figure 59 that the HOMO is primarily localised on the electron rich triphenylamine moieties, while the LUMO is primarily localised on the more electron deficient chrysene core. While this effect is evident in **122** (presumably due to the mildly electron withdrawing chloro functionalities) it is marked in **137** (due to the strongly electron withdrawing trifluoromethyl moieties). **137** in fact appears to experience a charge-transfer transition from the 4-

(diphenylamino)phenyl localised HOMO to the chrysene core localised LUMO in a process analogous with other donor-acceptor systems.[194] This occurs in spite of the presumably out-of-plane twisting of the 4-(diphenylamino)phenyl substituents at the 4,10-positions relative to the chrysene core. Contrasted with the apparent poor electronic communication between the 4,10-substituents and the chrysene core previously highlighted in other examples above (e.g. **132** and **133**), the effectiveness of this "A_2B_2" donor-acceptor substitution in increasing communication between substituents is considerable and may inform the future syntheses of relatively contorted conjugated structures.

2.2 Synthesis, Analysis and Application of Amphiphilic Graphene Stabilisers

2.2-1 Synthesis of Amphiphilic Graphene Stabilisers

Given the observations summarised in section 1.3-3 the synthesis of a variety of pyrene- and perylene-based amphiphilic graphene stabilisers was embarked upon. In both pyrene-based stabilisers (section 2.2-1.1) and perylene-based stabilisers (section 2.2-1.2) initial substitution focused on the installation of alkyl spacers of varying lengths; end functionalised with hydrophilic SO_3Na functionalities. These motifs were chosen as the final amphiphilic products would be asymmetrically functionalised with the sodium salt of the charged hydrophilic functionality, with alkyl spacers separating the hydrophilic and aromatic functionalities, thus fulfilling key structural requirements proposed in section 1.3-3. It was also identified that the application of the previously investigated iridium-catalysed aromatic C-H borylation and the subsequent substitution of these additional positons on the aromatic cores used, may enable the further tailoring of the synthesised stabilisers to maximise their potential performance.

2.2-1.1 Synthesis of Pyrene-Based Stabilisers

Upon analysis of the synthetic literature, it was noted that the Strecker sulfite alkylation offered a versatile and notionally simple route to alkylsulfonic acid salt functionalities *via* the reaction of an alkyl halide with sodium sulfite (Na_2SO_3). Utilising this as a key final step, the synthesis depicted in figure 60 was visualised, starting from the commercially available 1-pyrenebutyric acid, in which the pyrene core was already substituted at the 1-positon with a functionalised alkyl chain.

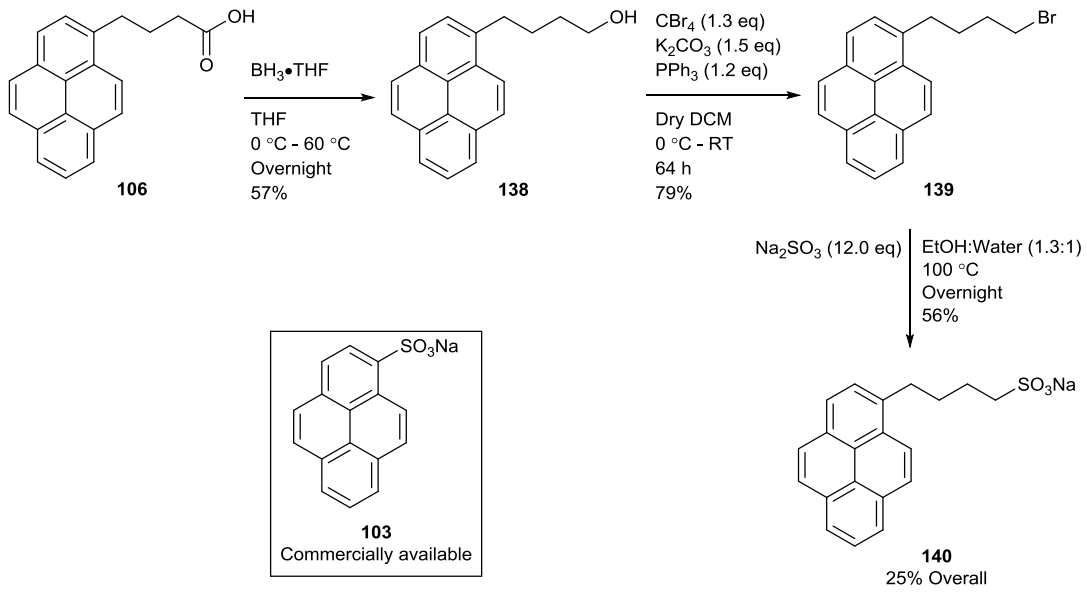

Figure 60 – Synthesis of pyrene-based stabiliser sodium 4-(pyren-1-yl)butane-1-sulfonate (**140**) compared to the commercially available sodium pyrene-1-sulfonate (**103**)

This proved to be a simple and direct synthesis of the stabiliser **140** in four steps and a 25% overall yield. It was designed to be directly comparable to the commercially available and commonly used[155, 195] stabiliser **103**, in the hope that the addition of an alkyl spacer between the hydrophilic and aromatic functionalities would result in improved stabiliser performance. This synthesis was simplified as bromoalkyl pyrene **139** was already known in the literature,[196] although literature procedures of Strecker sulfite alkylation reactions were largely limited to bromoalkyl substituted phenyls[197] or in one case naphthalene.[198] This raised concerns of the solubility of a larger pyrene-based system in the necessary alcohol/water-based solvents used in this reaction, however adaptation of literature procedures allowed the successful synthesis of **140** in a 56% yield with purification accomplished by recrystallisation from a ~1.3:1 ethanol:water mixture that was concentrated *in vacuo* to the crystallisation point. The material was additionally washed with DCM and water to ensure the removal of the starting materials, **139** and Na_2SO_3.

With this first stabiliser in hand a modification of the synthesis was proposed, using the previously explored iridium-catalysed aromatic C-H borylation to access the 7-position of the pyrene core. This borylation process was initially attempted from **139**

as in figure 61 using the MWI conditions successfully applied in the borylation of 4,10-dichlorochrysene (**32**) (figure 39, section 2.1-1.1).

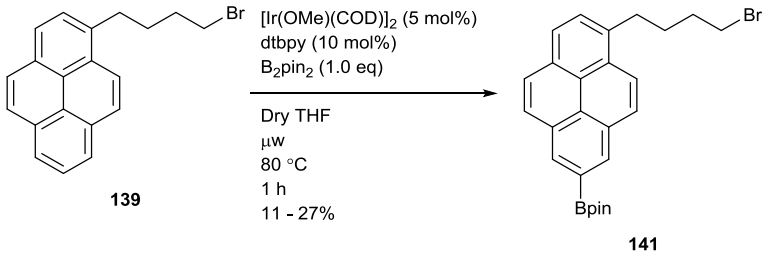

Figure 61 – Low yielding iridium-catalysed aromatic C-H borylation of bromoalkyl **139**

While this reaction was successful, it proved low yielding, with **141** initially isolated in only 11% yield after column chromatography, while a larger scale repeat synthesis isolated a 27% yield of lower purity product. These yields were far lower than anticipated (the diborylation of 4,10-dichlorochrysene (**32**) achieved isolated yields of 73%, with 90% conversion under MWI conditions) and in this case significant quantities of starting material were reclaimed from the reaction mixture, suggesting deactivation of the catalyst due to intolerance of bromoalkyl groups. Due to this functional group intolerance the reaction scheme as shown in figure 62 was settled upon, utilising an alternative route.

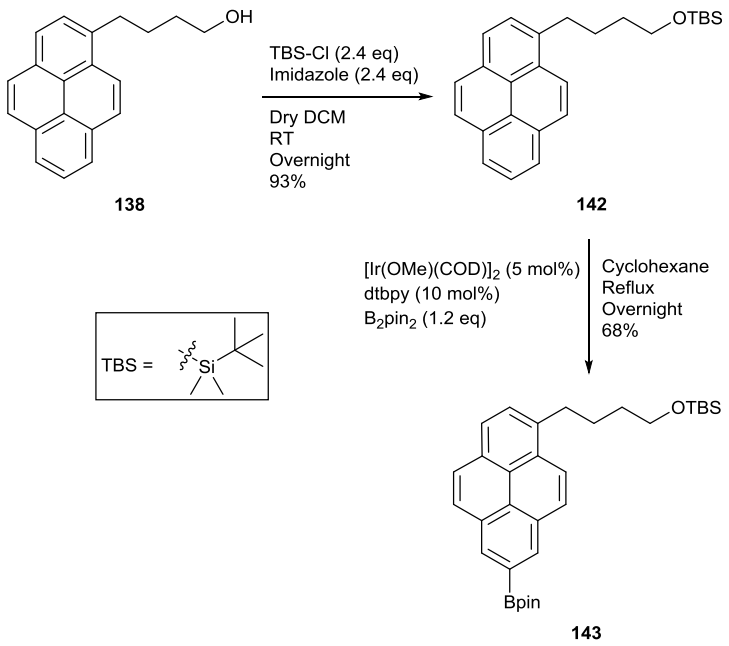

Figure 62 – Aromatic C-H borylation of TBS protected pyrene **142**

In this synthetic route the alcohol functionality of **138** was protected with a *tert*-butyldimethylsilyl (TBS) protecting group as it was strongly suspected such a functionality may once again interfere with the catalytic aromatic C-H borylation step.[199] Pleasingly the borylation of **142** featured a significantly improved crude ^{1}H NMR spectrum compared to the borylation of **139**, although notably the reaction did not proceed as smoothly as the aromatic C-H borylation of 4,10-dichlorochrysene (**32**) and column chromatography was required to obtain the pure product. This resulted in a 37% yield of analytically pure material, but after flushing the column and precipitating that flushed material three times from methanol, an overall 68% yield of ~95% pure product was obtained. Figure 63 compares the aromatic region of the ^{1}H NMR spectra of **142**, the crude borylated product and pure **143** indicating successful C-H borylation. The aromatic region of **143** integrates to one less proton compared to **142** and two low field 1 H singlets appear at ~8.6 ppm, presumably corresponding to the two protons *ortho*- to the borylated positon. Not shown is the additional 12 H singlet in the aliphatic region of the spectrum which corresponds to the boronic pinacol ester methyl groups of **143**.

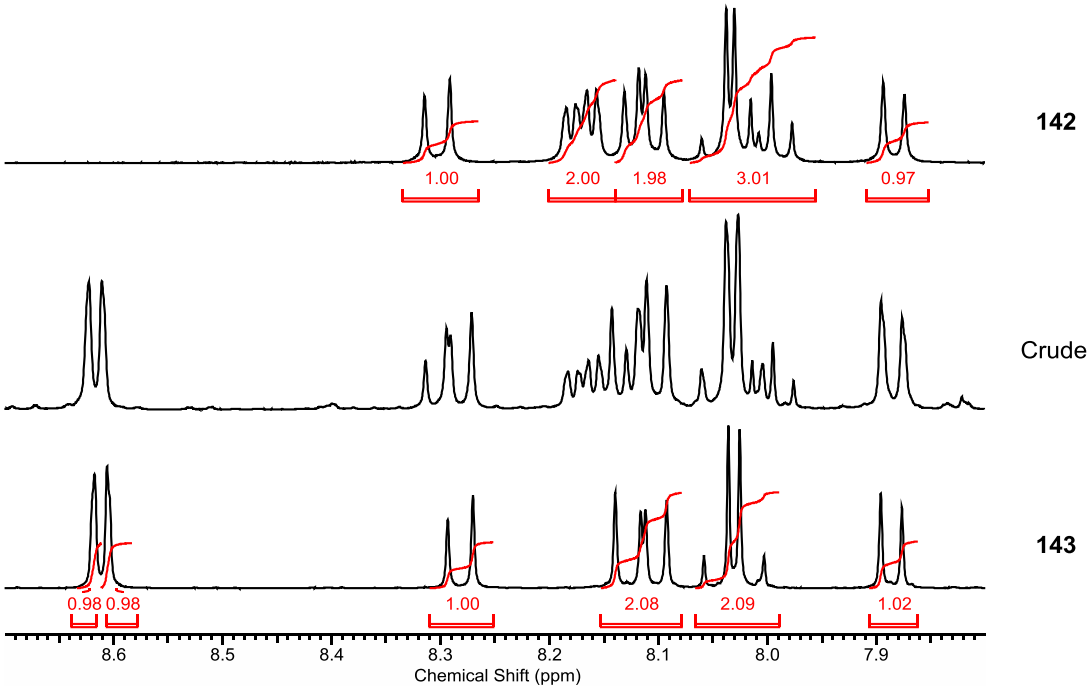

Figure 63 – ^{1}H NMR spectra (aromatic region) of **142**, the crude reaction mixture and **143**

The next step in this synthesis was to introduce an electronegative functionality at the borylated 7-position to both induce a dipole across the aromatic core and make the pyrene system more electronegative. A nitrile functionality was selected to do this, primarily as whilst being electron withdrawing, it would also maintain the planarity of the system, sterically hindering pyrene-graphene π-π interactions as little as possible. A variety of methods exist in the literature to cyanate borylated aromatics, for example **143** could be converted to the corresponding boronic acid and engage in a copper-catalysed cyanation as described by Liebeskind *et al*[200], however the most common method is a direct copper mediated cyanation utilising $ZnCN_2$ as a nitrile source.[201] This second method appeared more reliable, having been described by a variety of authors[124, 202] and having been performed on borylated pyrene derivatives previously (figure 25, section 1.2-3).[117] This method was additionally advantageous as it did not require prior conversion to the boronic acid, allowing its adaptation to **143** as in figure 64.

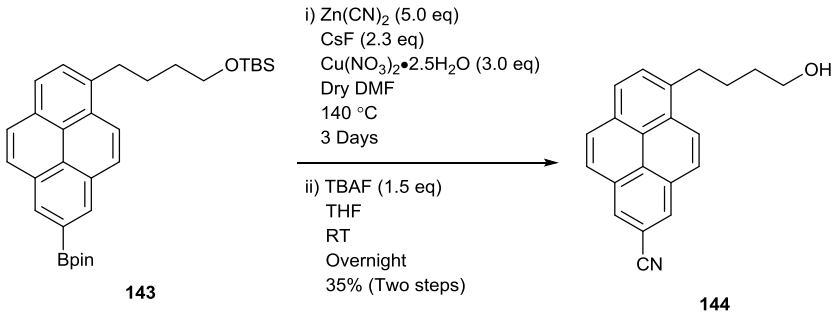

Figure 64 – Cyanation and TBS deprotection of boronic ester **143**

This cyanation methodology however did result in partial deprotection of the OTBS group of **143**, most likely due to the presence of CsF in the reaction mixture at high temperatures and over a prolonged reaction time. Due to this effect the formal deprotection reaction with TBAF was conducted on the crude reaction mixture directly after workup. This process yielded the cyanated, deprotected pyrene **144** in a 35% overall yield. At this stage **144** was then reacted analogously to **138** in two subsequent steps, forming bromoalkyl **145** and finally the alkylsulfonic acid salt **146** as in figure 65 below. This process yield the cyanated stabiliser **146** in a 6% overall yield as a more election deficient, stronger dipole containing product to complement **140**.

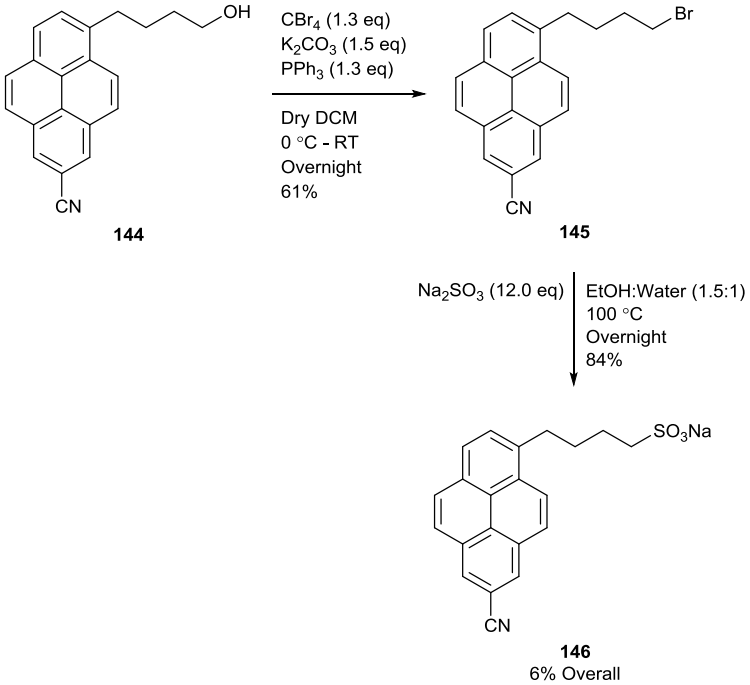

Figure 65 – Synthesis of nitrile containing pyrene-based stabiliser **146**

2.2-1.2 Synthesis of Perylene-Based Stabilisers

Following the successful synthesis of the pyrene-based stabilisers above (section 2.2-1.1) the synthesis of a variety of analogous perylene-based stabilisers was conducted. Not only did this enable the investigation of a larger aromatic core but due to the lack of commercially available substituted perylenes, this synthesis was conducted from the unsubstituted core perylene (**74**) enabling the installation of alkyl spacers of a variety of chain lengths. Once again, the first target compounds were the hydroxyalkyl substituted aromatic cores **157-159** as in figure 66 below.

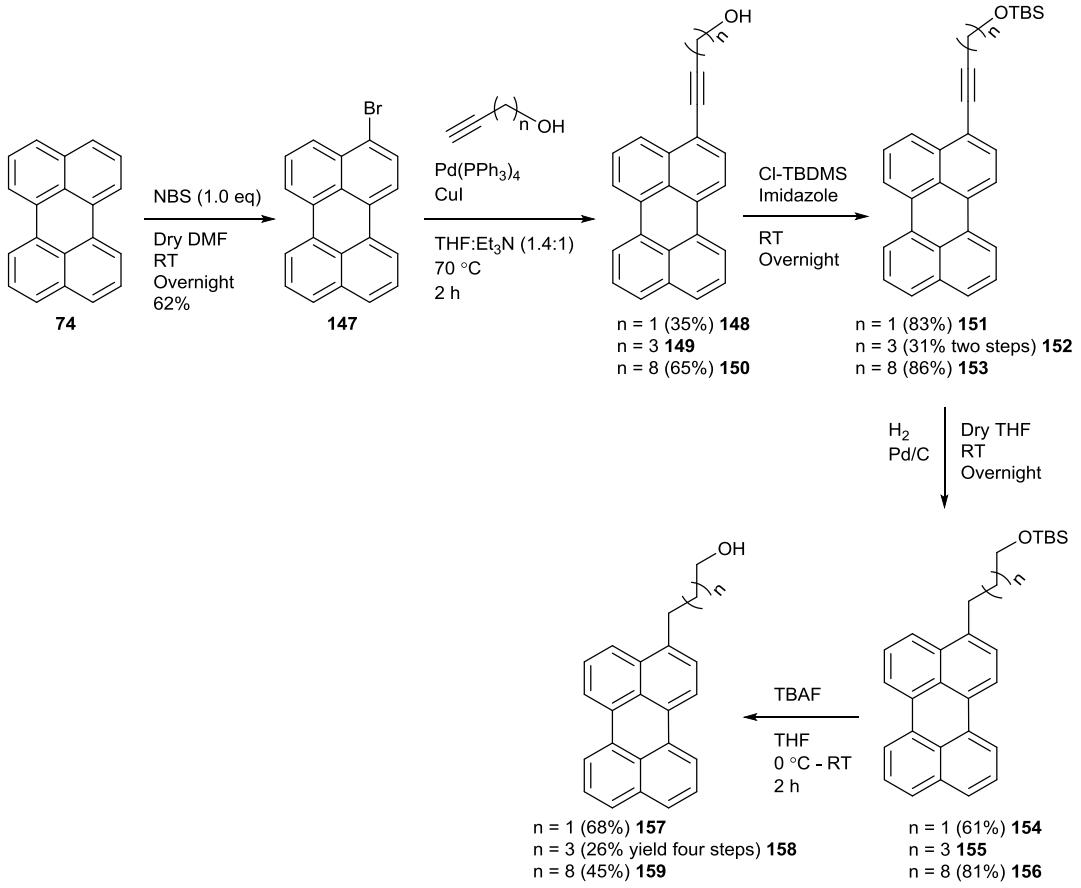

Figure 66 – Synthesis of hydroxyalkyl perylene derivatives of a variety of chain lengths

The synthetic route described in figure 66 was based on the work by Rebek *et al*[203] who previously demonstrated the synthesis of **158** *via* this route. After brominating the core perylene **74** with NBS, the brominated perylene **147** could then be further functionalised though a Sonogashira coupling with the desired alkynol. Of note in this synthesis is the practice of protecting the alcohol group after this coupling step,

which while not necessary to complete the reduction of the alkyne to the alkyl, significantly simplifies purification due to improved solubility. In particular the yield of **152** (as similarly reported by Rebek *et al*) is recorded over two steps due to the difficult and wasteful process of purifying **149** by column chromatography. As compounds **148** and **150** were novel, they were isolated directly after coupling, however yields were impacted by this, particularly **148** (isolated in a 35% yield) which featured extremely low solubility in common organic solvents necessitating NMR analysis in DMSO-d_6. It is noteworthy that in repeat syntheses of these compounds yields could be significantly improved by performing only partial purification of **148-150** (utilising a short silica plug, eluting with up to 100% ethyl acetate) and completing purification by controlled column chromatography and recrystallisation on the TBS protected perylene derivatives **151-153**. Solubilised perylenes **151-153** could then be reduced to their corresponding alkyl derivatives though treatment with palladium on carbon under a hydrogen atmosphere. These could then be subsequently deprotected by TBAF to yield the corresponding hydroxyalkyls **157-159**. **155** was carried directly though in the deprotection reaction (as reported by Rebek *et al*)[203] to yield **158** in a 26% yield over four steps while **154** and **156** were isolated and characterised. In order to isolate **154** and **156** it was important to maintain anhydrous conditions during the hydrogenation process as partial deprotection of the OTBS group was observed when the THF solvent was not appropriately dry. While unexpected, such observations have been previously noted in the literature when using non-anhydrous solvents under these hydrogenation conditions.[204]

The yields of this hydrogenation process are recorded as lower than would be expected. This was due to the appearance of a small quantity of unknown impurity after the hydrogenation step that proved difficult to remove by column chromatography and in **154** and **156** necessitated an additional recrystallisation step. This resulted in particularly low yields of **154** as the impurity was almost inseparable by column chromatography. It was noted when performing the TBAF deprotection and subsequent bromination steps (figure 68) of partially purified samples that the impurity propagated though each reaction, each time very similar in polarity (by TLC) to the desired product and therefore difficult to remove by column chromatography. Eventually when performing column chromatography of **160**

(figure 68) a purified sample of this impurity was isolated (albeit contaminated with a small quantity of the target compound), a proposed structure of which is identified in figure 67.

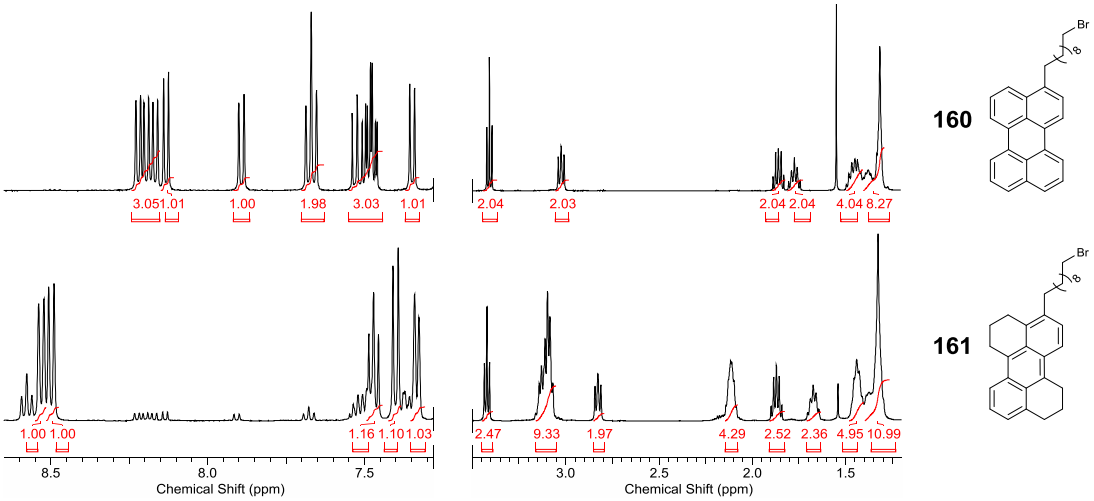

Figure 67 – ^{1}H NMR aromatic and aliphatic regions of target compound **160** and impurity **161**

It can be immediately suggested that the impurity arose from a reaction at the aromatic core of **151-153** as the impurity propagates though each additional step with similar polarity (by TLC) as that of the target compound. The ^{1}H NMR spectra in figure 67 indicates five aromatic protons compared to the 11 found in the target compound, consisting of four doublets and a triplet, each integrating to 1 H. In the aliphatic region a shift is observed in the benzylic protons of the alkyl substituent and also the introduction of new benzylic protons (~3.2 ppm) and new aliphatic protons (~2.2 ppm) is observed. This ^{1}H NMR data very strongly indicates the partially hydrogenated aromatic **161** suggested in figure 67, matching the expected aromatic signals and producing appropriate aliphatic and benzylic signals. This data is further compounded by analysis by mass spectrometry (APCI) which indicates two approximately equal intensity peaks at 477 and 479 corresponding to the $[M(^{79}Br) + H]^{+}$ and $[M(^{81}Br) + H]^{+}$ molecular ion peaks of the proposed impurity respectively, confirming the presence of bromine in the compound and its molecular weight to be that of the proposed structure **161**, as further confirmed by high resolution mass spectrometry. This observation of the partial hydrogenation of a perylene core is possibly the only reported example of the formation of a

hexahydroperylene by this method although examples do exist in the literature of the partial hydrogenation of hexabenzocoronene[205] and pyrene[206] cores under higher pressures and temperatures.

After the successful formation of **157-159** the subsequent Appel bromination and Strecker sulfite alkylation reactions could be performed as in figure 68 to isolate the final perylene-based alkylsulfonic acid salt substituted stabilisers **164-166**.

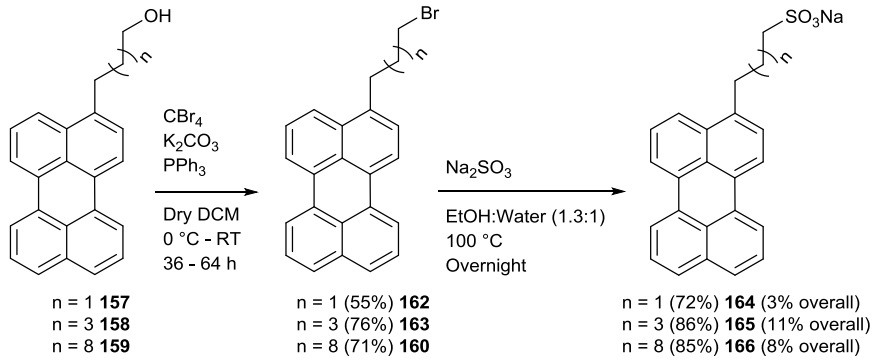

Figure 68 – Appel bromination and Strecker sulfite alkylation reactions of substituted perylene derivatives

The final desired perylene-based graphene stabilisers **164-166** were synthesised from unsubstituted perylene in overall yields of 3%, 11% and 8% respectively across seven synthetic steps. A likely reason for the low overall yield of **164** is the relative insolubility of its intermediate derivatives compared to those of **165** and **166**. Due to its relatively short alkyl chain, **157** and in particular its precursor acetylene **148** (figure 66) were more difficult to handle and purify than their related longer chained analogues (**148** for example being only sparingly soluble in DCM or chloroform). In addition the silylated derivative **154** (figure 66) was the most difficult to separate from its hexahydroperylene impurity lowering the yield of the hydrogenation of **151** to 61%.

With the successful synthesis of **164-166** completed, attention turned to the application of the previously investigated iridium-catalysed aromatic C-H borylation to a 3-substituted perylene core, in a process analogous to the functionalisation of pyrene derivative **142** (figure 62, section 2.2-1.1). Notably this borylation would be expected to produce a 5,8,11-triborylated perylene derivative with an entirely novel

perylene functionalisation pattern, as such aromatic C-H borylations have only been previously applied to perylene bisimides[125] (**87**, figure 27, section 1.2-3) and the tetraborylation of unsubstituted perylene (**74**, figure 24, section 1.2-3) as in the work of Perutz *et al.*[115] Additionally, the tetraborylated perylene **75** appears to have only been used in subsequent reactions twice in the literature, each time Suzuki coupled to an aromatic group, once to investigate assembly at metal-organic interfaces[207] and once as a spacer in multiporphyrin arrays.[208]

In order to test the selectivity of this borylation on a readily available precursor, 3-bromoperylene (**147**) was triborylated under MWI conditions as in figure 69 below.

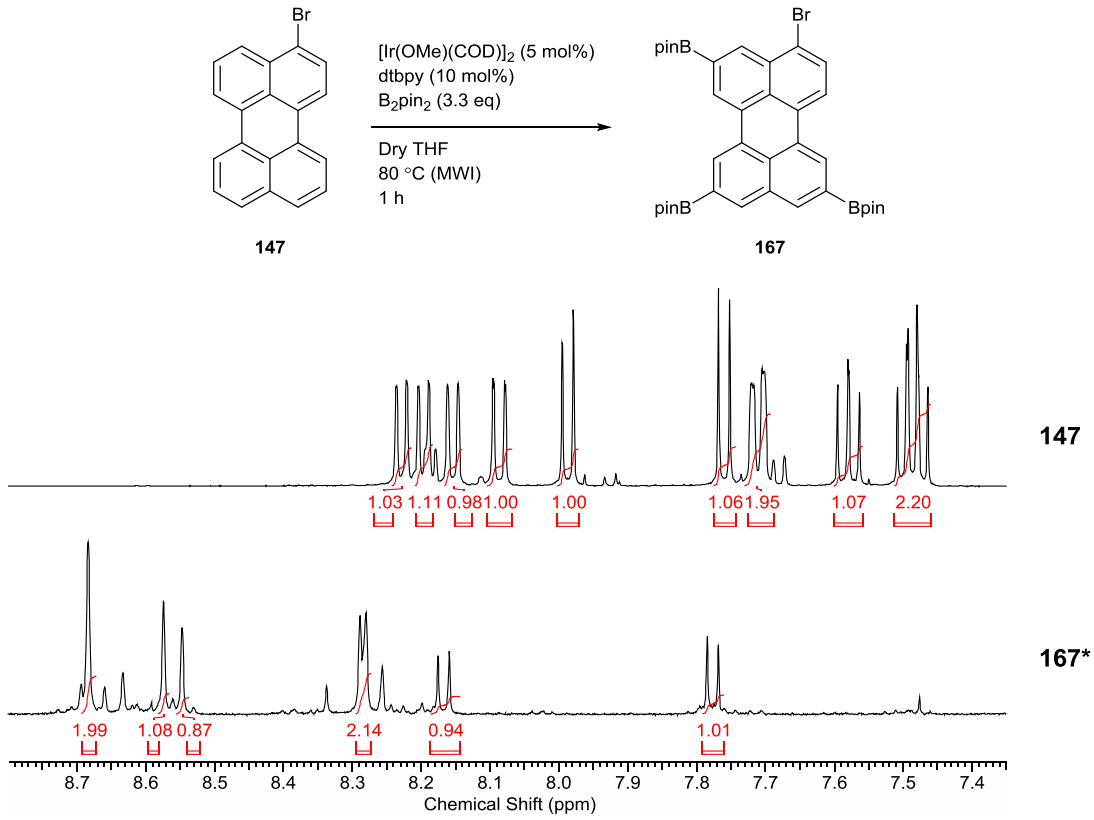

Figure 69 – Test borylation of **147** to form triborylated **167** and the associated ^{1}H NMR spectra (aromatic region) of the corresponding compounds. *^{1}H NMR spectra of **167** corresponds to the partially purified compound though trituration with methanol.

The reaction proved successful, although some associated additional products are present after trituration. Diborylated isomers from incomplete reactions along with

tetraborylated products (suggesting the possibility of limited borylation at the 1- or 2-positons) were identified by mass spectrometry. Such impurities appear to be minor however with the desired triborylation shown to proceed relatively smoothly by ^{1}H NMR spectrometry (figure 69).

With this promising test reaction in hand, TBS protected perylene **154** featuring a *n*-C_3H_6 alkyl spacer group was selected for additional functionalisation *via* this aromatic C-H borylation. **154** was chosen in particular as it was considered that additional functionalisation at the 5,8,11-positions may reduce the aqueous solubility of the final stabiliser and of the alkylsulfonic acid salt substituted derivatives **164-166**, **164** featuring the shortest chain also featured the highest aqueous solubility. **154** was therefore borylated under standard conditions utilising cyclohexane as a solvent (figure 70). Notably **154** featured far higher solubility in common organic solvents than **147**, hence microwave irradiation in a THF solvent system was unnecessary and "standard" reaction conditions (utilising cyclohexane as a solvent) were adopted.

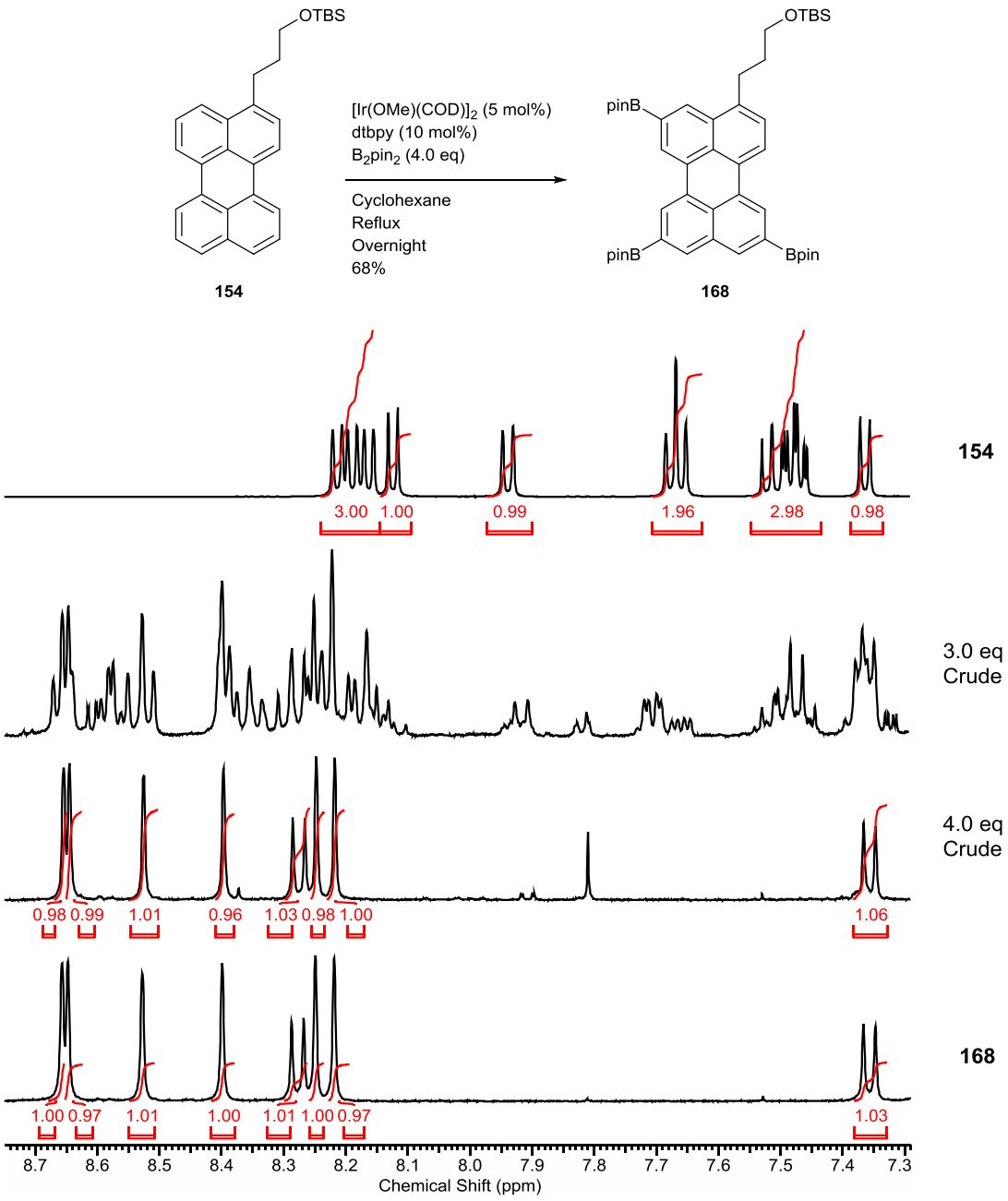

Figure 70 – The *tris* C-H borylation of **154** and the associated ^{1}H NMR spectra (aromatic region) of **154**, **168** and the crude reaction mixture when using 3.0 and 4.0 equivalents of B_2pin_2

As observed in figure 70 the use of 3.0 equivalents of B_2pin_2 resulted in a complex mixture of regioisomers while the use of 4.0 equivalents of B_2pin_2 drove the reaction to completion by ^{1}H NMR analysis. Interestingly, the borylation of 4,10-dichlorochrysene (**32**) proceeded essentially to completion with 2.0 equivalents of B_2pin_2, while the additional complexities and borylation sites of **154** require additional equivalents of B_2pin_2 to allow for inefficiencies in the borylation process,

indeed Perutz *et al*[115] when performing a tetraborylation of unsubstituted perylene used 4.4 equivalents of B_2pin_2 in order to obtain the desired product in an 83% yield.[115]

With the successful synthesis of triborylated perylene derivative **168**, the initial aim was to subject **168** to the same conditions previously used to successfully cyanate the analogous borylated pyrene **143** (figure 64). It was soon observed however that the reaction was not efficient enough to complete the tricyanation with meaningful yield. In the monosubstitution of **143**, **144** (figure 64) was isolated in a yield of 35% (over two steps). Given this, a tricyanation of **168** could be expected to provide yields as low as ~4%. This low value also does not take into account any deactivating effects that may occur as the compound is sequentially cyanated, a process that along with a potential decrease in solubility, may further depress potential yields.

At this stage alternative syntheses were considered, notably the bromination of **168** with $CuBr_2$, with the hope of preparing the corresponding 5,8,11-tribromo substituted perylene derivative (a methodology used in the literature to brominate borylated pyrene derivatives,[116, 117] figure 25, section 1.2-3). Such a brominated derivative could then be cyanated more reliably by treatment with CuCN.[209] Perylene derivative **168** however proved relatively unstable and disappointingly decomposed during the attempted reaction with $CuBr_2$.

It was therefore decided a more viable synthesis would be the oxidation of **168** to 5,8,11-trihydroxyperylene derivative **169** (figure 71). This was decided on the basis of both synthetic availability and the potential of such hydroxyl groups to enhance stabiliser performance. Indeed both Palermo *et al*[154] and Lukkari *et al*[156] studied hydroxyl containing stabilisers **108** (figure 31, section 1.3-2.1) and **117** (figure 34, section 1.3-2.4) showing them to enable the stabiliser to "slide" into π-π interactions with the graphene surface and to engage in graphene-OH interactions respectively.

This oxidation however proved more challenging than anticipated. 2,8-Diboryl-4,10-dichlorochrysene derivative (**118**) had previously been oxidised to the corresponding 2,8-diol (**131**, figure 44, section 2.1-1.2) using basic H_2O_2. In a test reaction these same conditions were applied to the readily available 5,8,11-triborylpeylene

derivative **167**, however it was observed to rapidly decompose under these conditions, perhaps indicating oxidative instability. In the literature a similar observation was noted by Shinokubo *et al*[119] in which a diboryl hexabenzocoronene derivative was observed to decompose when subjected to oxidation with H_2O_2. This was overcome though the use of Oxone® ($KHSO_5$•½$KHSO_4$•½K_2SO_4) as an oxidant in a THF:acetone:H_2O solvent system. These conditions could be successfully applied to **168** to form the target compound **169**, the presence of which was confirmed by ^{1}H NMR of the crude reaction mixture (figure 71) and by high resolution mass spectrometry.

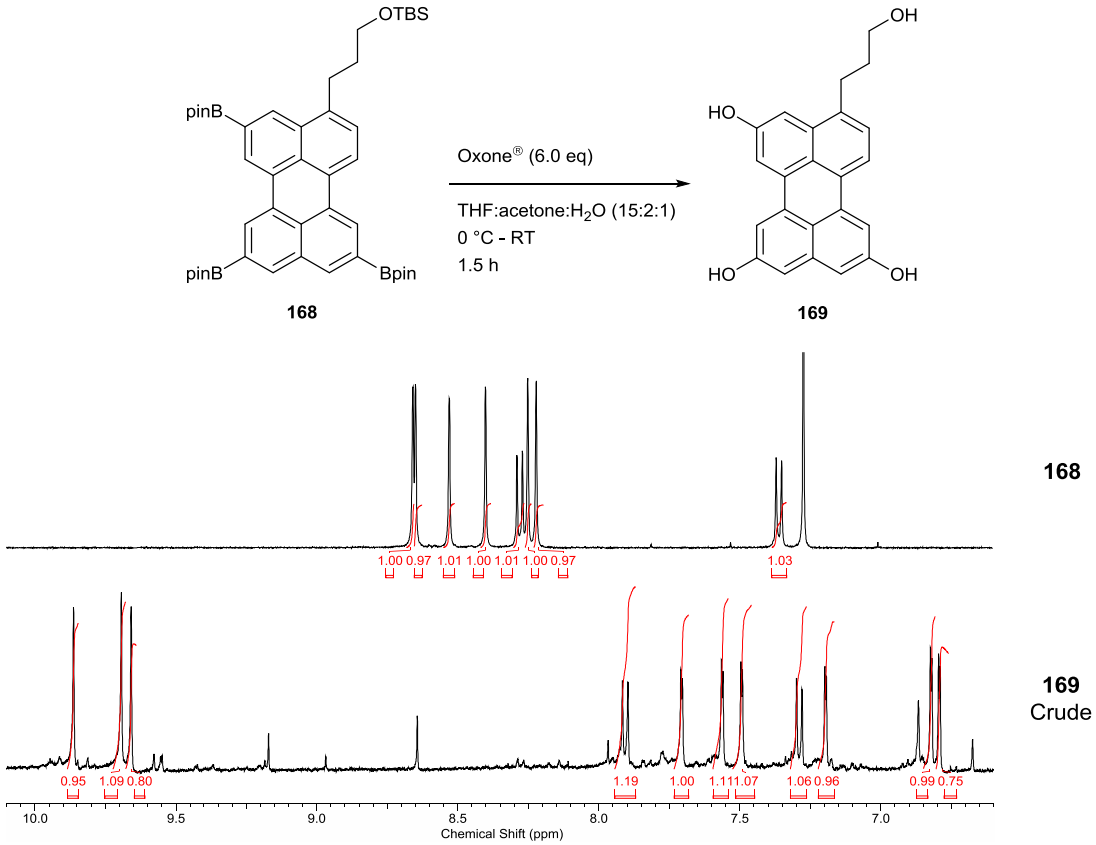

Figure 71 – Oxone® oxidation of triboryl perylene **168** to the TBS deprotected triol **169** and the associated ^{1}H NMR spectra (aromatic region) in $CDCl_3$ and DMSO-d_6 respectively

Utilising Oxone® the crude ^{1}H NMR spectrum indicated significant product formation, showing **169** to be the major component with little detectable decomposition and the clear appearance of three phenolic protons between 9.5-10 ppm (as expected in DMSO-d_6). Notably, the relatively acidic conditions associated

with Oxone® resulted in almost complete deprotection of the OTBS group and although this was not considered a disadvantage (as the following synthetic step was a TBS deprotection) resultant compound **169** was extremely polar and proved difficult to purify. Despite the promising crude ^{1}H NMR spectrum (figure 71) elution though a silica plug even with a solvent system as polar as 10% methanol in DCM resulted in the isolation of only a partially purified product in a yield as low as 11%. The reaction was repeated on multiple occasions with the intention of purifying the target compound by trituration or recrystallisation, however the results obtained in figure 71 proved irreproducible in subsequent attempts. In particular ^{1}H NMR and TLC analysis indicated difficulty quenching the reaction at the appropriate point, after the starting and intermediate materials had been consumed but before decomposition occurred. In an attempt to control the oxidation process the stepwise addition of a solution of Oxone® over 1.7 hours, followed by a formal deprotection of the OTBS group with TBAF (to ensure complete deprotection) was also attempted, however once again a complex mixture was formed that could only be partially purified though trituration. Frustratingly, when this method was applied to 2,5,8,11-tetraboryl perylene **75** (synthesised by adaptation of the literature procedure by Perutz *et al*[115], figure 24, section 1.2-3) the desired product (**170**) was successfully formed with relatively little decomposition and is clearly identifiable in the crude ^{1}H NMR spectrum (figure 72).

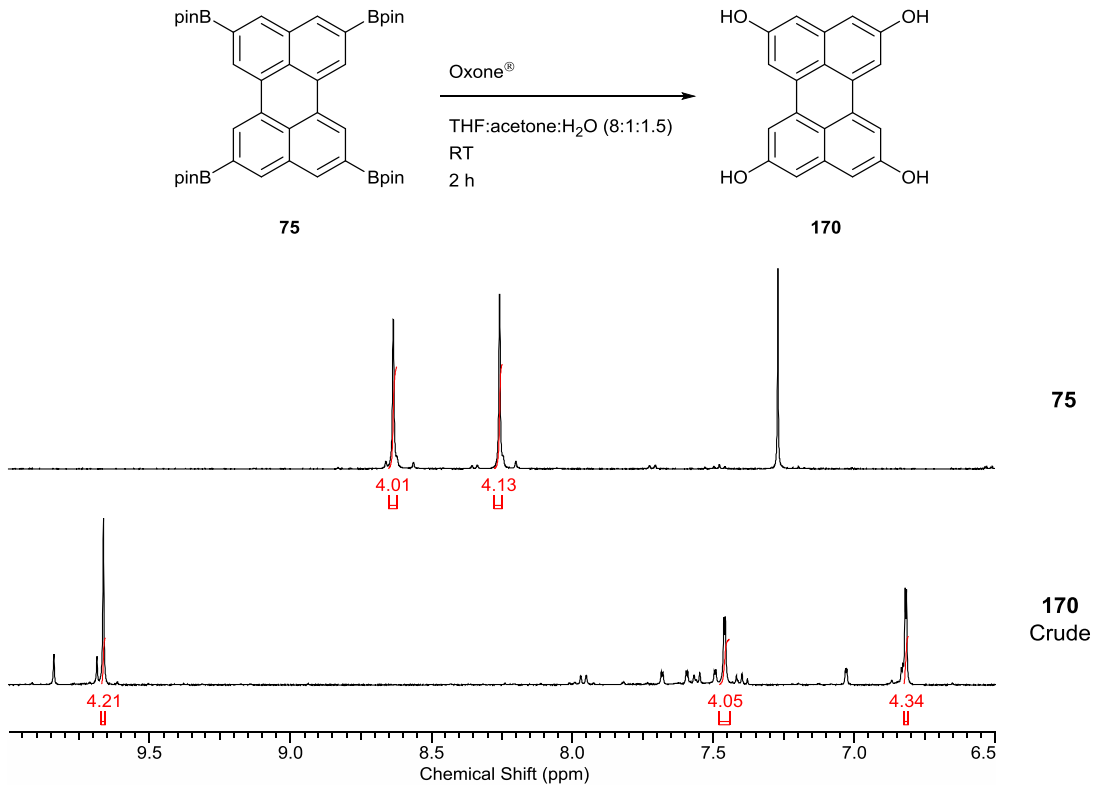

Figure 72 – Oxone® oxidation of perylene **75** to form tetrahydroxy perylene **170** and the associated ^{1}H NMR spectra (aromatic region) in $CDCl_3$ and DMSO-d_6 respectively.

Overall these results suggest that while the perylene core may not be intrinsically oxidatively unstable, it can be extremely sensitive to oxidising conditions (as perylene derivative **168** certainly demonstrates) and this will have to be taken into careful consideration when planning future syntheses. Ultimately the sensitivity of **168** to oxidative conditions prevented the isolation of **169** in sufficient quantities and purities to complete the proposed synthesis of **172** (figure 73).

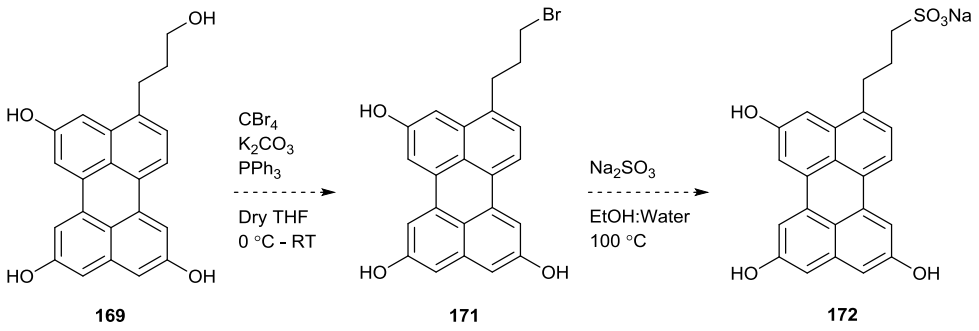

Figure 73 – The two remaining synthetic steps to stabiliser **172**

In order to complete the synthesis of target molecule **172** a milder oxidative method would first need to be identified in order to reliably access precursor **169** and this will be the subject of further work (section 3.2). It is however notable that the remaining synthetic steps to **171** and **172** should be readily be applicable to **169**. It is noted in the literature that both processes are tolerant of phenolic functional groups[210, 211] and as shown in this work, both can be readily applied to perylene-based derivatives (figure 68). The potential difficulties involved in purification and handling of intermediates **169** and **171** however remains a concern.

2.2-2 Computational Analysis of Amphiphilic Graphene Stabilisers

As the stabiliser synthesis described in section 2.2-1 evolved, the potential value of computational calculations regarding stabiliser performance became apparent. Computational molecular dynamics simulations were performed by our collaborators (Dr Flor Siperstein *et al* at the University of Manchester)[212] to help validate our proposed stabiliser designs. These investigations were inspired in part by the work of Palermo *et al*[154] (reviewed in section 1.3-2.1) where molecular dynamics simulations were utilised to help elucidate the mechanism by which different pyrene-based stabilisers approach the graphene surface in aqueous solution.

Using molecular dynamics simulations, potential of mean force (PMF) curves were generated for each of the stabilisers outlined in section 2.2-1 that we hoped to synthesise. These studies investigated the free energy of the stabiliser in an aqueous medium at various distances from the graphene surface. The computations were conducted using a simulation cell (3.68 nm × 3.83 nm × 5.00 nm) with the graphene sheet positioned in the x-y plane at z = 0. Periodic boundary conditions were used to simulate an infinite graphene sheet. The generated PMF curves of each stabiliser are shown in figure 74.

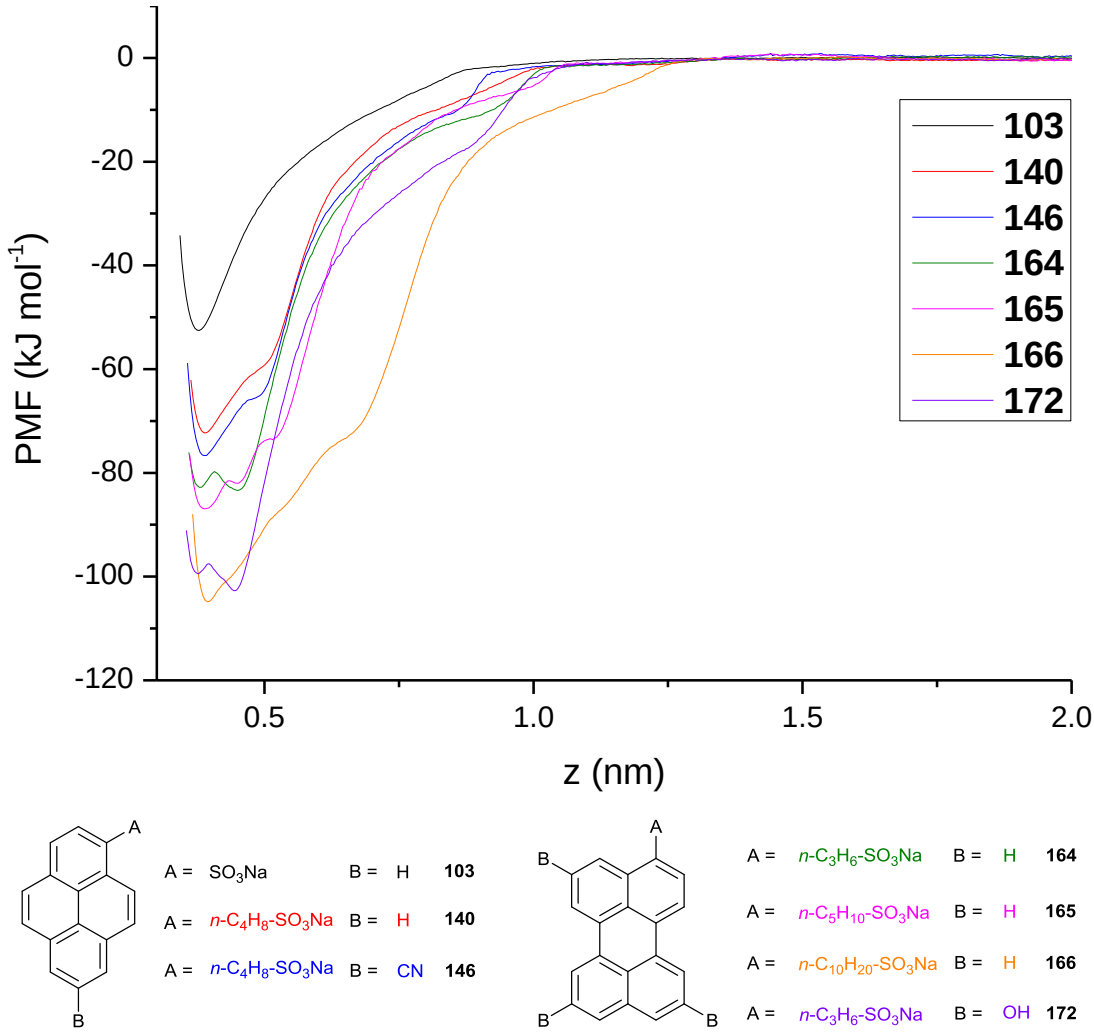

Figure 74 – Calculated PMF curves of each of the proposed stabilisers

As previously described figure 74 plots changes in the free energy of each stabiliser against the distance of the centre of mass of the stabiliser from the graphene surface on the z axis. As expected the general trend observed is that as the stabiliser approaches the surface, the free energy decreases to a minimum after which it sharply increases as repulsion overcomes the system. The adsorption free energy of each stabiliser (determined from the PMF minima) and the associated distance from the surface along the z axis can be summarised as table 6.

PAH Core	Motif	Derivative	Adsorption Free Energy (kJ mol^{-1})	z (nm)
Pyrene	A = SO_3Na B = H	**103**	-52.5 ± 0.2	0.38
	A = *n*-C_4H_8-SO_3Na B = H	**140**	-72.3 ± 0.8	0.39
	A = *n*-C_4H_8-SO_3Na B = CN	**146**	-76.7 ± 0.9	0.39
Perylene	A = *n*-C_3H_6-SO_3Na B = H	**164**	-83.4 ± 0.5	0.45
	A = *n*-C_5H_{10}-SO_3Na B = H	**165**	-86.9 ± 1.2	0.39
	A = *n*-$C_{10}H_{20}$-SO_3Na B = H	**166**	-104.8 ± 0.9	0.39
	A = *n*-C_3H_6-SO_3Na B = OH	**172**	-102.7 ± 0.8	0.44

Table 6 – Calculated adsorption free energies of each stabiliser investigated and the distance from the graphene sheet (z) with which they are associated

Considering these results, it is generally observed that the larger the aromatic core and the longer the alkyl spacer, the stronger the interaction of the stabiliser with the graphene surface. This is likely due to greater π-π interactions associated with larger aromatic cores and decreased steric interactions associated with the sulfonic acid group due to the alkyl spacer. There is however relatively little difference between **164** and **165** suggesting *n*-C_3H_6 and *n*-C_5H_{10} chains are sufficient to relieve steric interactions while **166** sees a significant decrease in adsorption free energy, possibly due to additional hydrophobic interactions.

These computations predict only a marginal improvement in stabiliser interaction with the installation of a nitrile group in **146** compared with **140**. This is likely due to the nature of the calculations performed which do not account for the potential decrease in electron density across the whole aromatic system (that could lead to charge-transfer π-π interactions) and only consider localised effects of the nitrile group. Conversely the installation of hydroxyl functionalities as in **172** produces a substantial decrease in the absorption free energy. Once again the effects of these functionalities are localised and the effect on the whole aromatic system is not considered but this result may suggest additional favourable interactions associated with the installation of phenolic functionalities.

Considering PMF curve shape, **146** exhibits similar features to that of **140** and appears to approach the graphene surface in much the same manner. Similarly while the installation of hydroxyl functionalities as in **172** produces a substantial decrease in the adsorption free energy compared to **164**, the overall PMF curve shape is also very similar, suggesting little change in manner in which the stabiliser approaches the graphene surface. This is in contrast to the results of Palermo *et al*[154] in which it was suggested that the hydroxyl functionalities present in **108** (figure 31, section 1.3-2.1) helped enable a "sliding effect" though the final layer of water molecules as the stabiliser approached the graphene surface due to an asymmetric polarity across the aromatic core. In this study we find that all of the asymmetric stabilisers investigated here approach the graphene surface initially with the sulfonic acid group orientated away from the graphene surface, before then "sliding" into a face-face π-π interaction despite a distinct lack in polarity across the aromatic core in the majority of cases.

The stabiliser graphene interactions investigated here can be exemplified by further analysis of the PMF curves of **140** and **166** as in figure 75 below, featuring associated snap shots of the orientation of the molecule as it approaches the graphene surface.

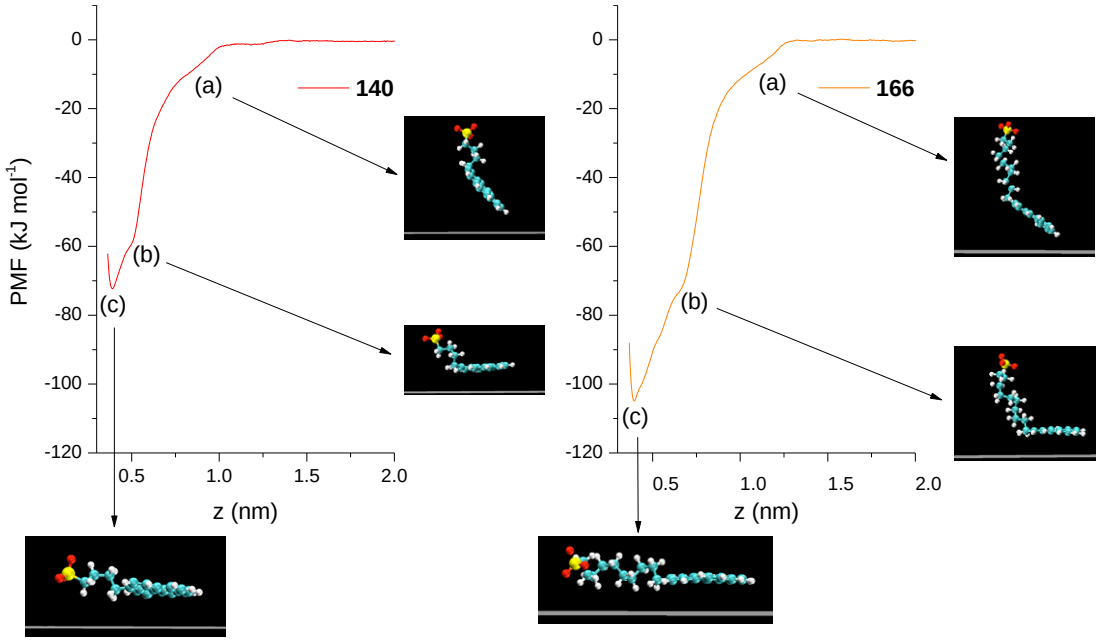

Figure 75 – Calculated PMF curves of **140** and **166** with representative snapshots of the stabiliser molecule at various stages of interaction

Considering figure 75 it is interesting to note that while it was anticipated that the sulfonic acid functionality would orientate itself away from the graphene surface after the π-π interactions of the aromatic core of the stabilisers had been maximised (b), we instead observe that the alkyl chain collapses to additionally interact with the graphene surface, eventually settling at an energy minimum with the sulfonic acid functionality far closer to the surface than expected (c). Also surprising is the degree to which these alkyl chains are calculated to aid the surface interaction, particularly in the case of **166** where the free energy decreases significantly after the π-π stacking interaction has been maximised (b) with significant additional interaction coming from the longer chain assuming a flattened orientation (c). Considering this it can also be observed in figure 74 that those compounds with *n*-C_3H_6 spacer groups (**164**, **172**) appear to have two free energy minima close to the surface in which the alkyl chain can either lay flat on the surface or be orientated into solution.

At this stage it is important to note that while these calculations are useful as a qualitative order of interaction, the values presented are not necessarily suitable as absolute interaction energies. Another important drawback of these calculations that must be considered is that only one stabiliser molecule is considered at a time. This later point is particularly significant as it was hoped that the installation of an alkyl spacer group would allow these stabilisers to perform more effectively at higher concentrations due to the separation of the charge from the graphene surface and the relief of steric interactions (section 1.3-2.1) as multiple stabilisers interact with the same graphene sheet. It should be further noted that these calculations do not directly indicate the stability of the dispersion that may be produced upon the interaction of these stabilisers with the graphene surface. The simulations used above measure the interaction of a single stabiliser with a single static infinite graphene sheet. For these reasons while it is predicted that the longer the alkyl spacer the stronger the interaction of the stabiliser, these computations would be expected to fail to communicate the point at which the stabiliser becomes too insoluble in aqueous solution to behave effectively as an aqueous stabiliser. For this reason the significance of longer chains may be overemphasised as the simulation begins to simply assign the most hydrophobic compound as the most effective as its interactions with the aqueous medium become increasingly unfavourable (and interactions with the graphene surface more favourable).

2.2-3 Initial Experimental Investigations of Stabiliser Performance

With the majority of synthetic pyrene and perylene-based stabiliser targets in hand (section 2.2-1) and computational analysis of those targets completed (section 2.2-2), investigations were begun with a supervised student[213] into the experimental performance of these stabilisers in the aqueous exfoliation of graphite to generate graphene dispersions. Such investigations are still ongoing and as yet in their early stages. These studies are additionally still limited to commercially available stabiliser sodium pyrene-1-sulfonate (**103**) and the simplest novel stabiliser sodium 4-(pyren-1-yl)butane-1-sulfonate (**140**). Limited results can however be tentatively included here to provide an insight into the potential graphene dispersion concentrations that may be accessed with these stabiliser designs.

Closely based on work undertaken by Green *et al*[144] (section 1.3-2.1) samples of **103** and **140** were tip sonicated in aqueous solution in the presence of graphite. The samples were then centrifuged at 5000 rpm for 4 hours and the supernatant removed for further analysis. As in previous work,[144, 148, 163] diluted samples were analysed by UV-vis spectroscopy and their absorbance at 660 nm (where pyrene and perylene-based materials feature no absorbance) used to determine their concentration according to the Beer-Lambert law. The extinction coefficient (ε) of these graphene dispersions was determined though the gravimetric analysis of a graphene dispersion (generated through the use of **103**) after the completion of UV-vis absorbance analysis. In these studies ε was determined to be 1700 mL mg^{-1} m^{-1}. This is at the lower end of the commonly accepted range of graphene dispersion ε values at 660 nm in aqueous media, which can vary between 1390 and 6600 mL mg^{-1} m^{-1}.[214, 215] It is likely these variations are dependent on the method used to produce the graphene dispersion and the quantity of few and single layer sheets suspended. Our determined value however compares well with that of Wang *et al*[148] who engaged in the similar tip sonication of natural graphite in aqueous solution with novel stabilisers **111** (figure 32, section 1.3-2.2) reported an ε value at 660 nm of 1506 mL mg^{-1} m^{-1}.

Initial experiments were based on the work of Green *et al*[144] sonicating **103** in aqueous solution at concentrations of 6.6, 9.9 and 13 mM with 9129 mg $mmol^{-1}$ (30 mass equivalents with respect to **103**) of natural graphite (used as an alternative to expanded graphite). As expected based on the results of Green *et al* a 9.9 mM

concentration was determined to provide the highest concentration graphene dispersion of ~0.4 mg mL^{-1} (compared to Green *et al*'s value of 0.8-1 mg mL^{-1} using expanded graphite). This experimental method was then applied to the synthesised stabiliser **140** initially using the same concentrations, then increasing them in increments of ~3.3 mM (corresponding to an increase of 1.0 mg mL^{-1} of **103**). UV-vis absorbance analyses at 660 nm of the resultant centrifuged solutions then allowed the construction of figure 76.

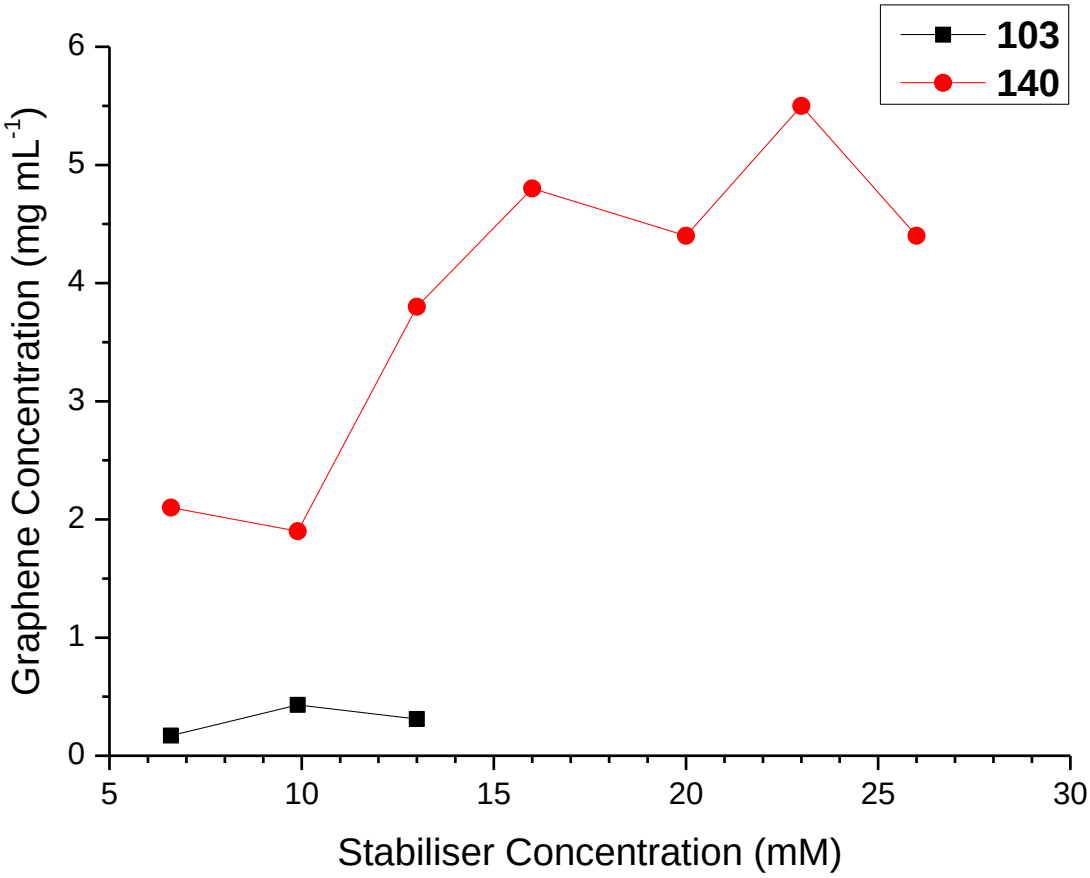

Figure 76 – Preliminary aqueous graphene dispersion concentrations (determined by UV-vis absorbance) obtained using **103** and **140** at various concentrations

Interpretations based on figure 76 are tentative and based on individual measurements. The reproducibility of these results has yet to be established and internal inconsistencies for stabiliser **140** at concentrations of 9.9 and 20 mM certainly suggest further methodological adjustments may be necessary to ensure reliable and reproducible results are collected. Notable in these results is the observation that stabiliser **140** continues to produce higher graphene concentrations

beyond the limit of its apparent solubility in water. Indeed while solutions of **103** are transparent prior to sonication at the concentrations investigated, those of **140** are dispersions that become increasingly opaque as the concentration is increased. This is important as brief solubility tests have raised concerns of the relative solubility of longer alkyl chain perylenes (in particular **166**) in aqueous solution. It may well be the case however that those stabilisers bearing solubilising groups, but that are not themselves entirely soluble in aqueous solution, may feature some of the best performance as their aromatic segment has a lower affinity to remain free in solution and a higher affinity to associate with the graphene sheet (however it is also expected a point will eventually be reached where the stabiliser simply becomes too insoluble in aqueous solution to behave appropriately). Considering this, the low solubility of **140** may also be a large source of error associated with the results in figure 76 as homogenous dispersions at concentrations at which it is largely insoluble are difficult to produce.

It should be noted at this early stage that owing to methodological concerns and the establishment of results with limited error, these samples have yet to be fully characterised by appropriate methods suitable to identify the quality and quantity of graphene present in solution. For instance optical microscopy, transmission electron microscopy (TEM), AFM, X-ray photoelectron spectroscopy (XPS) and Raman spectroscopy are still necessary to confirm the production of significant quantities of high quality graphene in these dispersions.[148, 154, 161] It is possible lower power/shorter sonication times may be necessary to produce higher quality dispersions, although this may in turn result in lower concentration dispersions.[130] Investigations may also need to be made into the removal of excess stabiliser in the graphene dispersions produced, particularly when relatively high concentrations of **140** might be used, as the presence of excess stabiliser can hamper potential applications and analyses. It should be noted however that such "washing" procedures may in turn reduce the final graphene concentration. Finally, given the high concentrations of graphene proposed in figure 76 and the low solubility of the stabiliser used, investigations into dispersion stability will also be required and may be probed through zeta potential measurements and recalculating the dispersion concentration after standing over a period of months.[148]

At face value the results in figure 76 are however very promising. These results suggest the production of graphene dispersions an order of magnitude higher in concentration than achieved with the commonly used, commercially available stabiliser **103**. Those results obtained with **140** suggest the production of dispersions up to ~5.5 mg mL^{-1} in concentration and while such dispersions are subject to further analysis and validation, the results appear quite exceptional. Comparison with those novel stabilisers reviewed in section 1.3-2 further highlights the unique performance observed as far more complex stabilisers **114** and **115** (figure 33, section 1.3-2.3) achieve graphene concentrations of 1.1 and 1.5 mg mL^{-1} (natural graphite, centrifugation at 1000-1300 rpm)[161, 162] and **111-a** (figure 32, section 1.3-2.2) treated in a similar manner as **140** (natural graphite, tip sonication, centrifugation at 5000 rpm) achieves a concentration of 1.2 mg mL^{-1} based on UV-vis absorbance at 660 nm using a similar ε value.[148]

These initial investigations are thus far limited to pyrene-based stabiliser **140**, the most accessible novel stabiliser. It is envisioned however that once the behaviour of **140** is fully assessed and a reliable methodology for the production of these graphene dispersions established, our additional more complex stabilisers which have already been synthesised but are as yet untested, may produce improved results and still higher graphene concentrations.

3 Conclusions and Further Work

3.1 Conclusions

3.1-1 Synthesis and Properties of "A_2B_2" Tetrasubstituted Chrysene Derivatives

The iridium-catalysed aromatic C-H diborylation of 4,10-dichlorochrysene (**32**) was observed to proceed with exceptional regioselectivity allowing the isolation of 2,8-substituted diboryl chrysene **118** in high yields *via* a simple recrystallisation of the crude reaction mixture. This key intermediate allowed access to a variety of 2,8-substituted chlorochrysene derivatives *via* the chemoselective Suzuki coupling of a variety of aryl iodides at the borylated 2,8-positions with preservation of the aryl chloride functionality. An assortment of aromatic functionalities were installed at the 2,8-positions including a variety of electron donating substituents. Additionally an electron withdrawing substituent was also installed *via* a copper mediated trifluoromethylation. The "A_2B_2" substitution pattern made available by this methodology was also explored *via* the subsequent palladium-catalysed Kumada coupling of the chlorinated 4,10-positions. This further allowed the installation of additional aromatic substituents and ultimately the synthesis of the first donor-acceptor chrysene derivative.

Analysis of the properties of the chrysene derivatives synthesised revealed broadened UV-vis absorption spectra, decreased E_g and increased HOMO levels. Triphenylamine-based materials **122** and donor-acceptor **137** in particular featured broadened absorption spectra and redshifted fluorescence spectra. This was further rationalised by subsequent computational studies which revealed a significant charge-transfer HOMO to LUMO transition in donor-acceptor chrysene **137** in spite of its contorted structure. **122**, **133** and **137** in particular featured increased HOMO levels and decreased E_g values compared to the parent chrysene and these compared well with bench mark literature materials. While the p-type device behaviour of such derivatives is subject to their crystal structure (**137** and **133** would be expected to feature limited π-π overlap) the expected contorted structure of **137** along with its suitable fluorescence make it a promising candidate for OLED applications. It is

further envisioned that the application of this halogen directed, aromatic C-H borylation protocol to higher polyaromatics may lead to a similar enhancement of photophysical and electrochemical properties and may be particularly applicable in the synthesis of tuneable emissive materials.

3.1-2 Synthesis, Analysis and Application of Amphiphilic Graphene Stabilisers

A series of pyrene- and perylene-based amphiphilic graphene stabilisers were successfully synthesised and characterised despite challenging purification protocols. Based on optimum requirements suggested in the literature, each stabiliser was asymmetrically substituted with a hydrophilic SO_3Na functionality separated by an alkyl spacer group. In comparison to the commercially available and commonly used sodium pyrene-1-sulfonate (**103**) the readily accessible stabiliser sodium 4-(pyren-1-yl)butane-1-sulfonate (**140**) was synthesised featuring a *n*-C_4H_8 alkyl spacer group. To further explore the effect of a variety of alkyl spacer lengths and the influence of a larger aromatic core on stabiliser performance, a series of SO_3Na substituted perylenes were additionally synthesised featuring *n*-C_3H_6, *n*-C_5H_{10} and *n*-$C_{10}H_{20}$ alkyl spacer groups. To enhance the asymmetric substitution pattern of these pyrene- and perylene-based stabilisers the previously explored iridium-catalysed aromatic C-H borylation was then revisited, enabling the regioselective mono- and tri-borylation of substituted pyrene and perylene cores respectively. This was successful, allowing subsequent functionalisation on the monoborylated pyrene core with a nitrile group. Significant attempts were made to reliably oxidise triboryl perylene (**168**) to generate a substituted trihydroxy perylene core, however oxidation procedures proved capricious and purification difficult due to the poor solubility and high polarity of the products produced.

Computational molecular dynamics simulations indicated the promise of these targeted stabilisers. Simulations particularly indicated the superior interaction of larger aromatic cores with longer alkyl chain spacer groups (although such simulations may over emphasise the importance of hydrophobic interactions). Interestingly these investigations suggested that alkyl spacer groups would lie flat on the graphene surface rather than being directed into solution as was expected. Meanwhile the results of brief initial investigations into the aqueous exfoliation of

graphite to graphene, focusing on the performance of the most synthetically accessible novel pyrene-based stabiliser **140**, suggest the generation of graphene dispersions an order of magnitude higher in concentration than obtained using its commercially available equivalent **103**. While interpretation of these results is still limited, they are very promising and it is hoped that the further application of our already synthesised but as yet untested stabilisers will yield further improvement on these results and allow the production of graphene dispersions of still higher concentrations in the near future.

3.1-3 Conclusions

In conclusion chrysene, pyrene and perylene polyaromatic cores have been substituted with a variety of functionalities in order to synthesise polyaromatic materials with enhanced properties. Chrysene was substituted with a variety of functionalities including electron releasing groups and electron withdrawing groups in a unique "A_2B_2" substitution pattern. Exploiting this methodology a donor-acceptor chrysene was accessed along with a variety of chrysene derivatives featuring enhanced photophysical and electrochemical properties (lower E_g, higher HOMO), significantly increasing their potential for application in organic electronic devices such OLEDs. In addition pyrene and perylene cores were asymmetrically substituted with hydrophilic SO_3Na functionalities equipped with alkyl spacer groups. This has enabled their application towards the aqueous stabilisation of exfoliated graphene dispersions with stabiliser **140** so far yielding positive results, indicating such stabiliser designs should prove effective at producing high concentration dispersions. Throughout these studies the iridium-catalysed aromatic C-H borylation of substrates has been a key process, essential to the "A_2B_2" substitution of the chrysene derivatives synthesised and pivotal in the late-stage asymmetric functionalisation of the pyrene and perylene cores investigated as amphiphilic graphene stabilisers.

Overall this thesis highlights the potential methodologies accessible *via* the late-stage aromatic C-H borylation of various substituted polyaromatic cores and the broad range of applications against which such synthesised derivatives may be applied. It is also apparent in this thesis the extent to which work in new areas of materials chemistry are aided though collaboration, with key insights in each project made

available through computational studies. The potential chemical space that may be accessed through the functionalisation methodologies applied here are far greater than there was sufficient time to explore, but the potential for tuning the properties of a variety of polyaromatic cores by these methods to suit a variety of applications has yet to be fully explored.

3.2 Further Work

As outlined in section 2.2-3 immediate ongoing work includes experimental graphene stabiliser performance studies. Stabiliser **140** has only been tested in a limited capacity and there are still unexplored pyrene- and perylene-based graphene stabilisers that have been synthesised but are as yet untested. The first challenge is the identification of a methodology for the reliable and replicable exfoliation of graphite in the presence of these synthesised stabilisers. The preliminary results so far collected (figure 76, section 2.2-3) feature inconsistencies in performance and require further investigation. It is proposed the major source for the observed error is the relative insolubility of the novel stabiliser **140** at the concentrations tested for graphite exfoliation, a problem that may only be compounded as larger polyaromatics with longer alkyl chain spacer groups are explored. While **140** has demonstrated that a dispersion of these stabilisers can be used effectively in the generation of aqueous graphene dispersions, a lack of homogeneity in the stabiliser dispersion is likely a large source of error, adding a significant amount of variation between exfoliation experiments. It is suggested this may be mitigated to some extent by ensuring the dispersion is as homogeneous as possible prior to the addition of graphite, perhaps by heating the stabiliser dispersion for longer periods or by an initial tip sonication process. Key in this work will also be the complete characterisation of the graphene dispersions produced, using optical microscopy, TEM, AFM, XPS and Raman spectroscopy to assess the quality and quantity of exfoliated graphene. Stability studies will also be performed, including zeta potential measurements and the repetition of UV-vis absorption analysis after a period of months to identify any changes in graphene concentration due to dispersion instability. It can be further noted that in the determination of the graphene extinction coefficient (ε) (section 4.1-2), filtered dispersions may in future also be subjected to thermogravimetric analysis after washing to confirm the compete removal of residual

stabiliser. This will ensure a more accurate filtered weight of graphene is obtained and in turn produce a more accurate measurement of the graphene ε value.

Key in further work of this project will also be the completion of the synthesis outlined in figure 73 (section 2.2-1.2) which will allow isolation of the desired hydroxyl functionalised perylene-based stabiliser **172**. Despite significant difficulties this synthesis is likely to be worthwhile revisiting, particularly as **172** is computationally predicted to have some of the strongest interactions with the graphene surface identified. These potentially strong interactions can be explained to some extent by the observations of Lukkari *et al*[156] and a proposed graphene-OH interaction (section 1.3-2.4). It may be useful given the potential importance of these interactions to investigate the synthesis of hydroxyl substituted pyrene-based stabiliser **174** as in figure 77 below.

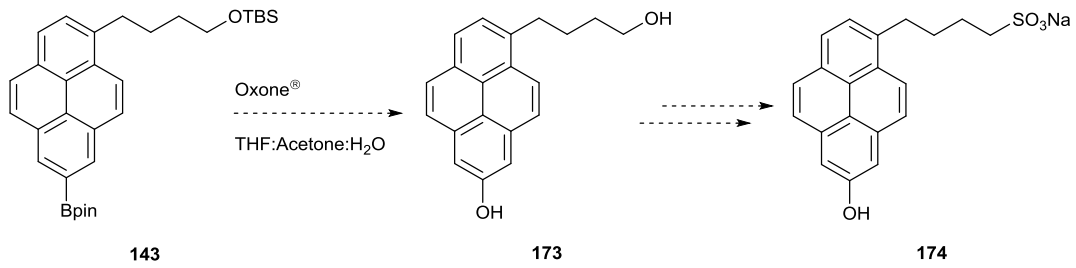

Figure 77 – Proposed synthesis of hydroxyl functionalised pyrene-based stabiliser **174**

The synthesis of **174** would allow a valuable comparison with nitrile substituted pyrene-based stabiliser **146** (figure 65, section 2.2-1.1) to be made. Both would feature an asymmetric polarisation across the aromatic core (suggested as an important feature of amphiphilic graphene stabilisers by Palermo *et al*[154]) and would therefore serve to deconvolute the benefits of this polarisation from those associated with an electron deficient aromatic core *vs* a possible graphene-OH based interaction.

Concerning the possibility of performing an "A_2B_2" synthesis such as that undertaken on 4,10-dichlorochrysene (**32**) but on a higher polyaromatic, the synthesis outlined in figure 78 below could be suggested.

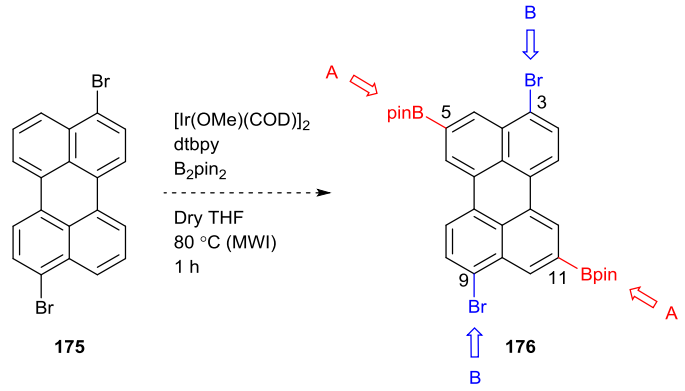

Figure 78 – Proposed "A_2B_2" functionalisation of a perylene core using a halogenation borylation methodology

This synthesis would involve starting with a relatively simple known compound such as 3,9-dibromoperylene (**175**),[216] synthesised in one step by the dibromination of perylene (although isomeric separation by recrystallisation may be required). The aromatic C-H borylation of this substrate would then be expected to proceed in the 5,11-positions, establishing **176** as a key intermediate for an "A_2B_2" style synthesis. It can be envisioned that such a process would result in similar substantial increases in HOMO level and decreases in E_g as observed in the substitution of **32**. By starting with a more conjugated, electron rich system however, the final compounds produced would be expected to be more tuneable and have superior properties compared to their equivalent chrysene derivatives. It would however have to be borne in mind at that stage that in such electron rich systems stability (a key advantage of chrysene and its derivatives) may begin to become a concern.

4 Experimental Procedures

4.1 General Remarks

All reactants and reagents were purchased from Sigma Aldrich, Fisher Scientific, Acros Organics, Apollo Scientific or Fluorochem and used without purification unless otherwise noted. Anhydrous THF was obtained from a sodium wire still with benzophenone indicator or purchased directly from Sigma Aldrich. Diethyl ether was dried over sodium wire. Acetone, chloroform and ethanol were dried over 4 Å molecular sieves. DCM was dried over 4 Å molecular sieves or obtained from an Innovative Technology Puresolv multi dispensary solvent purification system. All other anhydrous solvents and reagents were purchased as such and used without purification. Deionised water was used in synthetic reactions, recrystallisations and graphene exfoliation studies. Petroleum ether used was bp 40-60 °C. Reactions carried out under microwave irradiation were performed in a biotage initiator microwave reactor. TLC was carried out using DC-Fertigfolie POLYGRAM® SIL G/UV_{254} precoated TLC sheets with substrate detection by UV light (254 and 365 nm). Benchtop sonication was performed in in an Ultrawave SFE 590/1 sonicator bath. All reaction glassware was heated under vacuum prior to use unless otherwise noted.

All NMR spectra were recorded with using a Bruker Avance III 400, Bruker Avance III HD 400 (equipped with a broadband "prodigy" N_2 coldprobe), Bruker Avance II+ 500, Bruker Avance 500 DRX or Bruker Avance III HD 500 (equipped with a broadband "prodigy" N_2 coldprobe) spectrometer. ^{1}H and ^{13}C NMR spectra were referenced to the residual solvent peak as appropriate: $CDCl_3$ (7.27 or 77.00 ppm respectively), DMSO-d_6 (2.50 or 39.51 ppm respectively) or methanol-d_4 (3.31 or 49.15 ppm respectively). ^{19}F NMR spectra were recorded without reprocessing. Couplings are denoted as s (singlet), d (doublet), t (triplet), q (quartet), quin (quintet), m (multiplet) or any combination of these. All coupling constants (*J*) are given in Hz and reported to one decimal place.

MALDI mass spectra were recorded with a Shimadzu Biotech Axima Confidence spectrometer using a dithranol, DCTB, TCNQ or CHCA matrix as stated.

Atmospheric pressure chemical ionisation (APCI) mass spectra were recorded on a Micromass Platform II, Waters SQD2 Aquity System or Thermo Exactive Plus EMR Orbitrap spectrometer. Electrospray ionization (ESI) mass spectra were recorded on a Waters SQD2 Aquity System spectrometer. Gas chromatography (GC) mass spectra were recorded on a Perkin Elmer Auto System XL Arnel with a Perkin Elmer TurboMass Spectrometer or Agilent 5975C Triple Axis GC/MS spectrometer. Electron ionization (EI) high resolution mass spectra were recorded on a Thermo Finnigan MAT95XP spectrometer. High resolution ESI, heated electrospray ionization (HESI), APCI and atmospheric pressure photoionization (APPI) mass spectra were recorded on a Thermo Exactive Plus EMR Orbitrap spectrometer. Atmospheric solids analysis probe (ASAP) high resolution mass spectra were recorded on a Thermofisher LTQ Orbitrap XL spectrometer at the EPSRC national mass spectrometry facility (Swansea, UK).

Infrared spectra were obtained using a Thermo Scientific Nicolet iS5 spectrometer with an iDS ATR accessory.

Melting points were recorded on a Stuart SMP10 melting point apparatus or Gallenkamp Griffen melting point apparatus with a thermocouple attached to an Extech 380224 multimeter.

Gradient sublimation was performed using apparatus constructed by the Manchester Chemistry Department mechanical and electrical workshops. The gradient sublimation heating coil is controlled by a thermostat and a temperature gradient is maintained along a pathlength of 40 cm by air cooling over the cold zone. Vacuum was maintained by an Edwards TIC Pumping Station turbopump (pressure normally 1×10^{-7} to 1×10^{-6} mbar).

UV-vis absorption spectra were recorded on a Varian Cary 5000 UV-vis-NIR spectrophotometer and fluorescence spectra were recorded on a Varian Cary Eclipse fluorescence spectrophotometer. Spectra were recorded in DCM or in aqueous solution using a quartz curvet. Fluorescence measurements were conducted from samples diluted to a λ_{max} absorbance of ~0.1 in the absorption spectrum.

CV measurements were recorded on a Basi Epsilon instrument utilising a C3 Cell Stand in a standard three electrode setup with a working electrode (glassy carbon), counter electrode (platinum) and reference electrode ($Ag/AgNO_3$). CV measurements were made in DCM using a 0.1 M concentration of Tetrabutylammoniumhexafluorophosphate as the supporting electrolyte and a 1.0 mg mL^{-1} concentration of the analyte. All CV measurements were made with reference to ferrocene and were conducted at a scan speed of 100 mV S^{-1}.

4.1-1 Experimental Details of Computational Calculations

4.1-1.1 DFT Studies of Chrysene Derivatives

Computational DFT studies of chrysene derivatives (performed by Dr Joseph McDouall *et al* at the University of Manchester)[2] were performed using the Gaussian 09[217] software. All geometries were optimised in the gas phase at the B3LYP/6-31G(d,p) level.[218,219,220] UV-vis absorption spectra were obtained using TD-DFT at the B3LYP/6-311G(d,p)//B3LYP/6-31G(d,p) level. pK_a values were calculated using the methodology of Guo *et al*[166] at the B3LYP/6-31G(d,p) level.

4.1-1.2 Molecular Dynamic Simulations of Graphene Stabilisers

Using molecular dynamics simulations (performed by Dr Flor Siperstein *et al* at the University of Manchester)[212] the adsorption free energy for each stabiliser molecule transferring from bulk solution to the graphene surface was calculated by generating a potential of mean force (PMF), using molecular dynamics as implemented in the GROMACS software,[221] version 5.0.4. For each molecule, the initial configuration consisted of an orthorhombic simulation cell (3.68 nm × 3.83 nm × 5.00 nm), with the graphene sheet positioned in the x-y plane at z = 0, the stabiliser molecule was placed in the centre of the cell and the remainder of the free space solvated with water. One water molecule was then selected at random and swapped for the Na^+ counter ion. The simulation cell boundaries were periodic in all three dimensions, resulting in a graphene surface infinite in the x and y-dimensions.

Both the stabiliser molecules and graphene sheet were modeled using parameters taken from the CHARMM force field[222, 223, 224] and the TIP3P model[225] was used for water.

The adsorption free energy was calculated using the umbrella sampling technique.[226, 227] The initial configuration was minimized using the steepest descents algorithm. Then, the stabiliser molecule was pulled towards the graphene sheet using a harmonic potential with a force constant of 5000 kJ mol^{-1} nm^{-2} at a rate of 0.02 nm ps^{-1}. This simulation was used to generate the initial configurations for all of the umbrella sampling simulations, which were chosen on the basis of the z-component of the stabiliser centre of mass. Twenty simulations were performed for each stabiliser molecule, in the range z = 0.3-2.2 nm, with a spacing of 0.1 nm, employing a harmonic potential with a force constant of 2500 kJ mol^{-1} nm^{-2} to constrain the sampling. Only the z-coordinate of the stabiliser centre of mass was constrained by this potential, enabling the molecule to freely rotate and translate in the x and y directions. Each simulation was performed for a total of 20 ns and only the forces from the final 19 ns of simulation time were used to generate the PMF. The PMF was obtained by integrating the forces required to keep the molecule at a given z-coordinate, saved every 0.1 ps, with the weighted histogram analysis method (WHAM)[228] using the GROMACS analysis tool, g_wham.[229] The adsorption free energy was taken as the minimum value in the PMF after shifting the entire curve so that the free energy at z = 2.2 nm was equal to zero. The statistical uncertainty in the adsorption free energy was calculated using a bootstrapping resampling procedure with 100 bootstrap samples.

All simulations were performed in the canonical ensemble, with the graphene sheet held rigid for the duration of the simulation. The equations of motion were integrated using a leapfrog algorithm[230] and timestep of 1 fs. The long-range nature of electrostatic interactions was accounted for using the particle-mesh Ewald method (PME)[231, 232] using a real-space cut off of 1.2 nm, a maximum Fourier grid spacing of 0.12 nm and 4th order interpolation, resulting in electrostatic energies accurate to approximately 5×10^{-3} kJ mol^{-1}. Short-range, non-bonded, interactions were modified from 1.0 nm so that the potential tended smoothly to zero at 1.2 nm. A temperature of 298.15 K was regulated using the Nosé-Hoover thermostat[233, 234] with a relaxation time constant of 1 ps. The geometry of TIP3P water was constrained using the SETTLE algorithm.[235]

4.1-2 Experimental Details of Aqueous Graphene Exfoliation Studies

Natural graphite flakes were obtained from NGS Naturgraphit GmbH and tip sonication was performed with a Misonix Sonicator 3000 at an output voltage of 24 W. Centrifugation of graphene dispersions was completed with a Eppendorf 5418 centrifuge and the filtration of graphene dispersions was completed using Millipore 0.22 μm filter paper. Dilutions of graphene dispersions were conducted with a measuring cylinder (10.0 mL).

Aqueous graphene exfoliation studies were completed with a supervised student.[213] The requisite amount of stabiliser was added to 6.0 mL of water. This was then heated at 80-90 °C with stirring for 15 minutes to obtain a dispersion of stabiliser. Natural graphite flakes were then added and the sample placed in an ice bath while tip sonicated for 1 hour in 5 second pluses (2 hours total time). Each sample was then centrifuged for 4 hours at 5000 rpm and the supernatant collected for further analysis.

The concentrations of stabiliser investigated were based on the studies completed by Green *et al*[144]. In accordance with this work stabiliser concentrations were tested at various concentrations ranging from 6.6 to 26 mM, increasing the stabiliser concentration in ~3.3 mM increments (corresponding to increases of 1.0 mg mL^{-1} of sodium pyrene-1-sulfonate, **103**) utilising 9129 mg $mmol^{-1}$ of graphite flakes (corresponding to 30 mass equivalents of graphite with respect to **103**).

Graphene concentrations after centrifugation were determined by UV-vis absorbance of diluted solutions at 660 nm *via* the Beer-Lambert law using the determined extinction coefficient (ε) of these graphene dispersions.

The ε value of the graphene dispersions generated was determined by sonication of **103** (9.9 mM concentration) with graphite (using the above method) three times. The three samples were then combined and subjected to UV-vis absorption analysis. A Beer-Lambert plot was constructed, measuring the absorbance of the dispersion at 660 nm at a variety of dilutions. Subsequent filtration (followed by washing with water and ethanol to remove residual stabiliser) and gravimetric analysis of the

graphene dispersion indicated an initial concentration of 0.55 mg mL^{-1} demonstrating an ε value of 1700 mL mg^{-1} m^{-1}.

4.2 Synthetic Procedures

4.2-1 Chrysene Derivatives

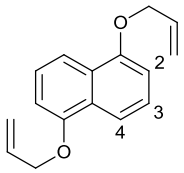

1,5-*Bis*(allyloxy)naphthalene (**29**)

Prepared by an adaptation of a literature synthesis[164]

1,5-Dihydroxynapthalene (**28**) (25.00 g, 156.1 mmol) and K_2CO_3 (51.75 g, 374.4 mmol) were added to a three neck RBF (1 L) which was then purged with N_2. Dry acetone (~400 mL) was then added *via* cannula before allyl bromide (32 mL, 370 mmol) was added to the stirring suspension *via* syringe and the reaction mixture heated to reflux overnight. The inorganic by-products were then removed by filtration though celite® and the solvent removed *in vacuo*. The resulting brown solid was then dissolved in diethyl ether (500 mL) and washed with NaOH solution (1 M) (2 × ~250 mL), water (1 × ~150 mL) and brine (1 × ~150 mL). The organic layer was then dried over $MgSO_4$ and the solvent removed *in vacuo* to afford the crude product which was then recrystallised twice from MeOH to afford the purified *title compound* (**29**) (16.96 g, 70.57 mmol, 45% yield) as a light brown solid. mp 95 °C (lit.,[236] 92-94.5 °C). δ_H (400 MHz; $CDCl_3$; $CHCl_3$) 4.73 (4 H, dt, *J* = 5.1, 1.5 Hz, O-C-H), 5.35 (2 H, dq, *J* = 10.5, 1.5, C=C-H), 5.54 (2 H, dq, *J* = 17.3, 1.5, C=C-H), 6.19 (2 H, ddt, *J* = 17.3, 10.5, 5.1, H-C=C), 6.86 (2 H, d, *J* = 7.7, C(2)H), 7.38 (2 H, dd, *J* = 8.5, 7.7, C(3)H), 7.92 (2 H, d, *J* = 8.5, C(4)H). δ_C (101 MHz; $CDCl_3$; $^{13}CDCl_3$) 68.9, 105.8, 114.5, 117.3, 125.1, 126.8, 133.3, 154.1. *m/z* (APCI) 241 ($[M + H]^+$, 100%), 200 ($[M - C_3H_5]^+$, 10). ^{1}H NMR comparable to that in the literature.[237]

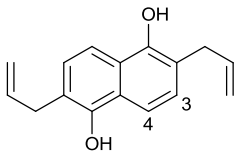

2,6-Diallyl-1,5-dihydroxynaphthalene (**30**)

Prepared by an adaptation of a literature synthesis[236]

1,5-*Bis*(allyloxy)napthalene (**29**) (7.00 g, 29.1 mmol) was added to a two neck RBF (100 mL) which was then purged with N_2. The material was then heated with stirring to 200 °C for 2 h. The product was assumed to be oxidatively unstable and so was used directly in the next step of the synthesis without purification. A quantitative yield of the *title compound* (**30**) as a dark brown solid was assumed. mp 139-141 °C (lit.,[236] 137-143 °C). δ_H (400 MHz; $CDCl_3$; $CHCl_3$) 3.58 (4 H, dt, *J* = 6.2, 1.5, Ar-C-H), 5.21 - 5.30 (4 H, m, C=C-H), 5.52 (2 H, s, Ar-O-H), 6.03 - 6.15 (2 H, m, H-C=C) 7.22 (2 H, d, *J* = 8.5, C(3)H), 7.71 (2 H, d, *J* = 8.5, C(4)H). δ_C (101 MHz; $CDCl_3$; $^{13}CDCl_3$) 35.7, 113.7, 117.0, 117.8, 125.2, 127.9, 136.1, 149.5. *m/z* (ESI$^-$) 239 ([M – H]$^-$, 100%). ^{1}H NMR comparable to that in the literature.[164]

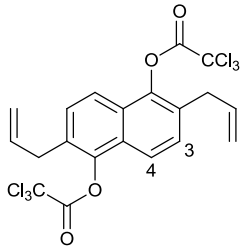

2,6-Diallyl-1,5-*bis*(2,2,2-trichloroacetyl)naphthalene (**31**)

Prepared by an adaptation of a literature synthesis[90]

2,6-Diallyl-1,5-dihydroxynapthalene (**30**) (~7.00 g, ~29.1 mmol) was added to a three neck RBF (250 mL) directly after its formation and the flask purged with N_2. Dry diethyl ether (185 mL) was then added, followed by dry pyridine (5.5 mL, 68 mmol). The reaction was then cooled to 0 °C in an ice bath before trichloroacetylchloride (8.0 mL, 72 mmol) was added, after which the reaction was allowed to stir to room temperature overnight. The reaction was then quenched by the slow addition (initially dropwise) of water (90 mL). The organic layer was then washed with saturated sodium hydrogen carbonate solution (2 × 50 mL), water (2 × 50 mL) and brine (2 × 50 mL) before drying over $MgSO_4$. The solution was then concentrated *in vacuo* to afford the *title compound* (**31**) (13.05 g, 24.57 mmol, 84% yield) as an orange yellow solid with no further purification. mp 125-128 °C (lit.,[90] 133 °C). δ_H (400 MHz; $CDCl_3$; $CHCl_3$) 3.53 (4 H, dt, *J* = 6.5, 1.4, Ar-C-H), 5.12 - 5.21 (4 H, m, C=C-H), 5.89 - 6.02 (2 H, m, H-C=C), 7.51 (2 H, d, *J* = 8.5, C(3)H), 7.84 (2 H, d, *J* = 8.5, C(4)H). δ_C (101 MHz; $CDCl_3$; $^{13}CDCl_3$) 34.0, 89.5, 117.5, 119.8, 126.6, 129.2, 129.3, 134.5, 143.6, 160.2. *m/z* (APCI) 552 ($[M(^{35}Cl_3 + {}^{37}Cl_3) + NH_4]^+$, 35%), 550 ($[M(^{35}Cl_4 + {}^{37}Cl_2) + NH_4]^+$, 80), 548 ($[M(^{35}Cl_5 + {}^{37}Cl) + NH_4]^+$, 100), 546 ($[M(^{35}Cl_6) + NH_4]^+$, 50). ^1H NMR comparable to that in the literature.[90]

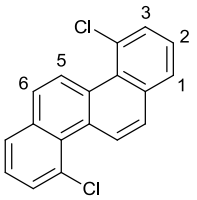

4,10-Dichlorochrysene (**32**)

Prepared by an adaptation of a literature synthesis[90]

2,6-Diallyl-1,5-*bis*(2,2,2-trichloroacetyl)naphthalene (**31**) (4.00 g, 7.53 mmol) and CuCl (75.2 mg, 0.760 mmol, 10 mol%) were added to a two neck RBF (100 mL) which was then purged with N_2. Dry diglyme (3.0 mL) was added *via* syringe and the reaction heated until a solution was formed. The solution was then vigorously degassed with N_2 for ~3 minutes before the reaction was heated to 160 °C for 2 h. The crude product was purified by directly dry loading the crude material *via* DCM/silica onto a chromatography column and eluting with a 20% DCM in petroleum ether solvent system to afford the *title compound* (**32**) (0.82 g, 2.6 mmol, 35% yield) as a colourless crystalline solid. mp 160-161 °C (lit.,[90] 159 °C). δ_H (400 MHz; $CDCl_3$; $CHCl_3$) 7.54 (2 H, t, *J* = 7.8, C(2)H), 7.77 (2 H, dd, *J* = 7.8, 1.2, C(3)H), 7.86 (2 H, d, *J* = 9.2, C(6)H), 7.91 (2 H, dd, *J* = 7.8, 1.2, C(1)H), 9.53 (2 H, d, *J* = 9.2, C(5)H). δ_C (101 MHz; $CDCl_3$; $^{13}CDCl_3$) 25.0, 126.4, 126.6, 127.4, 127.5, 129.8, 130.2, 131.4, 134.5. *m/z* (GC/MS) (EI) Single component: 298 ([M(^{35}Cl + ^{37}Cl)]$^+$, 60%), 296 ([M($^{35}Cl_2$)]$^+$, 100), 226 ([M – Cl_2]$^+$, 60), 208 (30), 112 (30). ^{1}H NMR comparable to that in the literature.[90]

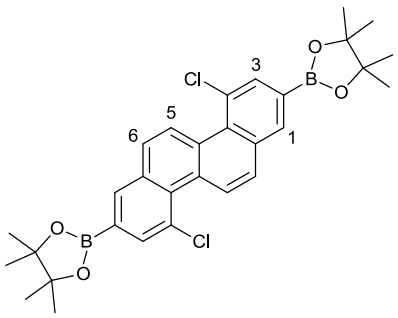

4,10-Dichloro-2,8-*bis*(4,4',5,5'-tetramethyl-1,3,2-dioxaborolan-2-yl)chrysene (**118**)

4,10-Dichlorochrysene (**32**) (500.5 mg, 1.684 mmol), *bis*(pinacolato)diboron (854.7 mg, 3.366 mmol), dtbpy (45.2 mg, 0.168 mmol, 10 mol%) and $[Ir(OMe)(COD)]_2$ (56.1 mg, 0.0846 mmol, 5 mol%) were added to a two neck RBF (100 mL) which was then purged with N_2. Cyclohexane (20 mL) was then added *via* syringe and the reaction heated to reflux overnight. The crude reaction mixture was then concentrated *in vacuo* and recrystallised from acetone to afford the purified *title compound* (**118**) (679.1 mg, 1.237 mmol, 73% yield) as a colourless powder. mp 268-269 °C. δ_H (400 MHz; $CDCl_3$; $CHCl_3$) 1.43 (24 H, s, Me), 7.88 (2 H, d, *J* = 9.2, C(6)H), 8.14 (2 H, d, *J* = 1.2, C(3)H), 8.36 (2 H, d, *J* = 1.2, C(1)H), 9.56 (2 H, d, *J* = 9.2, C(5)H). δ_C (125 MHz; $CDCl_3$; $^{13}CDCl_3$) 24.9, 84.4, 125.4, 126.4, 129.2, 130.4, 131.0, 134.2, 134.9, 135.0. NB: As is commonly reported,[128] the ^{13}C NMR spectrum features no signals from the carbon *ipso*- to the boron. *m/z* (MALDI-Dithranol) 550 ($[M(^{35}Cl + {}^{37}Cl)]^+$, 20%), 548 ($[M(^{35}Cl_2)]^+$, 40), 436 (25), 271 ($[M - C_{12}H_{24}BCl_2O_2 + H]^+$, 95), 247 (100), 228 (90). HR *m/z* (EI) $C_{30}H_{32}{}^{11}B_2{}^{35}Cl_2O_4$ requires 548.1858, found 548.1835. ν_{max}/cm^{-1} 3162w, 3076w, 3043w and 2995w (Ar C-H), 2975s and 2930 (C-H), 1613 and 1510 (Ar C=C).

Alternative preparation *via* MWI: An oven dried microwave vial equipped with a stirrer bar was placed under a flushing N_2 needle. 4,10-Dichlorochrysene (238.0 mg, 0.8009 mmol), *bis*(pinacolato)diboron (406.7 mg, 1.602 mmol), $[Ir(OMe)(COD)]_2$ (26.8 mg, 0.0404 mmol, 5 mol%) and dtbpy (21.7, 0.0808 mmol, 10 mol%) were then added against a flow of N_2. Dry THF (2.0 mL) was then added and the vial quickly capped as the N_2 needle was withdrawn. The reaction mixture was then heated at 80 °C for 1 h in a microwave reactor before concentration *in vacuo*.

Analysis of the crude sample by ^{1}H NMR indicated ~90% yield of the *title compound* (**118**) comparable with that achieved by conventional heating.

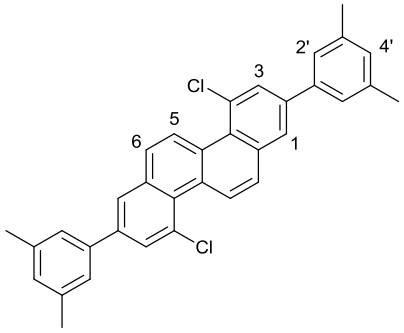

4,10-Dichloro-2,8-*bis*(3,5-dimethylphenyl)chrysene (**119**)

4,10-Dichloro-2,8-*bis*(4,4',5,5'-tetramethyl-1,3,2-dioxaborolan-2-yl)chrysene (**118**) (125.1 mg, 0.2278 mmol) was added to a pear shaped flask (10 mL) equipped with a Claisen adapter which was then purged with N_2. Toluene (3 mL), 1-iodo-3,5-dimethylbenzene (120.1 mg, 0.5175 mmol) and aliquat 336® (3 drops) were then added *via* syringe and the solution degassed with N_2 for 30 minutes with vigorous stirring. K_2CO_3 (414.8 mg, 3.001 mmol) was then dissolved in water (1.5 mL) to form a 2 M solution which after degassing for 15 minutes with N_2 was added to the reaction mixture. The toluene/water biphase was then degassed for a further 15 minutes before toluene (~1.0 mL) was removed by syringe and used to take up $Pd(PPh_3)_4$ (8.0 mg, 0.0069 mmol, 3 mol%) (under N_2) before reinjection into the reaction mixture. The reaction was then stirred at 80 °C overnight. The toluene layer was then collected and the water layer washed with toluene (5 mL). The combined organic extracts were then washed with water (2 × 5 mL) and brine (2 × 5 mL) before drying over $MgSO_4$ and concentrating *in vacuo* to isolate the crude product. Purification was then achieved by gradient sublimation to afford the *title compound* (**119**) (70.0 mg, 0.138 mmol, 77% yield) as an off-white solid. mp 344-346 °C. δ_H (400 MHz; $CDCl_3$; $CHCl_3$) 2.46 (12 H, m, Me), 7.09 (2 H, s, C(4')H), 7.41 (4 H, s, C(2')H), 7.93 (2 H, d, *J* = 9.4, C(6)H), 8.04 (2 H, d, *J* = 2.0, C(3)H), 8.10 (2 H, d, *J* = 2.0, C(1)H), 9.59 (2 H, d, *J* = 9.4, C(5)H). *m/z* (MALDI-dithranol) 506 ([M(^{35}Cl + ^{37}Cl)]$^+$, 60%), 504 ([M($^{35}Cl_2$)]$^+$, 70), 470 ([M – Cl]$^+$, 25), 249 (60), 227 (100). HR *m/z* (EI) $C_{34}H_{26}{}^{35}Cl_2$ requires 504.1406, found 504.1399. ν_{max}/cm^{-1} 3022 and 2910 (Ar C-H), 2852 and 2722w (C-H), 1603s, 1585w and 1507 (Ar C=C). Carbon spectrum unavailable due to insolubility in common organic solvents.

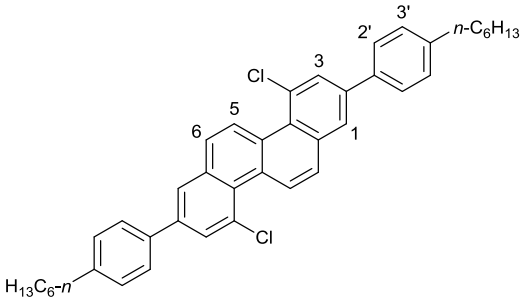

4,10-Dichloro-2,8-*bis*[4-(*n*-hexyl)phenyl]chrysene (**120**)

4,10-Dichloro-2,8-*bis*(4,4',5,5'-tetramethyl-1,3,2-dioxaborolan-2-yl)chrysene (**118**) (500.8 mg, 0.9120 mmol) was added to a three neck RBF (100 mL) which was then purged with N_2. Toluene (13 mL), 1-iodo-4-*n*-hexylbenzene (579.6 mg, 2.011 mmol) and aliquat 336® (8 drops) were then added *via* syringe and the solution degassed with N_2 for 30 minutes with vigorous stirring. K_2CO_3 (1.80 g, 13.0 mmol) was then dissolved in water (6.5 mL) to form a 2 M solution which after degassing for 15 minutes with N_2 was added to the reaction mixture. The toluene/water biphase was then degassed for a further 15 minutes before toluene (~1.5 mL) was removed by syringe and used to take up $Pd(PPh_3)_4$ (31.8 mg, 0.0275 mmol, 3 mol%) (under N_2) before reinjection into the reaction mixture. The reaction was then stirred at 80 °C overnight. The toluene layer was then collected and the water layer washed with toluene (10 mL). The combined organic layers were then washed with water (2 × 10 mL) and brine (2 × 10 mL) before drying over $MgSO_4$ and concentrating *in vacuo* to isolate the crude product. Purification was achieved by column chromatography utilising a 10% DCM in petroleum ether solvent system to isolate the purified *title compound* (**120**) (241.2 mg, 0.3905 mmol, 43% yield) as a colourless crystalline solid. mp 145-146 °C. δ_H (400 MHz; $CDCl_3$; $CHCl_3$) 0.93 (6 H, t, *J* = 7.0, Me), 1.27 - 1.47 (12 H, m, C-C-H), 1.69 (4 H, quin, *J* = 7.6, C-C-H), 2.70 (4 H, t, *J* = 7.6, Ar-C-H), 7.34 (4 H, d, *J* = 8.3, C(2':3')H), 7.69 (4 H, d, *J* = 8.3, C(2':3')H), 7.89 (2 H, d, *J* = 9.4, C(6)H), 8.03 (2 H, d, *J* = 2.0, C(3)H), 8.07 (2 H, d, *J* = 2.0, C(1)H), 9.56 (2 H, d, *J* = 9.4, C(5)H). δ_C (101 MHz; $CDCl_3$; $^{13}CDCl_3$) 14.1, 22.6, 29.0, 31.5, 31.8, 35.7, 124.8, 125.5, 126.3, 126.5, 127.1, 129.1, 129.2, 129.6, 131.7, 134.7, 136.3, 139.2, 143.1. *m/z* (MALDI-DCTB) 618 ($[M(^{35}Cl + ^{37}Cl)]^+$, 15%), 616 ($[M(^{35}Cl_2)]^+$, 20), 274 (100). HR *m/z* (EI) $C_{42}H_{42}{}^{35}Cl_2$ requires 616.2658, found 616.2635. ν_{max}/cm^{-1} 2953 and 2923 (Ar C-H), 2853 (C-H), 1609 and 1500 (Ar C=C).

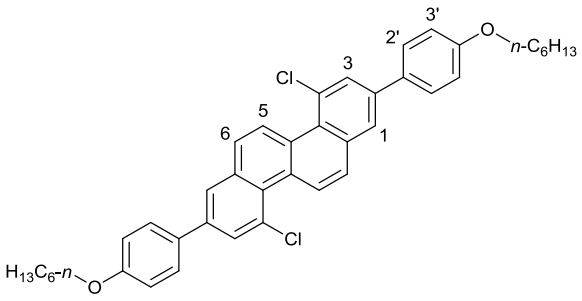

4,10-Dichloro-2,8-*bis*[4-(*n*-hexyloxy)phenyl]chrysene (**121**)

4,10-Dichloro-2,8-*bis*(4,4',5,5'-tetramethyl-1,3,2-dioxaborolan-2-yl)chrysene (**118**) (1.00 g, 1.82 mmol) was added to a three neck RBF (100 mL) which was then purged with N_2. Toluene (26 mL), 4-(*n*-hexyloxy)iodobenzene (**125**) (1.22 g, 4.01 mmol) and aliquat 336® (16 drops) were then added *via* syringe and the solution degassed with N_2 for 30 minutes with vigorous stirring. K_2CO_3 (3.59 g, 26.0 mmol) was then dissolved in water (13 mL) to form a 2 M solution which after degassing for 15 minutes with N_2 was added to the reaction mixture. The toluene/water biphase was then degassed for a further 15 minutes before toluene (~2 mL) was removed by syringe and used to take up $Pd(PPh_3)_4$ (64.1 mg, 0.0555 mmol, 3 mol%) (under N_2) before reinjection into the reaction mixture. The reaction was then stirred at 80 °C overnight. The toluene layer was then collected and the water layer washed with toluene (10 mL). The combined organic layers were then washed with water (2 × 20 mL) and brine (2 × 20 mL) before drying over $MgSO_4$ and concentrating *in vacuo* to isolate the crude product. Purification was achieved by column chromatography utilising a graded solvent system from 10% DCM in petroleum ether to 30% DCM in petroleum ether to isolate the purified *title compound* (**121**) (463.0 mg, 0.7126 mmol, 39% yield) as a colourless crystalline solid. mp 176-179 °C. δ_H (400 MHz; $CDCl_3$; $CHCl_3$) 0.94 (6 H, t, *J* = 7.0, Me), 1.32 - 1.44 (8 H, m, C-C-H), 1.45 - 1.55 (4 H, m, C-C-H), 1.83 (4 H, quin, *J* = 6.9, C-C-H), 4.02 (4 H, *t*, J = 6.9, Ar-O-C-H), 7.03 (4 H, d, *J* = 8.7, C(3')H), 7.68 (4 H, d, *J* = 8.7, C(2')H), 7.85 (2 H, d, *J* = 9.3, C(6)H), 7.97 (2 H, d, *J* = 2.0, C(3)H), 8.00 (2 H, d, *J* = 2.0, C(1)H), 9.53 (2 H, d, *J* = 9.3, C(5)H). δ_C (101 MHz; $CDCl_3$; $^{13}CDCl_3$) 14.0, 22.6, 25.7, 29.3, 31.6, 68.2, 115.0, 124.3, 125.4, 126.0, 126.5, 128.2, 129.0, 129.6, 131.2, 131.7, 134.8, 138.9, 159.3. *m/z* (MALDI-Dithranol-TCNQ) 652 ($[M(^{37}Cl_2)]^+$, 15%), 650 ($[M(^{35}Cl + ^{37}Cl)]^+$, 75), 648 ($[M(^{35}Cl_2)]^+$, 100), 616 ($[M(^{37}Cl) – Cl + H]^+$, 15), 614 ($[M(^{35}Cl) – Cl + H]^+$, 40), 580 (25). HR *m/z* (EI) $C_{42}H_{42}{}^{35}Cl_2O_2$ requires 648.2556, found 648.2547. ν_{max}/cm^{-1}

3160, 3057 and 3034 (Ar C-H), 2954, 2930s and 2870 (C-H), 1606s, 1574w, 1516 and 1502s (Ar C=C).

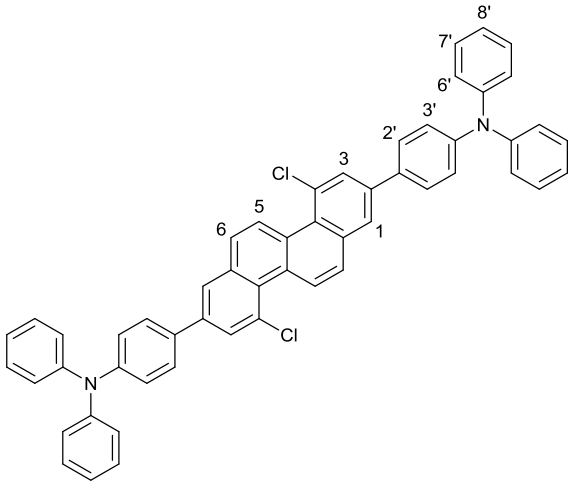

4,10-Dichloro-2,8-*bis*[4-(diphenylamino)phenyl]chrysene (**122**)

4,10-Dichloro-2,8-*bis*(4,4',5,5'-tetramethyl-1,3,2-dioxaborolan-2-yl)chrysene (**118**) (125.7 mg, 0.2289 mmol) and 4-iodo-N,N-diphenylaniline (**128**) (185.7, 0.5002 mmol) were added to a pear shaped flask (10 mL) equipped with a Claisen adapter which was then purged with N_2. Toluene (3 mL) and aliquat 336® (2 drops) were then added *via* syringe and the solution degassed with N_2 for 15 minutes with vigorous stirring. K_2CO_3 (415.6 mg, 3.007 mmol) was then dissolved in water (1.5 mL) to form a 2 M solution which after degassing for 15 minutes with N_2 was added to the reaction mixture. The toluene/water biphase was then degassed for a further 15 minutes before toluene (~1 mL) was removed by syringe and used to take up $Pd(PPh_3)_4$ (7.9 mg, 0.0068 mmol, 3 mol%) (under N_2) before reinjection into the reaction mixture. The reaction was then stirred at 80 °C overnight. The toluene layer was then collected and the water layer washed with toluene (5 mL). The combined organic layers were then washed with water (2 × 4 mL) and brine (2 × 4 mL) before concentration *in vacuo*, to isolate the crude product. Initial purification was achieved by dissolving the crude in an excess of hot DCM followed by concentration *in vacuo* to the point of precipitation (~10 mL) at which point the solution was added to a beaker of stirring petroleum ether (40 mL) and the precipitated product collected *via* filtration with a sintered funnel. The process was then repeated once more before final purification by column chromatography utilising a graded solvent system from 10% DCM in petroleum ether to 100% ethyl acetate to isolate the purified *title compound* (**122**) (63.9 mg, 0.0815 mmol, 36% yield) as a light green solid. mp 319-321 °C. δ_H (500 MHz; $CDCl_3$; $CHCl_3$) 7.09 (4 H, t, J = 7.6, C(8')H), 7.19 (8 H, d, J

= 7.6, C(6')H), 7.22 (4 H, d, *J* = 8.5, C(3')H), 7.31 (8 H, t, *J* = 7.6, C(7')H), 7.66 (4 H, d, *J* = 8.5, C(2')H), 7.90 (2 H, d, *J* = 9.3, C(6)H), 8.02 (2 H, d, *J* = 2.1, C(3)H), 8.07 (2 H, d, *J* = 2.1, C(1)H), 9.58 (2 H, d, *J* = 9.3, C(5)H). δ_C (126 MHz; $CDCl_3$; $^{13}CDCl_3$) 123.3, 123.6, 124.4, 124.7, 125.5, 126.2, 126.6, 127.9, 128.9, 129.4, 129.6, 131.8, 132.5, 134.8, 138.7, 147.5, 148.0. *m/z* (MALDI-TCNQ) 786 ($[M(^{37}Cl_2)]^+$, 30%), 784 ($[M(^{35}Cl + ^{37}Cl)]^+$, 90), 782 ($[M(^{35}Cl_2)]^+$, 100), 750 ($[M(^{37}Cl) – Cl + H]^+$, 10), 748 ($[M(^{35}Cl) – Cl + H]^+$, 20), 554 (35), 441 (10), 327 (15), 293 (20), 276 (15), 242 (20). HR *m/z* (ASAP) $C_{54}H_{36}{}^{35}Cl_2N_2$ + H requires 783.2328, found 783.2322. ν_{max}/cm^{-1} 3061, 3035, 2953, 2923w and 2870w (Ar C-H), 1611, 1588s and 1517 (Ar C=C).

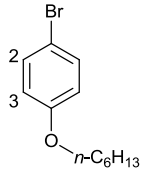

4-(*n*-Hexyloxy)bromobenzene (**124**)

Prepared by an adaptation of a literature synthesis[169]

4-Bromophenol (**123**) (1.00 g, 5.78 mmol) and K_2CO_3 (2.64 g, 19.1 mmol) were added to a two neck RBF (50 mL) equipped with a condenser which was then purged with N_2. Dry acetone (16 mL) and 1-bromohexane (1.05 g, 6.36 mmol) were then added *via* syringe before the reaction was heated to reflux overnight. The inorganic by-products were then removed by filtration though celite® and the solvent removed *in vacuo*. The resulting brown oil was then dissolved in DCM (50 mL) and washed with NaOH solution (1 M) (2 × 15 mL), water (2 × 20 mL) and brine (2 × 20 mL). The organic layer was then dried over $MgSO_4$ and concentrated *in vacuo* to isolate the crude product which was then purified by column chromatography with a graded solvent system from 100% petroleum ether to 10% DCM in petroleum ether to afford the purified *title compound* (**124**) (1.18 g, 4.59 mmol, 79% yield) as a yellow tinged oil. δ_H (500 MHz; $CDCl_3$; $CHCl_3$) 0.92 (3 H, t, *J* = 7.0, Me), 1.29 - 1.40 (4 H, m, C-C-H), 1.41 - 1.50 (2 H, m, C-C-H), 1.77 (2 H, quin, *J* = 6.9, C-C-H), 3.92 (2 H, t, *J* = 6.9, Ar-O-C-H), 6.75 - 6.81 (2 H, m, C(3)H), 7.34 - 7.40 (2 H, m, C(2)H). δ_C (126 MHz; $CDCl_3$; $^{13}CDCl_3$) 14.0, 22.6, 25.7, 29.1, 31.6, 68.3, 112.5, 116.3, 132.2, 158.3. *m/z* (GC/MS) (EI) Single component: 258.1 ($[M(^{81}Br)]^+$, 55%), 256.1 ($[M(^{79}Br)]^+$, 55), 174.0 ($[M(^{81}Br) - C_6H_{13} + H]^+$, 100), 172.0 ($[M(^{79}Br) - C_6H_{13} + H]^+$, 100), 157.0 ($[M(^{81}Br) - OC_6H_{13}]^+$, 15), 155.0 $[M(^{79}Br) - OC_6H_{13}]^+$, 15), 145.0 (15), 143.0 (15), 93.1 (10), 65.1 (20). ^1H NMR comparable to that in the literature.[169]

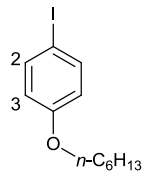

4-(*n*-Hexyloxy)iodobenzene (**125**)

4-(*n*-Hexyloxy)bromobenzene (**124**) (3.00 g, 11.7 mmol) was added *via* syringe to a three neck RBF (100 mL) which was then purged with N_2. Dry THF (33 mL) was then added *via* syringe and the solution cooled to -78 °C before *n*-butyllithium (1.6 M in hexanes) (8.0 mL, 13 mmol) was added dropwise *via* syringe. The solution was stirred at -78 °C for ~30 minutes before injection *via* syringe (4 × ~10 mL) into a solution of I_2 (3.55 g, 14.0 mmol) in dry THF (22 mL) in a three neck RBF (100 mL) at room temperature. The combined solution was then stirred at room temperature for ~1 h before it was concentrated *in vacuo*, re-dissolved in DCM (100 mL) and washed with water (50 mL), concentrated sodium thiosulfate solution (2 × 50 mL) and brine (2 × 50 mL) before drying over $MgSO_4$ and concentrating *in vacuo*. The crude product was then subjected to column chromatography in a graded solvent system from 100% petroleum ether to 10% DCM in petroleum ether to afford the *title compound* (**125**) (1.88 g, 6.18 mmol, 53% yield) as a colourless oil. δ_H (500 MHz; $CDCl_3$; $CHCl_3$) 0.91 (3 H, t, *J* = 7.0, Me), 1.31 - 1.37 (4 H, m, C-C-H), 1.40 - 1.50 (2 H, m, C-C-H), 1.77 (2 H, quin, *J* = 6.8, C-C-H), 3.92 (2 H, t, *J* = 6.8, Ar-O-C-H), 6.63 - 6.73 (2 H, m, C(3)H), 7.51 - 7.60 (2 H, m, C(2)H). δ_C (101 MHz; $CDCl_3$; $^{13}CDCl_3$) 14.0, 22.6, 25.7, 29.1, 31.5, 68.1, 82.4, 116.9, 138.1, 159.0. *m/z* (GC/MS) (EI) Single component: 304.1 ($[M]^+$, 40%), 220.1 ($[M - C_6H_{13} + H]^+$, 100), 93.2 ($[M - C_6H_{13} - I + H]^+$, 15), 65.2 (15). ^1H NMR comparable to that in the literature.[238]

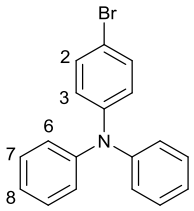

4-Bromo-N,N-diphenylaniline (**127**)

Prepared by an adaptation of a literature synthesis[170]

Triphenylamine (**126**) (5.00 g, 20.4 mmol) was added to a three neck RBF (250 mL) which was then purged with N_2. Dry chloroform (~150 mL) was then added *via* cannula and the solution cooled to ~-10 °C on a salt ice bath before NBS (3.66 g, 20.6 mmol) was added in three approximately equal portions, each 30 minutes apart. After the final addition the reaction mixture was allowed to stir to room temperature overnight. The reaction mixture was then concentrated *in vacuo* before being re-dissolved in DCM (100 mL) and washed with water (2 × 50 mL) and brine (2 × 50 mL), dried over $MgSO_4$ and concentrated *in vacuo*. The crude product was then recrystallized three times from MeOH to afford the purified *title compound* (**127**) (2.24 g, 6.91 mmol, 34% yield) as a colourless crystalline solid. mp 112-113 °C (lit.,[239] 106-111 °C). δ_H (500 MHz; $CDCl_3$; $CHCl_3$) 6.92 - 6.97 (2 H, m, C(3)H), 7.04 (2 H, tt, *J* = 8.0, 1.1, C(8)H), 7.08 (4 H, dd, *J* = 8.0, 1.1, C(6)H), 7.23 - 7.29 (4 H, m, C(7)H), 7.31 - 7.36 (2 H, m, C(2)H). δ_C (126 MHz; $CDCl_3$; $^{13}CDCl_3$) 114.8, 123.2, 124.4, 125.1, 129.4, 132.1, 147.0, 147.4. *m/z* (APCI) 326.0 ($[M(^{81}Br) + H]^+$, 15%), 324.0 ($[M(^{79}Br) + H]^+$, 15), 116.9 ($[M - C_{10}H_8Br + H]^+$, 30), 90.9 ($[M - C_{12}H_9Br]^+$, 35), 64.9 (15), 58.8 (100). ^1H NMR comparable to that in the literature.[240]

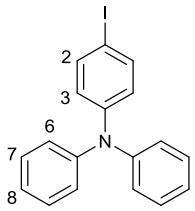

4-Iodo-N,N-diphenylaniline (**128**)

Prepared by an adaptation of a literature synthesis[171]

4-Bromo-N,N-diphenylaniline (**127**) (852.4 mg, 2.629 mmol) was added to a three neck RBF (100 mL) which was then purged with N_2. Dry THF (7.4 mL) was added and the solution cooled to -78 °C before *n*-butyllithium (1.6 M in hexanes) (1.8 mL, 2.9 mmol) was added. On addition a bright purple colour evolved before fading to brown. After 15 minutes the reaction was transferred to an acetonitrile dry ice bath to warm to ~-45 °C. After 30 minutes TLC analysis indicated incomplete consumption of the starting material so additional *n*-butyllithium (1.6 M in hexanes) (0.33 mL, 0.53 mmol) was added. The solution was stirred for a further 30 minutes before it was added *via* syringe to a solution of I_2 (801.2 mg, 3.157 mmol) in dry THF (5.0 mL) at -78 °C. The reaction was then allowed to warm to room temperature overnight. The solution was then concentrated *in vacuo* before taking up in DCM (~50 mL) and washing with water (2 × 25 mL), concentrated sodium bisulfite solution (2 × 25 mL) and brine (2 × 25 mL) before drying over $MgSO_4$ and concentrating *in vacuo*. The crude product was purified by column chromatography utilising a graded solvent system from petroleum ether to 10% DCM in petroleum ether to afford the purified (~85% pure by ^{1}H NMR) *title compound* (**128**) (321.2 mg, 0.8653 mmol, 33% yield) as a colourless crystalline solid. 4-Butyl-N,N-diphenylaniline was found to be the largely inseparable impurity, determined by GC/MS analysis. δ_H (500 MHz; $CDCl_3$; $CHCl_3$) 6.81 - 6.85 (2 H, m, C(3)H), 7.04 (2 H, tt, *J* = 8.0, 1.2, C(8)H), 7.08 (4 H, dd, *J* = 8.0, 1.2, C(6)H), 7.24 - 7.28 (4 H, m, C(7)H), 7.47 - 7.54 (2 H, m, C(2)H) (ignoring impurity peaks). *m/z* (GC/MS) (EI) First component: [4-(*n*-butyl)-N,N-diphenylaniline] 301.1 ($[M]^+$, 54%), 258 ($[M - C_3H_7]^+$, 100). Second Component: [4-Iodo-N,N-diphenylaniline] 371 ($[M]^+$, 100%), 243 ($[M - I - H]^+$, 18). ^{1}H NMR comparable to that in the literature.[241]

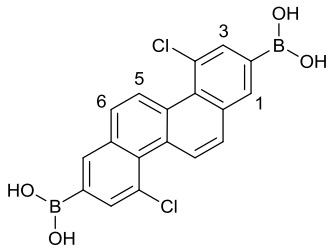

(4,10-Dichlorochrysene-2,8-diyl)diboronic acid (**129**)

4,10-Dichloro-2,8-*bis*(4,4',5,5'-tetramethyl-1,3,2-dioxaborolan-2-yl)chrysene (**118**) (100.5 mg, 0.1830 mmol) and $NaIO_4$ (234.3 mg, 1.095 mmol) were added to a two neck RBF (25 mL) which was then purged with N_2. A THF:water mixture (4:1) (1.5 mL) was then added *via* syringe and the reaction mixture stirred at room temperature for 30 minutes before HCl (1.2 M) (0.22 mL) was added *via* syringe and the reaction stirred at room temperature overnight. The reaction mixture was then diluted with water (10 mL) and extracted with ethyl acetate (2 × 20 mL). The combined organic extracts were then washed with water (2 × 20 mL) and brine (2 × 20 mL), dried over $MgSO_4$ and concentrated *in vacuo*. The crude product was then triturated with petroleum ether (3 × 3 mL) to afford the purified *title compound* (**129**) (60.5 mg, 0.1572 mmol, 86% yield) as an amorphous brown solid. mp 333-335 °C. δ_H (400 MHz; DMSO-d_6; DMSO-d_5) 8.07 (2 H, d, J = 9.2, C(6)H), 8.21 (2 H, d, J = 1.3, C(3)H), 8.50 (2 H, d, J = 1.3, C(1)H), 8.53 (4 H, s, B-OH), 9.47 (2 H, d, J = 9.2, C(5)H). δ_C (126 MHz; DMSO-d_6; DMSO-d_6) 125.7, 125.9, 127.5, 129.3, 129.6, 133.8, 134.6, 135.2. NB: As is commonly reported,[128] the ^{13}C NMR spectrum features no signals from the carbon *ipso*- to boron. *m/z* (MALDI-TCNQ-MeOH) 445 ($[M(^{37}Cl_2) - H_4 + (Me)_4 + H]^+$, 2%), 443 ($[M(^{35}Cl + ^{37}Cl) - H_4 + (Me)_4 + H]^+$, 8), 441 ($[M(^{35}Cl_2) - H_4 + (Me)_4 + H]^+$, 12), 440 ($[M(^{35}Cl_2) - H_4 + (Me)_4]^+$, 6), 431 ($[M(^{37}Cl_2) - H_3 + (Me)_3 + H]^+$, 2), 429 ($[M(^{35}Cl + ^{37}Cl) - H_3 + (Me)_3 + H]^+$, 6), 427 ($[M(^{35}Cl_2) - H_3 + (Me)_3 + H]^+$, 10), 426 ($[M(^{35}Cl_2) - H_3 + (Me)_3]^+$, 5), 417 ($[M(^{37}Cl_2) - H_2 + (Me)_2 + H]^+$, 4), 415 ($[M(^{35}Cl + ^{37}Cl) - H_2 + (Me)_2 + H]^+$, 19), 413 ($[M(^{35}Cl_2) - H_2 + (Me)_2 + H]^+$, 30), 412 ($[M(^{35}Cl_2) - H_2 + (Me)_2]^+$, 13), 403 ($[M(^{37}Cl_2) - H + Me + H]^+$, 3), 401 ($[M(^{35}Cl + ^{37}Cl) - H + Me + H]^+$, 14), 399 ($[M(^{35}Cl_2) - H + Me + H]^+$, 21), 398 ($[M(^{35}Cl_2) - H + Me]^+$, 9), 389 ($[M(^{37}Cl_2) + H]^+$, 7), 387 ($[M(^{35}Cl + ^{37}Cl) + H]^+$, 38), 385 ($[M(^{35}Cl_2) + H]^+$, 56), 384 ($[M(^{35}Cl_2)]^+$, 27), 328 (15), 294 (25), 274 (80), 233 (20), 207 (100). ν_{max}/cm^{-1} 3377 br (BOH_2), 3038w and 2961w (Ar C-H), 1700, 1609 and 1508 (Ar C=C).

Due to difficulty obtaining a high resolution mass spectrum of the boronic acid derivative, it was rederivatised with ethylene glycol *in situ* to the corresponding dioxaborolane prior to the mass measurement.

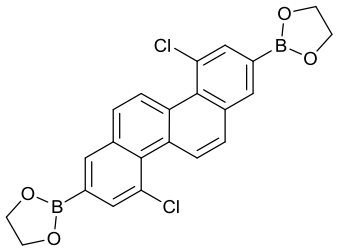

4,10-Dichloro-2,8-*bis*(1,3,2-dioxaborolan-2-yl)chrysene

HR *m/z* (ASAP) $C_{22}H_{16}{}^{11}B_2{}^{35}Cl_2O_4$ + H requires 437.0685 found 437.0685.

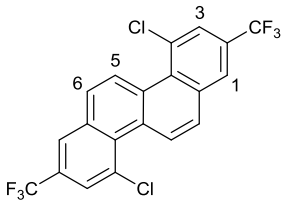

4,10-Dichloro-2,8-*bis*(trifluoromethyl)chrysene (**130**)

(4,10-Dichlorochrysene-2,8-diyl)boronic acid (**129**) (430.7 mg, 1.119 mmol), sodium triflinate (1.05 g, 6.73 mmol) and CuCl (221.8 mg, 2.240 mmol) were added to a single neck RBF (100 mL). A MeOH:DCM:water mixture (1:1:0.8) (3.7 mL) was then added and the flask stoppered under atmospheric conditions. TBHP (70 wt % in H_2O) (1.5 mL, 11 mmol) was then added dropwise *via* syringe at 0 °C and the reaction allowed to stir to room temperature overnight. The reaction was then extracted with DCM (2 × 25 mL) and the combined organic extracts washed with saturated sodium hydrogen carbonate solution (2 × 25 mL) and saturated sodium bisulfite solution (2 × 25) mL before drying over $MgSO_4$ and concentrating *in vacuo*. The crude product was then subjected to column chromatography utilising a petroleum ether solvent system to afford the purified *title compound* (**130**) (149.6 mg, 0.3454 mmol, 31% yield) as a colourless crystalline solid. mp 150-152 °C. δ_H (500 MHz; $CDCl_3$; $CHCl_3$) 7.97 (2 H, d, J = 9.1, C(6)H), 8.00 (2 H, d, J = 1.9, C(3)H), 8.22 (2 H, s, C(1)H), 9.62 (2 H, d, J = 9.1, C(5)H). δ_C (126 MHz; $CDCl_3$; $^{13}CDCl_3$) 123.3 (q, $J^1_{C\text{-}F}$ = 272.2), 124.7 (q, $J^3_{C\text{-}F}$ = 4.0), 125.7, 126.0 (q, $J^3_{C\text{-}F}$ = 3.3), 127.4, 129.0 (q, $J^2_{C\text{-}F}$ = 33.6), 129.1, 130.6, 132.6, 134.0. δ_F (376 MHz; $CDCl_3$) -62.41 (s). *m/z* (MALDI-TCNQ) 437 ([M($^{37}Cl_2$) + H]$^+$, 10%), 435 ([M(^{35}Cl + ^{37}Cl) + H]$^+$, 60), 433 ([M($^{35}Cl_2$) + H]$^+$, 90), 414 (25), 403 (25), 375 (40), 363 ([M – Cl_2 + H]$^+$, 15), 359 (50), 347 (25), 331 (100), 328 (55), 319 (55), 304 (65), 294 ([M – Cl_2 – CF_3 + H]$^+$, 25), 292 (15), 278 (15), 276 (95). HR *m/z* (EI) $C_{20}H_8{}^{35}Cl_2F_6$ requires 431.9902, found 431.9894. ν_{max}/cm^{-1} 3165w, 3087w, 2924w and 2851w (Ar C-H), 1627, 1512 and 1473 (Ar C=C).

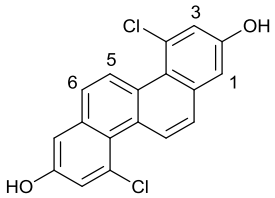

4,10-Dichloro-2,8-dihydroxychrsyene (**131**)

A sodium hydroxide pellet (55.3 mg, 1.38 mmol) was added to a two neck RBF (100 mL) which was then purged with N_2. THF (13 mL) was then added *via* syringe and the suspension stirred for ~15 mins before 4,10-dichloro-2,8-*bis*(4,4',5,5'-tetramethyl-1,3,2-dioxaborolan-2-yl)chrysene (**118**) (100.1 mg, 0.1823) was added against a flow of N_2. The solution was stirred for a further 10 mins before H_2O_2 (100 volumes, >30% w/v, 0.1 mL, ~0.9 mmol) was added *via* syringe. A yellow precipitate was observed after 1 h. The reaction was then stirred for an additional 1 h before concentration *in vacuo*. The crude product was then dissolved in DCM, acidified with HCl (~36 M, ~1 mL), washed with water (2 × 50 mL) and brine (2 × 50 mL), dried over $MgSO_4$ and concentrated in *vacuo*. Final purification was then achieved by column chromatography utilising a graded solvent system from 0.5% MeOH in DCM to 1.5% MeOH in DCM to afford the *title compound* (**131**) (7.8 mg, 0.024 mmol 13% yield) as a red/brown solid. mp 254-255 °C. δ_H (500 MHz; DMSO-d_6; DMSO-d_5) 7.32 (2 H, d, J = 2.7, C(3)H), 7.37 (2 H, d, J = 2.7, C(1)H), 7.81 (2 H, d, J = 9.1, C(6)H), 9.25 (2 H, d, J = 9.1, C(5)H), 10.33 (2 H, s, Ar-O-H). δ_C (126 MHz; DMSO-d_6; DMSO-d_6) 110.6, 120.4, 121.2, 124.8, 125.6, 127.4, 130.5, 134.9, 155.3. *m/z* (MALDI-Dithranol) 330 ([M(^{35}Cl + ^{37}Cl)]$^+$, 15%), 328 ([M(^{35}Cl$_2$)]$^+$, 25), 249 (20), 242 (10), 227 (100), 211 (25). HR *m/z* (APCI) $C_{18}H_{10}{}^{35}Cl_2O_2$ + H requires 329.0136, found 329.0146. ν_{max}/cm^{-1} 3233br (OH), 2923 and 2852 (Ar C-H), 1609 and 1515 (Ar C=C).

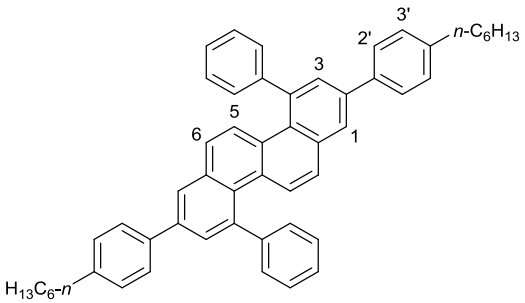

4,10-Diphenyl-2,8-*bis*[4-(*n*-hexyl)phenyl]chrysene (**132**)

Magnesium (387.6 mg, 15.94 mmol) was added to a three neck RBF and gently heated under vacuum before purging with N_2. Dry THF (6.0 mL) was then added *via* syringe before bromobenzene (2.00 g, 12.7 mmol) was slowly added *via* syringe without stirring. After the addition of approximately 50% of the bromobenzene, gentle heating was used to initiate the Grignard reaction. Stirring was then begun and the remaining bromobenzene was added dropwise so as to maintain reflux. After the reaction mixture had returned to room temperature and a colour change to a dark brown was observed, the consumption of bromobenzene was confirmed by GC/MS of a sample of the water quenched solution. 4,10-Dichloro-2,8-*bis*[4-(*n*-hexyl)phenyl]chrysene (**120**) (200.5 mg, 0.3246 mmol) and PEPPSI-IPr (17.9 mg, 0.0263 mmol, 8 mol%) were then added to a pear shaped flask (10 mL) equipped with a Claisen adaptor which was then purged with N_2. Dry THF (3.3 mL) was then added and the solution degassed with vigorous stirring. The reaction was then cooled to 0 °C in an ice bath before the previously formed phenylmagnesium bromide solution was added dropwise *via* syringe (0.46 mL, 0.97 mmol) and the reaction mixture stirred to room temperature overnight. An additional portion of the phenylmagnesium bromide solution (0.23 mL, 0.49 mmol) was then added and the reaction stirred at room temperature for 30 minutes before a third portion of the phenylmagnesium bromide solution (0.23 mL, 0.49 mmol) was added and the reaction stirred for a further 30 minutes at which point TLC analysis indicated the consumption of the starting material. The reaction mixture was then quenched by the dropwise addition of water (10 mL) before addition to a separating funnel with water (~45 mL) and toluene (~20 mL). The organic layer was then washed with water (2 × 10 mL) and brine (2 × 10 mL) before being dried over $MgSO_4$ and concentrated *in vacuo*. The crude product was partially purified by column chromatography with a graded solvent system from 5% DCM in petroleum ether to 10% DCM in petroleum

ether. The partially purified product was then recrystallised from petroleum ether to afford the *title compound* (**132**) (69.0 mg, 0.0984 mmol, 30% yield) as an off-white crystalline solid. mp 159-161 °C. δ_H (500 MHz; $CDCl_3$; $CHCl_3$) 0.92 (6 H, t, *J* = 7.0, Me), 1.30 - 1.45 (12 H, m, C-C-H), 1.68 (4 H, quin, *J* = 7.7, C-C-H), 2.69 (4 H, t, *J* = 7.7, Ar-C-H), 7.31 (4 H, d, *J* = 8.2, C(2':3')H), 7.44 - 7.53 (8 H, m, Ar-H + C(5)H), 7.54 - 7.59 (4 H, m, Ar-H), 7.69 (4 H, d, *J* = 8.2, C(2':3')H), 7.77 (2 H, d, *J* = 9.1, C(6)H), 7.80 (2 H, d, *J* = 2.1, C(1:3)H), 8.00 (2 H, d, *J* = 2.1, C(1:3)H). δ_C (126 MHz; $CDCl_3$; $^{13}CDCl_3$) 14.1, 22.6, 29.0, 31.5, 31.8, 35.7, 124.8, 125.2, 127.1, 127.2, 127.8, 128.0, 129.0, 129.2, 129.9, 130.4, 133.5, 137.7, 138.3, 140.8, 142.5, 145.0. NB: 16 Aromatic carbons detected rather than 17, this is assumed to be due to overlap. *m/z* (MALDI-DCTB) 701 ($[M + H]^+$, 70%), 592 (84), 413 (20), 271 (26), 249 (100), 227 (98), 211 (38). HR *m/z* (EI) $C_{54}H_{52}$ requires 700.4064, found 700.4069. ν_{max}/cm^{-1} 3051w and 3025w (Ar C-H), 2952, 2922s and 2852 (C-H) 1609, 1578w and 1511 (Ar C=C).

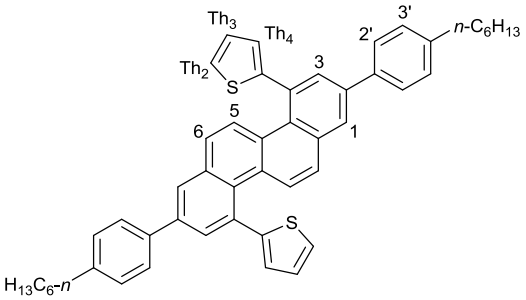

4,10-*Bis*(2-thienyl)-2,8-*bis*[4-(*n*-hexyl)phenyl]chrysene (**133**)

Prepared by a supervised student[2]

Magnesium turnings (179.0 mg, 7.36 mmol) were added to a three neck RBF (100 mL). Dry THF (10 mL) was then added *via* syringe before 2-bromothiophene (1.00 g, 6.13 mmol) was slowly added to the flask *via* syringe with vigorous stirring. Gentle heating was then used to initiate the Grignard reaction. After the reflux had ceased and the reaction cooled to room temperature the Grignard reagent solution was then cooled on ice to 0 °C. 4,10-Dichloro-2,8-*bis*[4-(*n*-hexylphenyl)]chrysene (**120**) (100.0 mg, 0.162 mmol) and PEPPSI-IPr (8.8 mg, 0.013 mmol, 8 mol%) were then added to a two neck RBF (50 mL) which was then purged with N_2. Thoroughly degassed dry THF (1.0 mL) was then added *via* syringe and the reaction cooled on ice to 0 °C before a portion of the previously formed Grignard reagent solution (2.8 mL, 1.7 mmol) was added dropwise *via* syringe. The reaction was then stirred to room temperature overnight. The reaction mixture was then taken up in toluene (20 mL), washed with with water (2 × 10 mL) and brine (2 × 10 mL), dried over $MgSO_4$ and concentrated *in vacuo*. The crude product was then purified by column chromatography eluting with a 10% DCM in petroleum ether solvent system to afford the *title compound* (**133**) (64.9 mg, 0.0910 mmol, 56% yield) as a pale green solid. mp 184-186 °C. δ_H (500 MHz; $CDCl_3$; $CHCl_3$) 0.91 (6 H, t, *J* = 7.1, Me), 1.29 - 1.43 (12 H, m, C-C-H), 1.67 (4 H, quin, *J* = 7.7, C-C-H), 2.68 (4 H, t, *J* = 7.7, Ar-C-H), 7.16 - 7.20 (4 H, m, C(Th_3)H + C(Th_4)H), 7.32 (4 H, d, *J* = 8.2, C(2':3')H), 7.47 (2 H, dd, *J* = 4.9, 1.4, C(Th_2)H), 7.55 (2 H, d, *J* = 9.1, C(5)H), 7.69 (4 H, d, *J* = 8.2, C(2':3')H), 7.92 (2 H, d, *J* = 2.1, C(1:3)H), 7.94 (2 H, d, *J* = 9.1, C(6)H), 8.03 (2 H, d, *J* = 2.1, C(1:3)H). δ_C (126 MHz; $CDCl_3$; $^{13}CDCl_3$) 14.1, 22.6, 29.0, 31.5, 31.7, 35.7, 124.8, 125.9, 126.1, 126.3, 127.15, 127.20, 127.7, 128.9, 129.0, 130.5, 130.6, 132.8, 133.6, 137.3, 138.2, 142.6, 146.4. *m/z* (MALDI-TCNQ) 713 ($[M + H]^+$, 100%), 436 (10), 381 (10), 327 (15), 323 (20), 219 (55). HR *m/z* (EI) $C_{50}H_{48}S_2$

requires 712.3192, found 712.3188. ν_{max}/cm^{-1} 3100w and 3025w (Ar C-H), 2952, 2918s and 2851 (C-H), 1608, 1519 and 1507 (Ar C=C).

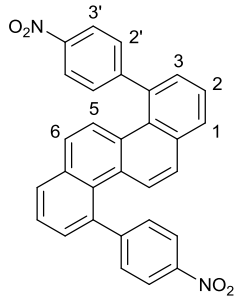

4,10-*Bis*(4-nitrophenyl)chrysene (**134**)

KO^{t}Bu (50.3 mg, 0.448 mmol) and PEPPSI-IPr (3.3 mg, 0.0049 mmol, 3 mol%) were added to a pear shaped flask (10 mL) equipped with a Claisen adapter which was then purged with N_2. Dry degassed EtOH (4.0 mL) was then added *via* syringe and the reaction stirred for 10 minutes to ensure activation of the catalyst. 4,10-Dichlorochrysene (**32**) (50. 3 mg, 0.169 mmol) and 4-nitrophenylboronic acid (68.3 mg, 0.409 mmol) were then added to the reaction flask against a flow of N_2. After 1.5 h additional PEPPSI-IPr (2.9 mg, 0.0043 mmol, 2.5 mol%) was added to the reaction flask against a flow of N_2 and the reaction stirred overnight. Purification was then achieved by directly dry loading the crude reaction mixture *via* DCM/silica onto a chromatography column and eluting with a 50% DCM in petroleum ether solvent system to obtain the partially purified product. The partially purified product was then recrystallised from toluene to obtain the pure *title compound* (**134**) (16.7 mg, 0.0355 mmol, 21% yield) as a green crystalline solid. mp >300 °C. δ_H (500 MHz; $CDCl_3$; $CHCl_3$) 7.48 (2 H, d, *J* = 9.1, C(5:6)H), 7.54 (2 H, dd, *J* = 7.6, 1.2, C(1:3)H), 7.60 (2 H, d, *J* = 9.1, C(5:6)H), 7.64 - 7.70 (6 H, m, C(2)H + C(2')H), 7.90 (2 H, dd, *J* = 7.6, 1.2, C(1:3)H), 8.35 (4 H, d, *J* = 8.8, C(3')H). δ_C (126 MHz; $CDCl_3$; $^{13}CDCl_3$) 124.3, 124.9, 126.2, 127.8, 128.6, 129.1, 130.0, 130.1, 130.9, 133.0, 137.9, 147.0, 151.6. *m/z* (MALDI-TCNQ) 471 ($[M + H]^+$, 100%). HR *m/z* (EI) $C_{30}H_{18}O_4N_2$ requires 470.1261, found 470.1277. ν_{max}/cm^{-1} 3105w, 3079w, 3042w, 2922 and 2849 (Ar C-H), 1591s (Ar C=C) 1508vs and 1340s (Ar NO_2).

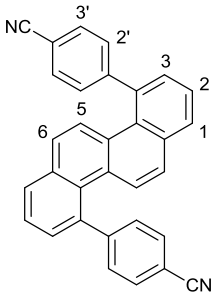

4,10-*Bis*(4-cyanophenyl)chrysene (**135**)

KO^{t}Bu (567.2 mg, 5.055 mmol) and PEPPSI-IPr (39.8 mg, 0.0586 mmol, 3 mol%) were added to three neck RBF (100 mL) which was then purged with N_2. Dry degassed EtOH (3.8 mL) was then added *via* syringe and the reaction stirred for 10 minutes to ensure activation of the catalyst (the evolution of a dark pink/red colouration was noted). Additional dry degassed EtOH (21 mL) was then added *via* syringe before 4,10-dichlorochrysene (**32**) (643.8 mg, 2.166 mmol) and 4-cyanophenylboronic acid (685.0 mg, 4.662 mmol) were added against a flow of N_2. Additional dry degassed EtOH (20 mL) was then added *via* syringe and the reaction stirred overnight. Purification was then achieved by directly dry loading the crude reaction mixture *via* DCM/silica onto a chromatography column and eluting with a graded solvent system from 10% ethyl acetate in petroleum ether to 30% ethyl acetate in petroleum ether to obtain the purified *title compound* (**135**) (106.3 mg, 0.2469 mmol, 11% yield) as a colourless crystalline solid. To obtain analytically pure material, an additional mixed solvent recrystallisation from a toluene/acetone and petroleum ether solvent system yielded the pure product 4,10-*bis*(4-cyanophenyl)chrysene (39.2 mg, 0.0911 mmol, 4% yield). mp 293-295 °C. δ_H (500 MHz; $CDCl_3$; $CHCl_3$) 7.47 (2 H, d, *J* = 9.0, C(5:6)H), 7.51 (2 H, dd, *J* = 7.7, 1.3, C(1:3)H, 7.58 (2 H, d, *J* = 9.0, C(5:6)H), 7.61 (4 H, d, *J* = 8.4, C(2')H), 7.65 (2 H, t, *J* = 7.7, C(2)H), 7.77 (4 H, d, *J* = 8.4, C(3')H), 7.90 (2 H, dd, *J* = 7.7, 1.3, C(1:3)H). δ_C (126 MHz; $CDCl_3$; $^{13}CDCl_3$) 110.9, 119.0, 124.8, 126.2, 127.7, 128.5, 128.9, 129.9, 130.1, 130.8, 132.8, 133.0, 138.2, 149.5. *m/z* (MALDI-TCNQ) 431 ([M + H]$^+$, 100%), 222 (25). HR *m/z* (EI) $C_{32}H_{18}N_2$ requires 430.1465, found 430.1450. ν_{max}/cm^{-1} 3039w, 2925w and 2852w (Ar C-H), 2227 (C≡N), 1602 (Ar C=C).

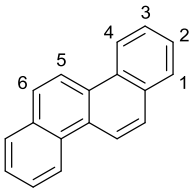

Chrysene (**25**)

Formed during the attempted preparation of:

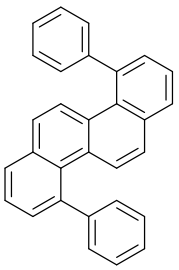

4,10-Diphenylchrysene (**51**)

4,10-Dichlorochrysene (**32**) (296.8 mg, 0.9987 mmol), Cs_2CO_3 (1.95 g, 5.98 mmol) and PEPPSI-IPr (68.1 mg, 0.100 mmol, 10 mol%) were added to a three neck RBF (100 mL) which was then purged with N_2. Degassed MeOH (3 mL) was then added, followed by degassed toluene (3 mL). With stirring, phenylboronic acid pinacol ester (0.47 g, 2.30 mmol) was then added *via* syringe and the reaction immediately placed in a pre-heated oil bath and stirred at 90 °C overnight. The crude product was then purified by directly dry loading the crude material *via* DCM/silica onto a chromatography column and eluting with 10% DCM in petroleum ether solvent system to afford the *title compound* (**25**) (170.0 mg, 0.7447 mmol, 75% yield) as a colourless crystalline solid. mp 253-254 °C (lit.,[97] 254-255 °C). δ_H (500 MHz; $CDCl_3$; $CHCl_3$) 7.63 - 7.68 (2 H, m, C(2)H), 7.71 - 7.75 (2 H, m, C(3)H), 7.98 - 8.07 (4 H, m, C(1)H + C(6)H), 8.75 (2 H, d, *J* = 8.8, C(5)H), 8.81 (2 H, d, *J* = 8.5, C(4)H). δ_C (126 MHz; $CDCl_3$; $^{13}CDCl_3$) 121.2, 123.2, 126.4, 126.7, 127.3, 128.2, 128.6, 130.6, 132.2. *m/z* (MALDI-TCNQ) 362 (15%), 292 (35), 229 ($[M + H]^+$, 100). ^{1}H NMR comparable to that in the literature.[97]

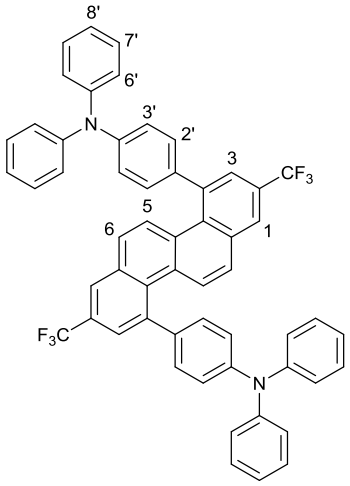

4,10-*Bis*[4-(diphenylamino)phenyl]-2,8-*bis*(trifluoromethyl)chrysene (**137**)

Magnesium turnings (375.7 mg, 15.45 mmol) were added to a three neck RBF (100 mL) which was then purged with N_2 and the turnings dry stirred overnight. Dry degassed THF (2.0 mL) was then added and the magnesium activated by the addition of 1,2-dibromoethane (0.30 mL, 3.5 mmol). Once the reaction had cooled to room temperature, without stirring, a crystal of I_2 was added, and a solution of 4-bromo-N,N-diphenylaniline (**127**) (2.00 g, 6.17 mmol) in dry degassed THF (3.5 mL) was added to the magnesium around the I_2 crystal. Stirring was then restarted and the reaction heated to ~60 °C at which point it began to reflux and a colour change to light green/brown was observed. The reaction was then immediately taken off heat and allowed to cool to room temperature, at which point it was placed in an ice water bath. 4,10-Dichloro-2,8-*bis*(trifluoromethyl)chrysene (**130**) (33.9 mg, 0.0783 mmol) and PEPPSI-IPr (4.8 mg, 0.0071 mmol, 9 mol%) were then added to a pear shaped flask (10 mL) equipped with a Claisen adapter, which was then purged with N_2 before dry degassed THF (0.8 mL) was added. The flask was then cooled to 0 °C in an ice bath and a portion of the previously formed 4-(diphenylamino)phenylmagnesium bromide (**136**) solution (0.21 mL, 0.24 mmol) added dropwise *via* syringe. A deep red colour was observed upon addition and the reaction was stirred at 0 °C for 30 minutes and then at room temperature for a further 30 minutes. Following the reaction by TLC analysis, further portions of 4-(diphenylamino)phenylmagnesium bromide (**136**) solution ([0.21 mL, 0.24 mmol] and [0.35 mL, 0.39 mmol]) were added dropwise at room temperature *via* syringe 30 minutes apart and the reaction stirred overnight after the final addition. The reaction

was then quenched by the addition of water (5 mL) and the reaction extracted with DCM (3 × 5 mL). The combined organic extracts were then washed with water (2 × 10 mL) and brine (2 × 10 mL) and dried over $MgSO_4$ before being concentrated *in vacuo*. The crude product was then subjected to column chromatography with a graded solvent system from 100% petroleum ether to 5% DCM in petroleum ether to obtain the purified product. Final purification was achieved *via* trituration with hot acetone (3 × 7 mL) to obtain the *title compound* (**137**) (31.2 mg, 0.0367 mmol, 47% yield) as a light green solid. mp 345-347 °C. δ_H (500 MHz; $CDCl_3$; $CHCl_3$) 7.08 (4 H, tt, *J* = 7.3, 1.1, C(8')H), 7.17 (4 H, d, *J* = 8.8, C(3')H), 7.22 (8 H, dd, *J* = 8.7, 1.1, C(6')H), 7.29 - 7.35 (12 H, m, C(2')H + C(7')H), 7.58 (2 H, d, *J* = 9.1, C(5)H), 7.76 (2 H, d, *J* = 1.9, C(1:3)H), 8.01 (2 H, d, *J* = 9.1, C(6)H), 8.12 (2 H, s, C(1:3)H). δ_C (126 MHz; $CDCl_3$; $^{13}CDCl_3$) 123.3, 123.7, 124.2 (q, $J^1_{C\text{-}F}$ = 272.3), 124.5 (q, $J^3_{C\text{-}F}$ = 4.1), 124.7, 124.8, 125.8 (q, $J^3_{C\text{-}F}$ = 3.2), 128.0 (q, $J^2_{C\text{-}F}$ = 32.8), 128.4, 129.4, 129.8, 130.8, 131.5, 132.8, 137.0, 141.5, 147.5, 147.6. δ_F (376 MHz; $CDCl_3$) -62.16 (s). *m/z* (MALDI-TCNQ) 850 ($[M]^+$, 70%), 648 (15), 620 ($[M - C_{18}H_{15} + H]^+$, 30), 592 (10), 500 (30), 477 (55), 437 (25), 413 (10), 400 (10), 381 (25), 374 (15), 358 (25), 353 (15), 330 (55), 318 (20), 302 (40), 293 (12), 274 (55), 250 (100). HR *m/z* (ASAP) $C_{56}H_{36}F_6N_2$ + H requires 851.2855, found 851.2844. ν_{max}/cm^{-1} 3036w and 2954w (Ar C-H), 1610, 1591s and 1504 (Ar C=C).

4.2-2 Pyrene Derivatives

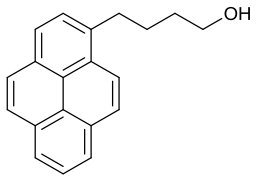

4-(Pyren-1-yl)butan-1-ol (**138**)

Prepared by the adaptation of a literature synthesis[242]

1-Pyrenebutyric acid (**106**) (0.30 g, 1.0 mmol) was added to a three neck RBF (100 mL) which was then purged with N_2. The flask was then cooled to 0 °C in an ice bath before borane tetrahydrofuran complex solution (1.0 M) (5.0 mL, 5.0 mmol) was added *via* syringe. The reaction was stirred for 10 minutes at 0 °C and then 10 minutes at room temperature. Additional borane tetrahydrofuran complex solution (1M) (2.0 mL, 2.0 mmol) was then added *via* syringe and the reaction heated to 60 °C overnight. The reaction was then cooled to room temperature before MeOH (7.0 mL) was added *via* syringe and the reaction stirred for 5 h. K_2CO_3 (200 mg, 1.45 mmol) was then added and after 10 minutes water (3.5 mL) was added *via* syringe. The reaction was then added to a separating funnel with water (30 mL) and extracted with DCM (2 × 15 mL). The combined organic extracts were then washed with water (15 mL) and brine (15 mL) before drying over $MgSO_4$ and concentrating *in vacuo*. The crude product was then purified by column chromatography with a graded solvent system from 20% ethyl acetate in petroleum ether to 30% ethyl acetate in petroleum ether to afford the *title compound* (**138**) (156.6 mg, 0.5708 mmol, 57% yield) as an off-colour oil which crystallised on standing to an off-white solid. mp 76-77 °C (lit.,[243] 72.5-74.5 °C). δ_H (400 MHz; $CDCl_3$; $CHCl_3$) 1.33 (1 H, s, OH), 1.70 - 1.81 (2 H, m, C-C-H), 1.89 - 2.00 (2 H, m, C-C-H), 3.38 (2 H, t, *J* = 7.7, Ar-C-H), 3.71 (2 H, t, *J* = 6.4, O-C-H), 7.88 (1 H, d, *J* = 7.8, Ar-H), 7.97 - 8.07 (3 H, m, Ar-H), 8.09 - 8.14 (2 H, m, Ar-H), 8.17 (2 H, dd, *J* = 7.7, 2.1, Ar-H), 8.29 (1 H, d, *J* = 9.3, Ar-H). δ_C (101 MHz; $CDCl_3$; $^{13}CDCl_3$) 27.9, 32.7, 33.2, 62.8, 123.4, 124.7, 124.75, 124.82, 125.0, 125.1, 125.8, 126.6, 127.19, 127.22, 127.5, 128.6, 129.8, 130.9, 131.4, 136.6. *m/z* (MALDI-Dithranol) 274 ($[M]^+$, 100%), 225 (45). ^{1}H NMR comparable to that in the literature.[196]

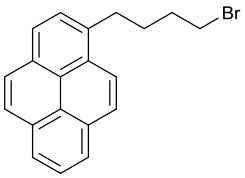

1-(4-Bromobutyl)pyrene (**139**)

Prepared by the adaptation of a literature synthesis[196]

CBr_4 (5.43 g, 16.4 mmol) and K_2CO_3 (2.70 g, 19.5 mmol) were added to a three neck RBF (250 mL) which was then purged with N_2. 4-(Pyren-1-yl)butan-1-ol (**138**) (3.59 g, 13.1 mmol) under N_2 was then taken up in dry DCM (62 mL) *via* syringe and injected into the reaction mixture, which was then cooled to 0 °C in an ice bath. PPh_3 (4.21 g, 16.1 mmol) in dry DCM (23 mL) was then added dropwise *via* syringe and the reaction mixture allowed to stir to room temperature for ~64 h. The crude product was purified by directly dry loading the crude material via DCM/silica onto a chromatography column and eluting with a 10% DCM in petroleum ether solvent system to afford the *title compound* (**139**) (3.52 g, 10.4 mmol, 79% yield) as a colourless oil which crystallised on standing into a colourless solid. mp 73-74 °C (lit.,[244] 71-72 °C). δ_H (500 MHz; $CDCl_3$; $CHCl_3$) 2.00 - 2.09 (4 H, m, C-C-H), 3.36 - 3.42 (2 H, m, Ar-C-H), 3.46 - 3.50 (2 H, m, Br-C-H), 7.87 (1 H, d, *J* = 8.5, Ar-H), 7.97 - 8.07 (3 H, m, Ar-H), 8.13 (2 H, d, *J* = 8.5, Ar-H), 8.18 (2 H, dd, *J* = 7.6, 3.5, Ar-H), 8.28 (1 H, d, *J* = 8.5, Ar-H). δ_C (126 MHz; $CDCl_3$; $^{13}CDCl_3$) 30.2, 32.6, 33.6, 123.2, 124.7, 124.8, 124.9, 125.0, 125.1, 125.8, 126.7, 127.2, 127.3, 127.5, 128.6, 129.9, 130.9, 131.4, 136.0. NB: Three aliphatic carbons detected rather than four due to overlap (as previously reported in the literature[196] and indicated by HSQC NMR spectroscopy). *m/z* (MALDI-Dithranol) 339 ($[M(^{81}Br) + H]^+$, 100%), 337 ($[M(^{79}Br) + H]^+$, 95), 227 (15). ^1H NMR comparable to that in the literature.[196]

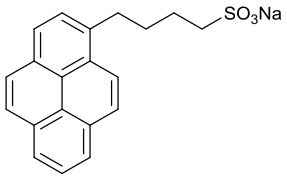

Sodium 4-(pyren-1-yl)butane-1-sulfonate (**140**)

Na_2SO_3 (4.48 g, 35.5 mmol) was added to a two neck RBF (250 mL) which was then purged with N_2. 1-(4-Bromobutyl)pyrene (**139**) (1.00 g, 2.97 mmol) was then ground with pestle and mortar before being taken up in portions into EtOH (6 × 10 mL) with sonication and injected into the reaction flask *via* syringe. Remaining unsuspended material after sonication in a final portion of EtOH (10 mL) was then added against a flow of N_2. Water (54 mL) was then added *via* syringe and the reaction heated to 100 °C overnight. The crude reaction mixture was then concentrated *in vacuo* and trituated with DCM (2 × 10 mL). The crude product was then recrystallised from an EtOH:water mixture (~1.3:1) (concentrating *in vacuo*) washing the filtered solid with ice cold water (10 mL) and DCM (10 mL). The partially purified material was then recrystallised one further time from an EtOH:water mixture (~1.3:1) (concentrating *in vacuo*) to afford the purified *title compound* (**140**) (604.3 mg, 1.677 mmol, 56% yield) as a colourless powder. mp >300 °C. δ_H (500 MHz; methanol-d_4; methanol-d_3) 1.94 - 2.03 (4 H, m, C-C-H), 2.87 - 2.92 (2 H, m, SO_3Na-C-H), 3.35 - 3.41 (2 H, m, Ar-C-H), 7.90 (1 H, d, J = 7.9, Ar-H), 7.95 - 8.04 (3 H, m, Ar-H), 8.08 - 8.13 (2 H, m, Ar-H), 8.13 - 8.18 (2 H, m, Ar-H), 8.32 (1 H, d, J = 9.14, Ar-H). δ_C (126 MHz, methanol-d_4; methanol-d_4) 26.4, 32.3, 34.3, 52.7, 124.6, 125.9, 126.0, 126.1, 126.3, 126.4, 127.0, 127.7, 128.4, 128.6, 128.7, 130.0, 131.4, 132.5, 133.0, 138.1. *m/z* (ESI^-) 697 ($[M - Na + M]^-$, 15%), 337 ($[M - Na]^-$, 100). (ESI^+) 743 ($[M + M + Na]^+$, 30%), 383 ($[M + Na]^+$, 100). HR *m/z* (ESI^+) $C_{20}H_{17}NaO_3S$ + Na requires 383.0694, found 383.0689. ν_{max}/cm^{-1} 3528br and 3475br ($SO_3Na•H_2O$), 3040 (Ar C-H), 2934 and 2868 (C-H), 1621, 1603 and 1586 (Ar C=C).

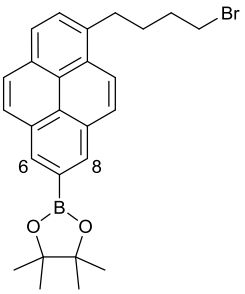

1-(4-Bromobutyl)-7-(4,4',5,5'-tetramethyl-1,3,2-dioxaborolan-2-yl)pyrene (**141**)

An oven dried microwave vial equipped with a stirrer bar was placed under a flushing N_2 needle. 1-(4-Bromobutyl)pyrene (**139**) (281.3 mg, 0.8341 mmol), *bis*(pinacolato)diboron (212.1 mg, 0.8352 mmol), $[Ir(OMe)(COD)]_2$ (28.0 mg, 0.0422 mmol, 5 mol%) and dtbpy (22.6 mg, 0.0842 mmol, 10 mol%) were then added against a flow of N_2. Dry THF (2.0 mL) was then added and the vial quickly capped as the N_2 needle was withdrawn. The reaction mixture was then heated at 80 °C for 1 h in a microwave reactor before concentration *in vacuo*. The crude product was then purified by column chromatography with a graded solvent system from 10% DCM in petroleum ether to 50% DCM in petroleum ether to obtain the *title compound* (**141**) (42.0 mg, 0.0907 mmol, 11% yield) as an off-white solid. mp 115-116 °C. δ_H (400 MHz;$CDCl_3$; $CHCl_3$) 1.48 (12 H, s, Me), 1.98 - 2.10 (4 H, m, C-C-H), 3.38 (2 H, t, *J* = 6.9, Ar-C-H), 3.48 (2 H, t, *J* = 6.2, Br-C-H), 7.88 (1 H, d, *J* = 7.8, Ar-H), 7.99 - 8.08 (2 H, m, Ar-H), 8.11 (1 H, d, *J* = 7.8, Ar-H), 8.15 (1 H, d, *J* = 9.3, Ar-H), 8.26 (1 H, d, *J* = 9.3, Ar-H), 8.62 (1 H, s, C(6:8)H), 8.63 (1 H, s, C(6:8)H). δ_C (101 MHz; CDCl3; $^{13}CDCl_3$) 25.0, 30.2, 32.6, 32.7, 33.6, 84.1, 123.1, 124.7, 125.0, 126.7, 127.1, 127.3, 127.67, 127.73, 129.1, 130.1, 130.4, 130.7, 131.2, 131.3, 135.9. NB: As is commonly reported,[128] the ^{13}C NMR spectrum features no signals from the carbon *ipso*- to the boron. *m/z* (MALDI-Dithranol) 464 ($[M(^{81}Br)]^+$, 50%), 462 ($[M(^{79}Br)]^+$, 50), 243 (80), 227 ([dithranol + H]$^+$, 100), 211 (15). HR *m/z* (APCI) $C_{26}H_{28}{}^{11}B^{79}BrO_2$ + H requires 463.1438, found 463.1442. ν_{max}/cm^{-1} 3040w and 2976 (Ar C-H), 2932 and 2865w (C-H), 1602 and 1552 (Ar C=C).

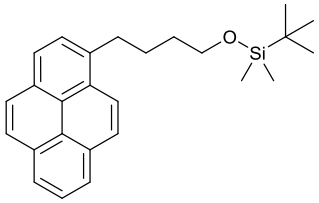

tert-Butyldimethyl(4-(pyren-1-yl)butoxy)silane (**142**)

4-(Pyren-1-yl)butan-1-ol (**138**) (1.66 g, 6.05 mmol), *tert*-butyldimethylsilyl chloride (2.19 g, 14.5 mmol) and imidazole (991.3 mg, 14.56 mmol) were added to a two neck RBF (100 mL) which was then purged with N_2. Dry DCM (25 mL) was then added *via* syringe and the reaction stirred at room temperature overnight. Purification was then achieved by directly dry loading the crude reaction mixture *via* DCM/silica onto a chromatography column and eluting with a graded solvent system from 20% DCM in petroleum ether to 30% DCM in petroleum ether solvent system to afford the *title compound* (**142**) (2.20 g, 5.65 mmol, 93% yield) as a colourless oil that crystallised on standing to a colourless crystalline solid. mp 43-44 °C. δ_H (400 MHz; $CDCl_3$; $CHCl_3$) 0.06 (6 H, s, Si-Me), 0.90 (9 H, s, Si-C-Me), 1.73 (2 H, quin, *J* = 7.3, C-C-H), 1.93 (2 H, quin, *J* = 7.3, C-C-H), 3.37 (2 H, t, *J* = 7.3, Ar-C-H), 3.70 (2 H, t, *J* = 7.3, O-C-H), 7.88 (1 H, d, *J* = 7.8, Ar-H), 7.96 - 8.06 (3 H, m, Ar-H), 8.08 - 8.14 (2 H, m, Ar-H), 8.17 (2 H, dd, *J* = 7.6, 3.4), 8.30 (1 H, d, *J* = 9.3, Ar-H). δ_C (101 MHz; $CDCl_3$; $^{13}CDCl_3$) -5.3, 18.4, 26.0, 28.1, 32.8, 33.3, 62.9, 123.5, 124.6, 124.8, 125.00, 125.03, 125.7, 126.5, 127.1, 127.2, 127.5, 128.6, 129.7, 130.9, 131.4, 137.1. NB: 15 Aromatic carbons detected rather than 16, this is presumed to be due to overlap. *m/z* (MALDI-DCTB) 388 ($[M]^+$, 100%). HR *m/z* (APCI) $C_{26}H_{32}OSi$ + H requires 389.2295, found 389.2294. ν_{max}/cm^{-1} 3040w (Ar C-H), 2943, 2924, 2892 and 2854 (C-H), 1602w and 1564 (Ar C=C).

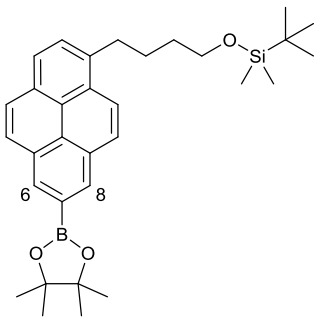

tert-Butyldimethyl(4-[7-(4,4',5,5'-tetramethyl-1,3,2-dioxaborolan-2-yl) pyren-1-yl]butoxy)silane (**143**)

tert-Butyldimethyl(4-(pyren-1-yl)butoxy)silane (**142**) (942.3 mg, 2.425 mmol), *bis*(pinacolato)diboron (740.0 mg, 2.914 mmol), $[Ir(OMe)(COD)]_2$ (81.2 mg, 0.122 mmol, 5 mol%) and dtbpy (65.9 mg, 0.246 mmol, 10 mol%) were added to a two neck RBF (100 mL) equipped with a condenser and purged with N_2. Cyclohexane (29 mL) was then added *via* syringe and the reaction heated to reflux overnight. The crude reaction mixture was then concentrated *in vacuo* and the product purified by column chromatography utilising a graded solvent system from 30% DCM in petroleum ether to 50% DCM in petroleum ether to isolate the analytically pure *title compound* (**143**) (459.9 mg, 0.8937 mmol, 37% yield) as a colourless solid. Additional product could be obtained by flushing the chromatography column, with 100% ethyl acetate followed by 10% MeOH in DCM. The flushed material was then dissolved in MeOH and purified by a precipitation process, concentrating the solution *in vacuo* to the point of precipitation, cooling the mixture to 0 °C and filtering the precipitate. This process was repeated with the filtrate two further times to maximise yield. The precipitated material was then combined with the initial columned material to obtain the partially purified (~95% pure) *title compound* (**143**) (851.0 mg, 1.654 mmol, 68% yield) as an off-white solid. mp 101-103 °C. δ_H (400 MHz; $CDCl_3$; $CHCl_3$) 0.06 (6 H, s, Si-Me), 0.90 (9 H, s, Si-C-Me), 1.47 (12 H, s, Me), 1.73 (2 H, quin, *J* = 6.8, C-C-H), 1.86 - 1.99 (2 H, m, C-C-H), 3.36 (2 H, t, *J* = 7.9, Ar-C-H), 3.70 (2 H, t, *J* = 6.8, O-C-H), 7.89 (1 H, d, *J* = 7.7, Ar-H), 7.99 - 8.07 (2 H, m, Ar-H), 8.08 - 8.15 (2 H, m, Ar-H), 8.28 (1 H, d, *J* = 9.3, Ar-H), 8.61 (1 H, s, C(6:8)H), 8.62 (1 H, s, C(6:8)H). δ_C (101 MHz; $CDCl_3$; $^{13}CDCl_3$) -5.3, 18.3, 25.0, 26.0, 28.1, 32.9, 33.3, 62.9, 84.1, 123.4, 124.7, 125.0, 126.8, 126.9, 127.4, 127.5, 127.7, 129.1, 130.20, 130.22, 130.7, 131.0, 131.1, 137.0. NB: As is commonly

reported,[128] the ^{13}C NMR spectrum features no signals from the carbon *ipso*- to the boron. *m/z* (MALDI-Dithranol) 515 ($[M + H]^+$, 100%). HR *m/z* (APCI) $C_{32}H_{43}{}^{11}BO_3Si$ + H requires 515.3147, found 515.3149. ν_{max}/cm^{-1} 3035w (Ar C-H), 2976, 2953, 2932 and 2857 (C-H), 1602 and 1552 (Ar C=C).

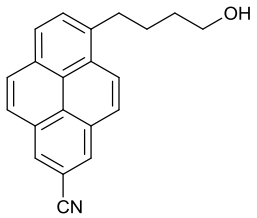

4-(7-Cyanopyren-1-yl)butan-1-ol (**144**)

Caution: Zinc cyanide is fatal if swallowed, in contact with skin or if inhaled and should be handled with great care. All gloves, spatulas, glassware and aqueous extracts to contact zinc cyanide should be quenched in 10% sodium hypochlorite solution overnight after use.

tert-Butyldimethyl(4-[7-(4,4',5,5'-tetramethyl-1,3,2-dioxaborolan-2-yl)pyren-1-yl]butoxy)silane (**143**) (684.5 mg, 1.330 mmol), $Zn(CN)_2$ (782.9 mg, 6.668 mmol), CsF (459.2 mg, 3.023 mmol) and $Cu(NO_3)_2 \bullet 2.5H_2O$ (928.8 mg, 3.993 mmol) were added to a three neck RBF (250 mL) against a flow of N_2. Dry DMF (90 mL) was then added *via* syringe and the reaction heated at 140 °C for 3 days. The crude reaction mixture was then added to a separating funnel with water (200 mL) and extracted with DCM (2 × 20 mL). The organic extracts were then washed with 5 wt% aqueous LiCl solution (2 × 100 mL) and brine (2 × 100 mL) extracting the aqueous layer each time with DCM (1 × 10 mL). The combined organic extracts were then dried over $MgSO_4$, and concentrated *in vacuo* into a single neck RBF (100 mL). A stirrer bar was added and this flask was then flushed with N_2 and placed under an N_2 needle before THF (7.5 mL) was added *via* syringe. The reaction mixture was then cooled to 0 °C in an ice bath before TBAF (1.0 M in THF) (2.0 mL, 2.0 mmol) was added dropwise *via* syringe and the reaction stirred to room temperature overnight. The reaction was then quenched by the addition of ammonium chloride (50 mL) and extracted with DCM (3 × 10 mL). The combined organic extracts were then dried over $MgSO_4$ and concentrated *in vacuo*. The crude product was then purified by column chromatography utilising a graded solvent system from 100% petroleum ether to 40% ethyl acetate in petroleum ether to obtain the *title compound* (**144**) (140.4 mg, 0.4690 mmol, 35% yield) as an off-white brown solid. mp 134-135 °C. δ_H (400 MHz; $CDCl_3$; $CHCl_3$) 1.27 (1 H, s, OH), 1.73 - 1.82 (2 H, m, C-C-H), 1.92 - 2.02 (2 H, m, C-C-H), 3.42 (2 H, t, *J* = 7.7, Ar-C-H), 3.74 (2

H, t, *J* = 6.1, O-C-H), 7.97 - 8.05 (2 H, m, Ar-H), 8.11 (1 H, d, *J* = 9.3, Ar-H), 8.14 (1 H, d, *J* = 8.9, Ar-H), 8.21 (1 H, d, *J* = 7.8, Ar-H), 8.37 - 8.43 (3 H, m, Ar-H). δ_C (101 MHz; $CDCl_3$; $^{13}CDCl_3$) 28.1, 32.6, 33.2, 62.7, 108.9, 119.7, 124.2, 125.2, 125.7, 126.0, 126.4, 126.5, 127.1, 127.2, 128.9, 129.1, 129.3, 130.2, 131.0, 131.5, 138.2. *m/z* (GC/MS) (EI) Single component: 299 ($[M]^+$, 35%), 240 ($[M - C_3H_6OH]^+$, 100). HR *m/z* (APCI) $C_{21}H_{17}NO$ + H requires 300.1383, found 300.1380. ν_{max}/cm^{-1} 3282br (OH), 3042w (Ar C-H), 2929, 2870 and 2835w (C-H), 2231 and 2218 (C≡N), 1602 and 1508w (Ar C=C).

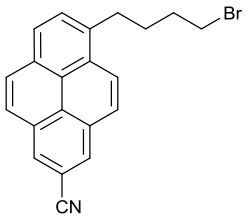

1-(4-Bromobutyl)-7-cyanopyrene (**145**)

4-(7-Cyanopyren-1-yl)butan-1-ol (**144**) (145.2 mg, 0.4850 mmol), CBr_4 (210.8 mg, 0.6356 mmol) and K_2CO_3 (102.3 mg, 0.7402 mmol) were added to a three neck RBF (100 mL) which was then purged with N_2. Dry DCM (3.5 mL) was then added *via* syringe and the reaction cooled to 0 °C in an ice bath. PPh_3 (163.2 mg, 0.6222 mmol) in dry DCM (1.0 mL) was then added dropwise and the reaction stirred to room temperature overnight. The product was purified by directly dry loading the crude reaction mixture *via* DCM/silica onto a chromatography column and eluting with a graded solvent system from 10% ethyl acetate in petroleum ether to 20% ethyl acetate in petroleum ether to afford the *title compound* (**145**) (110.9 mg, 0.3061 mmol, 61% yield) as an off-white brown solid. mp 117-118 °C. δ_H (400 MHz; $CDCl_3$; $CHCl_3$) 2.02 - 2.08 (4 H, m, C-C-H), 3.38 - 3.43 (2 H, m, Ar-C-H), 3.47 - 3.51 (2 H, m, Br-C-H), 7.99 (1 H, d, *J* = 7.8, Ar-H), 8.03 (1 H, d, *J* = 8.8, Ar-H), 8.10 - 8.17 (2 H, m, Ar-H), 8.21 (1 H, d, *J* = 7.8, Ar-H), 8.36 - 8.42 (3 H, m, Ar-H). δ_C (101 MHz; $CDCl_3$; $^{13}CDCl_3$) 30.2, 32.48, 32.54, 33.5, 109.0, 119.7, 124.2, 125.1, 125.8, 126.1, 126.5, 127.1, 127.3, 128.8, 129.1, 129.3, 130.3, 131.0, 131.5, 137.6. NB: 15 aromatic carbons observed rather than 16, this is assumed to be due to overlap. *m/z* (MALDI-Dithranol) 628 (35%), 363 ($[M(^{81}Br)]^+$, 80), 361 ($[M(^{79}Br)]^+$, 80), 282 ($[M - Br]^+$, 30), 240 ($[M - C_3H_6Br]^+$, 20), 227 (85), 226 ($[Dithranol]^+$, 100), 225 (100). HR *m/z* (APCI) $C_{21}H_{16}{}^{79}BrN$ + H requires 362.0539, found 362.0525. ν_{max}/cm^{-1} 3061 and 3039 (Ar C-H), 2942, 2871 and 2832w (C-H), 2233 and 2219 (C≡N), 1602, 1549w and 1508w (Ar C=C).

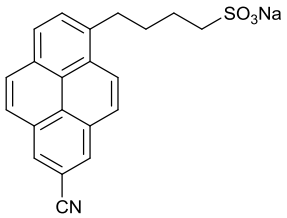

Sodium 4-(7-cyanopyren-1-yl)butane-1-sulfonate (**146**)

Na_2SO_3 (751.0 mg, 5.958 mmol) was added to a two neck RBF (100 mL) which was then purged N_2. 1-(4-Bromobutyl)-7-cyanopyrene (**145**) (179.9 mg, 0.4966 mmol) was ground into a powder with a pestle and mortar before being taken up in portions into EtOH (2 × 5.0 mL) with sonication and injected in to the reaction flask *via* syringe. Remaining unsuspended material after sonication in a final portion of EtOH (5.0 mL) was then added against a flow of N_2. Water (10 mL) was then added *via* syringe and the reaction heated to 100 °C overnight. The crude reaction mixture was then concentrated *in vacuo* and trituated with DCM (2 × 10 mL). The crude product was recrystallised from an EtOH:water mixture (~1.3:1) (concentrating *in vacuo*) washing the filtered solid with ice cold water (2 × 7 mL). The isolated material was then finally triturated with DCM (2 × 5 mL) to afford the pure *title compound* (**146**) (159.9 mg, 0.4149 mmol, 84% yield) as an off-white yellow amorphous solid. mp >300 °C. δ_H (400 MHz; methanol-d_4; methanol-d_3) 1.97 - 2.02 (4 H, m, C-C-H), 2.87 - 2.94 (2 H, m, SO_3Na-C-H), 3.40 - 3.47 (2 H, m, Ar-C-H), 8.03 - 8.10 (2 H, m, Ar-H), 8.18 (2 H, d, J = 9.1, Ar-H), 8.24 (1 H, d, J = 7.8, Ar-H), 8.44 - 8.51 (3 H, m, Ar-H). δ_C (126 MHz; DMSO-d_6; DMSO-d_6) 25.2, 31.0, 32.5, 51.4, 108.2, 119.5, 123.3, 125.5, 125.66, 125.74, 126.1, 126.5, 127.2, 127.3, 128.6, 129.2, 129.3, 129.7, 130.7, 131.2, 138.6. *m/z* (ESI$^-$) 747 ([M – Na + M]$^-$, 10%), 362 ([M – Na]$^-$, 100). HR *m/z* (ESI$^-$) $C_{21}H_{16}NNaO_3S$ – Na requires 362.0856, found 362.0844. ν_{max}/cm^{-1} 3424br ($SO_3Na•H_2O$), 3066w and 3021w (Ar C-H), 2933, 2905 and 2851 (C-H), 2219 (C≡N), 1692, 1656 and 1603 (Ar C=C).

4.2-3 Perylene Derivatives

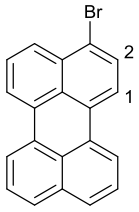

3-Bromoperylene (**147**)

Prepared by the adaptation of a literature synthesis[245]

Perylene (**74**) (2.00 g, 7.93 mmol) was added to a three neck RBF (1 L) which was then purged with N_2. Dry DMF (~500mL) was then added *via* cannula and the reaction vessel covered in foil. In a separate three neck RBF (100 mL), freshly recrystallised NBS (1.41 g, 7.92 mmol) was added and the flask purged with N_2. Dry DMF (40 mL) was then added *via* syringe and the NBS dissolved. With vigorous stirring, the solution of NBS was then immediately injected into the perylene reaction mixture which was then stirred at room temperature overnight. Water (2 × 250 mL) was then added and the reaction mixture extracted with DCM (4 × 100 mL). The combined organic extracts were then washed with aqueous HCl (~1 M) (4 × 200 mL), water (250 mL) and brine (250 mL) extracting the aqueous phase each time with DCM (~20 mL). The combined organic extracts were then dried over $MgSO_4$ and concentrated *in vacuo*. The crude product was then recrystallised twice from toluene to afford the purified (~90% pure by ^{1}H NMR) *title compound* (**147**) (1.64 g, 62% yield) as a yellow solid. Perylene was found to be the major impurity, observed by ^{1}H NMR and mass spectrometry. δ_H (500 MHz; $CDCl_3$; $CHCl_3$) 7.45 - 7.52 (2 H, m, Ar-H), 7.58 (1 H, t, *J* = 7.8, Ar-H), 7.69 - 7.73 (2 H, m, Ar-H), 7.76 (1 H, d, *J* = 8.2, C(2)H), 7.99 (1 H, d, *J* = 8.2, C(1)H), 8.09 (1 H, dd, *J* = 7.8, 0.8, Ar-H), 8.15 (1 H, d, *J* = 7.6, Ar-H), 8.20 (1 H, d, *J* = 7.6, Ar-H), 8.23 (1 H, d, *J* = 7.8, Ar-H) (ignoring impurity peaks). *m/z* (APCI) 333 ([M(^{81}Br) + H]$^+$, 10%), 331 ([M(^{79}Br) + H]$^+$, 10), 253 ([perylene + H]$^+$, 15), 214 (100), 158 (15). ^{1}H NMR comparable to that the literature.[245]

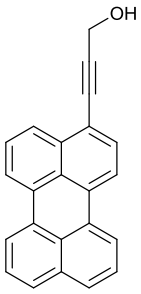

3-(Perylen-3-yl)prop-2-yn-1-ol (**148**)

3-Bromoperylene (**147**) (2.00 g, 6.04 mmol), $Pd(PPh_3)_4$ (390.4 mg, 0.3375 mmol, 6 mol%) and CuI (104.3 mg, 0.5477 mmol, 9 mol%) were added to a three neck RBF (250 mL) which was then purged with N_2. Dry THF (70 mL) and Et_3N (50 mL) were then added to a separate three neck RBF (250 mL) *via* syringe and the solution degassed for 20 minutes before the addition of propargyl alcohol (0.87 mL, 15 mmol). The solution was then degassed for a further 10 minutes before injection *via* syringe into the reaction flask, which was then heated at 70 °C for 2 h. The crude reaction mixture was then directly dry loaded *via* DCM/silica onto a chromatography column and eluted with a graded solvent system from 20% ethyl acetate in petroleum ether to 90% ethyl acetate in petroleum ether to obtain the pure *title compound* (**148**) (641.0 mg, 2.092 mmol, 35% yield) as a yellow orange solid. mp 208-210 °C. δ_H (400 MHz; DMSO-d_6; DMSO-d_5) 4.48 (2 H, d, J = 5.9, O-C-H), 5.51 (1 H, t, J = 5.9, O-H), 7.53 - 7.61 (2 H, m, Ar-H), 7.64 - 7.71 (2 H, m, Ar-H), 7.81 - 7.87 (2 H, m, Ar-H), 8.16 (1 H, d, J = 8.1, Ar-H), 8.31 - 8.49 (4 H, m, Ar-H). δ_C (126 MHz; DMSO-d_6; DMSO-d_6) 49.8, 81.8, 96.2, 119.5, 120.2, 121.3, 121.4, 121.5, 125.6, 126.96, 127.01, 127.6, 127.75, 127.77, 128.3, 128.6, 129.8, 130.1, 130.9, 131.0, 131.1, 134.0, 134.2. *m/z* (MALDI-CHCA) 306 ($[M]^+$, 100%), 227 (25). HR *m/z* (APCI) $C_{23}H_{14}O$ + H requires 307.1123, found 307.1121. ν_{max}/cm^{-1} 3247br (OH), 3047, 2912w and 2860w (Ar C-H), 2217w (C≡C), 1590w, 1575w and 1499 (Ar C=C).

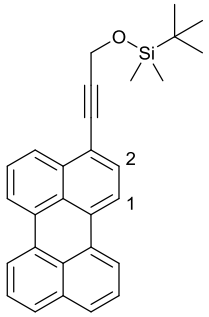

tert-Butyldimethyl([3-(perylen-3-yl)prop-2-yn-1-yl]oxy)silane (**151**)

tert-Butyldimethylsilyl chloride (709.3 mg, 4.706 mmol) and imidazole (320.0 mg, 4.700 mmol) were added to a three neck RBF (100 mL) which was then purged with N_2. 3-(Perylen-3-yl)prop-2-yn-1-ol (**148**) (599.0 mg, 1.955 mmol) under N_2 was then taken up in dry DMF (2 × 4.0 mL) and injected into the reaction flask *via* syringe. Additional dry DMF (2.0 mL) was then added *via* syringe and the reaction mixture stirred at room temperature overnight. The reaction mixture was then diluted with water (100 mL) and extracted with DCM (4 × 15 mL). The combined organic extracts were then washed with brine (3 × 65 mL) extracting the aqueous layer with DCM (2 × 12 mL) after each wash. The organic extracts were then dried over $MgSO_4$ before directly dry loading the crude product *via* DCM/silica onto a chromatography column which was then eluted with a graded solvent system from 10% DCM in petroleum ether to 35% DCM in petroleum ether to obtain the purified *title compound* (**151**) (680.6 mg, 1.618 mmol, 83% yield) as an orange solid. mp 162-163 °C. δ_H (500 MHz; $CDCl_3$; $CHCl_3$) 0.24 (6 H, s, Si-Me), 1.00 (9 H, s, Si-C-Me), 4.73 (2 H, s, O-C-H), 7.45 - 7.51 (2 H, m, Ar-H), 7.55 (1 H, t, *J* = 7.9, Ar-H), 7.64 (1 H, d, *J* = 8.0, C(2)H), 7.67 - 7.71 (2 H, m, Ar-H), 8.10 (1 H, d, *J* = 8.0, C(1)H), 8.14 - 8.24 (4 H, m, Ar-H). δ_C (126 MHz; $CDCl_3$; $^{13}CDCl_3$) -5.0, 18.4, 25.9, 52.5, 83.3, 93.8, 119.5, 120.0, 120.5, 120.6, 120.8, 126.1, 126.55, 126.62, 127.1, 128.0, 128.3, 128.4, 130.7, 131.0, 131.1, 131.4, 131.8, 134.6, 134.7. NB: 19 Aromatic carbons detected rather than 20, this is assumed to be due to overlap. *m/z* (MALDI-Dithranol) 421 ($[M + H]^+$, 100%), 290 ($[M – C_6H_{15}OSi + H]^+$, 10), 228 (10). HR *m/z* (EI) $C_{29}H_{28}OSi$ requires 420.1904, found 420.1912. ν_{max}/cm^{-1} 3050 (Ar C-H), 2951, 2927, 2884 and 2855 (C-H), 2217w (C≡C), 1600w, 1590w, 1574w and 1499 (Ar C=C).

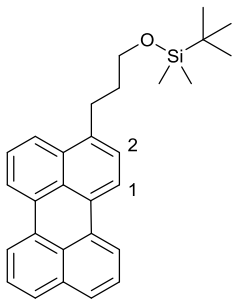

tert-Butyldimethyl[3-(perylen-3-yl)propoxy]silane (**154**)

Palladium (10 wt% on activated carbon) (179.6 mg) was added to a three neck RBF (100 mL) which was then purged with N_2. *tert*-Butyldimethyl([3-(perylen-3-yl)prop-2-yn-1-yl]oxy)silane (**151**) (638.1 mg, 1.517 mmol) under N_2 was then taken up in dry THF (13 mL) and added *via* syringe. Using a balloon, H_2 gas was then bubbled though the stirring solution *via* syringe for three minutes, before a fresh H_2 balloon was added and the solution left under an atmosphere of H_2 overnight. The crude reaction mixture was then filtered through celite® washing with ethyl acetate and the solvent removed *in vacuo*. The crude product was then recrystallised from petroleum ether to afford the pure *title compound* (**154**) (395.3 mg, 0.9309 mmol, 61% yield) as a yellow solid. mp 125 °C. δ_H (500 MHz; $CDCl_3$; $CHCl_3$) 0.12 (6 H, s, Si-Me), 0.98 (9 H, s, Si-C-Me), 1.94 - 2.04 (2 H, m, C-C-H), 3.11 (2 H, t, *J* = 7.8, Ar-C-H), 3.76 (2 H, t, *J* = 6.0, O-C-H), 7.36 (1 H, d, *J* = 7.6, C(2)H), 7.44 - 7.54 (3 H, m, Ar-H), 7.67 (2 H, t, *J* = 8.0, Ar-H), 7.94 (1 H, d, *J* = 8.2, Ar-H), 8.12 (1 H, d, *J* = 7.6, C(1)H), 8.15 - 8.23 (3 H, m, Ar-H). δ_C (126 MHz; $CDCl_3$; $^{13}CDCl_3$) -5.2, 18.4, 26.0, 29.5, 33.6, 62.5, 119.7, 120.06, 120.09, 123.9, 126.3, 126.5, 126.6, 126.9, 127.3, 127.7, 128.5, 129.1, 129.5, 131.50, 131.52, 131.7, 133.1, 134.7, 138.5. NB: 19 Aromatic carbons detected rather than 20, this is assumed to be due to overlap. *m/z* (MALDI-Dithranol) 425 ($[M + H]^+$, 100%), 228 (10). HR *m/z* (EI) $C_{29}H_{32}OSi$ requires 424.2217 found 424.2211. ν_{max}/cm^{-1} 3047w (Ar C-H), 2951, 2928, 2885 and 2855 (C-H), 1591w and 1501 (Ar C=C).

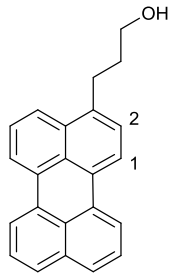

3-(Perylen-3-yl)propan-1-ol (**157**)

tert-Butyldimethyl[3-(perylen-3-yl)propoxy]silane (**154**) (355.5 mg, 0.8371 mmol) was taken up in THF (4.7 mL) and added to a three neck RBF (100 mL) under N_2 *via* syringe. The reaction mixture was then cooled to 0 °C in an ice bath before TBAF (1.0 M in THF) (1.2 mL, 1.2 mmol) was added dropwise *via* syringe. After 15 minutes the reaction mixture was allowed to warm to room temperature with stirring for a further 2 h. The reaction was then quenched by the addition of saturated aqueous NH_4Cl solution (50 mL) and extracted with ethyl acetate (3 × 30 mL). The combined organic extracts were then washed with brine (50 mL), dried over $MgSO_4$ and concentrated *in vacuo*. The crude product was then purified by column chromatography utilising a graded solvent system from 30% ethyl acetate in petroleum ether to 50% ethyl acetate in petroleum ether to afford the pure *title compound* (**157**) (175.7 mg, 0.5660 mmol, 68% yield) as a yellow solid. mp 161-162 °C. δ_H (500 MHz; $CDCl_3$; $CHCl_3$) 1.36 (1 H, s, O-H), 2.01 - 2.10 (2 H, m, C-C-H), 3.15 (2 H, t, *J* = 7.7, Ar-C-H), 3.80 (2 H, t, *J* = 6.2, O-C-H), 7.38 (1 H, d, *J* = 7.7, C(2)H), 7.46 - 7.56 (3 H, m, Ar-H), 7.68 (2 H, t, *J* = 7.9, Ar-H), 7.92 (1 H, d, *J* = 8.2, Ar-H), 8.14 (1 H, d, *J* = 7.7, C(1)H), 8.15 - 8.25 (3 H, m, Ar-H). δ_C (126 MHz; $CDCl_3$; $^{13}CDCl_3$) 29.5, 33.2, 62.5, 119.7, 120.0, 120.1, 120.2, 123.7, 126.4, 126.5, 126.6, 126.9, 127.4, 127.7, 128.5, 129.1, 129.7, 131.4, 131.8, 133.0, 134.6, 137.9. NB: 19 Aromatic carbons detected rather than 20, this is assumed to be due to overlap. *m/z* (MALDI-Dithranol) 311 ($[M + H]^+$, 100%). HR *m/z* (EI) $C_{23}H_{18}O$ requires 310.1352, found 310.1358. ν_{max}/cm^{-1} 3305br (OH), 3048 (Ar C-H), 2934 and 2866 (C-H), 1590 and 1501 (Ar C=C).

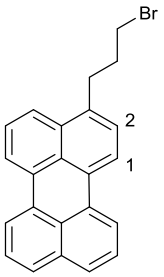

3-(3-Bromopropyl)perylene (**162**)

CBr_4 (192.6 mg, 0.5808 mmol) and K_2CO_3 (95.1 mg, 0.688 mmol) were added to a three neck RBF (100 mL) which was then purged with N_2. 3-(Perylen-3-yl)propan-1-ol (**157**) (142.0 mg, 0.4575 mmol) under N_2 was then taken up in dry DCM (10 mL) and added *via* syringe before the reaction mixture was cooled to 0 °C in an ice bath. PPh_3 (150.1 mg, 0.5723 mmol) in dry DCM (0.8 mL) was then added dropwise *via* syringe. The reaction was then allowed to warm to room temperature with stirring for ~64 h. The crude reaction mixture was then directly dry loaded *via* DCM/silica onto a chromatography column and eluted with a 10% DCM in petroleum ether solvent system to obtain the pure *title compound* (**162**) (93.5 mg, 0.250 mmol, 55% yield) as a yellow solid. mp 155-156 °C. δ_H (400 MHz; $CDCl_3$; $CHCl_3$) 2.28 - 2.36 (2 H, m, C-C-H), 3.20 (2 H, t, *J* = 7.4, Ar-C-H), 3.51 (2 H, t, *J* = 6.4, Br-C-H), 7.38 (1 H, d, *J* = 7.5, C(2)H), 7.44 - 7.57 (3 H, m, Ar-H), 7.64 - 7.71 (2 H, m, Ar-H), 7.88 (1 H, d, *J* = 8.3, Ar-H), 8.12 (1 H, d, *J* = 7.5, C(1)H), 8.14 - 8.25 (3 H, m, Ar-H). δ_C (101 MHz; $CDCl_3$; $CHCl_3$) 31.4, 33.1, 33.6, 119.9, 120.0, 120.18, 120.23, 123.5, 126.52, 126.54, 126.6, 127.3, 127.5, 127.8, 128.5, 129.2, 130.0, 131.26, 131.29, 131.9, 132.9, 134.6, 136.4. *m/z* (APCI) 375 ([M(^{81}Br) + H]$^+$, 100%), 373 ([M(^{79}Br) + H]$^+$, 95), 293 ([M – Br]$^+$, 40). HR *m/z* (APCI) $C_{23}H_{17}{}^{79}Br$ + H requires 373.0592, found 373.0586. ν_{max}/cm^{-1} 3046 and 3007 (Ar C-H), 2957 and 2860 (C-H), 1588 and 1500 (Ar C=C).

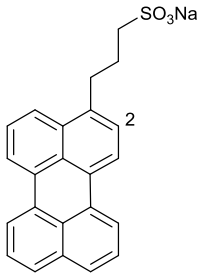

Sodium 3-(perylen-3-yl)propane-1-sulfonate (**164**)

Na_2SO_3 (218.9 mg, 1.737 mmol) was added to a three neck RBF (100 mL) which was then purged with N_2. 3-(3-Bromopropyl)perylene (**162**) (53.8 mg, 0.144 mmol) was ground into a powder with a pestle and mortar and suspended in portions into EtOH (3 × 2.4 mL) with sonication before addition to the reaction mixture *via* syringe. Water (5.5 mL) was then added *via* syringe and the reaction heated to 100 °C overnight. The reaction mixture was then concentrated *in vacuo* and triturated with DCM (10 mL + 5 mL). The crude material was then recrystallised from an EtOH:water mixture (1.3:1) (concentrating *in vacuo*) washing the filtered solid with DCM (2 × 2 mL) and ice cold water (2 × 2 mL). To afford the pure *title compound* (**164**) (40.8 mg, 72% yield) as a yellow amorphous solid. mp >300 °C. δ_H (400 MHz; methanol-d_4; methanol-d_3) 2.19 - 2.29 (2 H, m, C-C-H), 2.91 - 2.98 (2 H, m, NaO_3S-C-H), 3.20 (2 H, t, *J* = 7.8, Ar-C-H), 7.43 (1 H, d, *J* = 7.6, C(2)H), 7.45 - 7.51 (2 H, m, Ar-H), 7.53 - 7.58 (1 H, m, Ar-H), 7.66 - 7.72 (2 H, m, Ar-H), 8.00 (1 H, d, *J* = 8.6, Ar-H), 8.19 - 8.33 (4 H, m, Ar-H). δ_C (101 MHz; DMSO-d_6; DMSO-d_6) 26.4, 31.6, 51.1, 120.2, 120.56, 120.60, 120.62, 124.3, 126.7, 126.88, 126.93, 127.2, 127.4, 127.7, 127.8, 128.3, 128.7, 130.75, 130.78, 130.9, 132.6, 134.3, 138.8. *m/z* (ESI$^-$) 373 ([M – Na]$^-$, 100%). HR *m/z* (APPI) $C_{23}H_{17}NaO_3S$ + H requires 397.0869, found 397.0867. ν_{max}/cm^{-1} 3501br and 3427br (SO_3Na•H_2O), 3047 (Ar C-H), 2918 and 2849 (C-H), 1685, 1661, 1589 and 1500 (Ar C=C).

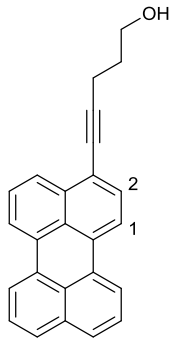

5-(Perylen-3-yl)pent-4-yn-1-ol (**149**)

Prepared by the adaptation of a literature synthesis[203]

3-Bromoperylene (**147**) (2.00 g, 6.04 mmol), $Pd(PPh_3)_4$ (391.6 mg, 0.3389 mmol, 6 mol%) and CuI (105.6 mg, 0.5545 mmol, 9 mol%) were added to a three neck RBF (250 mL) which was then purged with N_2. Dry THF (70 mL) and Et_3N (50 mL) were then added to a separate three neck RBF (250 mL) *via* syringe and the solution degassed for 20 minutes before the addition of 4-pentyn-1-ol (1.4 mL, 15 mmol). The solution was then degassed for a further 15 minutes before injection *via* syringe into the reaction flask, which was then heated at 70 °C for 2 h. The crude reaction mixture was then directly dry loaded *via* DCM/silica onto a chromatography column and eluted initially with a 30% DCM in petroleum ether solvent system followed by a graded solvent system from 40% ethyl acetate in petroleum ether to 100% ethyl acetate, to afford the partially purified *title compound* (**149**) (2.10 g) as a dark red/orange solid. δ_H (400 MHz; $CDCl_3$; $CHCl_3$) 1.49 (1 H, br s, OH), 2.00 (2 H, quin, *J* = 6.6, C-C-H), 2.74 (2 H, t, *J* = 6.6, C≡C-C-H), 3.93 (2 H, t, *J* = 6.6, O-C-H), 7.45 - 7.51 (2 H, m, Ar-H), 7.55 (1 H, t, *J* = 7.9, Ar-H), 7.60 (1 H, d, *J* = 7.8, C(2)H), 7.68 (2 H, d, *J* = 8.3, Ar-H), 8.09 (1 H, d, *J* = 7.8, C(1)H), 8.12 - 8.25 (4 H, m, Ar-H) (ignoring impurity peaks). Homocoupled starting material 4,6-decadiyn-1,10-diol was found to be the major impurity, determined by comparison of ^1H and ^{13}C NMR with the literature.[246] *m/z* (MALDI-Dithranol) 429 (10%), 334 ($[M]^+$, 100), 226 ($[Dithranol]^+$, 55), 225 (95). ^1H NMR (ignoring impurity peaks) was found to be comparable with the literature.[203]

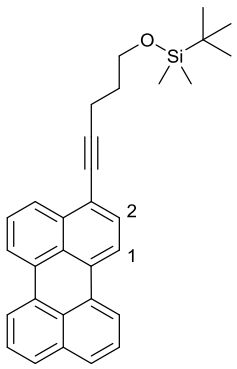

tert-Butyldimethyl([5-(perylen-3-yl)pent-4-yn-1-yl]oxy)silane (**152**)

Prepared by the adaptation of a literature synthesis[203]

Partially purified 5-(perylen-3-yl)pent-4-yn-1-ol (**149**) (2.16 g), imidazole (1.06 g, 15.6 mmol) and *tert*-butyldimethylsilyl chloride (2.35 g, 15.6 mmol) were added to a three neck RBF (100 mL) which was then purged with N_2. Dry DCM (11 mL) was then added *via* syringe and the reaction stirred at room temperature overnight. The crude reaction mixture was then directly dry loaded *via* DCM/silica onto a chromatography column and eluted with a graded solvent system from 10% DCM to 30% DCM in petroleum ether. The partially purified product was then recrystallised twice from petroleum ether to afford the *title compound* (**152**) (847.1 mg, 1.888 mmol, 31% yield over 2 steps) as an orange solid. mp 129-131 °C. δ_H (400 MHz; $CDCl_3$; $CHCl_3$) 0.13 (6 H, s, Si-Me), 0.95 (9 H, s, Si-C-Me), 1.94 (2 H, quin, *J* = 6.6, C-C-H), 2.70 (2 H, t, *J* = 6.6, C≡C-C-H), 3.87 (2 H, t, *J* = 6.6, O-C-H), 7.45 - 7.51 (2 H, m, Ar-H), 7.55 (1 H, t, *J* = 7.8, Ar-H), 7.61 (1 H, d, *J* = 7.9, C(2)H), 7.69 (2 H, d, *J* = 8.1, Ar-H), 8.10 (1 H, d, J = 7.9, C(1)H), 8.13 - 8.25 (4H, m, Ar-H). δ_C (101 MHz; $CDCl_3$; $^{13}CDCl_3$) -5.3, 16.3, 18.4, 26.0, 31.9, 61.7, 79.1, 96.1, 119.6, 120.4, 120.6, 121.2, 126.3, 126.5, 126.6, 126.9, 127.9, 128.1, 128.46, 128.48, 130.7, 130.9, 131.0, 131.1, 131.4, 134.6, 134.8. NB: 19 Aromatic carbons detected rather than 20, this is assumed to be due to overlap. *m/z* (MALDI-TCNQ) 448 ($[M]^+$, 100%), 391 ($[M - C_4H_9]^+$, 20). ^{1}H NMR comparable to that in the literature.[203]

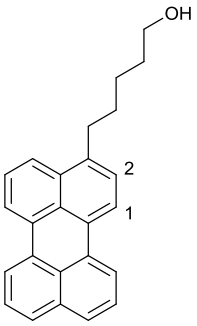

5-(Perylen-3-yl)pentan-1-ol (**158**)

Prepared by the adaptation of a literature synthesis[203]

Palladium (10 wt% on activated carbon) (810.2 mg) was added to a three neck RBF (100 mL) followed by partially purified *tert*-butyldimethyl([5-(perylen-3-yl)pent-4-yn-1-yl]oxy)silane (**152**) (3.09 g) washed in with THF (60 mL). Using a balloon, H_2 gas was then bubbled though the stirring solution *via* syringe for three minutes, before a fresh H_2 balloon was added and the solution left under an atmosphere of H_2 overnight. The crude reaction mixture was then filtered through celite® washing with ethyl acetate and the solvent removed *in vacuo*. The crude product was then dissolved in THF (40 mL) and added against a flow of N_2 to a three neck RBF (100 mL) and the reaction mixture cooled to 0 °C in an ice bath before the addition of TBAF (1.0 M in THF) (9.5 mL, 9.5 mmol) dropwise. After 15 minutes the reaction was allowed to warm to room temperature and stirred for a further 2 h. The reaction was quenched by the addition of saturated NH_4Cl solution (100 mL) and extracted with ethyl acetate (3 × 50 mL). The combined organic extracts were then dried over $MgSO_4$ and concentrated *in vacuo*. The crude product was then partially purified utilising a silica plug, eluting initially with 30% DCM in petroleum ether then 100% ethyl acetate. Final purification was achieved by column chromatography utilising a graded solvent system from 10% ethyl acetate in petroleum ether to 40% ethyl acetate in petroleum ether to isolate the *title compound* (**158**) (539.8 mg, 1.595 mmol, 26% yield over four steps) as a yellow solid. mp 157-160 °C. δ_H (400 MHz; $CDCl_3$; $CHCl_3$) 1.30 (1 H, br s, OH), 1.48 - 1.58 (2 H, m, C-C-H), 1.62 - 1.71 (2 H, m, C-C-H), 1.80 (2 H, quin, *J* = 7.8, C-C-H), 3.03 (2 H, t, *J* = 7.8, Ar-C-H), 3.68 (2 H, t, *J* = 6.4, O-C-H), 7.33 (1 H, d, *J* = 7.8, C(2)H), 7.44 - 7.54 (3 H, m, Ar-H), 7.67 (2 H, t, *J* = 7.3, Ar-H), 7.87 (1 H, d, *J* = 8.3, Ar-H), 8.11 (1 H, d, *J* = 7.8, C(1)H), 8.13 - 8.23 (3 H, m, Ar-H). δ_C (101 MHz; $CDCl_3$; $^{13}CDCl_3$) 25.9, 30.3, 32.7, 33.3,

62.9, 119.7, 120.0, 120.06, 120.09, 123.7, 126.3, 126.5, 126.6, 126.8, 127.3, 127.7, 128.5, 129.1, 129.4, 131.42, 131.44, 131.7, 133.0, 134.6, 138.6. *m/z* (MALDI-TCNQ) 338 ($[M]^+$, 100%). ^{1}H NMR comparable to that in the literature.[203]

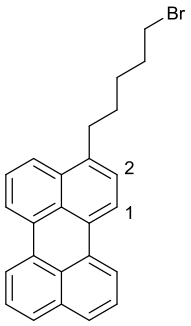

3-(5-Bromopentyl)perylene (**163**)

5-(Perylen-3-yl)pentan-1-ol (**158**) (505.5 mg, 1.494 mmol), K_2CO_3 (309.4 mg, 2.239 mmol) and CBr_4 (619.0 mg, 1.867 mmol) were added to a three neck RBF (100 mL) which was then purged with N_2. Dry DCM (7.0 mL) was then added *via* syringe and the reaction mixture cooled to 0 °C in an ice bath. PPh_3 (490.8 mg, 1.871 mmol) in dry DCM (2.8 mL) was then added dropwise *via* syringe and the reaction mixture allowed to warm to room temperature with stirring for ~40 h. The crude reaction mixture was then purified by directly dry loading the crude material *via* DCM/silica onto a chromatography column and eluting with a graded solvent system from 10% DCM in petroleum either to 20% DCM in petroleum ether to afford the *title compound* (**163**) (457.1 mg, 1.139 mmol, 76% yield) as a yellow solid. mp 118-119 °C. δ_H (400 MHz; $CDCl_3$; $CHCl_3$) 1.58 - 1.66 (2 H, m, C-C-H), 1.80 (2 H, quin, *J* = 7.8, C-C-H), 1.95 (2 H, quin, *J* = 7.1, C-C-H), 3.03 (2 H, t, *J* = 7.8, Ar-C-H), 3.44 (2 H, t, *J* = 7.1, Br-C-H), 7.33 (1 H, d, *J* = 7.7, C(2)H), 7.44 - 7.55 (3 H, m, Ar-H), 7.67 (2 H, t, *J* = 7.1, Ar-H), 7.85 (1 H, d, *J* = 8.3, Ar-H), 8.12 (1 H, d, *J* = 7.7, C(1)H), 8.14 - 8.23 (3 H, m, Ar-H). δ_C (126 MHz; $CDCl_3$; $^{13}CDCl_3$) 28.3, 29.6, 32.7, 33.2, 33.8, 119.7, 120.0, 120.10, 120.14, 123.6, 126.3, 126.5, 126.6, 126.8, 127.4, 127.7, 128.5, 129.1, 129.6, 131.4, 131.8, 133.0, 134.7, 138.3. NB: 19 Aromatic carbons detected rather than 20, this is assumed to be due to overlap. *m/z* (MALDI-TCNQ) 400 ($[M(^{79}Br)]^+$, 100%), 402 ($[M(^{81}Br)]^+$, 100). HR *m/z* (EI) $C_{25}H_{21}{}^{79}Br$ requires 400.0821, found 400.0820. ν_{max}/cm^{-1} 3054w (Ar C-H), 2938 and 2864 (C-H), 1588, 1570w and 1500 (Ar C=C).

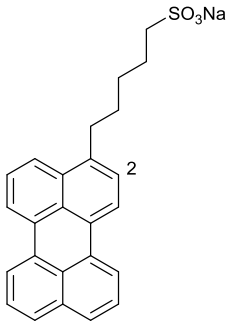

Sodium 5-(perylen-3-yl)pentane-1-sulfonate (**165**)

Na_2SO_3 (1.86 g, 14.8 mmol) was added to a three neck RBF (250 mL) which was then purged with N_2. 3-(5-Bromopentyl)perylene (**163**) (493.8 mg, 1.230 mmol) was ground into a powder with a pestle and mortar and suspended in portions into EtOH (4 × 7.5 mL) with sonication before addition to the reaction mixture *via* syringe. Water (23 mL) was then added *via* syringe and the reaction heated to 100 °C overnight. The reaction mixture was then concentrated *in vacuo* and triturated with DCM (13 mL). Purification was then achieved by a repeated trituration/recrystallisation process. The crude material was suspended in an EtOH:water mixture (~1.3:1) (~500 mL) heated at ~80 °C before concentration *in vacuo* to ~100 mL. The suspension was then cooled to 0 °C in an ice bath and the filtered solid washed with water (10 mL). Repetition of this process two further times yielded purified product (206.0 mg, 0.4853 mmol) after which concentration of the final filtrate *in vacuo* to the point of precipitation and cooling to 0 °C allowed filtration of additional purified product (240.7 mg, 0.5670 mmol). This process allowed isolation of pure *title compound* (**165**) (446.7 mg, 1.052 mmol, 86% yield) as a yellow amorphous solid. mp >300 °C. δ_H (500 MHz; DMSO-d_6; DMSO-d_5) 1.42 - 1.51 (2 H, m, C-C-H), 1.61 - 1.72 (4 H, m, C-C-H), 2.37 - 2.44 (2 H, m, NaO_3S-C-H), 2.99 (2 H, t, *J* = 7.7, Ar-C-H), 7.41 (1 H, d, *J* = 7.9, C(2)H), 7.50 - 7.56 (2 H, m, Ar-H), 7.59 (1 H, t, *J* = 8.1, Ar-H), 7.77 (2 H, t, *J* = 8.8, Ar-H), 7.94 (1 H, d, *J* = 8.1, Ar-H), 8.27 - 8.33 (2 H, m, Ar-H), 8.34 - 8.41 (2 H, m, Ar-H). δ_C (126 MHz; DMSO-d_6; DMSO-d_6) 25.1, 28.6, 30.2, 32.5, 51.5, 120.2, 120.59, 120.64, 124.0, 126.8, 126.90, 126.94, 127.0, 127.5, 127.7, 127.8, 128.3, 128.6, 130.7, 130.8, 131.0, 132.6, 134.3, 138.8. NB: 19 Aromatic carbons detected rather than 20, this is assumed to be due to overlap. *m/z* (ESI$^-$) 401 ([M – Na]$^-$, 100%). (ESI$^+$) 463 (60%), 447 ([M + Na]$^+$, 100), 229 (55). HR *m/z* (ESI$^-$) $C_{25}H_{21}NaO_3S$ – Na requires

401.1211, found 401.1212. ν_{max}/cm^{-1} 3464br ($SO_3Na•H_2O$), 3047 (Ar C-H), 2925 and 2854 (C-H), 1647, 1589 and 1500 (Ar C=C).

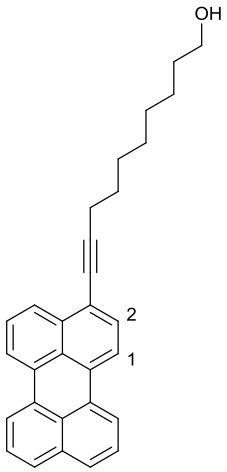

10-(Perylen-3-yl)dec-9-yn-1-ol (**150**)

3-Bromoperylene (**147**) (2.00 g, 6.04 mmol), $Pd(PPh_3)_4$ (390.3 mg, 0.3378 mmol, 6 mol%) and CuI (104.1 mg, 0.5466 mmol, 9 mol%) were added to a three neck RBF (250 mL) which was then purged with N_2. Dry THF (70 mL) and Et_3N (50 mL) were then added to a separate three neck RBF (250 mL) *via* syringe and the solution degassed for 20 minutes before the addition of 9-decyn-1-ol (2.31 g, 15.0 mmol). The solution was then degassed for a further 15 minutes before injection *via* syringe into the reaction flask, which was then heated at 70 °C for 2 h. The crude reaction mixture was then directly dry loaded *via* DCM/silica onto a chromatography column and eluted with a graded solvent system from 30% ethyl acetate in petroleum ether to 50% ethyl acetate in petroleum ether. The partially purified product was then recrystallised twice from acetone to afford the pure *title compound* (**150**) (1.58 g, 3.91 mmol, 65% yield) as an orange yellow solid. mp 129-130 °C. δ_H (400 MHz; $CDCl_3$; $CHCl_3$) 1.23 (1 H, s, O-H), 1.37 - 1.47 (6 H, m, C-C-H), 1.52 - 1.65 (4 H, m, C-C-H), 1.74 (2 H, quin, *J* = 7.2, C-C-H), 2.60 (2 H, t, *J* = 7.2, C≡C-C-H), 3.66 (2 H, t, *J* = 6.4, O-C-H), 7.45 - 7.52 (2 H, m, Ar-H), 7.56 (1 H, t, *J* = 7.9, Ar-H), 7.61 (1 H, d, *J* = 7.9, C(2)H), 7.69 (2 H, d, *J* = 8.1, Ar-H), 8.11 (1 H, d, *J* = 7.9, C(1)H), 8.15 - 8.26 (4 H, m, Ar-H). δ_C (126 MHz; $CDCl_3$; $^{13}CDCl_3$) 19.8, 25.7, 28.9, 29.0, 29.1, 29.3, 32.8, 63.1, 79.1, 96.6, 119.6, 120.4, 120.6, 121.2, 126.3, 126.55, 126.59, 126.9, 127.9, 128.0, 128.46, 128.50, 130.6, 130.86, 130.91, 131.1, 131.4, 134.6, 134.8. NB: 19 Aromatic carbons detected rather than 20, this is assumed to be due to overlap. *m/z* (MALDI-Dithranol) 404 ($[M]^+$, 100%). HR *m/z* (APCI) $C_{30}H_{28}O$ + H requires 405.2218, found 405.2234. ν_{max}/cm^{-1} 3309br (OH), 3048 (Ar C-H), 2926 and 2851 (C-H), 2218w (C≡C), 1590w and 1575w (Ar C=C).

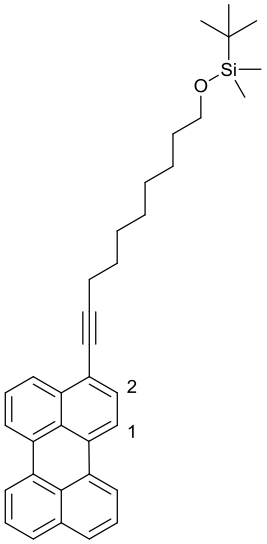

tert-Butyldimethyl([10-(perylen-3-yl)dec-9-yn-1-yl]oxy)silane (**153**)

10-(Perylen-3-yl)dec-9-yn-1-ol (**150**) (1.54 g, 3.81 mmol), *tert*-butyldimethylsilyl chloride (1.38 g, 9.16 mmol) and imidazole (622.9 mg, 9.150 mmol) were added to a three neck RBF (100 mL) which was then purged with N_2. Dry DMF (25 mL) was then added *via* syringe and the reaction mixture stirred at room temperature overnight. The reaction mixture was then diluted with water (75 mL) and extracted with DCM (3 × 20 mL). The combined organic extracts were then washed with brine (3 × 75 mL) extracting the aqueous layer each time with DCM (2 × 10 mL). The organic layer was then dried over $MgSO_4$ before dry loading the crude product *via* DCM/silica onto a silica plug which was then eluted with a graded solvent system from 10% DCM in petroleum ether to 30% DCM in petroleum ether. The partially purified product was then triturated with petroleum ether to afford the pure *title compound* (**153**) as a yellow solid (1.70 g, 3.28 mmol, 86% yield). mp 105 °C. δ_H (500 MHz; $CDCl_3$; $CHCl_3$) 0.06 (6 H, s, Si-Me), 0.91 (9 H, s, Si-C-Me), 1.33 - 1.44 (6 H, m, C-C-H), 1.50 - 1.60 (4 H, m, C-C-H), 1.74 (2 H, quin, *J* = 7.3, C-C-H), 2.60 (2 H, t, *J* = 7.3, C≡C-C-H), 3.62 (2 H, t, *J* = 6.6, O-C-H), 7.45 - 7.52 (2 H, m, Ar-H), 7.56 (1 H, t, *J* = 7.9, Ar-H), 7.61 (1 H, d, *J* = 7.9, C(2)H), 7.69 (2 H, d, *J* = 8.2, Ar-H), 8.11 (1 H, d, *J* = 7.9, C(1)H), 8.14 - 8.25 (4 H, m, Ar-H). δ_C (126 MHz; CDCl3; ^{13}CDCl3) -5.3, 18.4, 19.9, 25.8, 26.0, 28.9, 29.0, 29.2, 29.4, 32.9, 63.3, 79.0, 96.7, 119.7, 120.4, 120.6, 121.3, 126.3, 126.56, 126.61, 127.0, 127.9, 128.0, 128.50, 128.52, 130.7, 130.9, 131.2, 131.4, 134.6, 134.8. NB: 18 Aromatic carbons detected rather than 20, this is assumed to be due to overlap. *m/z* (MALDI-Dithranol) 518

([M]$^+$, 100%), 404 ([M – $C_6H_{15}Si$ + H]$^+$, 25), 226 (35). HR *m/z* (APCI) $C_{36}H_{42}OSi$ + H requires 519.3083, found 519.3091. ν_{max}/cm^{-1} 3051w (Ar C-H), 2926, 2904 and 2855 (C-H), 2222w (C≡C), 1589w, 1574 and 1500 (Ar C=C).

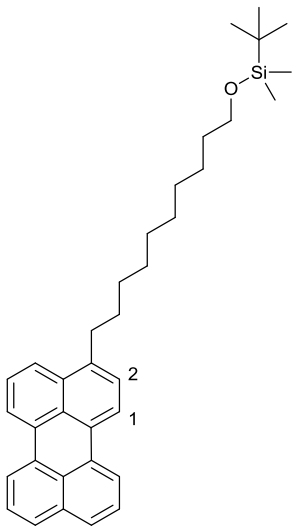

tert-Butyldimethyl[10-(perylen-3-yl)decoxy]silane (**156**)

Palladium (10 wt% on activated carbon) (372.2 mg) and *tert*-butyldimethyl([10-(perylen-3-yl)dec-9-yn-1-yl]oxy)silane (**153**) were added to a three neck RBF (100 mL) which was then purged with N_2. Dry THF (27 mL) was then added *via* syringe. Using a balloon, H_2 gas was then bubbled though the stirring solution *via* syringe for three minutes, before a fresh H_2 balloon was added and the solution left under an atmosphere of H_2 overnight. The crude reaction mixture was then filtered through celite® washing with ethyl acetate and the solvent removed *in vacuo*. The crude product was then partially purified by column chromatography eluting with a graded solvent system from 10% DCM in petroleum ether to 20% DCM in petroleum ether. The partially purified product was then recrystallised from petroleum ether to afford the pure *title compound* (**156**) (1.35 g, 2.58 mmol, 81% yield) as an amorphous yellow solid. mp 90-91 °C. δ_H (400 MHz; $CDCl_3$; $CHCl_3$) 0.05 (6 H, s, Si-Me), 0.90 (9 H, s, Si-C-Me), 1.28 - 1.41 (10 H, m, C-C-H), 1.42 - 1.54 (4 H, m, C-C-H), 1.71 - 1.82 (2 H, m, C-C-H), 3.02 (2 H, t, *J* = 7.8, Ar-C-H), 3.60 (2 H, t, *J* = 6.7, O-C-H), 7.35 (1 H, d, *J* = 7.7, C(2)H), 7.44 - 7.56 (3 H, m, Ar-H), 7.67 (2 H, t, *J* = 7.6, Ar-H), 7.89 (1 H, d, *J* = 8.1, Ar-H), 8.14 (1 H, d, *J* = 7.7, C(1)H), 8.15 - 8.25 (3 H, m, Ar-H). δ_C (126 MHz; $CDCl_3$; $^{13}CDCl_3$) -5.3, 18.4, 25.8, 26.0, 29.4, 29.5, 29.58, 29.63, 29.8, 30.6, 32.9, 33.4, 63.3, 119.6, 120.0, 120.1, 123.9, 126.2, 126.5, 126.6, 126.7, 127.2, 127.6, 128.5, 129.1, 129.3, 131.50, 131.53, 131.7, 133.1, 134.7, 139.1. NB: 19 Aromatic carbons detected rather than 20, this is assumed to be due to overlap. *m/z* (MALDI-Dithranol) 523 ($[M + H]^+$, 100%). HR *m/z* (APCI) $C_{36}H_{46}OSi$ + H

requires 523.3396, found 523.3393. ν_{max}/cm^{-1} 3048 (Ar C-H), 2925s and 2853s (C-H), 1590w and 1501 (Ar C=C).

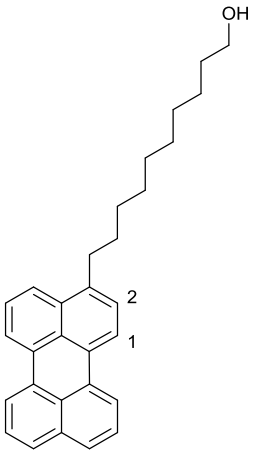

10-(Perylen-3-yl)decan-1-ol (**159**)

tert-Butyldimethyl[10-(perylen-3-yl)decoxy]silane (**156**) (1.27 g, 2.43 mmol) was added to a three neck RBF (100 mL) which was then purged with N_2. THF (14 mL) was then added *via* syringe and the reaction mixture and cooled to 0 °C in an ice bath before TBAF (1.0 M in THF) (3.4 mL, 3.4 mmol) was added dropwise *via* syringe. After 15 minutes the reaction mixture was allowed to warm to room temperature with stirring for a further 2 h. The reaction mixture was then directly dry loaded *via* DCM/silica onto a silica plug and eluted with a 30% DCM in petroleum ether solvent system, followed by a graded solvent system from 30% ethyl acetate in petroleum ether to 100% ethyl acetate to afford the pure *title compound* (**159**) (442.3 mg, 1.083 mmol, 45% yield) as yellow solid. mp 151-152 °C. δ_H (500 MHz; $CDCl_3$; $CHCl_3$) 1.24 (1 H, br s, OH), 1.28 - 1.41 (10 H, m, C-C-H), 1.42 - 1.50 (2 H, m, C-C-H), 1.53 - 1.62 (2 H, m, C-C-H), 1.77 (2 H, quin, *J* = 7.8, C-C-H), 3.02 (2 H, t, *J* = 7.8, Ar-C-H), 3.64 (2 H, t, *J* = 6.8, O-C-H), 7.34 (1 H, d, *J* = 7.6, C(2)H), 7.44 - 7.54 (3 H, m, Ar-H), 7.66 (2 H, t, *J* = 8.5, Ar-H), 7.89 (1 H, d, *J* = 8.5, Ar-H), 8.12 (1 H, d, *J* = 7.6, C(1)H), 8.14 - 8.23 (3 H, m, Ar-H). δ_C (126 MHz; $CDCl_3$; $^{13}CDCl_3$) 25.7, 29.4, 29.5, 29.6, 29.8, 30.6, 32.8, 33.4, 63.1, 119.6, 120.0, 120.1, 123.8, 126.2, 126.5, 126.6, 126.7, 127.3, 127.7, 128.5, 129.1, 129.3, 131.49, 131.52, 131.7, 133.1, 134.7, 139.0. NB: 19 Aromatic carbons detected rather than 20 and 9 aliphatic carbons detected rather than 10, this is assumed to be due to overlap. *m/z* (MALDI-Dithranol) 409 ($[M + H]^+$, 100%). HR *m/z* (EI) $C_{30}H_{32}O$ requires 408.2448 found 408.2450. ν_{max}/cm^{-1} 3318br (OH), 3048 (Ar C-H), 2920s and 2850s (C-H), 1590 and 1501 (Ar C=C).

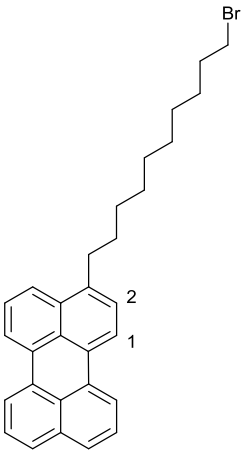

3-(10-Bromodecyl)perylene (**160**)

10-(Perylen-3-yl)decan-1-ol (**159**) (373.0 mg, 0.9129 mmol), CBr_4 (378.4 mg, 1.141 mmol), and K_2CO_3 (189.4 mg, 1.370 mmol) were added to a three neck RBF (100 mL) which was then purged with N_2. Dry DCM (5.5 mL) was then added *via* syringe and the reaction mixture cooled to 0 °C in an ice bath. PPh_3 (299.9 mg, 1.143 mmol) in dry DCM (1.6 mL) was then added dropwise *via* syringe and the reaction allowed to warm to room temperature with stirring for ~36 h. The crude reaction mixture was then directly dry loaded *via* DCM/silica onto a chromatography column and eluted with a 20% DCM in petroleum ether solvent system to obtain the pure *title compound* (**160**) (305.4 mg, 0.6477 mmol, 71%) as a yellow solid. mp 93-94 °C. δ_H (500 MHz; $CDCl_3$; $CHCl_3$) 1.28 - 1.50 (12 H, m, C-C-H), 1.77 (2 H, quin, *J* = 7.8, C-C-H), 1.86 (2 H, quin, *J* = 7.1, C-C-H), 3.02 (2 H, t, *J* = 7.8, Ar-C-H), 3.41 (2 H, t, *J* = 7.1, Br-C-H), 7.35 (1 H, d, *J* = 7.7, C(2)H), 7.45 - 7.55 (3 H, m, Ar-H), 7.67 (2 H, t, *J* = 8.4, Ar-H), 7.89 (1 H, d, *J* = 8.2, Ar-H), 8.13 (1 H, d, *J* = 7.7, C(1)H), 8.15 - 8.24 (3 H, m, Ar-H). δ_C (126 MHz; $CDCl_3$; $^{13}CDCl_3$) 28.2, 28.8, 29.4, 29.5, 29.8, 30.5, 32.8, 33.4, 34.0, 119.6, 120.05, 120.07, 123.8, 126.2, 126.5, 126.6, 126.7, 127.3, 127.7, 128.5, 129.1, 129.4, 131.50, 131.53, 131.8, 133.1, 134.7, 139.0. NB: 19 Aromatic carbons detected rather than 20 and 9 aliphatic carbons detected rather than 10, this is assumed to be due to overlap. *m/z* (APCI) 473 ($[M(^{81}Br) + H]^+$, 100%), 471 ($[M(^{79}Br) + H]^+$, 100), 391 ($[M - Br]^+$, 20). HR *m/z* (APCI) $C_{30}H_{31}{}^{79}Br$ + H requires 471.1687, found 471.1709. ν_{max}/cm^{-1} 3046 (Ar C-H), 2922s and 2850 (C-H), 1590 and 1501 (Ar C=C).

From the reaction of a partially purified sample of **159**, column chromatography allowed isolation of a partially pure sample (suitable for partial characterisation) of the corresponding hexahydroperylene **161**, an impurity carried forward from the hydrogenation of **153**.

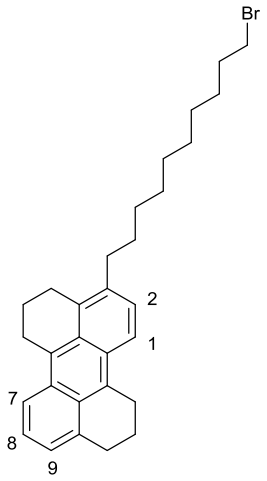

3-(10-Bromodecyl)-4,5,6,10,11,12-hexahydroperylene (**161**)

δ_H (500 MHz; $CDCl_3$; $CHCl_3$) 1.26 - 1.40 (m, C-C-H), 1.41 - 1.49 (m, C-C-H), 1.67 (2 H, quin, *J* = 7.7, C-C-H), 1.87 (~2 H, quin, *J* = 7.0, C-C-H), 2.06 - 2.16 (4 H, m, C-C-H), 2.83 (2 H, t, *J* = 7.7, Ar-C-H), 3.04 - 3.17 (m, Ar-C-H), 3.42 (~2 H, t, *J* = 7.0, Br-C-H), 7.33 (1 H, d, *J* = 7.7, C(9)H), 7.40 (1 H, d, *J* = 8.5, C(2)H), 7.47 (1 H, t, *J* = 7.7, C(8)H), 8.50 (1 H, d, *J* = 8.5, C(1)H), 8.53 (1 H, d, *J* = 7.7, C(7)H) (ignoring impurity peaks, approximate integrations given where appropriate, integrations not given where significant impurity overlap present). *m/z* (APCI) 479 ($[M(^{81}Br) + H]^+$, 45%), 477 ($[M(^{79}Br) + H]^+$, 45), 214 (100), 158 (60), 141 (35). HR *m/z* (APPI) $C_{30}H_{37}{}^{79}Br$ requires 476.2073, found 476.2073.

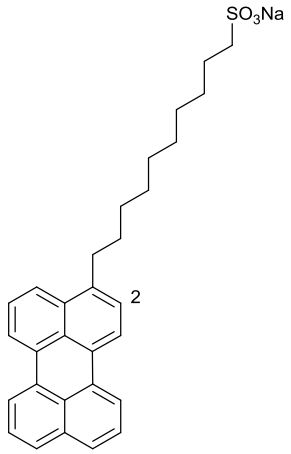

Sodium 10-(perylen-3-yl)decane-1-sulfonate (**166**)

Na_2SO_3 (1.53 g, 12.1 mmol) was added to a three neck RBF (250 mL) which was then purged with N_2. 3-(10-Bromodecyl)perylene (**160**) (476.1 mg, 1.010 mmol) was ground into a powder with a pestle and mortar and suspended in portions into EtOH (7 × 9 mL) with sonication before addition to the reaction mixture *via* syringe. Water (48 mL) was then added *via* syringe and the reaction heated to 100 °C overnight. The reaction mixture was then concentrated *in vacuo* and triturated with DCM (2 × 12 mL). The crude material was then purified by a trituration/recrystallisation process. The crude material was triturated with an EtOH:water mixture (1:1) (500 mL) heated at ~80 °C. The suspension was then cooled to 0 °C in an ice bath and the filtered precipitate washed with water (2 × 10 mL) and DCM (10 mL). The filtrate could then be concentrated *in vacuo* to the point of precipitation, cooled to 0 °C and the filtered precipitate washed with water (2 × 5 mL) and DCM (5 mL), allowing isolation of additional purified product. This process afforded the pure *title compound* (**166**) (427.1 mg, 0.8635 mmol, 85% yield) as a yellow amorphous solid. mp 263-265 °C. δ_H (400 MHz; DMSO-d_6; DMSO-d_5) 1.19 - 1.46 (12 H, m, C-C-H), 1.48 - 1.58 (2 H, m, C-C-H), 1.62 - 1.72 (2 H, m, C-C-H), 2.35 (2 H, t, *J* = 7.8, NaO_3S-C-H), 2.99 (2 H, t, *J* = 7.7, Ar-C-H), 7.41 (1 H, d, *J* = 7.8, C(2)H), 7.48 - 7.62 (3 H, m, Ar-H), 7.77 (2 H, t, *J* = 7.9, Ar-H), 7.93 (1 H, d, *J* = 8.3, Ar-H), 8.25 - 8.41 (4 H, m, Ar-H). δ_C (126 MHz; DMSO-d_6; DMSO-d_6) 25.1, 28.5, 28.9, 29.0, 29.1, 30.2, 32.5, 51.6, 120.1, 120.55, 120.57, 124.0, 126.7, 126.85, 126.90, 127.0, 127.4, 127.7, 127.8, 128.3, 128.6, 130.70, 130.73, 130.9, 132.5, 134.3, 138.8. NB: 19 Aromatic carbons detected rather than 20 and 8 aliphatic carbons detected rather than 10, this is assumed to be due to overlap. *m/z* (ESI$^-$) 471

([M – Na]$^-$, 100%), 421 (25). HR *m/z* (ESI$^-$) $C_{30}H_{31}NaO_3S$ – Na requires 471.1994, found 471.2006. ν_{max}/cm^{-1} 3533br and 3482br ($SO_3Na•H_2O$), 3049 (Ar C-H), 2918s and 2849 (C-H), 1626, 1591 and 1502 (Ar C=C).

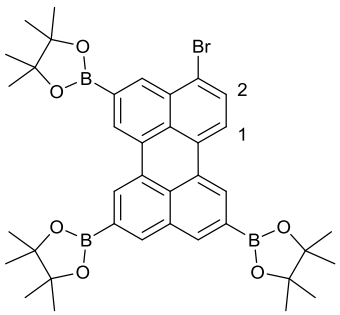

3-Bromo-5,8,11-*tris*(4,4',5,5'-tetramethyl-1,3,2-dioxaborolan-2-yl)perylene (**167**)

An oven dried microwave vial equipped with a stirrer bar was placed under a flushing N_2 needle. 3-Bromoperylene (**147**) (275.4 mg, 0.8315 mmol), *bis*(pinacolato)diboron (696.0 mg, 2.7408 mmol), $[Ir(OMe)(COD)]_2$ (27.7 mg, 0.0418 mmol, 5 mol%) and dtbpy (22.7 mg, 0.0846 mmol, 10 mol%) were then added against a flow of N_2. Dry THF (2.0 mL) was then added and the vial quickly capped as the N_2 needle was withdrawn. The reaction mixture was then heated at 80 °C for 1 h in a microwave reactor before concentration *in vacuo*. The crude sample was then trituated with MeOH to afford a partially purified sample of the *title compound* (**167**) suitable for partial characterisation. δ_H (500 MHz; $CDCl_3$; $CHCl_3$) 1.42 (~12 H, s, Me), 1.45 (s, Me), 1.46 (s, Me), 7.78 (1 H, d, *J* = 8.2, C(2)H), 8.17 (1 H, d, *J* = 8.2, C(1)H), 8.28 (1 H, s, Ar-H), 8.29 (1 H, s, Ar-H), 8.55 (1 H, s, Ar-H), 8.57 (1 H, s, Ar-H), 8.68 (2 H, s, Ar-H) (ignoring impurity peaks, approximate integrations given where appropriate, integrations not given where significant impurity overlap present). *m/z* (MALDI-Dithranol) 836 ($[M(^{81}Br) – H + Bpin]^+$, 20%), 834 ($[M(^{79}Br) – H + Bpin]^+$, 15), 756 ($[M – Br + Bpin]^+$, 25), 710 ($[M(^{81}Br)]^+$, 50), 708 ($[M(^{79}Br)]^+$, 55), 630 ($[M – Br + H]^+$, 15), 584 ($[M(^{81}Br) – Bpin + H]^+$, 5), 582 ($[M(^{79}Br) – Bpin + H]^+$, 5), 227 ($[Dithranol + H]^+$, 100). HR *m/z* (APCI) $C_{38}H_{44}{}^{11}B_3{}^{79}BrO_6$ + H requires 709.2673, found 709.2648.

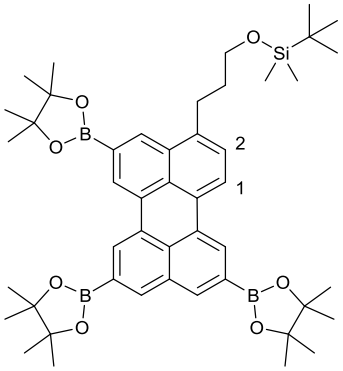

tert-Butyldimethyl(3-[5,8,11-*tris*(4,4',5,5'-tetramethyl-1,3,2-dioxaborolan-2-yl)perylen-3-yl]propoxy)silane (**168**)

tert-butyldimethyl[3-(perylen-3-yl)propoxy]silane (**154**) (249.9 mg, 0.5885 mmol), $[Ir(OMe)(COD)]_2$ (20.2 mg, 0.0305 mmol, 5 mol%), dtbpy (15.9 mg, 0.0592 mmol, 10 mol%) and *bis*(pinacolato)diboron (598.3 mg, 2.356 mmol) were added to a two neck RBF (100 mL) equipped with a condenser which was then purged with N_2. Cyclohexane (7 mL) was then added *via* syringe and the reaction heated to reflux overnight. The crude reaction mixture was then concentrated *in vacuo* and purification achieved by adaptation of a similar literature process.[126] The crude product was sonicated with MeOH (15 mL) and the residual solid filtered and washed with MeOH (7 mL). Repetition of this process two further times afforded the pure *title compound* (**168**) (319.3 mg, 0.3979 mmol, 68% yield) as a yellow solid. mp 157-158 °C. δ_H (400 MHz; $CDCl_3$; $CHCl_3$) 0.12 (6 H, s, Si-Me), 0.96 (9 H, s, Si-C-Me), 1.42 (12 H, s, Me), 1.44 (24 H, s, Me), 2.02 (2 H, quin, *J* = 7.1, C-C-H), 3.16 (2 H, t, *J* = 7.1, Ar-C-H), 3.77 (2 H, t, *J* = 7.1. O-C-H), 7.36 (1 H, d, *J* = 7.8, C(2)H), 8.22 (1 H, s, Ar-H), 8.25 (1 H, s, Ar-H), 8.28 (1 H, d, *J* = 7.8, C(1)H), 8.40 (1 H, s, Ar-H), 8.53 (1 H, s, Ar-H), 8.65 (1 H, s, Ar-H), 8.66 (1 H, s, Ar-H). δ_C (101 MHz; $CDCl_3$; $^{13}CDCl_3$) -5.2, 18.4, 25.0, 26.1, 29.3, 33.6, 62.7, 83.96, 83.98, 84.01, 121.3, 125.1, 125.3, 126.1, 126.6, 129.4, 130.5, 130.7, 130.8, 130.9, 131.6, 131.7, 132.3, 133.2, 136.2, 136.7, 138.9. NB: As is commonly reported,[128] the ^{13}C NMR spectrum features no signals from carbons *ipso*- to boron. *m/z* (MALDI-Dithranol) 825 ($[M + Na]^+$, 10%), 802 ($[M]^+$, 100). HR *m/z* (APCI) $C_{47}H_{65}{}^{11}B_3O_7Si$ requires 802.4773, found 802.4751. ν_{max}/cm^{-1} 2977 (Ar C-H), 2929 and 2856 (C-H), 1610 and 1509w (Ar C=C).

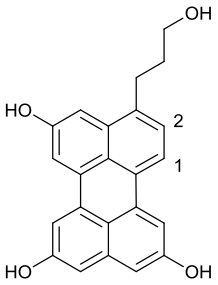

3-(5,8,11-Trihydroxyperylen-3-yl)propan-1-ol (**169**)

tert-butyldimethyl(3-[5,8,11-*tris*(4,4',5,5'-tetramethyl-1,3,2-dioxaborolan-2-yl)perylen-3-yl]propoxy)silane (**168**) (100.7 mg, 0.1255 mmol) and Oxone® (230.8 mg, 0.7509 mmol) were added to a single neck RBF (100 mL) which was then flushed with N_2 and placed under an N_2 needle. The flask was then cooled to 0 °C in an ice bath before an ice cold degassed THF:acetone:water mixture (15:2:1) (9.0 mL) was added *via* syringe. The reaction mixture was stirred at 0 °C for 30 minutes and then at room temperature for 1 h before the reaction was quenched by the addition of saturated sodium thiosulfate solution (100 mL) at 0 °C and extracted with ethyl acetate (3 × 20 mL). The combined organic extracts were then washed with water (100 mL) and brine (100 mL), extracting the aqueous layer each time with ethyl acetate (1 × 20 mL). The organic extracts were then dried over $MgSO_4$ and concentrated *in vacuo*. The crude product was then triturated with DCM (2 × 5 mL) before being subjected to column chromatography, utilising a short silica plug, eluting with a 10% MeOH in DCM solvent system to obtain the partially purified *title compound* (**169**) (5.0 mg, 0.0140 mmol, 11% yield) as a dark brown solid suitable for partial characterisation. δ_H (400 MHz; DMSO-d_6; DMSO-d_5) 1.81 (2 H, quin, *J* = 7.4, C-C-H), 2.90 (2 H, t, *J* = 7.4, Ar-C-H), 3.49 - 3.55 (~2 H, m, O-C-H), 6.79 (1 H, d, *J* = 2.1, Ar-H), 6.82 (1 H, d, *J* = 2.1, Ar-H), 7.20 (1 H, d, *J* = 2.1, Ar-H), 7.29 (1 H, d, *J* = 7.8, C(2)H), 7.49 (1 H, d, *J* = 2.1, Ar-H), 7.56 (1 H, d, *J* = 2.1, Ar-H), 7.71 (1 H, d, *J* = 2.1, Ar-H), 7.91 (1 H, d, *J* = 7.8, C(1)H), 9.66 (1 H, s, Ar-O-H), 9.69 (1 H, s, Ar-O-H), 9.86 (1 H, s, Ar-O-H) (ignoring impurity peaks, approximate integrations given where appropriate). *m/z* (MALDI-TCNQ) 715 ([M – H + M]$^+$, 50%), 477 (25), 358 ([M]$^+$, 100), 250 (55). HR *m/z* (APCI) $C_{23}H_{18}O_4$ + H requires 359.1278, found 359.1277.

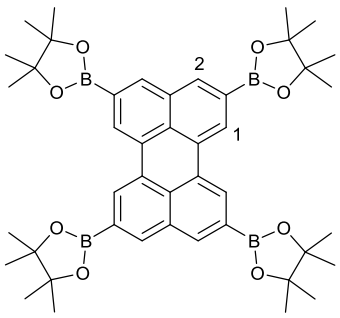

2,5,8,11-*Tetrakis*(4,4',5,5'-tetramethyl-1,3,2-dioxaborolan-2-yl)perylene (**75**)

Prepared by adaptation of a literature synthesis[115]

Perylene (**74**) (250.9 mg, 0.9944 mmol), *bis*(pinacolato)diboron (1.3091 g, 5.1552 mmol), $[Ir(OMe)(COD)]_2$ (33.1 mg, 0.0499 mmol, 5 mol%) and dtbpy (26.8 mg, 0.0999 mmol, 10 mol%) were added to a two neck RBF (100 mL) equipped with a condenser which was then purged with N_2. Cyclohexane (12 mL) was then added *via* syringe and the reaction heated to reflux overnight. The crude reaction mixture was then concentrated *in vacuo* and purification achieved by adaptation of a similar literature procedure.[126] The crude product was sonicated with MeOH (10 mL) and the residual solid filtered and washed with MeOH (5 mL) to obtain the partially purified product (674.4 mg). Material suitable for characterisation was obtained by the recrystallisation of the partially purified product twice from toluene, allowing the isolation of purified *title compound* (**75**) (195.6 mg, 0.2587 mmol, 26% yield). mp >300 °C. δ_H (400 MHz; $CDCl_3$; $CHCl_3$) 1.44 (48 H, s, Me), 8.26 (4 H, s, C(2)H), 8.63 (4 H, s, C(1)H). δ_C (126 MHz; $CDCl_3$; $^{13}CDCl_3$) 24.9, 84.0, 126.0, 130.4, 131.9, 133.3, 136.9. NB: As is commonly reported,[128] the ^{13}C NMR spectrum features no signals from carbons *ipso*- to boron. *m/z* (MALDI-TCNQ) 757 ($[M + H]^+$, 100%), 631 ($[Perylen\text{-}(Bpin)_3 + H]^+$, 10), 227 ($[TCNQ + Na]^+$, 65). ^1H NMR comparable to that in the literature.[115]

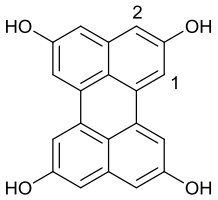

2,5,8,11-Tetrahydroxyperylene (**170**)

2,5,8,11-*tetrakis*(4,4',5,5'-tetramethyl-1,3,2-dioxaborolan-2-yl)perylene (**75**) (49.8 mg, 0.0659 mmol) was added to a two neck RBF (100 mL) which was then purged with N_2. A degassed THF:acetone mixture (8:1) (4.5 mL) was then added *via* syringe. To a separate two neck RBF (100 mL) Oxone® (162.4 mg, 0.5283 mmol) was added and the flask purged with N_2 before the addition of degassed water (1.0 mL) *via* syringe. At 30 minutes intervals the Oxone® solution was added in portions (3 × 0.25 mL, 3 × 0.13 mmol) to the reaction flask *via* syringe, following the reaction by TLC analysis. After 1.5 h product formation was noted. With no further additions, the reaction was stirred for an additional 30 minutes before cooling to 0 °C. Saturated sodium thiosulfate solution (70 mL) was then added and the reaction extracted with ethyl acetate (2 × 20 mL). The combined organic extracts were then washed with brine (2 × 20 mL), dried over $MgSO_4$ and concentrated *in vacuo* to isolate the crude *title compound* (**170**) suitable for partial characterisation. δ_H (400 MHz; DMSO-d_6; DMSO-d_5) 6.82 (4 H, d, J = 2.3, C(2)H), 7.46 (4 H, d, J = 2.3, C(1)H), 9.66 (4 H, s, Ar-O-H) (ignoring impurity peaks). HR *m/z* (HESI$^-$) $C_{20}H_{12}O_4$ – H requires 315.0663, found 315.0663.

5 References

1. C. H. Lo, MChem Report, University of Manchester, 2014.
2. K. W. J. Heard, J. J. Morrison, L. Weston, C. H. Lo, L. Pirvu, J. Raftery, M. S. Little, J. J. W. McDouall, S. G. Yeates and P. Quayle, *Chem. Commun.*, 2015, **51**, 6115-6118.
3. R. G. Harvey, *Polycyclic Aromatic Hydrocarbons Chemistry and Carcinogenicity*, Cambridge University Press, Cambridge, 2011, 1-3.
4. B. T Haire, K. W. J. Heard, M. S. Little, A. V. S. Parry, J. Raftery, P. Quayle and S. G. Yeates, *Chem. Eur. J.*, 2015, **21**, 9970-9974.
5. G. Horowitz, in *Organic Electronics: Materials, Manufacturing and Applications*, ed. H. Klauk, Wiley-VCH, Mörlenbach, 2006, vol. 1, ch. 1, pp. 3-10, 25.
6. M. Muccini, *Nature Materials*, 2006, **5**, 605-613.
7. C. Ruiz, E. M. García-Frutos, G. Hennrich and B. Gómez-Lor, *J. Phys. Chem. Lett.*, 2012, **3**, 1428-1436.
8. M. Kaltenbrunner, T. Sekitani, J. Reeder, T. Yokota, K. Kuribara, T. Tokuhara, M. Drack, R. Schwödiauer, I. Graz, S. Bauer-Gogonea, S. Bauer and T. Someya, *Nature*, 2013, **499**, 458-463.
9. M. Kaltenbrunner, M. S. White, E. D. Głowacki, T. Sekitani, T. Someya, N. S. Sariciftci and S. Bauer, *Nat. Commun.*, 2012, **3**, 770.
10. K. Lee, J. Y. Kim, S. H. Park, S. H. Kim, S. Cho, and A. J. Heeger, *Adv. Mater.*, 2007, **19**, 2445-2449.
11. R. R. Søndergaard, M. Hösel, F. C. Krebs, *J. Polym. Sci. Part B*, 2013, **51**, 16-34.
12. L. Wang, G. Nan, X. Yang, Q. Peng, Q. Li and Z. Shuai, *Chem. Soc. Rev.*, 2010, **39**, 423-434.
13. A. R. Murphy and J. M. J. Fréchet, *Chem. Rev.*, 2007, **107**, 1066-1096.
14. C. R. Newman, C. D. Frisbie, D. A. da Silva Filho, J. Brédas, P. C. Ewbank and K. R. Mann, *Chem. Mater.*, 2004, **16**, 4436-4451.
15. N. C. Greenham, S. C. Moratti, D. D. C. Bradley, R. H. Friend and A. B. Holmes, *Nature*, 1993, **365**, 628-630.

16. N. R. Armstrong, W. Wang, D. M. Alloway, D. Placencia, E. Ratcliff, M. Brumbach, *Macromol. Rapid Commun.*, 2009, **30**, 717-731.
17. G. Witte and C. Wöll, *J. Mater. Res.*, 2004, **19**, 1889-1916.
18. M. Mas-Torrent and C. Rovira, *Chem. Soc. Rev.*, 2008, **37**, 827-838.
19. A. Mishra and P. Bäuerle, *Angew. Chem. Int. Ed.*, 2012, **51**, 2020-2067.
20. C. Wang, H. Dong, W. Hu, Y. Liu and D. Zhu, *Chem. Rev.*, 2012, **112**, 2208-2267.
21. H. Klauk, M. Halik, U. Zschieschang, G. Schmid, W. Radlik and W. Weber, *J. Appl. Phys.*, 2002, **92**, 5259-5263.
22. O. D. Jurchescu, J. Baas and T. T. M. Palstra, *Appl. Phys. Lett.*, 2004, **84**, 3061-3063.
23. M. Watanabe, W. Su, K. Chen, C. Chien, T. Chao, Y. J. Chang, S. Liu and T. J. Chow, *Chem. Commun.*, 2013, **49**, 2240-2242.
24. M. Watanabe, Y. J. Chang, S. Liu, T. Chao, K. Goto, M. M. Islam, C. Yuan, Y. Tao, T. Shinmyozu and T. J. Chow, *Nat. Chem.*, 2012, **4**, 574-578.
25. H. Chang, W. Li, H. Tian, Y. Geng, H. Wang, D. Yan, T. Wang, *Org. Electron.*, 2015, **20**, 43-48.
26. J. Takeya, M. Yamagishi, Y. Tomina, R. Hirahara, Y. Nakazawa, T. Nishikawa, T. Kawase, T. Shimoda and S. Ogawa, *Appl. Phys. Lett.*, 2007, **90**, 102120.
27. G. R. Llorente, M. Dufourg-Madec, D. J. Crouch, R. G. Pritchard, S. Ogier and S. G. Yeates, *Chem. Commun.*, 2009, 3059-3061.
28. R. K. Hallani, K. J. Thorley, Y. Mei , S. R. Parkin, O. D. Jurchescu and J. E. Anthony, *Adv. Funct. Mater.*, 2015, DOI: 10.1002/adfm.201502440.
29. L. Zhang, A. Fonari, Y. Liu, A. M. Hoyt, H. Lee, D. Granger, S. Parkin, T. P. Russell, J. E. Anthony, J. Brédas, V. Coropceanu and A. L. Briseno, *J. Am. Chem. Soc.*, 2014, **136**, 9248-9251.
30. T. Minari, P. Darmawan, C. Liu, Y. Li, Y. Xu and K. Tsukagoshi, *Appl. Phys. Lett.*, 2012, **100**, 093303.
31. H. Minemawari, T. Yamada, H. Matsui, J. Tsutsumi, S. Haas, R. Chiba, R. Kumai and T. Hasegawa, *Nature*, 2011, **475**, 364-367.

32. R. Hofmockel, U. Zschieschang, U. Kraft, R. Rödel, N. H. Hansen, M. Stolte, F. Würthner, K. Takimiya, K. Kern, J. Pflaum and H. Klauk, *Org. Electron.*, 2013, **14**, 3213-3221.
33. T. Okamoto, C. Mitsui , M. Yamagishi , K. Nakahara, J. Soeda, Y. Hirose, K. Miwa, H. Sato, A. Yamano, T. Matsushita, T. Uemura and J. Takeya, *Adv. Mater.*, 2013, **25**, 6392-6397.
34. W. Wu, Y. Liu and D. Zhu, *Chem. Soc. Rev.*, 2010, **39**, 1489-1502.
35. J. S. Brooks, T. Tokumoto, E. S. Choi, D. Graf, N. Biskup, D. L. Eaton, J. E. Anthony and S. A. Odom, *J. Appl. Phys.*, 2004, **96**, 3312-3318.
36. Q. Ye and C. Chi, *Chem. Mater.*, 2014, **26**, 4046-4056.
37. M. Kytka, A. Gerlach, F. Schreiber and J. Kováč, *Appl. Phys. Lett.*, 2007, **90**, 131911.
38. Y. Yuan, G. Giri, A. L. Ayzner, A. P. Zoombelt, S. C. B. Mannsfeld, J. Chen, D. Nordlund, M. F. Toney, J. Huang and Z. Bao, *Nat. Commun.*, 2014, **5**, 3005.
39. K. Nakayama , Y. Hirose, J. Soeda, M. Yoshizumi, T. Uemura, M. Uno, W. Li, M. J. Kang, M. Yamagishi, Y. Okada, E. Miyazaki, Y. Nakazawa, A. Nakao, K. Takimiya and J. Takeya, *Adv. Mater.*, 2011, **23**, 1626-1629.
40. Z. Ding, G. Abbas, H. E. Assender, J. J. Morrison, S. G. Yeates, E. R. Patchett and D. M. Taylor, *ACS Appl. Mater. Interfaces*, 2014, **6**, 15224-15231.
41. J. E. Anthony, A. Facchetti, M. Heeney, S. R. Marder and X. Zhan, *Adv. Mater.*, 2010, **22**, 3876-3892.
42. M. Chikamatsu, A. Itakura, Y. Yoshida, R. Azumi and K. Yase, *Chem. Mater.*, 2008, **20**, 7365-7367.
43. B. A. Jones, A. Facchetti, M. R. Wasielewski, and T. J. Marks, *J. Am. Chem. Soc.*, 2007, **129**, 15259-15278.
44. D. Shukla, S. F. Nelson, D. C. Freeman, M. Rajeswaran, W. G. Ahearn, D. M. Meyer and J. T. Carey, *Chem. Mater.*, 2008, **20**, 7486-7491.
45. F. Zhang, Y. Hu, T. Schuettfort, C. Di, X. Gao, C. R. McNeill, L. Thomsen, S. C. B. Mannsfeld, W. Yuan, H. Sirringhaus and D. Zhu, *J. Am. Chem. Soc.*, 2013, **135**, 2338-2349.

46. Y. Inoue, Y. Sakamoto, T. Suzuki, M. Kobayashi, Y. Gao and S. Tokito, *Jpn. J. Appl. Phys.*, 2005, **44**, 3663-3668.
47. S. W. Yun, J. H. Kim, S. Shin, H. Yang, B. An, L. Yang and S. Y. Park, *Adv. Mater.*, 2012, **24**, 911-915.
48. T. D. Anthopoulos, B. Singh, N. Marjanovic, N. S. Sariciftci, A. M. Ramil, H. Sitter, M. Cölle and D. M. de Leeuw, *Appl. Phys. Lett.*, 2006, **89**, 213504.
49. A. Gupta, A. Ali, T. B. Singh, A. Bilic, U. Bach and R. A. Evans, *Tetrahedron*, 2012, **68**, 9440-9447.
50. A. Ajayaghosh, *Chem. Soc. Rev.*, 2003, **32**, 181-191.
51. J. Dai, X. Jiang, H. Wang and D. Yan, *Appl. Phys. Lett.*, 2007, **91**, 253503.
52. P. Gautam, R. Maragani, R. Misra, *Tetrahedron Lett.*, 2014, **55**, 6827-6830.
53. J. Zhou, Y. Zuo, X. Wan, G. Long, Q. Zhang, W. Ni, Y. Liu, Z. Li, G. He, C. Li, B. Kan, M. Li and Y. Chen, *J. Am. Chem. Soc.*, 2013, **135**, 8484-8487.
54. H. Jiang, *Macromol. Rapid Commun.*, 2010, **31**, 2007-2034.
55. Z. Chen, M. J. Lee, R. S. Ashraf, Y. Gu, S. Albert-Seifried, M. M. Nielsen, B. Schroeder, T. D. Anthopoulos, M. Heeney, I. McCulloch and H. Sirringhaus, *Adv. Mater.*, 2012, **24**, 647-652.
56. M. L. Tang, A. D. Reichardt, N. Miyaki, R. M. Stoltenberg and Z. Bao, *J. Am. Chem. Soc.*, 2008, **130**, 6064-6065.
57. M. L. Tang, J. H. Oh, A. D. Reichardt and Z. Bao, *J. Am. Chem. Soc.*, 2009, **131**, 3733-3740.
58. L. Tan, Y. Guo, Y. Yang, G. Zhang, D. Zhang, G. Yu, W. Xu and Y. Liu, *Chem. Sci.*, 2012, **3**, 2530-2541.
59. K. A. McGarry, W. Xie, C. Sutton, C. Risko, Y. Wu, V. G. Young Jr., J. Brédas, C. D. Frisbie and C. J. Douglas, *Chem. Mater.*, 2013, **25**, 2254-2263.
60. W. Xie, P. L. Prabhumirashi, Y. Nakayama, K. A. McGarry, M. L. Geier, Y. Uragami, K. Mase, C. J. Douglas, H. Ishii, M. C. Hersam and C. D. Frisbie, *ACS Nano*, 2013, **7**, 10245-10256.
61. M. Mas-Torrent and C. Rovira, *J. Mater. Chem.*, 2006, **16**, 433-436.
62. N. E. Gruhn, D. A. da Silva Filho, T. G. Bill, M. Malagoli, V. Coropceanu, A. Kahn and J. Brédas, *J. Am. Chem. Soc.*, 2002, **124**, 7918-7919.
63. S. S. Lee and Y. Loo, *Annu. Rev. Chem. Biomol. Eng.*, 2010, **1**, 59-78.

64. W. Shao, H. Dong, L. Jiang and W. Hu, *Chem. Sci.*, 2011, **2**, 590-600.

65. D. B. Hall, P. Underhill and J. M. Torkelson, *Polym. Eng. Sci.*, 1998, **38**, 2039-2045.

66. C. W. Sele, B. K. C. Kjellander, B. Niesen, M. J. Thornton, J. B. P. H. van der Putten, K. Myny, H. J. Wondergem, A. Moser, R. Resel, A. J. J. M. van Breemen, N. van Aerle, P. Heremans, J. E. Anthony and G. H. Gelinck, *Adv. Mater.*, 2009, **21**, 4926-4931.

67. J. Jang, S. Nam, K. Im, J. Hur, S. N. Cha, J. Kim, H. B. Son, H. Suh, M. A. Loth, J. E. Anthony, J. Park, C. E. Park, J. M. Kim and K. Kim, *Adv. Funct. Mater.*, 2012, **22**, 1005-1014.

68. W. H. Lee, D. H. Kim, Y. Jang, J. H. Cho, M. Hwang, Y. D. Park, Y. H. Kim, J. I. Han and K. Cho, *Appl. Phys. Lett.*, 2007, **90**, 132106.

69. Y. Su, X. Gao, J. Liu, R. Xingab and Y. Han, *Phys. Chem. Chem. Phys.*, 2013, **15**, 14396-14404.

70. G. Giri, E. Verploegen, S. C. B. Mannsfeld, S. Atahan-Evrenk, D. H. Kim, S. Y. Lee, H. A. Becerril, A. Aspuru-Guzik, M. F. Toney and Z. Bao, *Nature*, 2011, **480**, 504-508.

71. Y. Diao, B. C-K. Tee, G. Giri, J. Xu, D. H. Kim, H. A. Becerril1, R. M. Stoltenberg, T. H. Lee, G. Xue, S. C. B. Mannsfeld and Z. Bao, *Nat. Mater.*, **12**, 2013, 665-671.

72. G. Portella, J. Poater, J. M. Bofill, P. Alemany and M. Solà, *J. Org. Chem.*, 2005, **70**, 2509-2521.

73. H. Cho, S. Lee, N. S. Cho, G. Jabbour, J. Kwak, D. Hwang and C. Lee, *ACS Appl. Mater. Interfaces*, 2013, **5**, 3855−3860.

74. M. H. Hoang, D. N. Nguyen and D. H. Choi, *Adv. Nat. Sci. Nanosci. Nanotechnol.*, 2011, **2**, 035002.

75. S. Shinamura, E. Miyazaki and K. Takimiya, *J. Org. Chem.*, 2010, **75**, 1228-1234.

76. F. Cicoira, C. Santato, A. Dadvand, C. Harnagea, A. Pignolet, P. Bellutti, Z. Xiang, F. Rosei, H. Meng and D. F. Perepichka, *J. Mater. Chem.*, 2008, **18**, 158-161.

77. A. R. Murphy, J. Liu, C. Luscombe, D. Kavulak, J. M. J. Fréchet, R. J. Kline and M. D. McGehee, *Chem. Mater.*, 2005, **17**, 4892-4899.
78. S. Shinamura, I. Osaka, E. Miyazaki and K. Takimiya, *Heterocycles*, 2011, **83**, 1187-1204.
79. Y. Kubozono, X. He, S. Hamao, K. Teranishi, H. Goto, R. Eguchi, T. Kambe, S. Gohda and Y. Nishihara, *Eur. J. Inorg. Chem.*, 2014, 3806-3819.
80. Y. Kunugi, Y. M. Ikari and K. Okamoto, *ECS Trans.*, 2010, **25**, 11-17.
81. Y. Kunugi, T. Arai, N. Kobayashi, H. Otsuki, T. Nishinaga and K. Okamoto, *J. Photopolym. Sci. Technol.*, 2011, **24**, 345-348.
82. Y. Kunugi, H. Hoshino, H. Otsuki and K. Okamoto, *Electrochemistry*, 2013, **81**, 402-404.
83. Y. Kunugi, A. Mada, H. Otsuki and K. Okamoto, *Bull. Chem. Soc. Jpn.*, 2015, **88**, 1347-1349.
84. F. Zhang, X. Guoa and H. Zhang , *Open Org. Chem. J.*, 2011, **5**, 87-111.
85. D. Biermann and W. Schmidt, *J. Am. Chem. Soc.*, 1980, **102**, 3163-3173.
86. M. Solà, *Front. Chem.*, 2013, **1**, 00022.
87. J. Aihara, *J. Phys. Chem. A*, 1999, **103**, 7487-7495.
88. K. B. Wiberg, *J. Org. Chem.*, 1997, **62**, 5720-5727.
89. J. A. Bull, M. G. Hutchings and P. Quayle, *Angew. Chem. Int. Ed.*, 2007, **46**, 1869-1872.
90. M. Little, H. Lan, J. Raftery, J. J. Morrison, J. J. W. McDouall, S. G. Yeates and P. Quayle, *Eur. J. Org. Chem.*, 2013, 6038-6041.
91. B. K. Banik and F. F. Becker, *Eur. J. Med. Chem.*, 2010, **45**, 4687-4691.
92. A. J. Ashe, J. W. Kampf and P. M. Savla, *J. Org. Chem.*, 1990, **55**, 5558-5559.
93. O. Khorev, C. D. Bösch, M. Probst and R. Häner, *Chem. Sci.*, 2014, **5**, 1506-1512.
94. Y. Chung, L. Sheng, X. Xing, L. Zheng, M. Bian, Z. Chen, L. Xiao and Q. Gong, *J. Mater. Chem. C*, 2015, **3**, 1794-1798.
95. B. K. Banik, M. S. Venkatraman, I. Banik and M. K. Basu, *Tetrahedron Lett.*, 2004, **45**, 4737-4739.

96. A. S. Ionkin, W. J. Marshall, B. M. Fish, L. M. Bryman and Y. Wang, *Chem. Commun.*, 2008, 2319-2321.
97. T. Wu, H. Chou, P. Huang, C. Cheng and R. Liu, *J. Org. Chem.*, 2014, **79**, 267-274.
98. H. Isobe, S. Hitosugi, T. Matsuno, T. Iwamoto and J. Ichikawa, *Org. Lett.*, 2009, **11**, 4026-4028.
99. S. Hitosugi, W. Nakanishi, T. Yamasaki and H. Isobe, *Nat. Commun.*, 2011, **2**, 492.
100. S. Hitosugi, T. Yamasaki and H. Isobe, *J. Am. Chem. Soc.*, 2012, **134**, 12442-12445.
101. H. Shinokubo, *Proc. Jpn. Acad., Ser. B*, 2014, **90**, 1-11.
102. K. M. Waltz, X. He, C. Muhoro and J. F. Hartwig, *J. Am. Chem. Soc.*, 1995, **117**, 11357-11358.
103. C. N. Iverson and M. R. Smith III, *J. Am. Chem. Soc.*, 1999, **121**, 7696-7697.
104. J. Cho, C. N. Iverson and M. R. Smith III, *J. Am. Chem. Soc.*, 2000, **122**, 12868-12869.
105. J. Cho, M. K. Tse, D. Holmes, R. E. Maleczka Jr. and M. R. Smith III, *Science*, 2002, **295**, 305-308.
106. H. Tamura, H. Yamazaki, H. Sato and S. Sakaki, *J. Am. Chem. Soc.*, 2003, **125**, 16114-16126.
107. T. Ishiyama, J. Takagi, K. Ishida, N. Miyaura, N. R. Anastasi and J. F. Hartwig, *J. Am. Chem. Soc.*, 2002, **124**, 390-391.
108. T. Ishiyama, J. Takagi, J. F. Hartwig and N. Miyaura, *Angew. Chem. Int. Ed.*, 2002, **41**, 3056-3058.
109. T. Ishiyama, Y. Nobuta, J. F. Hartwig and N. Miyaura, *Chem. Commun.*, 2003, 2924-2925.
110. S. M. Preshlock, B. Ghaffari, P. E. Maligres, S. W. Krska, R. E. Maleczka Jr and M. R. Smith III, *J. Am. Chem. Soc.*, 2013, **135**, 7572-7582.
111. G. A. Chotana, M. A. Rak and M. R. Smith III, *J. Am. Chem. Soc.*, 2005, **127**, 10539-10544.

112. H. Tajuddin, P. Harrisson, B. Bitterlich, J. C. Collings, N. Sim, A. S. Batsanov, M. S. Cheung, S. Kawamorita, A. C. Maxwell, L. Shukla, J. Morris, Z. Lin, T. B. Marder and P. G. Steel, *Chem. Sci.*, 2012, **3**, 3505-3515.
113. T. M. Boller, J. M. Murphy, M. Hapke, T. Ishiyama, N. Miyaura and J. F. Hartwig, *J. Am. Chem. Soc.*, 2005, **127**, 14263-14278.
114. B. A. Vanchura II, S. M. Preshlock, P. C. Roosen, V. A. Kallepalli, R. J. Staples, R. E. Maleczka Jr, D. A. Singleton and M. R. Smith III, *Chem. Commun.*, 2010, **46**, 7724-7726.
115. D. N. Coventry, A. S. Batsanov, A. E. Goeta, J. A. K. Howard, T. B. Marder and R. N. Perutz, *Chem. Commun.*, 2005, 2172-2174.
116. A. G. Crawford, Z. Liu, I. A. I. Mkhalid, M. Thibault, N. Schwarz, G. Alcaraz, A. Steffen, J. C. Collings, A. S. Batsanov, J. A. K. Howard and T. B. Marder, *Chem. Eur. J.*, 2012, **18**, 5022-5035.
117. L. Ji, A. Lorbach, R. M. Edkins and T. B. Marder, *J. Org. Chem.*, 2015, **80**, 5658-5665.
118. R. Yamaguchi, S. Hiroto and H. Shinokubo, *Org. Lett.*, 2012, **14**, 2472-2475.
119. R. Yamaguchi, S. Ito, B. S. Lee, S. Hiroto, D. Kim and H. Shinokubo, *Chem. Asian J.*, 2013, **8**, 178-190.
120. R. Ozawa, K. Yoza and K. Kobayashi, *Chem. Lett.*, 2011, **40**, 941-943.
121. T. Kimoto, K. Tanaka, Y. Sakai, A. Ohno, K. Yoza and K. Kobayashi, *Org. Lett.*, 2009, **11**, 3658-3661.
122. K. Kurotobi, M. Miyauchi, K. Takakura, T. Murafuji and Y. Sugihara, *Eur. J. Org. Chem.*, 2003, 3663-3665.
123. T. Matsuno, S. Kamata, S. Hitosugi and H. Isobe, *Chem. Sci.*, 2013, **4**, 3179-3183.
124. S. Shinamura, R. Sugimoto, N. Yanai, N. Takemura, T. Kashiki, I. Osaka, E. Miyazaki and K. Takimiya, *Org. Lett.*, 2012, **14**, 4718-4721.
125. T. Teraoka, S. Hiroto and H. Shinokubo, *Org. Lett.*, 2011, **13**, 2532-2535.
126. M. N. Eliseeva and L. T. Scott, *J. Am. Chem. Soc.*, 2012, **134**, 15169-15172.
127. L. Ji, K. Fucke, S. K. Bose and T. B. Marder, *J. Org. Chem.*, 2015, **80**, 661-665.

128. S. Hitosugi, Y. Nakamura, T. Matsuno, W. Nakanishi and H. Isobe, *Tetrahedron Lett.*, 2012, **53**, 1180-1182.
129. A. K. Geim, *Science*, 2009, **324**, 1530-1534.
130. A. Ciesielski and P. Samorì, *Chem. Soc. Rev.*, 2014, **43**, 381-398.
131. K. S. Novoselov, A. K. Geim, S. V. Morozov, D. Jiang, Y. Zhang, S. V. Dubonos, I. V. Grigorieva, A. A. Firsov, *Science*, 2004, **306**, 666-669.
132. F. Bonaccorso, A. Lombardo, T. Hasan, Z. Sun, L. Colombo and A. C. Ferrari, *Mater. Today*, 2012, **15**, 564-589.
133. A. N. Obraztsov, *Nat. Nanotechnol.*, 2009, **4**, 212-213.
134. S. Bae, H. Kim, Y. Lee, X. Xu, J. Park, Y. Zheng, J. Balakrishnan, T. Lei, H. R. Kim, Y. I. Song, Y. Kim, K. S. Kim, B. Özyilmaz, J. Ahn, B. H. Hong and S. Iijima, *Nat. Nanotechnol.*, 2010, **5**, 574-578.
135. Q. Yu, L. A. Jauregui, W. Wu, R. Colby, J. Tian, Z. Su, H. Cao, Z. Liu, D. Pandey, D. Wei, T. F. Chung, P. Peng, N. P. Guisinger, E. A. Stach, J. Bao, S. Pei and Y. P. Chen, *Nat. Mater.*, 2011, **10**, 443-449.
136. W. Du, X. Jiang and L. Zhu, *J. Mater. Chem. A*, 2013, **1**, 10592-10606.
137. K. V. Emtsev, A. Bostwick, K. Horn, J. Jobst, G. L. Kellogg, L. Ley, J. L. McChesney, T. Ohta, S. A. Reshanov, J. Röhrl, E. Rotenberg, A. K. Schmid, D. Waldmann, H. B.Weber and T. Seyller, *Nat. Mater.*, 2009, **8**, 203-207.
138. L. Zhi and K. Müllen, *J. Mater. Chem.*, 2008, **18**, 1472-1484.
139. X. Yan, B. Li and L. Li, *Acc. Chem. Res.*, 2013, **46**, 2254-2262.
140. A. Narita, X. Feng and K. Müllen, *Chem. Rec.*, 2015, **15**, 295-309.
141. C. D. Simpson, J. D. Brand, A. J. Berresheim, L. Przybilla, H. J. Räder and K. Müllen, *Chem. Eur. J.*, 2002, **8**, 1424-1429.
142. L. Chen, Y. Hernandez, X. Feng and K. Müllen, *Angew. Chem. Int. Ed.*, 2012, **51**, 7640-7654.
143. A. Narita, X. Feng, Y. Hernandez, S. A. Jensen, M. Bonn, H. Yang, I. A. Verzhbitskiy, C. Casiraghi, M. R. Hansen, A. H. R. Koch, G. Fytas, O. Ivasenko, B. Li, K. S. Mali, T. Balandina, S. Mahesh, S. De Feyter and K. Müllen, *Nat. Chem.*, 2014, **6**, 126-132.
144. D. Parviz, S. Das, H. S. T. Ahmed, F. Irin, S. Bhattacharia and M. J. Green, *ACS Nano*, 2012, **6**, 8857-8867.

145. Z. Liu, D. He, Y. Wang, H. Wu, J. Wang, H. Wang, *Sol. Energ. Mat. Sol. Cells*, 2010, **94**, 2148-2153.

146. A. Shukla, R. Kumar, J. Mazher, A. Balan, *Solid State Commun.*, 2009, **149**, 718-721.

147. S. Dhar, A. R. Barman, G. X. Ni, X. Wang, X. F. Xu, Y. Zheng, S. Tripathy, Ariando, A. Rusydi, K. P. Loh, M. Rubhausen, A. H. C. Neto, B. Őzyilmaz and T. Venkatesan, *AIP Adv.*, 2011, **1**, 022109.

148. L. Zhang, Z. Zhang, C. He, L. Dai, J. Liu and L. Wang, *ACS Nano*, 2014, **8**, 6663-6670.

149. X. An, T. Simmons, R. Shah, C. Wolfe, K. M. Lewis, M. Washington, S. K. Nayak, S. Talapatra and S. Kar, *Nano Lett.*, 2010, **10**, 4295-4301.

150. R. J. Chen, Y. Zhang, D. Wang and H. Dai, *J. Am. Chem. Soc.*, 2001, **123**, 3838-3839.

151. N. Nakashima, Y. Tomonari and H. Murakamiy, *Chem. Lett.*, 2002, **31**, 638-639.

152. T. J. Simmons, J. Bult, D. P. Hashim, R. J. Linhardt and P. M. Ajayan, *ACS Nano*, 2009, **3**, 865-870.

153. W. Wenseleers, I. I. Vlasov, E. Goovaerts, E. D. Obraztsova, A. S. Lobach and A. Bouwen, *Adv. Funct. Mater.*, 2004, **14**, 1105-1112.

154. A. Schlierf, H. Yang, E. Gebremedhn, E. Treossi, L. Ortolani, L. Chen, A. Minoia, V. Morandi, P. Samorì, C. Casiraghi, D. Beljonne and V. Palermo, *Nanoscale*, 2013, **5**, 4205-4216.

155. H. Yang, Y. Hernandez, A. Schlierf, A. Felten, A. Eckmann, S. Johal, P. Louette, J. Pireaux, X. Feng, K. Müellen, V. Palermo, C. Casiraghi, *Carbon*, 2013, **53**, 357-365.

156. A. Viinikanoja, J. Kauppila, P. Damlin, E. Mäkilä, J. Leiro, T. Ääritalo, J. Lukkari, *Carbon*, 2014, **68**, 195-209.

157. J. M. Englert, J. Röhrl, C. D. Schmidt, R. Graupner, M. Hundhausen, F. Hauke and A. Hirsch, *Adv. Mater.*, 2009, **21**, 4265-4269.

158. A. Ghosh, K. V. Rao, S. J. George and C. N. R. Rao, *Chem. Eur. J.*, 2010, **16**, 2700-2704.

159. S. Sampath , A. N. Basuray , K. J. Hartlieb, T. Aytun, S. I. Stupp and J. F. Stoddart, *Adv. Mater.*, 2013, **25**, 2740-2745.
160. C. D. Schmidt, C. Böttcher and A. Hirsch, *Eur. J. Org. Chem.*, 2007, 5497-5505.
161. R. Kabe, X. Feng, C. Adachi and K. Müllen, *Chem. Asian J.*, 2014, **9**, 3125-3129.
162. D. Lee, T. Kim and M. Lee, *Chem. Commun.*, 2011, **47**, 8259-8261.
163. P. He, C. Zhou, S. Tian, J. Sun, S. Yang, G. Ding, X. Xie and M. Jiang, *Chem. Commun.*, 2015, **51**, 4651-4654.
164. K. C. Majumdar, B. Chattopadhyay, and S. Chakravorty, *Synthesis*, 2009, 674-680.
165. J. M. Murphy, C. C. Tzschucke and J. F. Hartwig, *Org. Lett.*, 2007, **9**, 757-760.
166. K. Shen, Y. Fu, J. Li, L. Liu and Q. Guo, *Tetrahedron*, 2007, **63**, 1568-1576.
167. P. Harrisson, J. Morris, T. B. Marder and P. G. Steel, *Org. Lett.*, 2009, **11**, 3586-3589.
168. L. Zeqing, L. Zhibin, W. Yuqiang Y. Pei, *Res. Chem. Intermed.*, 2013, **39**, 1917-1926.
169. H. Peng, Y. Chen, L. Chen, X. He and F. Li, *J. Polym. Sci. A Polym. Chem.*, 2010, **48**, 5679-5692.
170. X. Yang, Y. Zhao, X. Zhang, R. Li, J. Dang, Y. Li, G. Zhou, Z. Wu, D. Ma, W. Wong, X. Zhao, A. Ren, L. Wang and X Hou, *J. Mater. Chem.*, 2012, **22**, 7136-7148.
171. J. Fang, D. An, K. Wakamatsu, T. Ishikawa, T. Iwanaga, S. Toyota, D. Matsuo, A. Orita and J. Otera, *Tetrahedron Lett.*, 2010, **51**, 917-920.
172. C. C. Tzschucke, J. M. Murphy and J. F. Hartwig, *Org Lett.*, 2007, **9**, 761-764.
173. Y. Ye, S. A. Künzi and M. S. Sanford, *Org. Lett.*, 2012, **14**, 4979-4981.
174. J. Nasielski, N. Hadei, G. Achonduh, E. A. B. Kantchev, C. J. O'Brien, A. Lough and M. G. Organ, *Chem. Eur. J.*, 2010, **16**, 10844-10853.
175. J. Svoboda, P, Stenclová, F. Uhlík, J. Zedník, J. Vohlídal, *Tetrahedron*, 2011, **67**, 75-79.

176. N. Deshapande, N. S. Belavagi, M. G. Sunagar, S. Gaonkar, G. H. Pujar, M. N. Wari, S. R. Inamdar and I. A. M. Khazi, *RSC Adv.*, 2015, **5**, 86685-86696.
177. P. J. Low, M. A. J. Paterson, D. S. Yufit, J. A. K. Howard, J. C. Cherryman, D. R. Tackley, R. Brook and B. Brown, *J. Mater. Chem.*, 2005, **15**, 2304-2315.
178. A. Keerthi, Y. Liu, Q. Wang and S. Valiyaveettil, *Chem. Eur. J.*, 2012, **18**, 11669-11676.
179. J. Balandier, F. Quist, N. Sebaihi, C. Niebel, B. Tylleman, P. Boudard, S. Bouzakraoui, V. Lemaur, J. Cornil, R. Lazzaroni, Y. H. Geerts, S. Stas, *Tetrahedron*, 2011, **67**, 7156-7161.
180. Y. Lim, Y. Shu, S. R. Parkin, J. E. Anthony and G. G. Malliaras, *J. Mater. Chem.*, 2009, **19**, 3049-3056.
181. S. Yamada, K. Kinoshita, S. Iwama, T. Yamazaki, T. Kubota and Tomoko Yajima, *RSC Adv.*, 2013, **3**, 6803-6806.
182. J. Schwaben, N. Münster, T. Breuer, M. Klues, K. Harms, G. Witte and U. Koert, *Eur. J. Org. Chem.*, 2013, 1639-1643.
183. G. A. Mabbot, *J. Chem. Educ.*, 1983, **60**, 697-702.
184. I. Seguy, P. Jolinat, P. Destruel, R. Mamy, H. Allouchi, C. Courseille, M. Cotrait and H. Bock, *ChemPhysChem*, 2001, **2**, 448-452.
185. T. Chen and R. Liu, *Org. Lett.*, 2011, **13**, 4644-4647.
186. G. Hughes, C. Wang, A. S. Batsanov, M. Fern, S. Frank, M. R. Bryce, I. F. Perepichka, A. P. Monkman and B. P. Lyons, *Org. Biomol. Chem.*, 2003, **1**, 3069-3077.
187. P. K. Nayak, N. Periasamy, *Org. Electron.*, 2009, **10**, 1396-1400.
188. Z. Chen, P. Müller and T. M. Swager, *Org. Lett.*, 2006, **8**, 273-276.
189. H. Klauk, U. Zschieschang, R. T. Weitz, H. Meng, F. Sun, G. Nunes, D. E. Keys, C. R. Fincher and Z. Xiang, *Adv. Mater.*, 2007, **19**, 3882-3887.
190. T. Yamamoto and K. Takimiya, *J. Am. Chem. Soc.*, 2007, **129**, 2224-2225.
191. R. J. Chesterfield, J. C. McKeen, C. R. Newman, P. C. Ewbank, D. A. da Silva Filho, J. Brédas, L. L. Miller, K. R. Mann and C. D. Frisbie, *J. Phys. Chem. B*, 2004, **108**, 19281-19292.

192. P. R. L. Malenfant, C. D. Dimitrakopoulos, J. D. Gelorme, L. L. Kosbar, T. O. Graham, A. Curioni and W. Andreoni, *Appl. Phys. Lett.*, 2002, **80**, 2517-2519.

193. Y. Zhou, C. Fuentes-Hernandez, J. Shim, J. Meyer, A. J. Giordano, H. Li, P. Winget, T. Papadopoulos, H. Cheun, J. Kim, M. Fenoll, A. Dindar, W. Haske, E. Najafabadi, T. M. Khan, H. Sojoudi, S. Barlow, S. Graham, J. Brédas, S. R. Marder, A. Kahn and B. Kippelen, *Science*, 2012, **336**, 327-332.

194. J. A. Marsden, J. J. Miller, L. D. Shirtcliff and M. M. Haley, *J. Am. Chem. Soc.*, 2005, **127**, 2464-2476.

195. B. Q. Su, S. Pang, V. Alijani, C. Li, X. Feng and K. Müllen, *Adv. Mater.*, 2009, **21**, 3191-3195.

196. A. J. Lampkins, E. J. O'Neil and B. D. Smith, *J. Org. Chem.*, 2008, **73**, 6053-6058.

197. N. K. Zenkov, E. B. Menshchikova, N. V. Kandalintseva, A. S. Oleynik, A. E. Prosenko, O. N. Gusachenko, O. A. Shklyaeva, V. A. Vavilin and V. V. Lyakhovich, *Biochem. (Mosc.)*, 2007, **72**, 644-651.

198. L. D. Sasiambarrena, A. S. Cánepa, C. N. Luna and R. D. Bravo, *Tetrahedron Lett.*, 2015, **56**, 2054-2058.

199. L. J. Marshall, K. M. Cable, N. P. Botting, *Tetrahedron Lett.*, 2010, **51**, 2690-2692.

200. Z. Zhang and L. S. Liebeskind, *Org. Lett.*, 2006, **8**, 4331-4333.

201. C. W. Liskey, X. Liao and J. F. Hartwig, *J. Am. Chem. Soc.*, 2010, **132**, 11389-11391.

202. L. Zou, X. Wang, X. Zhang, Y. Dai, Y. Wu, J. Wang and J. Pei, *Chem. Commun.*, 2015, **51**, 12585-12588.

203. E. S. Barrett, T. J. Dale and J. Rebek Jr., *Chem. Commun.*, 2007, 4224-4226.

204. T. Ikawa, K. Hattori, H. Sajiki and K. Hirota, *Tetrahedron*, 2004, **60**, 6901-6911.

205. M. D. Watson, M. G. Debije, J. M. Warman and K. Müllen, *J. Am. Chem. Soc.*, 2004, **126**, 766-771.

206. J. M. Casas-Solvas, J. D. Howgego and A. P. Davis, *Org. Biomol. Chem.*, 2014, **12**, 212-232.
207. A. D. Pia, M. Riello, A. Floris, D. Stassen, T. S. Jones, D. Bonifazi, A. De Vita and G. Costantini, *ACS Nano*, 2014, **8**, 12356-12364.
208. S. Ikeda, N. Aratani and A. Osuka, *Chem. Commun.*, 2012, **48**, 4317-4319.
209. S. Kawano, M. Baumgarten, D. Chercka, V. Enkelmann and K. Müllen, *Chem. Commun.*, 2013, **49**, 5058-5060.
210. C. Chang, *J. Chin. Chem. Soc.*, 2011, **58**, 286-289.
211. A. S. Oleynik, T. S. Kuprina, N. Y. Pevneva, A. F. Markov, N. V. Kandalintseva, A. E. Prosenko and I. A. Grigor'ev, *Russ. Chem. Bull., Int. Ed.*, 2007, **56**, 1135-1143.
212. C. D. Williams and F. R. Siperstein, unpublished work.
213. J. Zhang, K. W. J. Heard, P. Quayle and S. G. Yeates, unpublished work.
214. M. Lotya, Y. Hernandez, P. J. King, R. J. Smith, V. Nicolosi, L. S. Karlsson, F. M. Blighe, S. De, Z. Wang, I. T. McGovern, G. S. Duesberg and J. N. Coleman, *J. Am. Chem. Soc.*, 2009, **131**, 3611-3620.
215. M. Lotya, P. J King, U. Khan, S. De and J. N. Coleman, *ACS Nano*, 2010, **4**, 3155-3162.
216. J. Kim, H. U. Kim, D. Mi, S. Jin, W. S. Shin, S. C. Yoon, I. Kang and D. Hwang, *Macromolecules*, 2012, **45**, 2367-2376.

217. Gaussian 09, Revision D.01, M. J. Frisch, G. W. Trucks, H. B. Schlegel, G. E. Scuseria, M. A. Robb, J. R. Cheeseman, G. Scalmani, V. Barone, B. Mennucci, G. A. Petersson, H. Nakatsuji, M. Caricato, X. Li, H. P. Hratchian, A. F. Izmaylov, J. Bloino, G. Zheng, J. L. Sonnenberg, M. Hada, M. Ehara, K. Toyota, R. Fukuda, J. Hasegawa, M. Ishida, T. Nakajima, Y. Honda, O. Kitao, H. Nakai, T. Vreven, J. A. Montgomery, Jr., J. E. Peralta, F. Ogliaro, M. Bearpark, J. J. Heyd, E. Brothers, K. N. Kudin, V. N. Staroverov, R. Kobayashi, J. Normand, K. Raghavachari, A. Rendell, J. C. Burant, S. S. Iyengar, J. Tomasi, M. Cossi, N. Rega, J. M. Millam, M. Klene, J. E. Knox, J. B. Cross, V. Bakken, C. Adamo, J. Jaramillo, R. Gomperts, R. E. Stratmann, O. Yazyev, A. J. Austin, R. Cammi, C. Pomelli, J. W. Ochterski, R. L. Martin, K. Morokuma, V. G. Zakrzewski, G. A. Voth, P. Salvador, J. J. Dannenberg, S. Dapprich, A. D. Daniels, Ö. Farkas, J. B. Foresman, J. V. Ortiz, J. Cioslowski and D. J. Fox, Gaussian, Inc., Wallingford CT, 2009.

218. C. Lee, W. Yang and R. G. Parr, *Phys. Rev. B*, 1988, **37**, 785-789.

219. A. D. Becke, *Phys. Rev. A*, 1988, **38**, 3098-3100.

220. A. D. Becke, *J. Chem. Phys.*, 1993, **98**, 5648-5652.

221. D. Van der Spoel, E. Lindahl, B. Hess, G. Groenhof, A. E. Mark and H. J. C. Berendsen, *J. Comput. Chem,*. 2005, **26**, 1701-1718.

222. A. D. Mackerell, D. Bashford, M. Bellott, R. L. Dunbrack, J. D. Evanseck, M. J. Field, S. Fischer, J. Gao, H. Guo, S. Ha, D. Joseph-McCarthy, L. Kuchnir, K. Kuczera, F. T. K. Lau, C. Mattos, S. Michnick, T. Ngo, D. T. Nguyen, B. Prodhom, W. E. Reiher, B. Roux, M. Schlenkrich, J. C. Smith, R. Stote, J. Straub, M. Watanabe, J. Wiorkiewicz-Kuczera, D. Yin and M. Karplus, *J. Phys. Chem. B*, 1998, **102**, 3586-3616.

223. E. Vanommeslaeghe, C. Hatcher, S. Acharya, S. Kundu, S. Zhong, J. Shim, E. Darian, O. Guvench, P. Lopes, I. Vorobyov and A. D. Mackerell, *J. Comput. Chem.*, 2010, **31**, 671-690.

224. C. Kramer, P. Gedeck and M. Meuwly, *J. Chem. Theory Comput.*, 2013, **9**, 1499-1511.

225. W. L. Jorgensen, J. Chandrasekhar, J. D. Madura, R. W. Impey and M. L. Klein, *J. Chem. Phys.*, 1983, **2**, 926-935.
226. G. M. Torrie and J. P. Valleau, *Chem. Phys. Lett.*, 1974, **28**, 578-581.
227. G. M. Torrie and J. P. Valleau, *J. Comput. Phys.*, 1977, **23**, 187-199.
228. S. Kumar, D. Bouzida, R. H. Swendsen, P. A. Kollman and J. M. Rosenberg, *J. Comput. Chem.*, 1992, **13**, 1011-1021.
229. J. S. Hub, B. L. de Groot and D. van der Spoel, *J. Chem. Theory Comput.*, 2010, **6**, 3713-3720.
230. M. P. Allen and D. J. Tildesley, *Computer Simulation of Liquids*, Clarendon Press, Oxford, 1989.
231. T. Darden, D. York and L. Pedersen, *J. Chem. Phys.*, 1993, **98**, 10089-10092.
232. U. Essmann, L. Perera, M. L. Berkowitz, T. Darden, H. Lee and L. G. Pedersen, *J. Chem. Phys.*, 1995, **103** , 8577-8593.
233. S. Nose, *Mol. Phys.*, 1984, **52**, 255-268.
234. W. G. Hoover, *Phys. Rev. A*, 1985, **31**, 1695-1697.
235. S. Miyamoto and P. A. Kollman, *J. Comput. Chem.*, 1992, **13**, 952-962.
236. I. Takahashi, A. Nomura and H. Kitajima, *Synth. Commun.*, 1990, **20**, 1569-1575.
237. W. Zhu, S. Tao, C. Tao, W. Li, C. Lin, M. Li, Y. Wen and G. Li, *Langmuir*, 2011, **27**, 8451-8457.
238. L. Cai, T. Moehl, S. Moon, J. Decoppet, R. Humphry-Baker, Z. Xue, L, Bin, S. M. Zakeeruddin, and M. Grätzel, *Org. Lett.*, 2014, **16**, 106-109.
239. Y. Kanazawa, T. Yokota, H. Ogasa, H. Watanabe, T. Hanakawa, S. Soga, M. Kawatsura, *Tetrahedron*, 2015, **71**, 1395-1402.
240. M. Yang, X. Chen, Y. Zou, C. Pan, B. Liu, H. Zhong, *J. Mater. Sci.*, 2013, **48**, 1014-1020.
241. C. Wang, L. Pålsson, A. S. Batsanov and M. R. Bryce, *J. Am. Chem. Soc.*, 2006, **128**, 3789-3799.
242. L. Bogani, C. Danieli, E. Biavardi, N. Bendiab, A. Barra, E. Dalcanale, W. Wernsdorfer and A. Cornia, *Angew. Chem. Int. Ed.*, 2009, **48**, 746-750.
243. L. J. O'Driscoll, D. J. Welsh, S. W. D. Bailey, D. Visontai, H. Frampton, M. R. Bryce and C. J. Lambert, *Chem. Eur. J.*, 2015, **21**, 3891-3894.

244. V. B. Kurteva, A. G. Santos and C. A. M. Afonso, *Org. Biomol. Chem.*, 2004, **2**, 514-523.

245. S. Nagarajan, C. Barthes, N. K. Girdhar, T. T. Dang and A. Gourdon, *Tetrahedron*, 2012, **68**, 9371-9375.

246. R. Takahashi, T. Nunokawa, T. Shibuya, R. Tomita, Y. Tatewaki, S. Okada, T. Kimura, S. Shimada and H. Matsuda, *Bull. Chem. Soc. Jpn.*, 2012, **85**, 236-244.

6 Appendix

6.1 UV-vis Absorption and Fluorescence Spectra

6.1-1 2,8-Substituted 4,10-Dichlorochrysene Derivatives

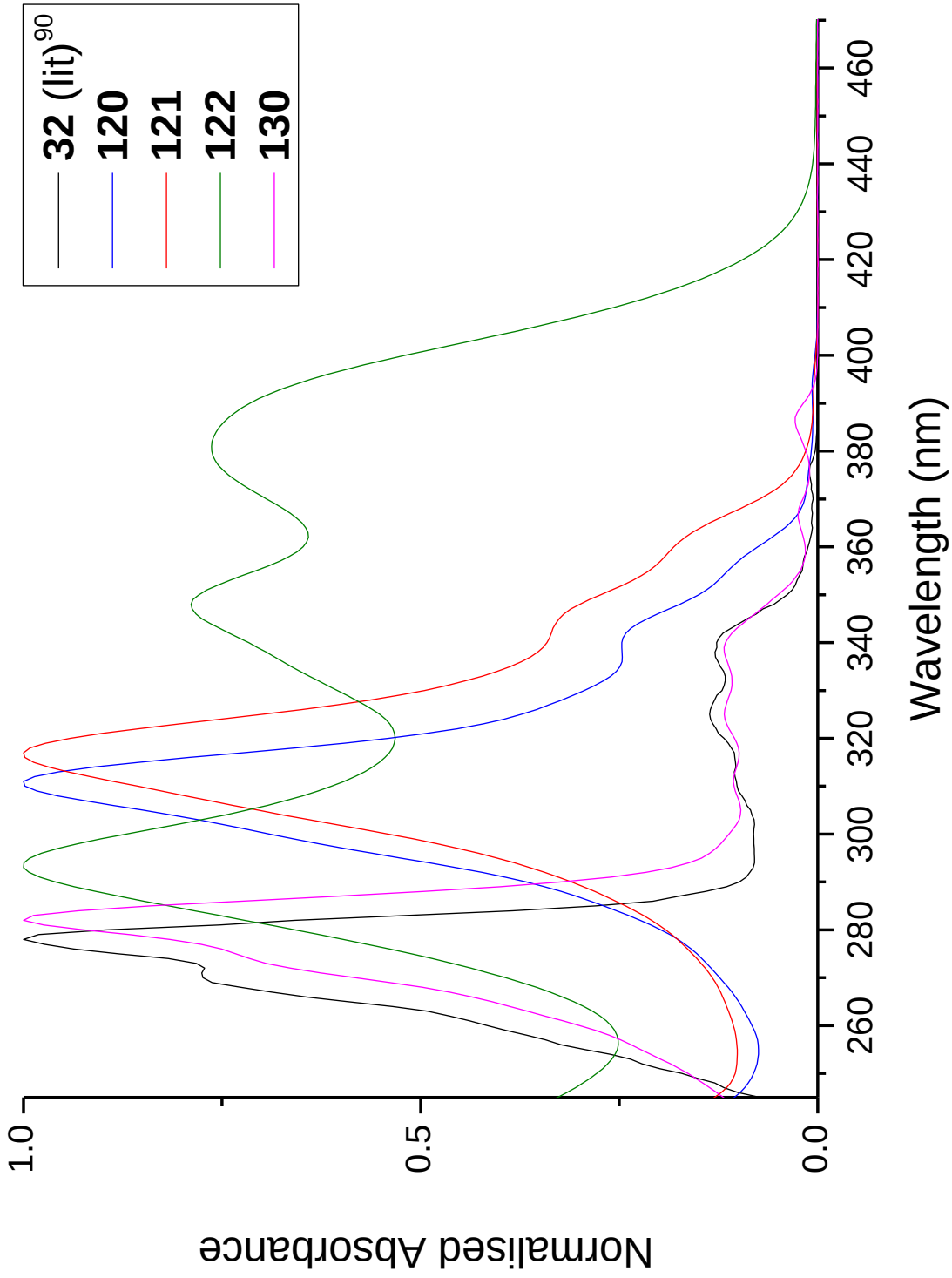

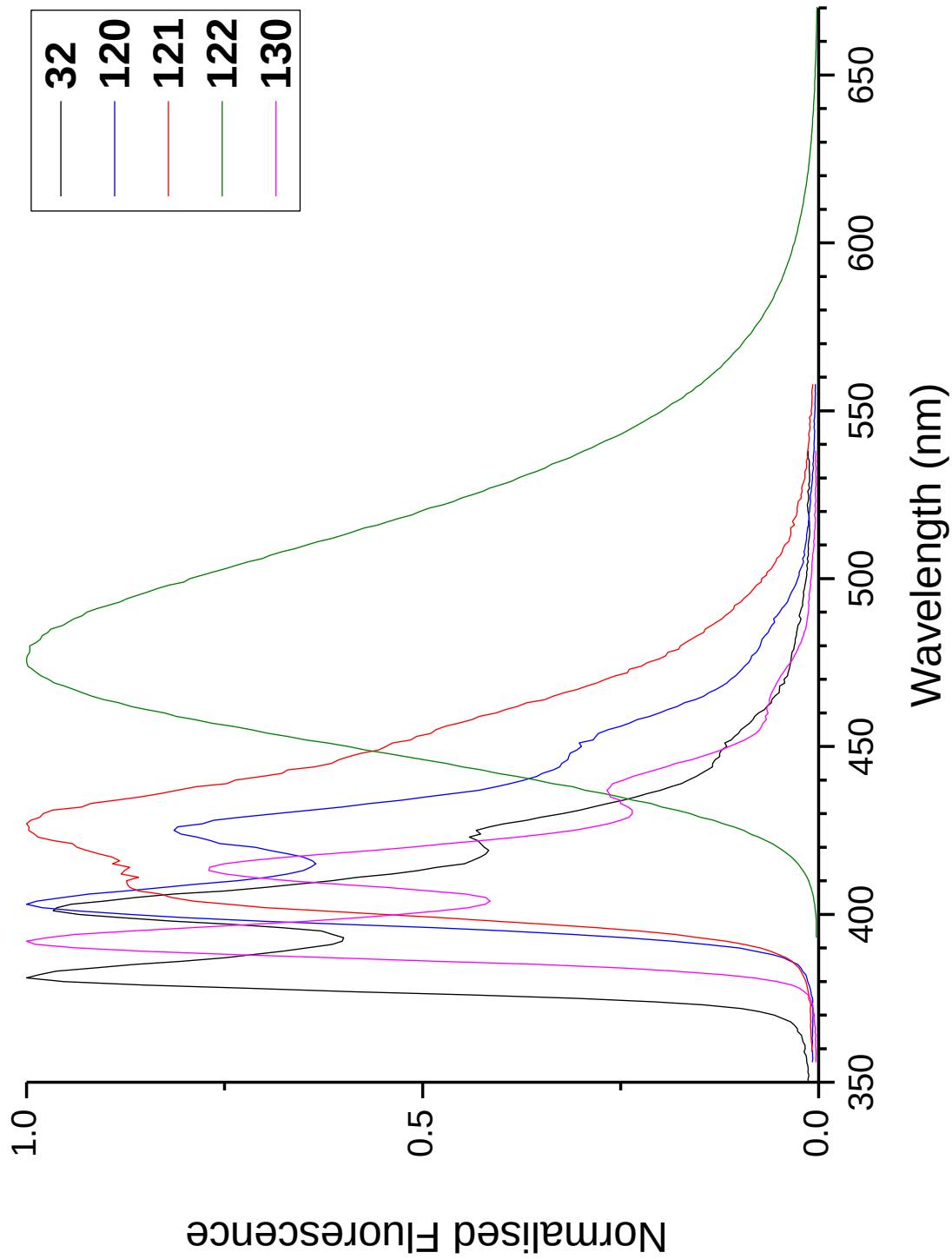
32
120
121
122
130
Normalised Fluorescence
1.0
0.5
0.0
350
400
450
500
550
600
650
Wavelength (nm)

6.1-2 “A_2B_2” Tetrasubstituted Chrysene Derivatives

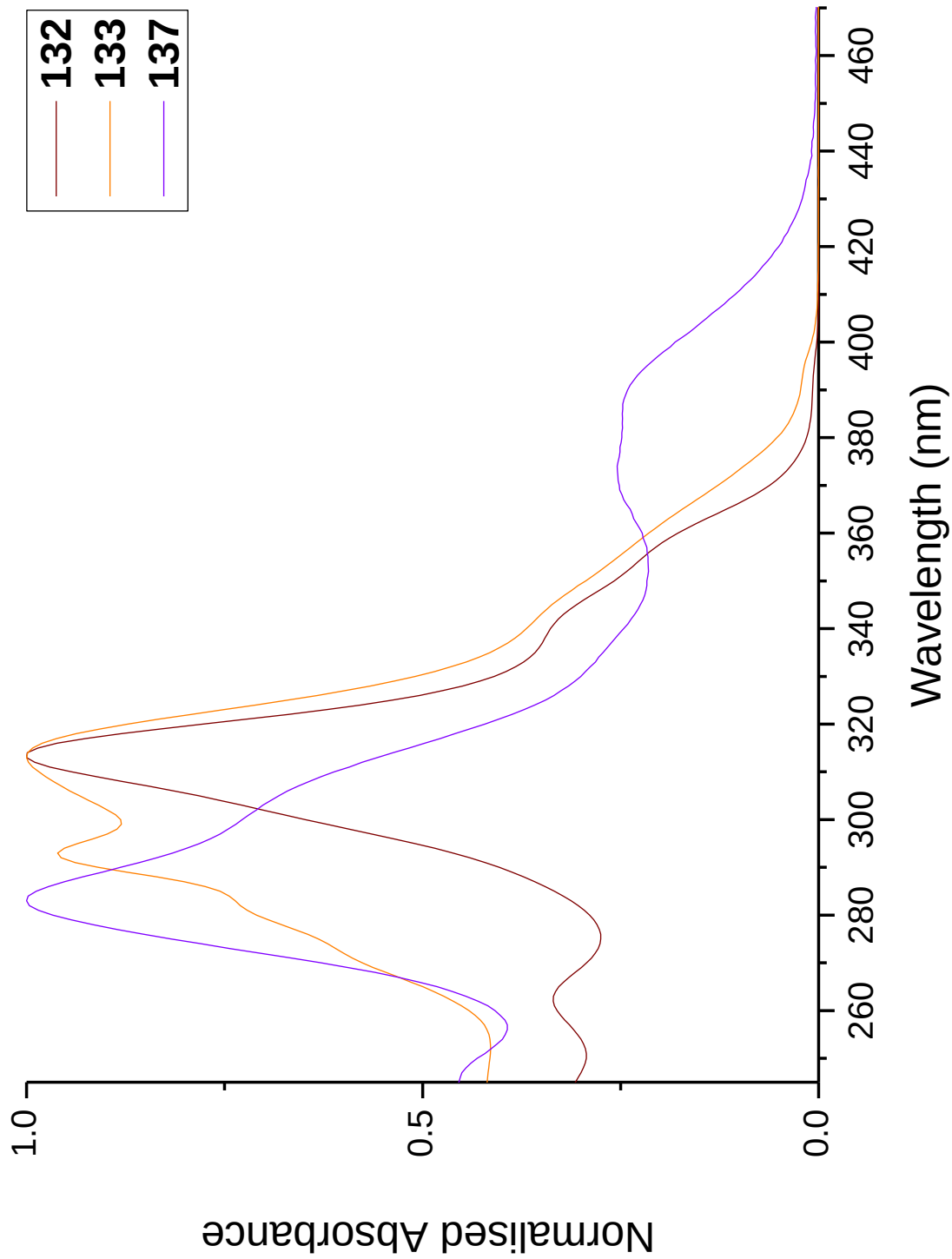

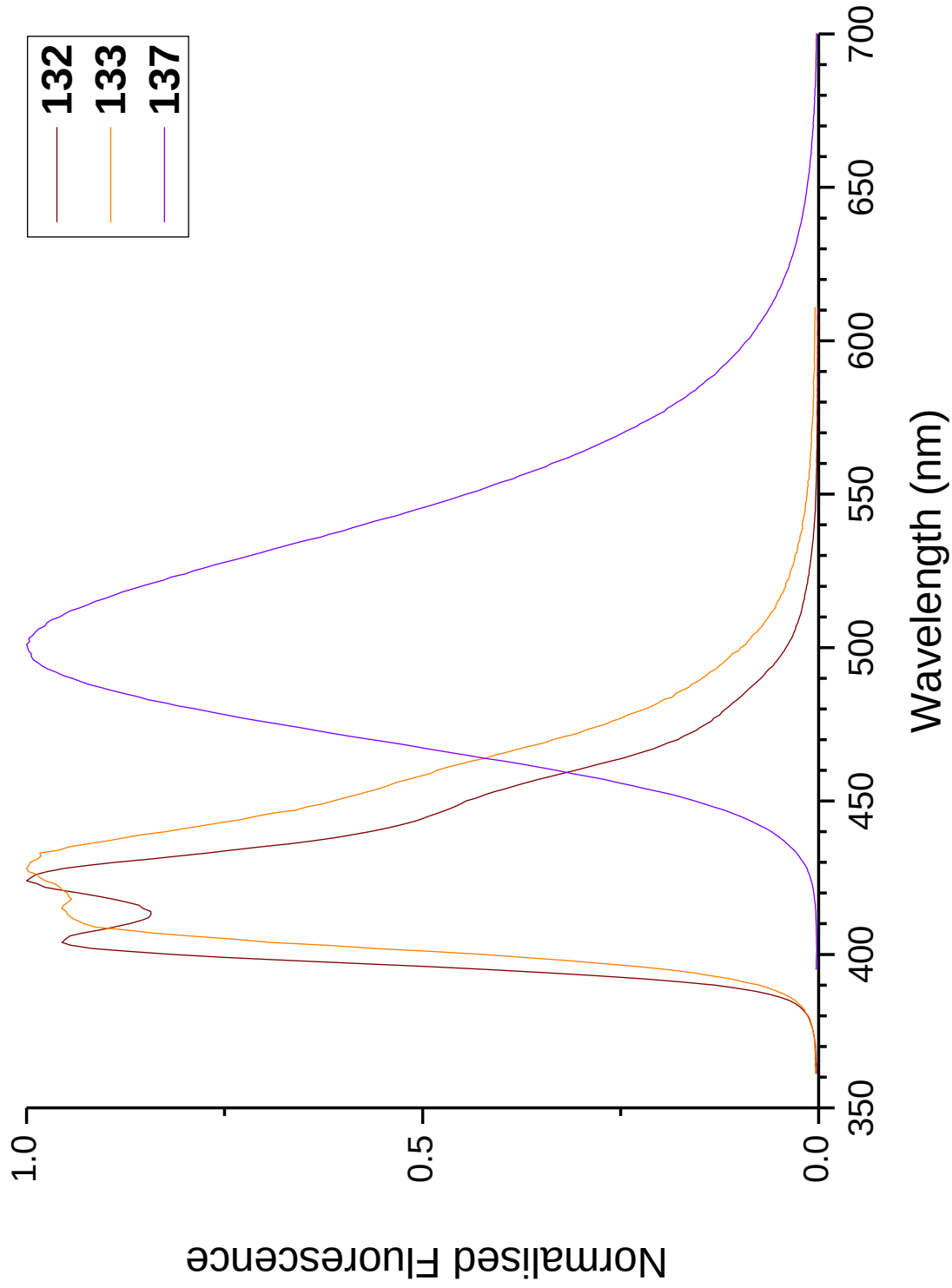
132
133
137
1.0
0.5
0.0
Normalised Fluorescence
350
400
450
500
550
600
650
700
Wavelength (nm)

6.2 ^{1}H and ^{13}C NMR Spectra of Key Compounds

6.2-1 Chrysene Derivatives

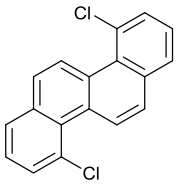

4,10-Dichlorochrysene (**32**)

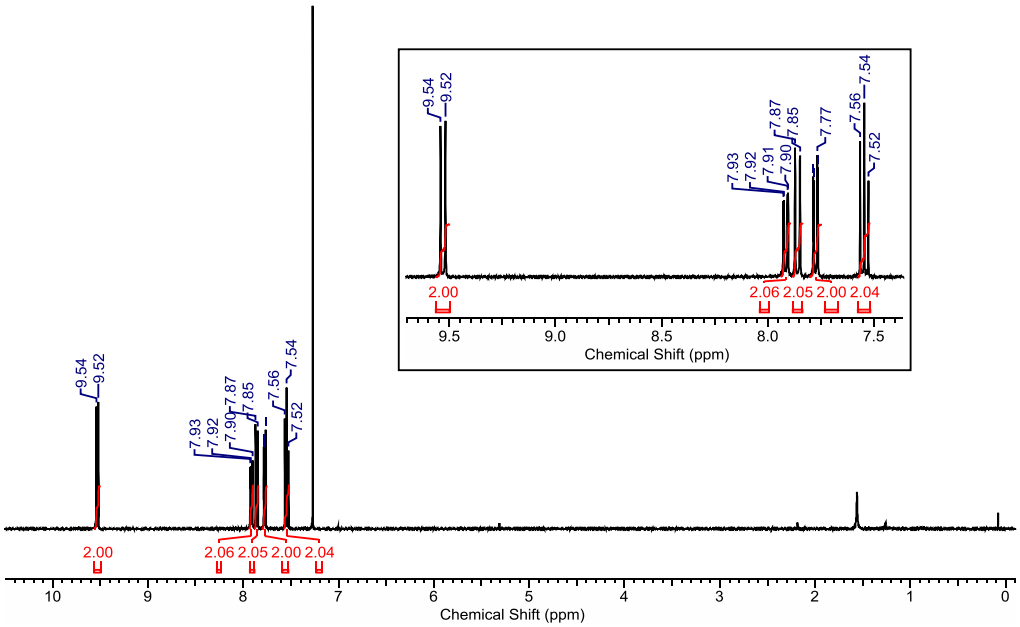

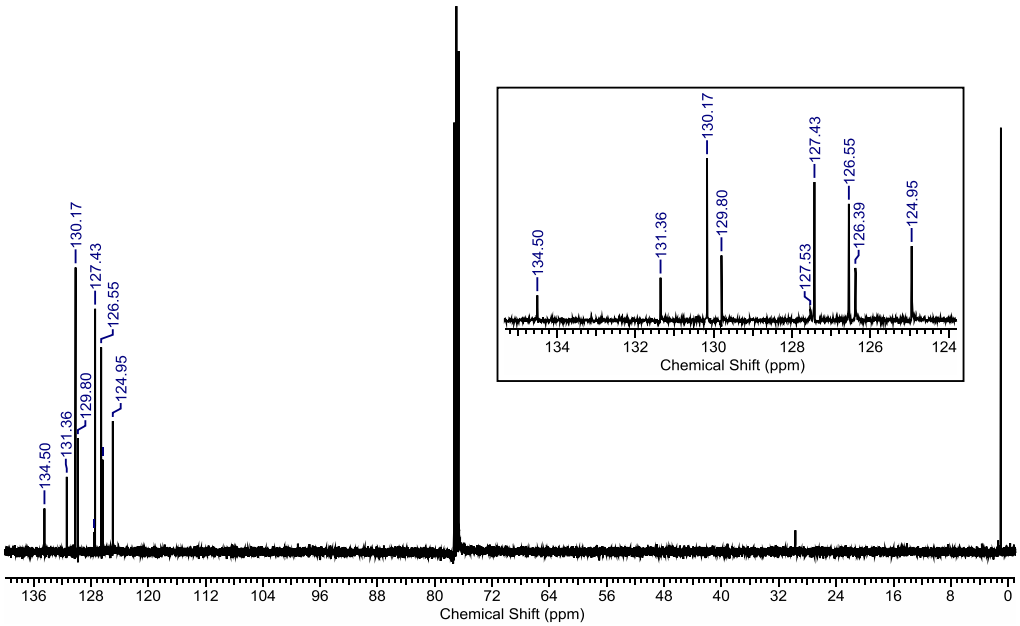

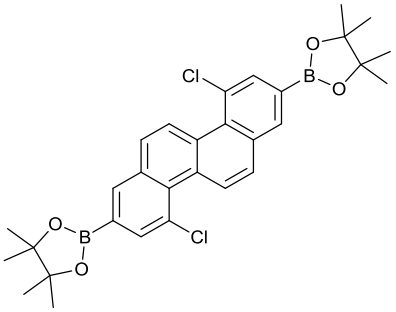

4,10-Dichloro-2,8-*bis*(4,4’,5,5’-tetramethyl-1,3,2-dioxaborolan-2-yl)chrysene (**118**)

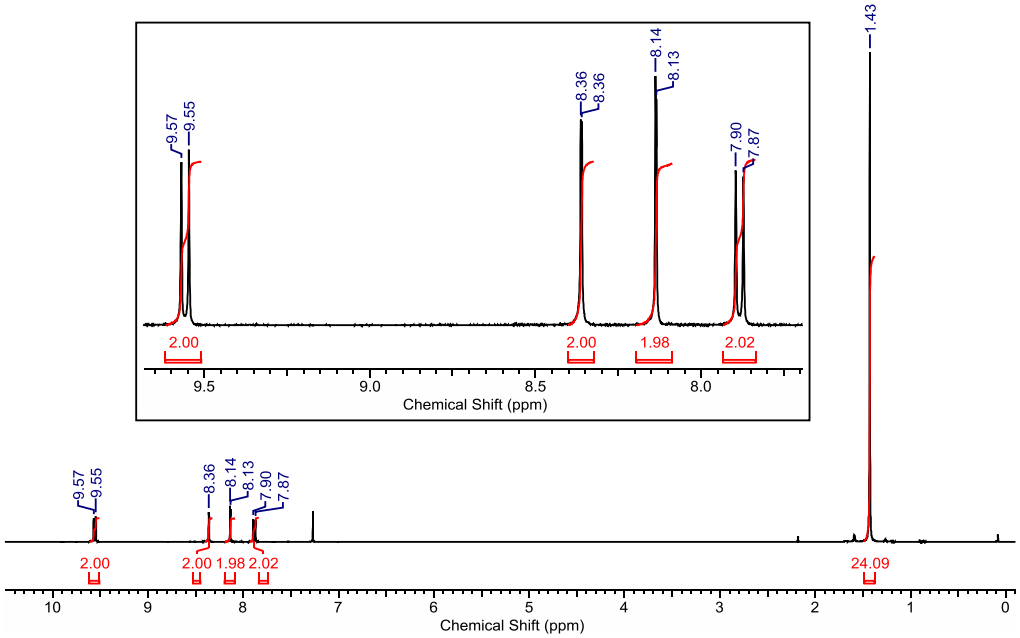

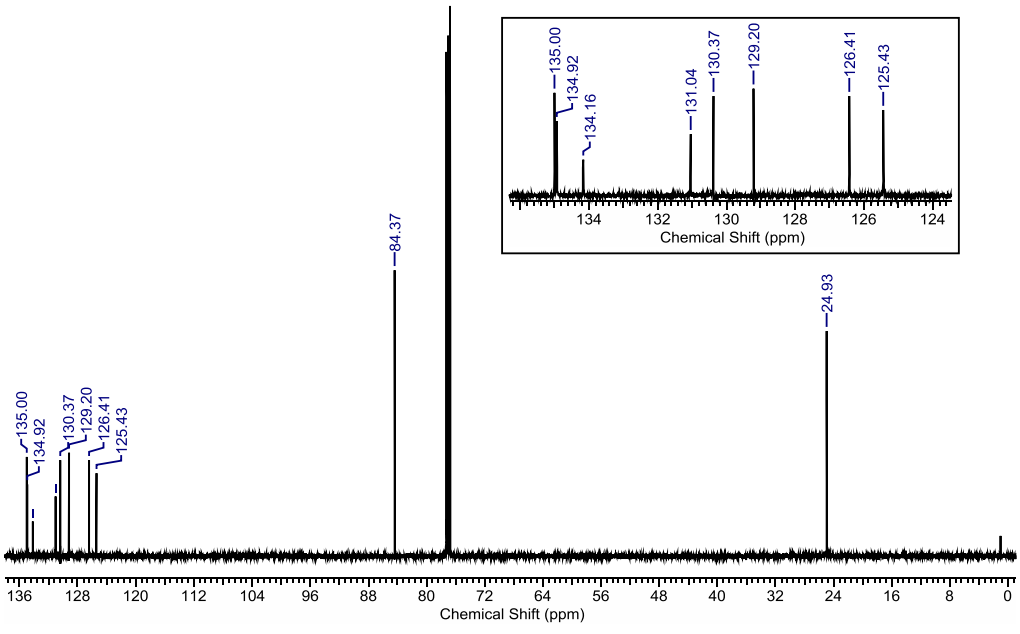

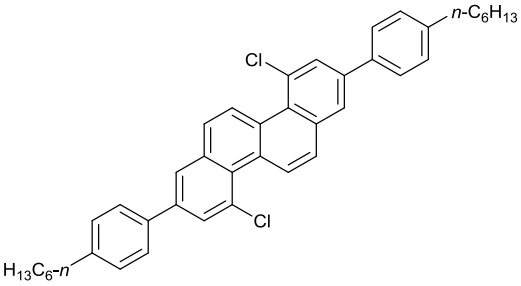

4,10-Dichloro-2,8-*bis*[4-(*n*-hexyl)phenyl]chrysene (**120**)

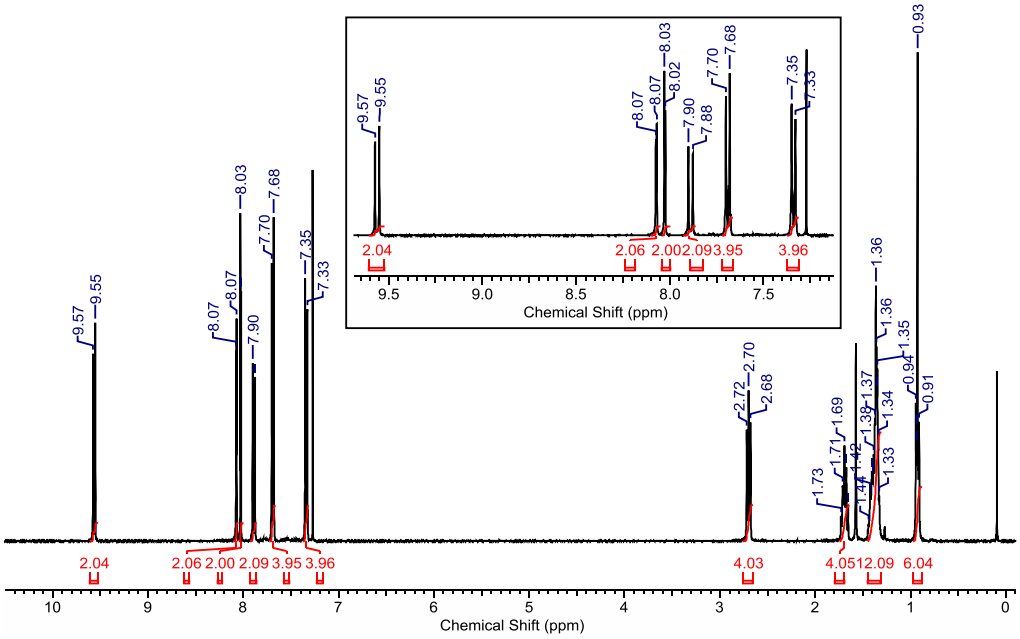

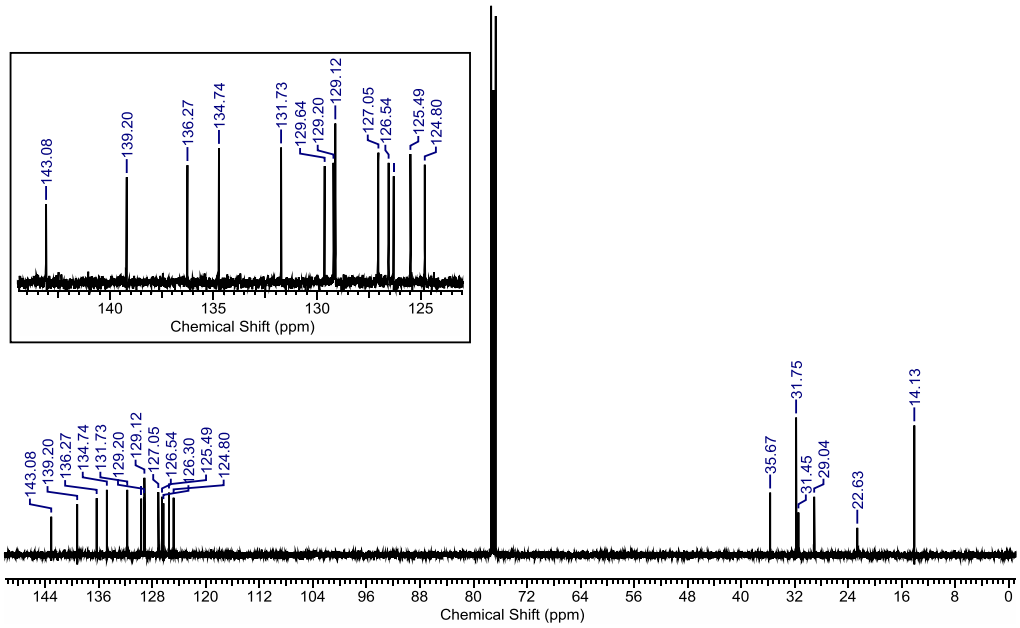

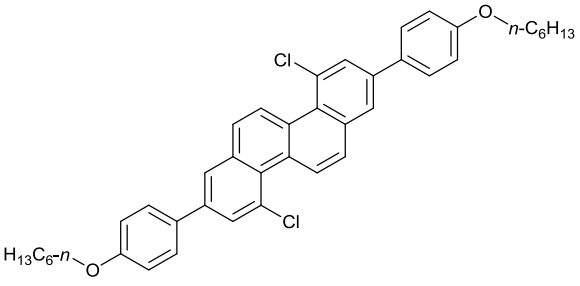

4,10-Dichloro-2,8-*bis*[4-(*n*-hexyloxy)phenyl]chrysene (**121**)

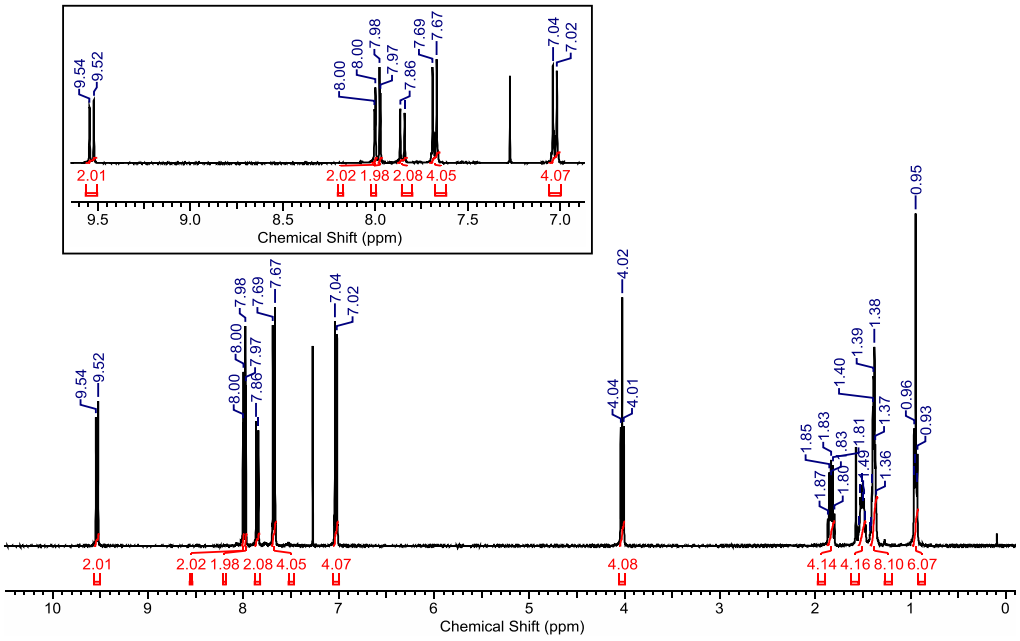

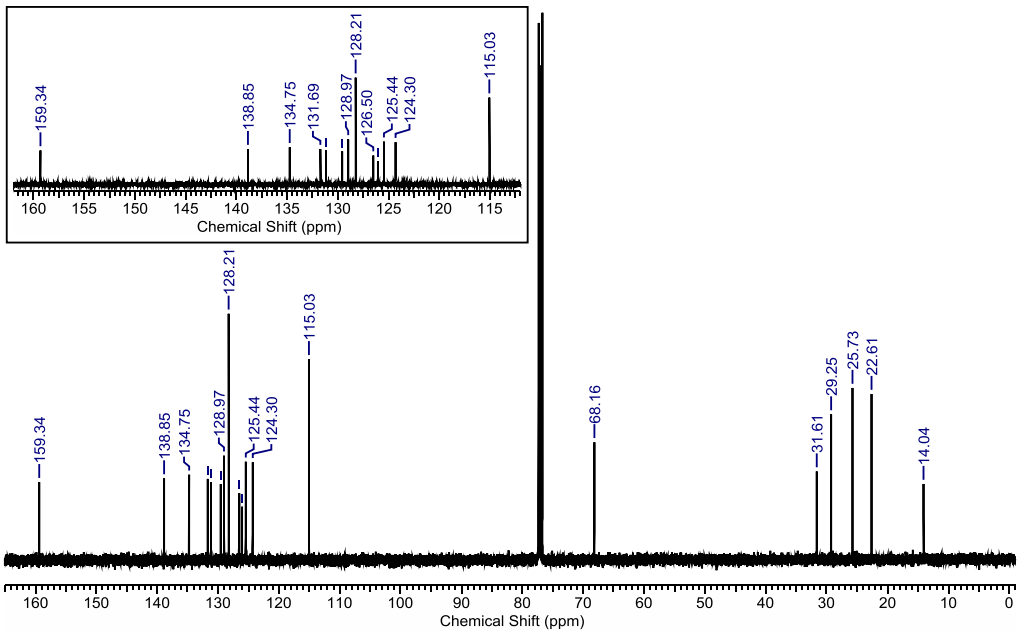

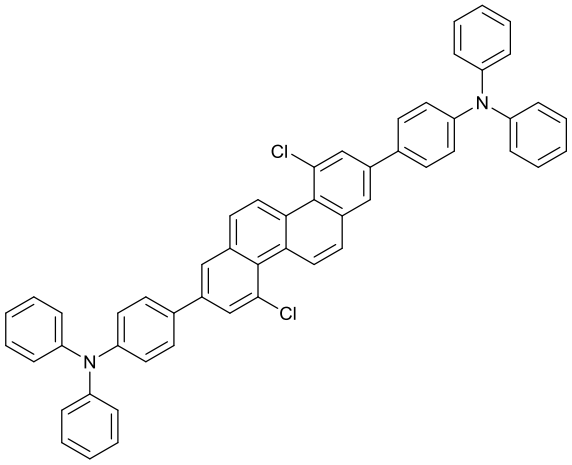

4,10-Dichloro-2,8-*bis*[4-(diphenylamino)phenyl]chrysene (**122**)

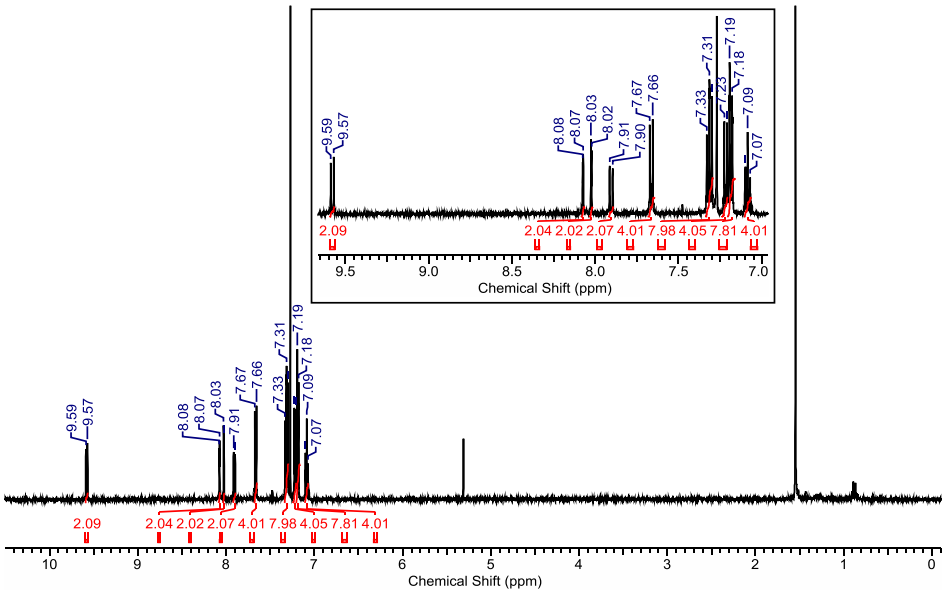

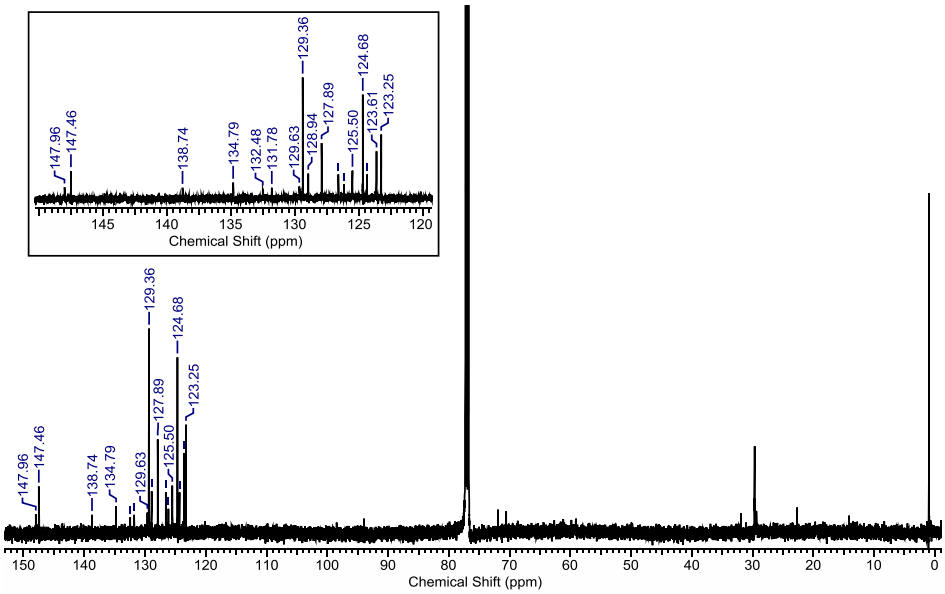

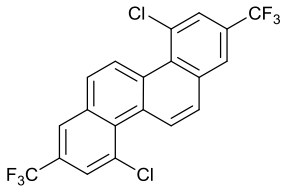

4,10-Dichloro-2,8-*bis*(trifluoromethyl)chrysene (**130**)

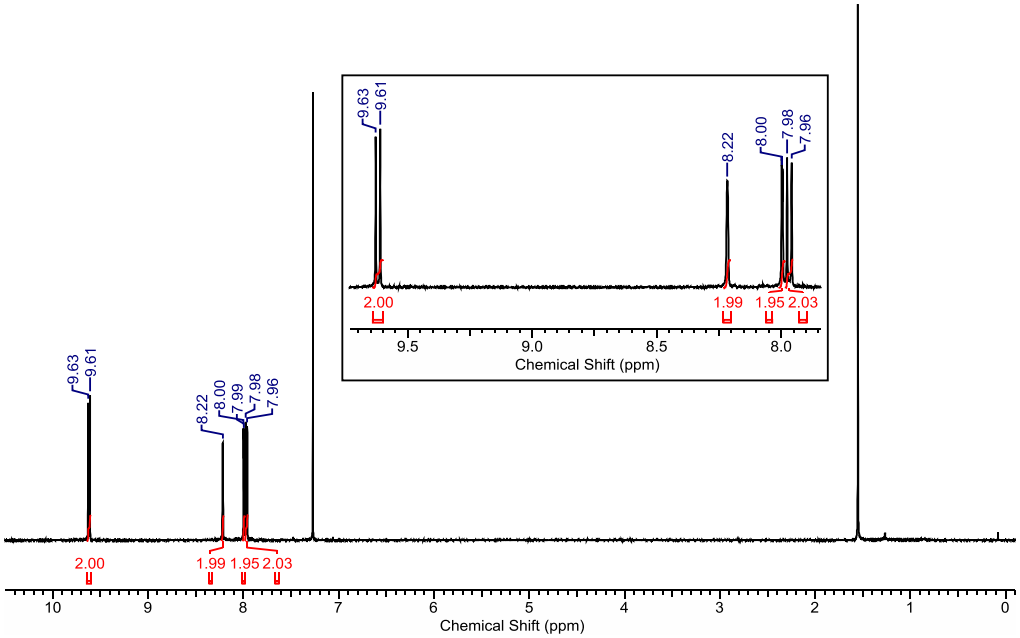

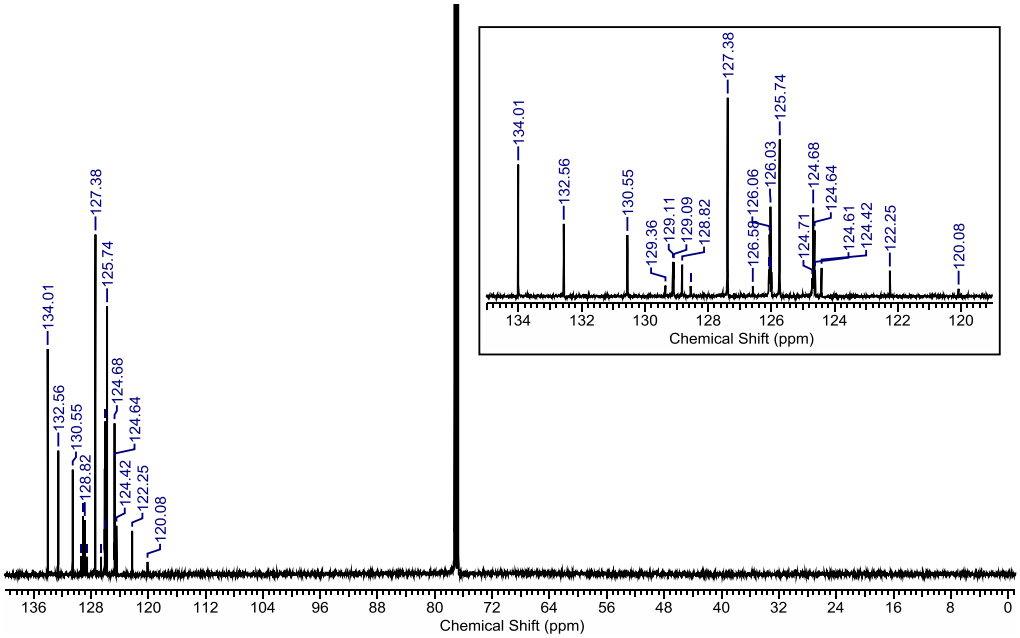

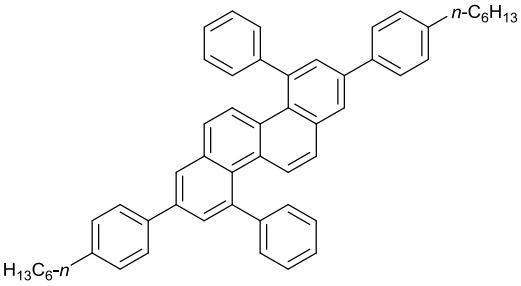

4,10-Diphenyl-2,8-*bis*[4-(*n*-hexyl)phenyl]chrysene (**132**)

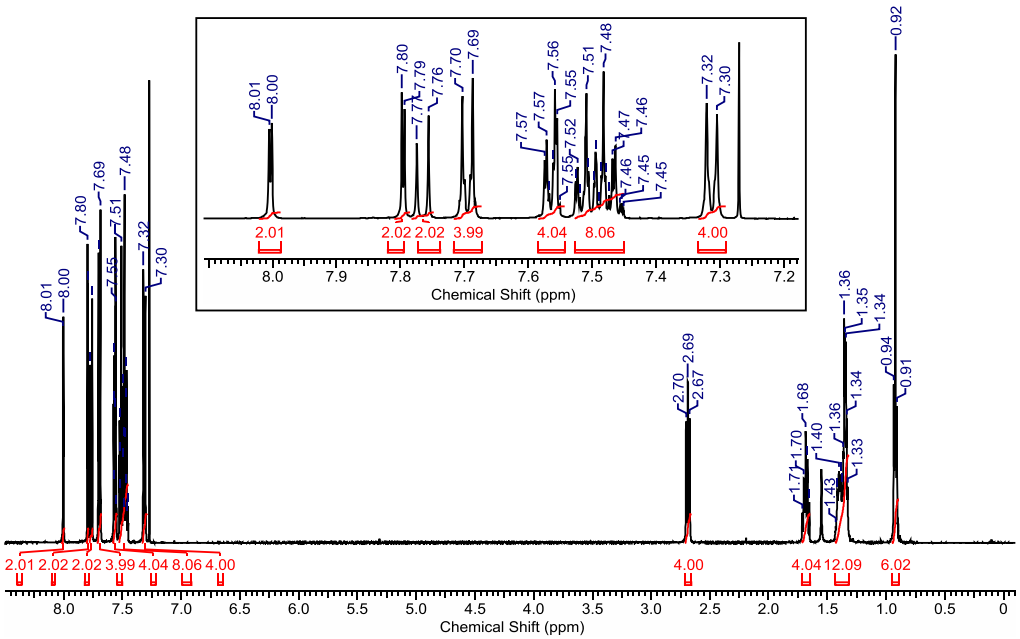

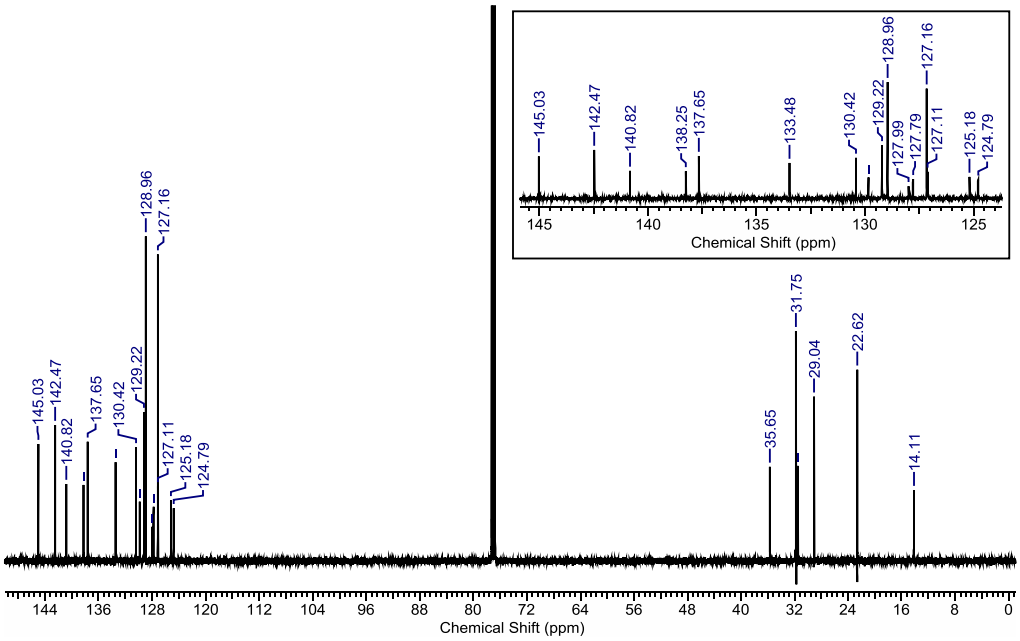

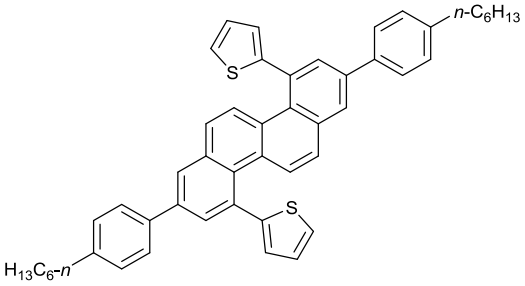

4,10-*Bis*(2-thienyl)-2,8-*bis*[4-(*n*-hexyl)phenyl]chrysene (**133**)

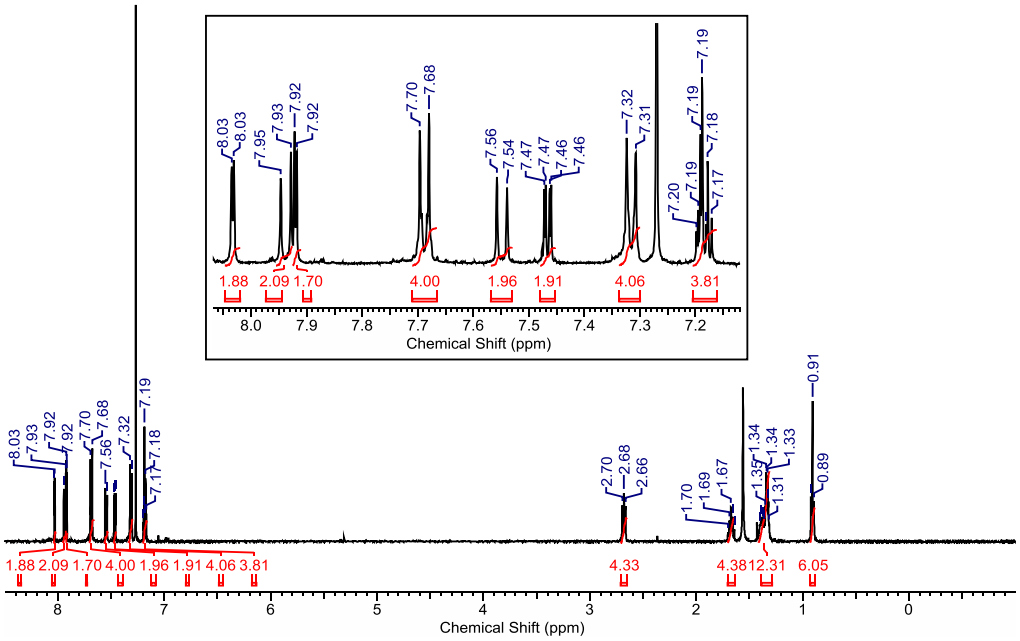

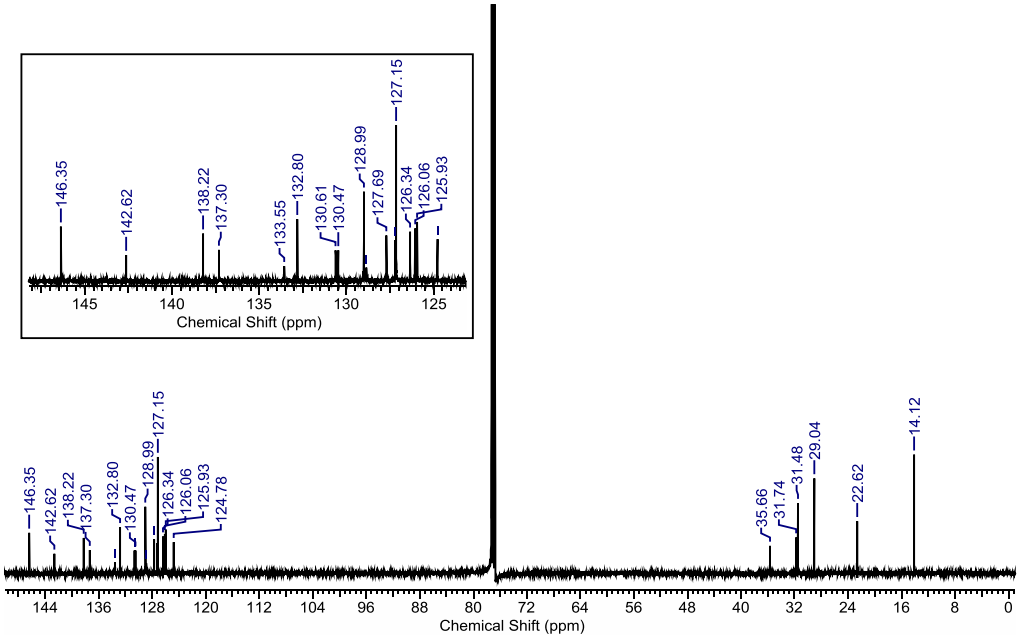

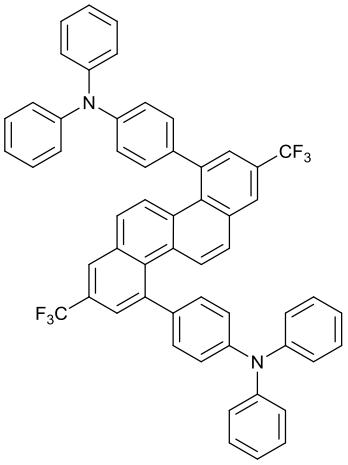

4,10-*Bis*[4-(diphenylamino)phenyl]-2,8-*bis*(trifluoromethyl)chrysene (**137**)

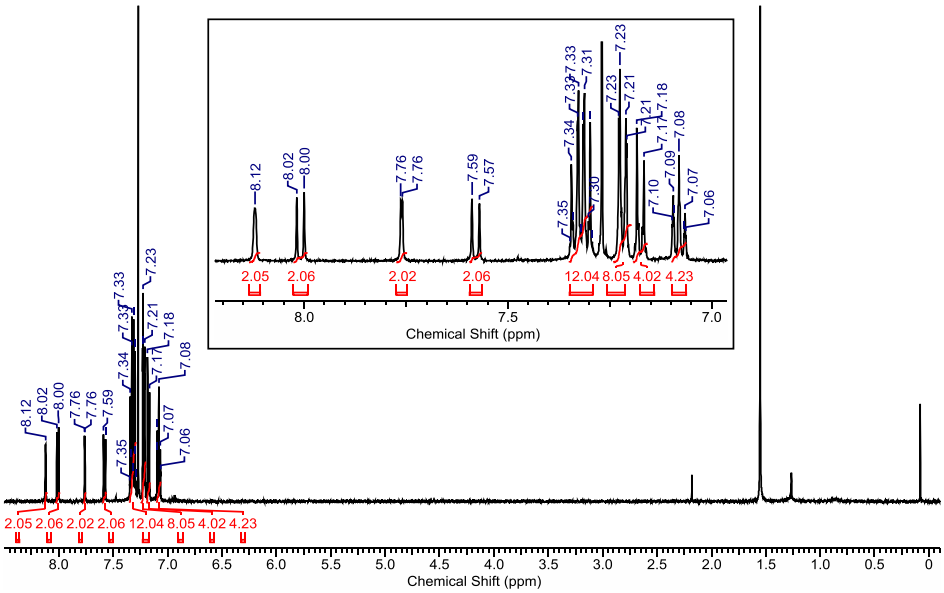

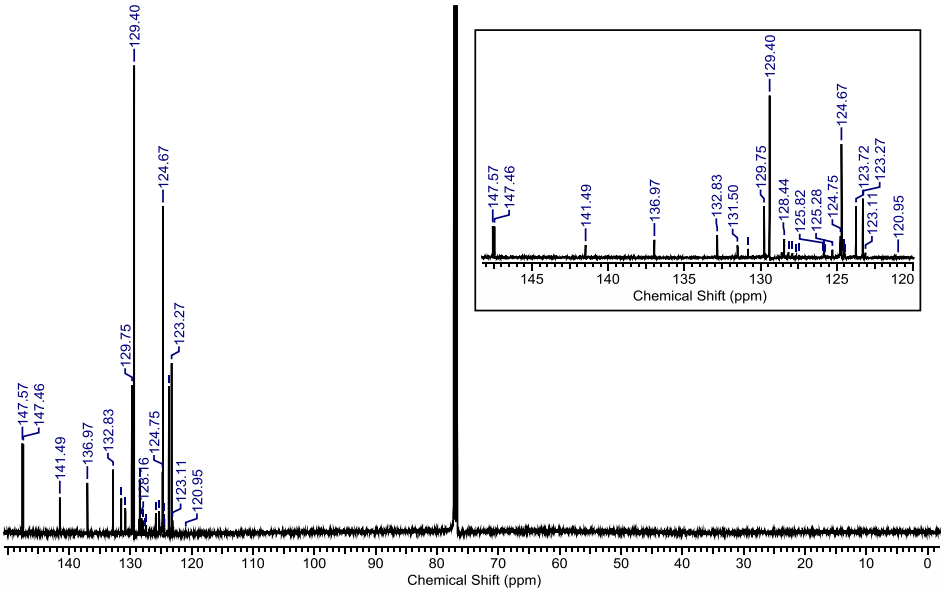

6.2-2 Pyrene Derivatives

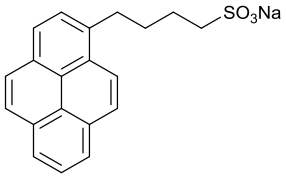

Sodium 4-(pyren-1-yl)butane-1-sulfonate (**140**)

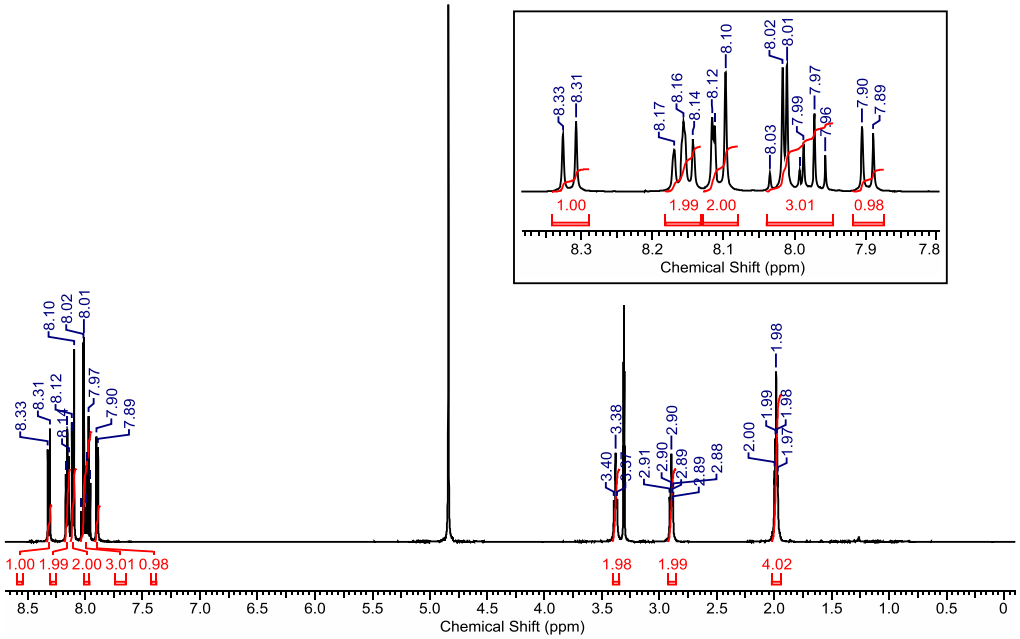

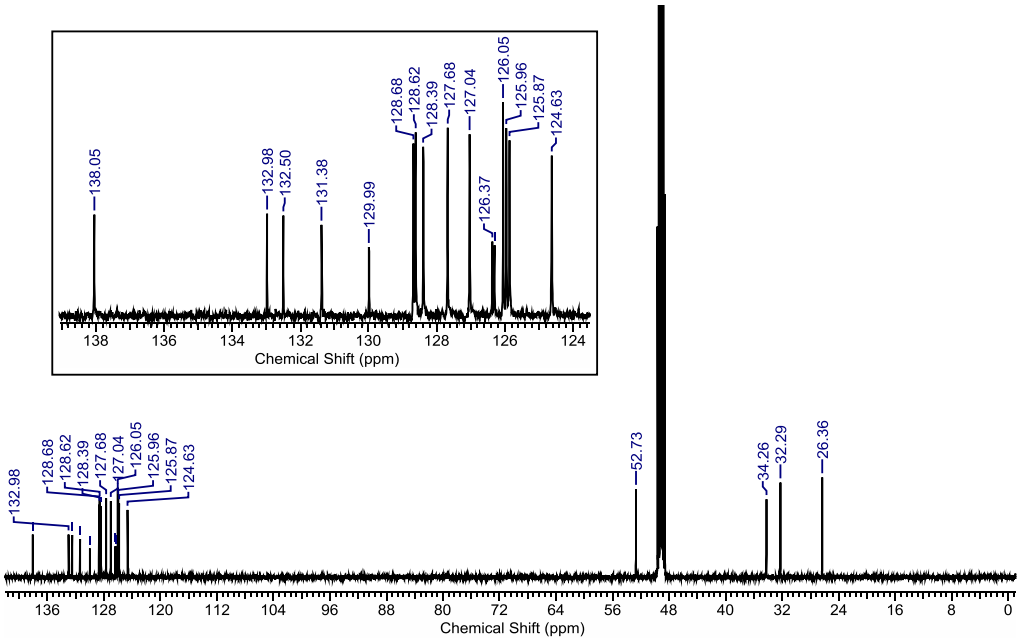

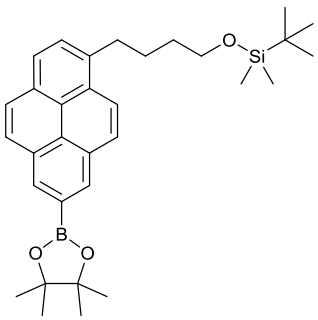

tert-Butyldimethyl(4-[7-(4,4’,5,5’-tetramethyl-1,3,2-dioxaborolan-2-yl) pyren-1-yl]butoxy)silane (**143**)

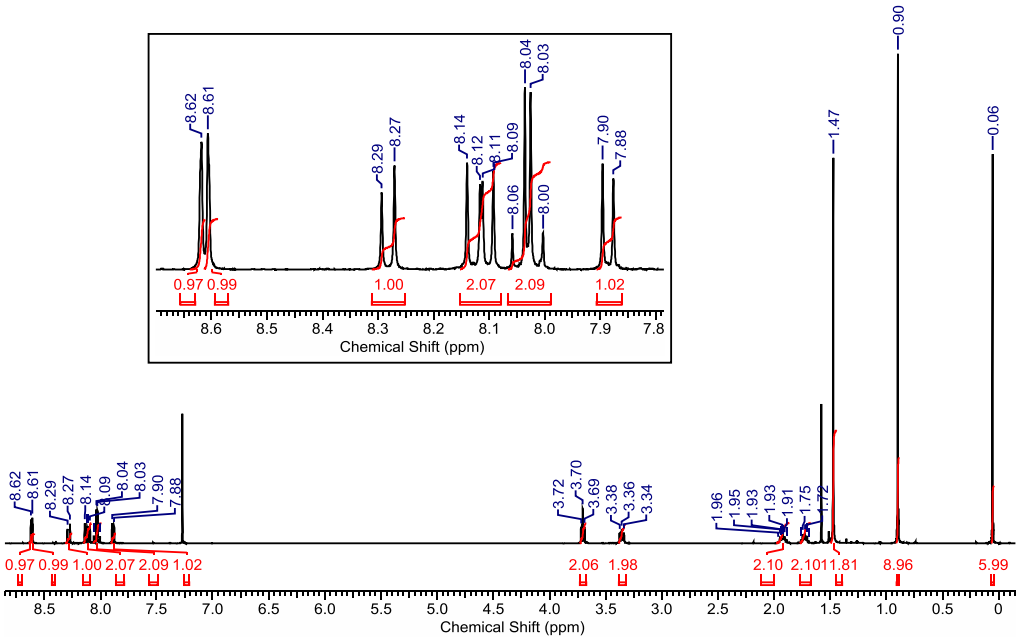

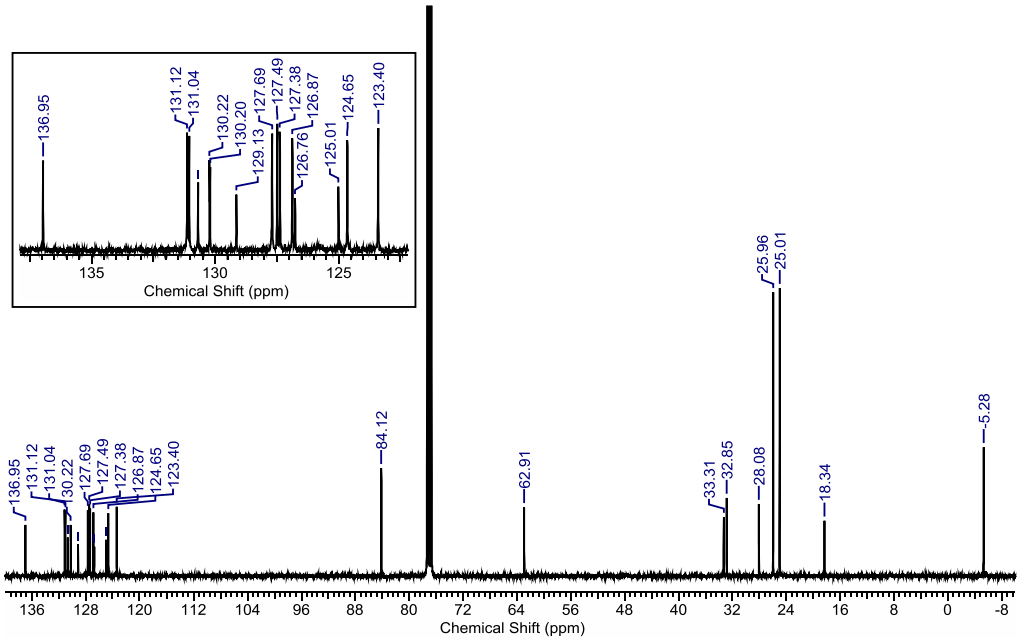

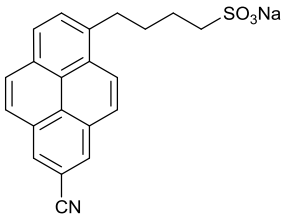

Sodium 4-(7-cyanopyren-1-yl)butane-1-sulfonate (**146**)

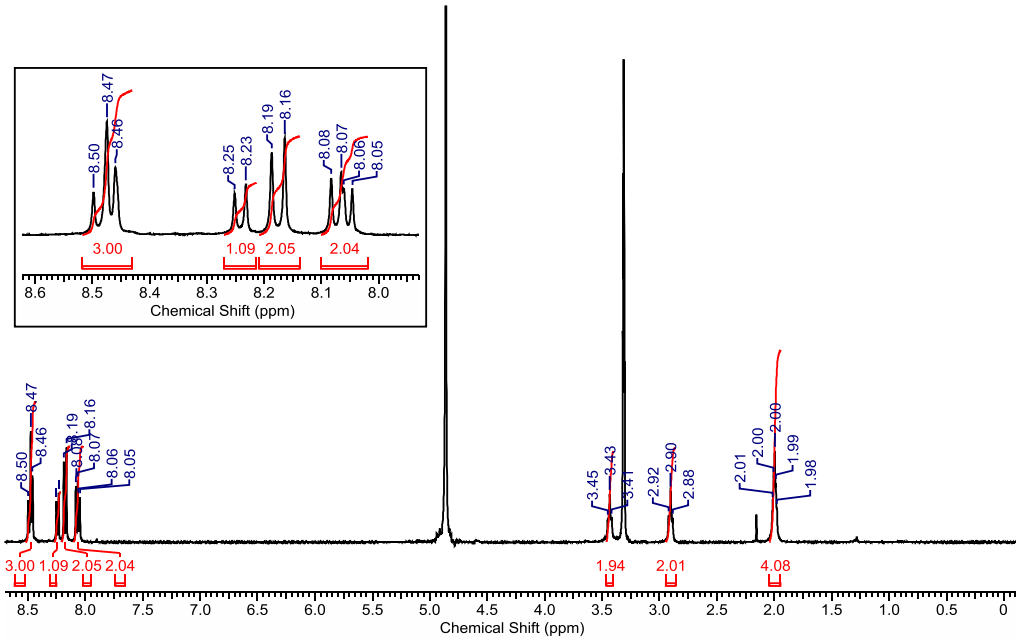

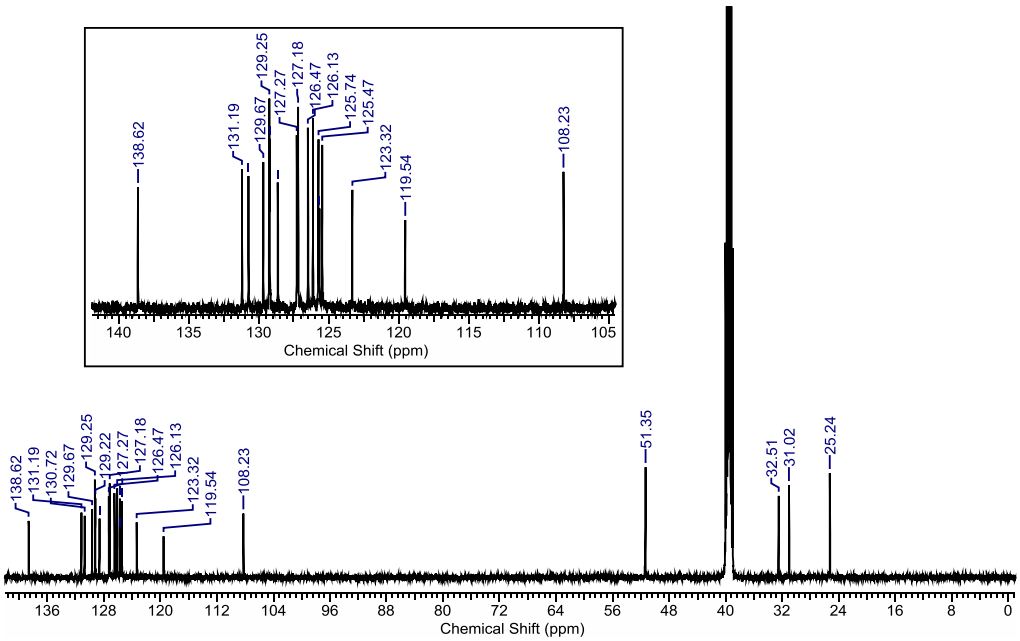

6.2-3 Perylene Derivatives

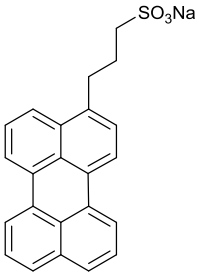

Sodium 3-(perylen-3-yl)propane-1-sulfonate (**164**)

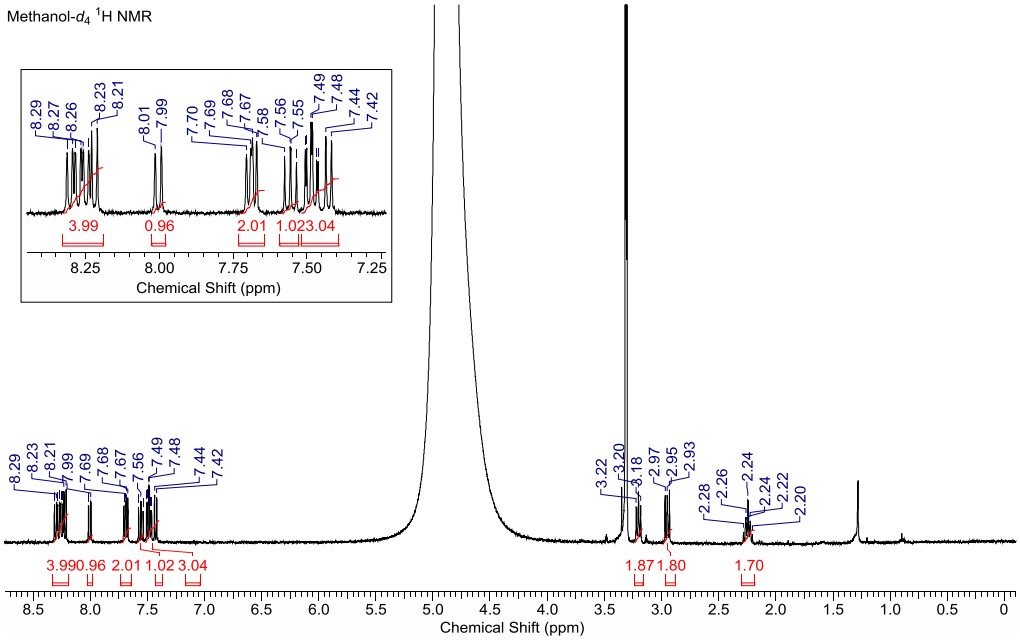

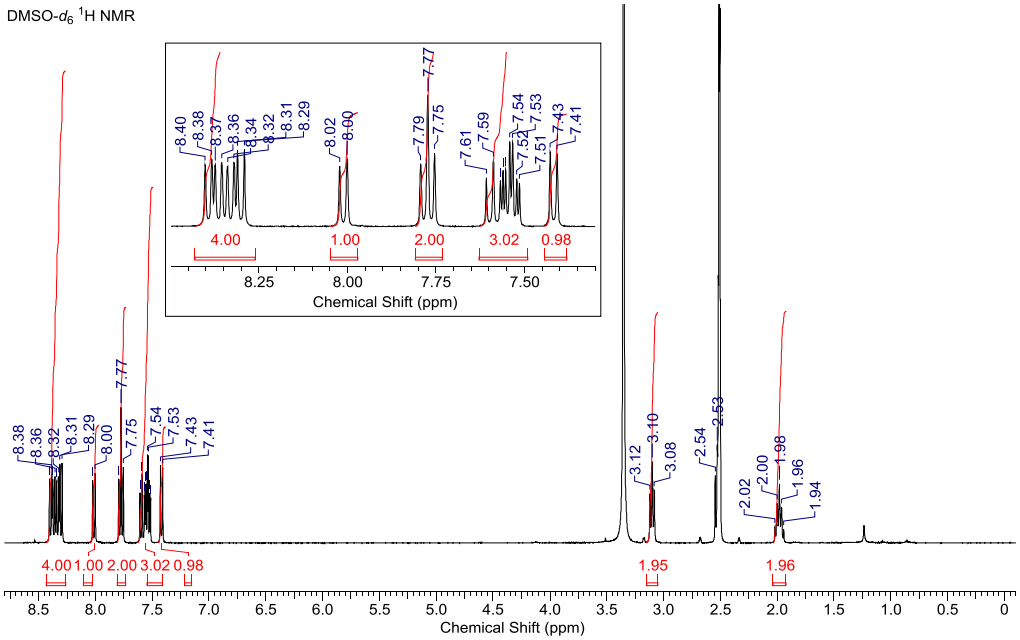

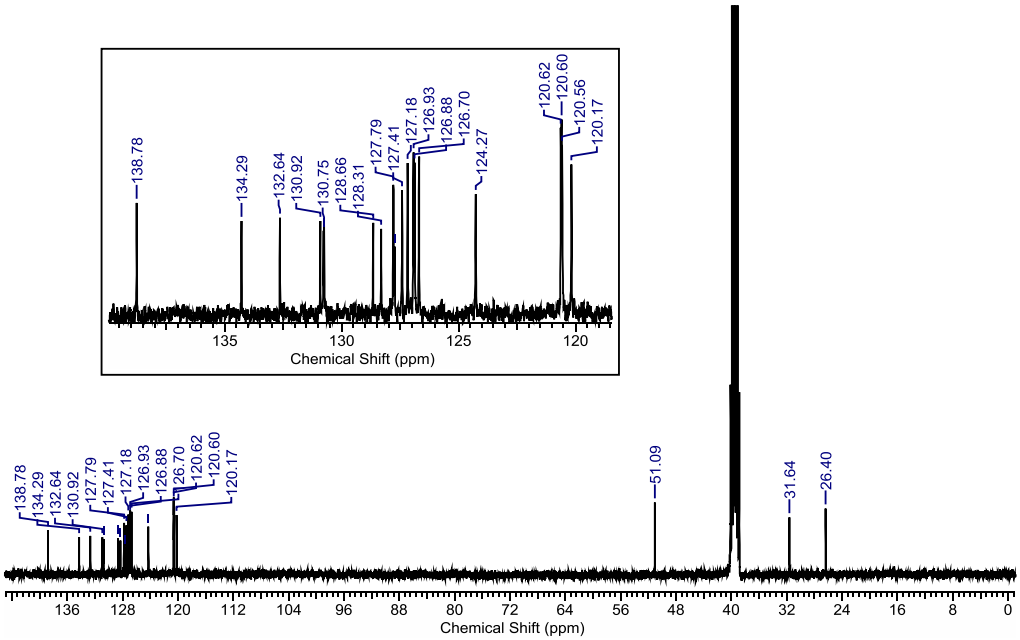
138.78
134.29
132.64
130.92
130.75
128.66
128.31
127.79
127.41
127.18
126.93
126.88
126.70
124.27
120.62
120.60
120.56
120.17
135
130
125
120
Chemical Shift (ppm)
138.78
134.29
132.64
130.92
127.79
127.41
127.18
126.93
126.88
126.70
120.62
120.60
120.17
51.09
31.64
26.40
136
128
120
112
104
96
88
80
72
64
56
48
40
32
24
16
8
0
Chemical Shift (ppm)

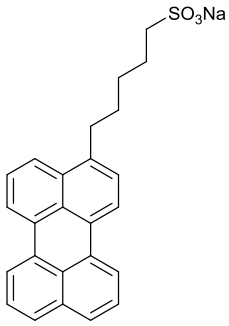

Sodium 5-(perylen-3-yl)pentane-1-sulfonate (**165**)

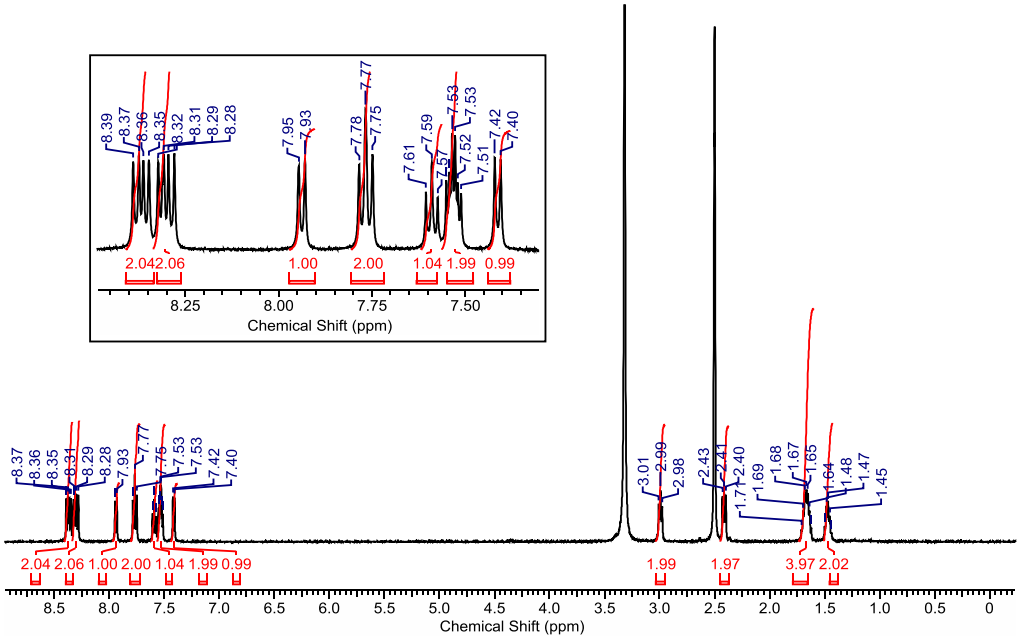

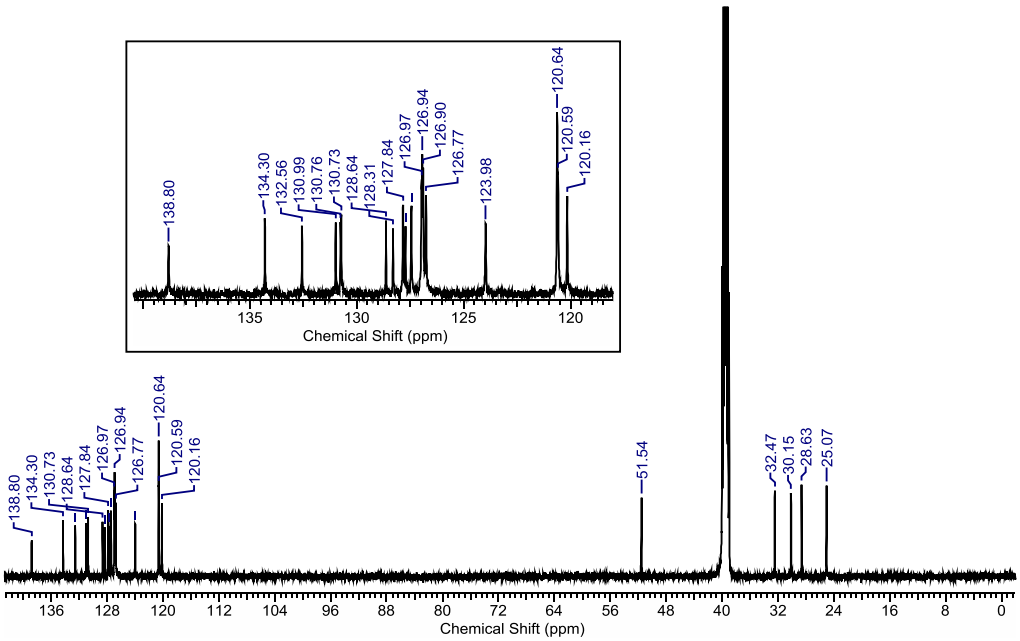

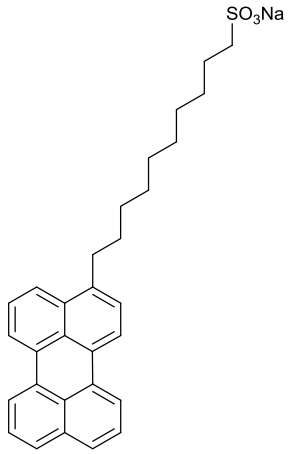

Sodium 10-(perylen-3-yl)decane-1-sulfonate (**166**)

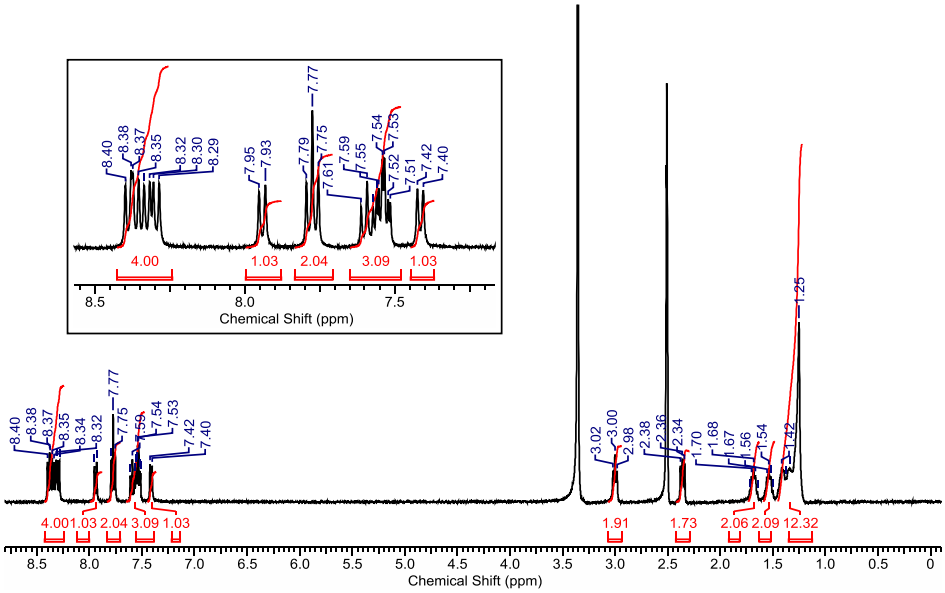

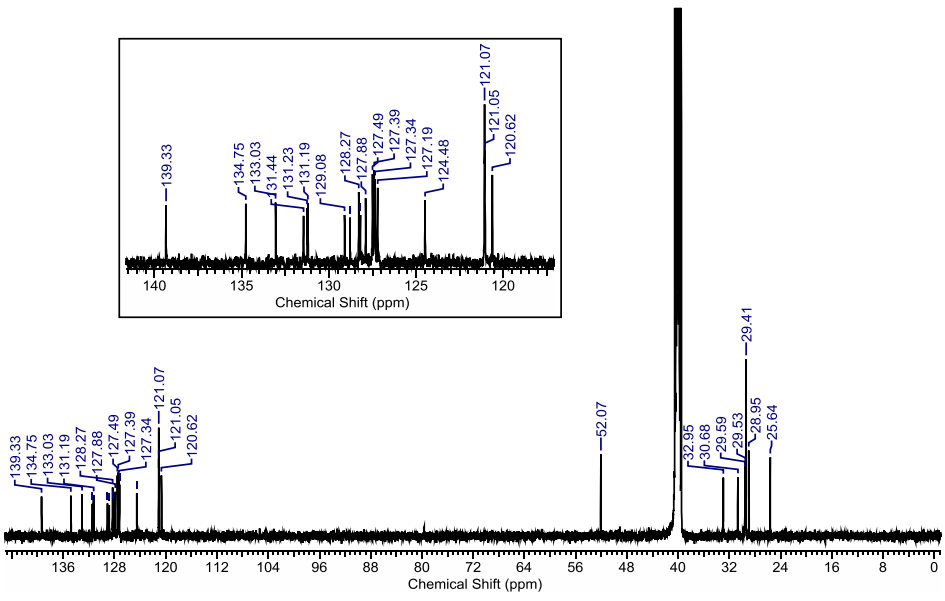

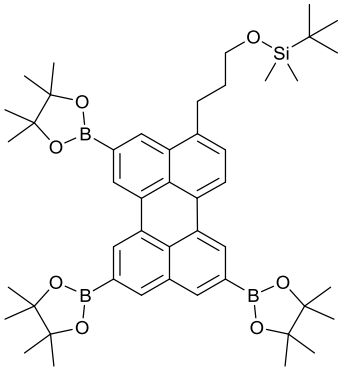

tert-Butyldimethyl(3-[5,8,11-*tris*(4,4,5,5-tetramethyl-1,3,2-dioxaborolan-2-yl)perylen-3-yl]propoxy)silane (**168**)

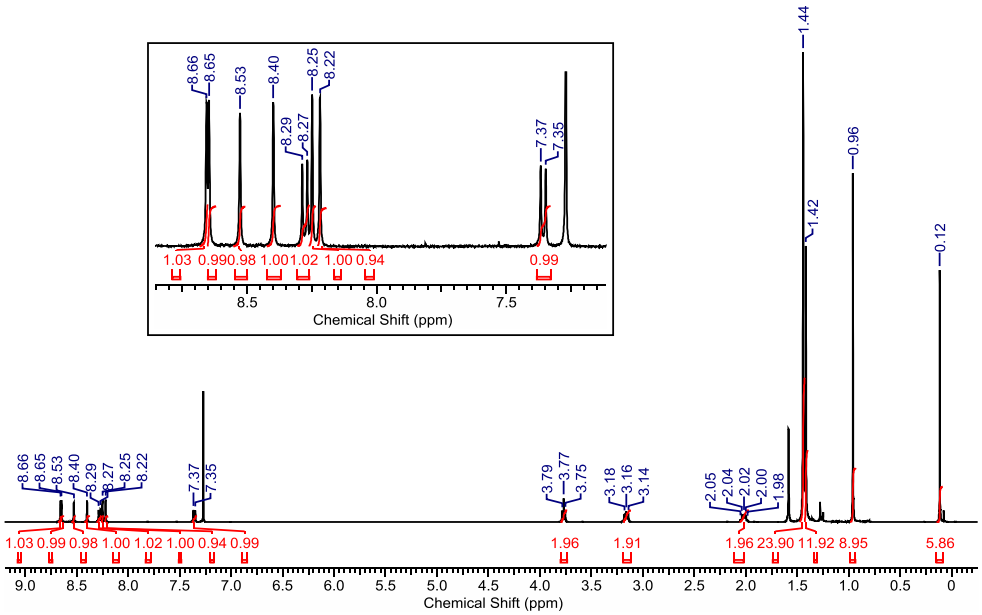

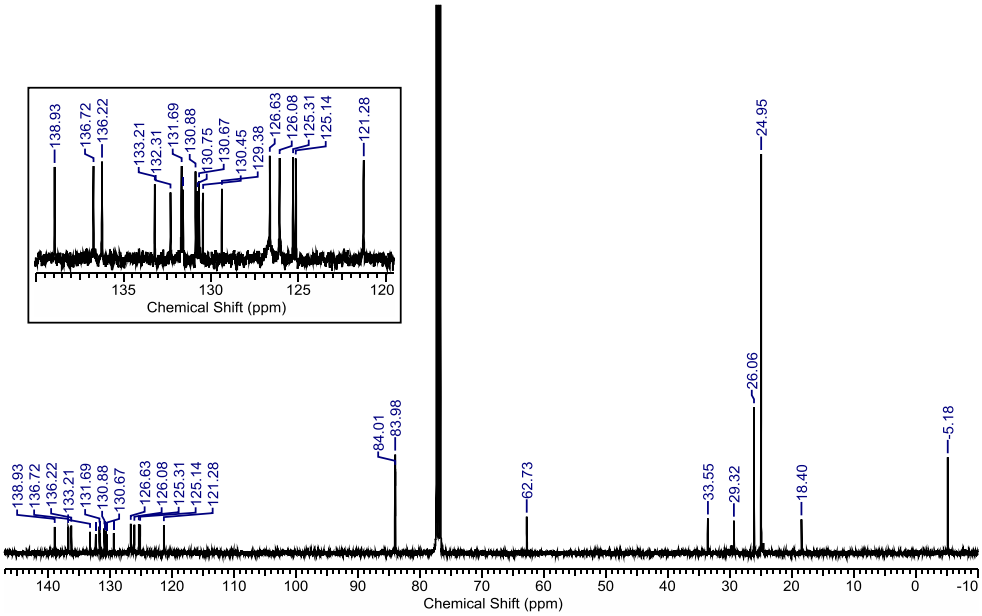

6.3 Appendices of Computational Analysis of Substituted Chrysenes

6.3-1 4,10-Dichloro-2,8-*bis*[4-(diphenylamino)phenyl]chrysene (122)

Optimised Gas Phase Geometry of 122:

From above:

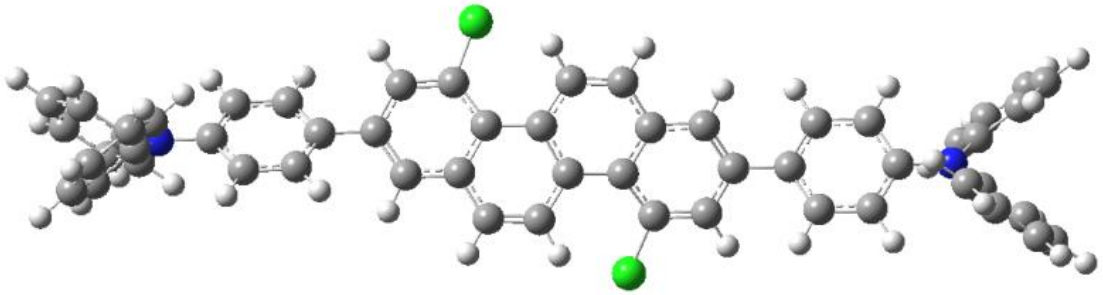

From side:

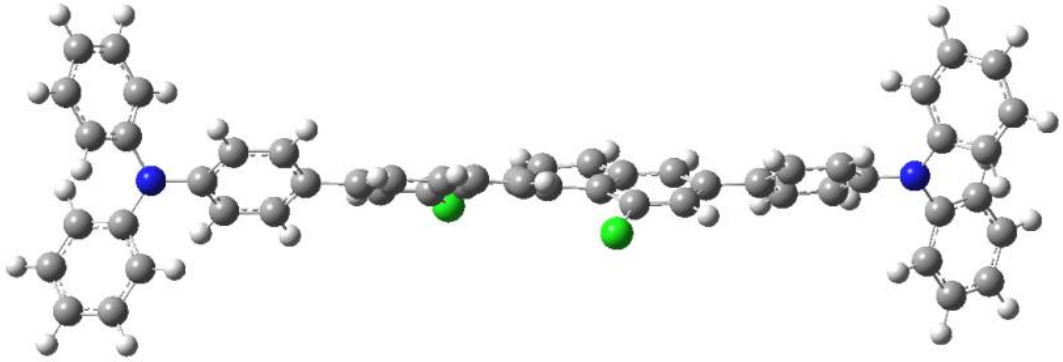

The central chrysene is predicted to be 21.16 ° out-of-plane across the bay region.

Key Molecular Orbitals of 122:

HOMO-2

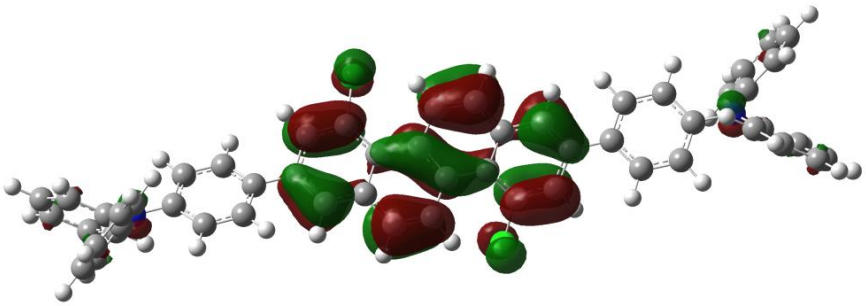

HOMO-1

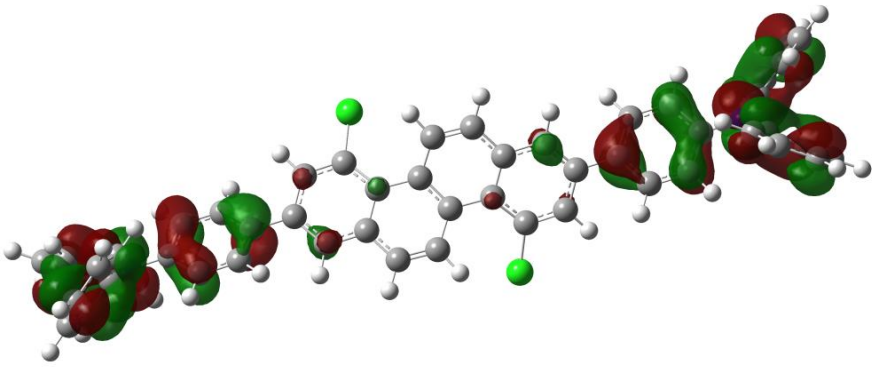

HOMO

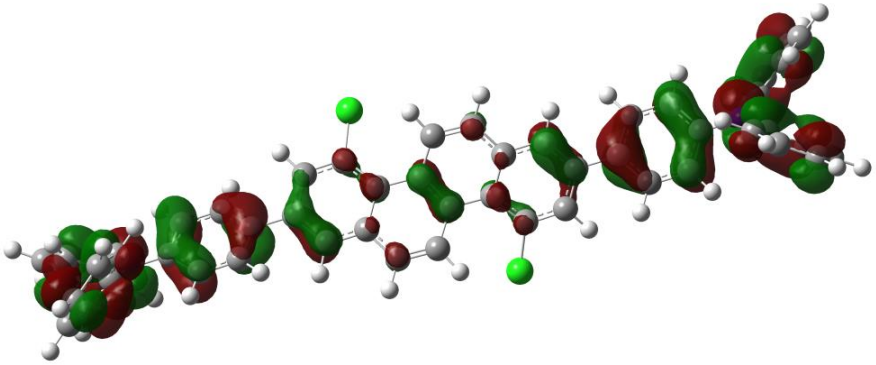

LUMO

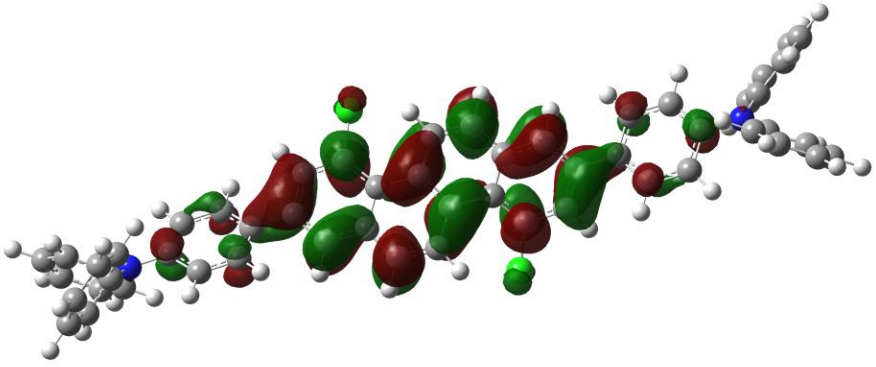

LUMO+1

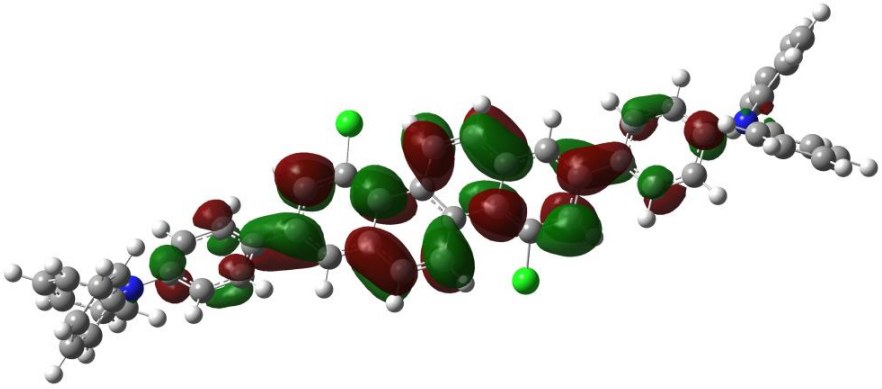

LUMO+2

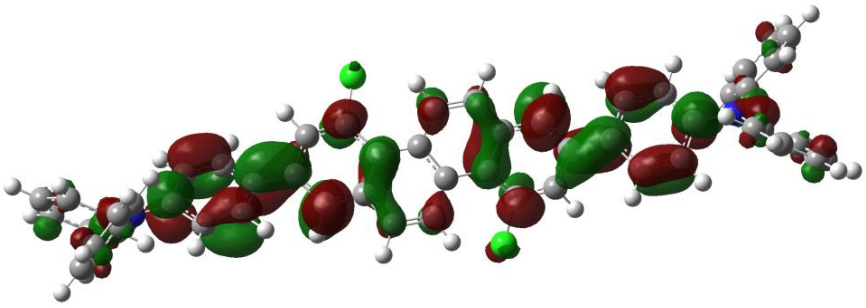

Optimised Gaussian Coordinates of 122:

Cl	-2.02143200	1.69608200	-2.73492700
Cl	2.02516100	-3.21262500	1.68730800
C	-2.64251600	0.93074500	-1.26027500
C	-4.02189100	0.89684400	-1.19326800
H	-4.58784000	1.40632300	-1.96419200
C	-4.70178700	0.22012000	-0.15552300
C	-3.92403200	-0.45908300	0.76799800
H	-4.39605100	-1.05988700	1.53930100
C	-2.51487600	-0.44106300	0.71230300
C	-1.80578600	0.31515800	-0.27978700
C	-0.35061800	0.36320200	-0.20299200
C	0.40756000	1.39504600	-0.84204100
H	-0.10575100	2.18105900	-1.37205000

C	1.76227200	1.45997800	-0.72789700
H	2.30508600	2.28867900	-1.17337000
C	2.50864600	0.44645400	-0.05950300
C	3.91781300	0.51789300	-0.05100000
H	4.38638300	1.37994500	-0.51600700
C	4.69647100	-0.46062100	0.54338400
C	4.01903600	-1.56870600	1.10303900
H	4.58998600	-2.40586700	1.48636300
C	2.64064700	-1.65121000	1.11275300
C	1.80127500	-0.62075300	0.58735400
C	0.34584600	-0.55955400	0.63119000
C	-0.41427700	-1.31152400	1.58270700
H	0.09804000	-1.92049500	2.30992500
C	-1.76976400	-1.21299200	1.65082000
H	-2.31469600	-1.74911200	2.42241800
C	-6.18214800	0.20752700	-0.09673200
C	-6.85992300	0.20403100	1.13439100
C	-6.96498000	0.19054500	-1.26375600
C	-8.24769900	0.17155100	1.20155100
H	-6.29039500	0.23797400	2.05823200
C	-8.35353800	0.17423500	-1.20846100
H	-6.48144900	0.17463800	-2.23579700
C	-9.02105600	0.15877000	0.02819000
H	-8.74127900	0.16449000	2.16708900
H	-8.92996400	0.16348300	-2.12694100
C	6.17573000	-0.39219100	0.56474900
C	6.91185800	-0.88061500	1.65760300
C	6.89812400	0.16245900	-0.50551700
C	8.30054200	-0.82492600	1.68223500
H	6.38875700	-1.30300700	2.51040900
C	8.28559600	0.23610800	-0.48493900
H	6.36573800	0.53118600	-1.37700000
C	9.01266900	-0.26204900	0.60977400

H	8.84200300	-1.21368700	2.53772900
H	8.81639200	0.67139800	-1.32464200
N	10.42788400	-0.20085900	0.62847500
N	-10.43556400	0.13024500	0.08907500
C	-11.17875800	-0.63452600	-0.85400200
C	-10.76536600	-1.92805100	-1.21018600
C	-12.34145400	-0.10587000	-1.43635200
C	-11.49586300	-2.66798100	-2.13774100
H	-9.87260100	-2.34636800	-0.75754300
C	-13.07563900	-0.86103900	-2.34858900
H	-12.66300300	0.89512000	-1.16874700
C	-12.65655200	-2.14306800	-2.70941200
H	-11.16198400	-3.66717400	-2.40247100
H	-13.97305400	-0.43697300	-2.78986600
H	-13.22695700	-2.72562100	-3.42616000
C	-11.12508300	0.85202200	1.10413300
C	-12.19682300	0.26125700	1.79155400
C	-10.74793000	2.16503800	1.42748900
C	-12.87825100	0.97474300	2.77550500
H	-12.48974300	-0.75465100	1.54881700
C	-11.42379800	2.86374600	2.42580200
H	-9.92591400	2.63007200	0.89360700
C	-12.49455400	2.27662800	3.10280700
H	-13.70541300	0.50306500	3.29822800
H	-11.11945900	3.87893800	2.66381100
H	-13.02345100	2.82684300	3.87482500
C	11.11608900	0.08831900	1.84009700
C	12.26457300	-0.63606100	2.19648300
C	10.65959700	1.10554700	2.69340100
C	12.94302100	-0.33998800	3.37696500
H	12.61969800	-1.42675200	1.54411600
C	11.33422500	1.38129600	3.88089300
H	9.77738800	1.67466000	2.41989200

C	12.48136100	0.66532300	4.22878100
H	13.83024500	-0.90992700	3.63772800
H	10.96745800	2.17157900	4.52970300
H	13.00858100	0.88809700	5.15118600
C	11.16953700	-0.44512900	-0.56161200
C	12.26897600	0.36262600	-0.89243100
C	10.81668800	-1.50027400	-1.41780700
C	13.00103600	0.11146500	-2.05114800
H	12.54403500	1.18193300	-0.23675700
C	11.54351100	-1.73155200	-2.58384400
H	9.97371900	-2.13414000	-1.16371600
C	12.64168700	-0.93193800	-2.90649300
H	13.84922200	0.74583600	-2.29227500
H	11.25684300	-2.55214200	-3.23525500
H	13.21022600	-1.11973100	-3.81203200

6.3-2 4,10-*Bis*[4-(diphenylamino)phenyl]-2,8-*bis*(trifluoromethyl)chrysene (137)

Optimised Gas Phase Geometry of 137:

From above:

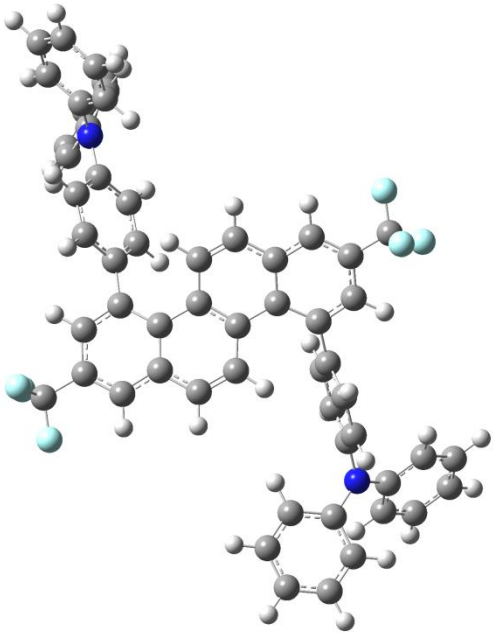

From side:

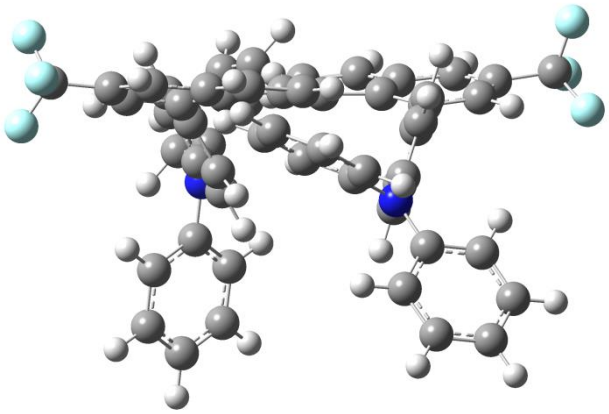

The central chrysene is predicted to be 17.57 ^{o} out-of-plane across the bay region.

Key Molecular Orbitals of 137:

HOMO-2

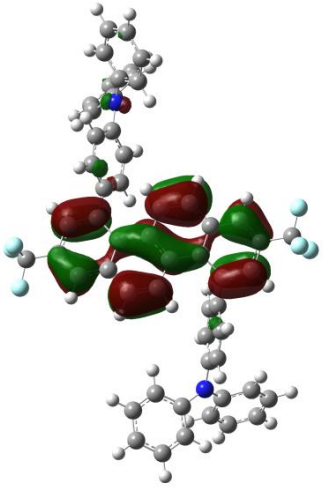

HOMO-1

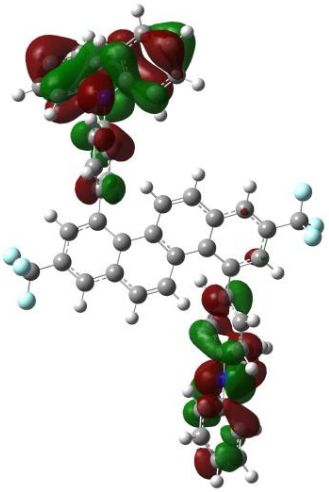

HOMO

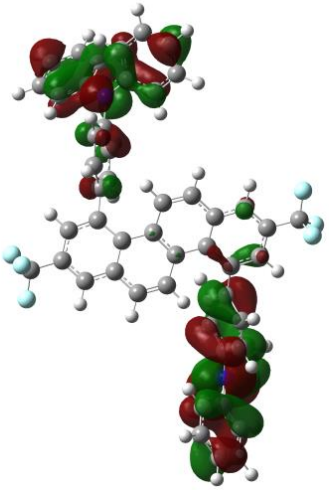

LUMO

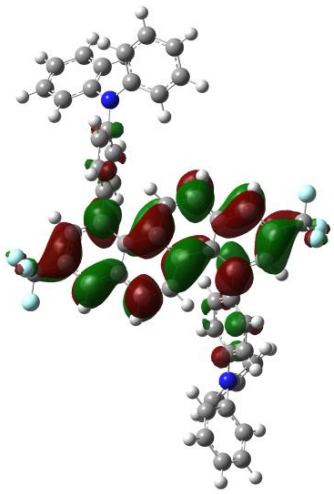

LUMO+1

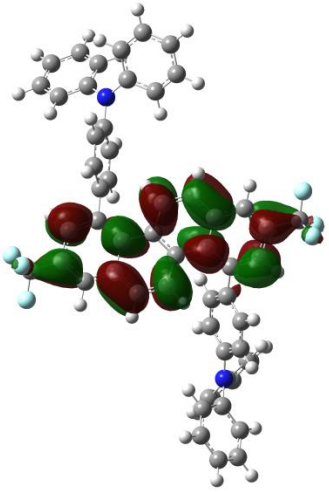

LUMO+2

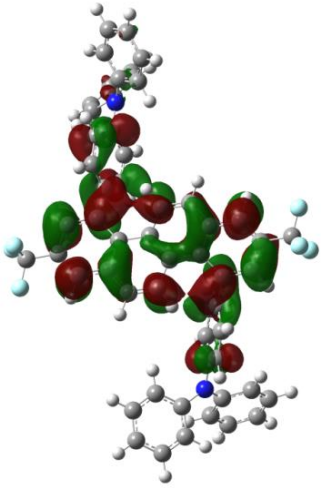

Optimised Gaussian Coordinates of 137:

C	-0.97879100	1.72751000	2.95632100
C	-0.01507000	1.67557100	3.98001100

H	0.83145700	1.00565200	3.87500400
C	-0.14704700	2.40514200	5.15333700
C	-1.27179900	3.28706200	5.32276500
C	-1.45304100	4.21703100	6.43515600
C	-3.68537900	4.77341300	5.58889500
H	-4.59739800	5.34525500	5.66640000
C	-3.46298600	4.03569200	4.46673500
H	-4.19894600	4.02538500	3.66785400
C	-2.27752500	3.26120600	4.30477400
C	-2.11050500	2.48916500	3.13311300
H	-2.88803800	2.50270600	2.37695200
C	-0.75327700	0.95260800	1.68803100
F	0.09830000	1.59776800	0.85608100
F	-1.89986800	0.75171900	1.00262400
F	-0.20893100	-0.26140000	1.93403800
C	-3.06331700	7.66480300	9.87497800
C	-4.22365900	7.22180500	9.21426400
H	-5.18885700	7.59669400	9.53739400
C	-4.18508600	6.26317600	8.20936000
C	-2.91192200	5.74053100	7.78288800
C	-2.70319700	4.87539300	6.62501700
C	-0.35920700	4.59374300	7.27726800
H	0.61877300	4.17777600	7.09886000
C	-0.49824700	5.53924600	8.24690800
H	0.36666300	5.85940200	8.82093800
C	-1.76128200	6.12707000	8.53999700
C	-1.85132100	7.09501600	9.56608600
H	-0.95393500	7.38111200	10.10341000
C	-3.18839800	8.72663200	10.93081400
F	-4.10733100	8.39261000	11.86718200
F	-2.02253000	8.95424000	11.57247900
F	-3.59159300	9.90490500	10.39973400
C	-5.51999400	5.78063400	7.74447400

C	-5.89768100	4.43442300	7.88180000
C	-6.48456800	6.68397500	7.27233400
C	-7.17917400	4.00797500	7.55448600
H	-5.17473600	3.71187200	8.24794500
C	-7.77387500	6.26824000	6.95130500
H	-6.22280000	7.73234600	7.16142100
C	-8.14303200	4.92095900	7.08971200
H	-7.44639300	2.96307000	7.66797600
H	-8.50205200	6.98968500	6.59732500
C	0.87419700	2.10451500	6.20664300
C	0.52314600	1.35202300	7.33816000
C	2.21330500	2.49450500	6.05444000
C	1.47305600	1.02123100	8.30010900
H	-0.50648800	1.03210800	7.46659000
C	3.16428900	2.18129600	7.02388800
H	2.50685000	3.06205000	5.17592900
C	2.80170500	1.44594100	8.15977700
H	1.19226600	0.43807500	9.17121600
H	4.19457900	2.50182100	6.90736700
N	3.77261100	1.14139600	9.16082600
N	-9.45609700	4.48937000	6.77805900
C	-10.15375300	5.05766300	5.67553700
C	-9.50216500	5.25635500	4.44797800
C	-11.50304200	5.42639800	5.79725100
C	-10.18325700	5.82409200	3.37378000
H	-8.46231200	4.96443800	4.34454700
C	-12.18126500	5.97580900	4.71092200
H	-12.01270800	5.28009900	6.74361600
C	-11.52720200	6.18395300	3.49525700
H	-9.66293900	5.97190900	2.43181000
H	-13.22509700	6.25557100	4.82225700
H	-12.05707800	6.61956400	2.65407600
C	-10.10933900	3.53898000	7.61348600

C	-10.86584200	2.50020200	7.04897300
C	-10.01159100	3.63000600	9.01102500
C	-11.51497800	1.57929600	7.86883700
H	-10.94119900	2.42252100	5.96946700
C	-10.64892100	2.69305200	9.82205400
H	-9.43609700	4.43568100	9.45419000
C	-11.40742400	1.66555400	9.25837300
H	-12.09696900	0.78156800	7.41644600
H	-10.56296800	2.77810300	10.90150200
H	-11.90878900	0.94182000	9.89349500
C	4.05302500	-0.21456900	9.46645800
C	4.03065600	-1.18428800	8.44939700
C	4.34831900	-0.61840200	10.78009300
C	4.30010800	-2.51948500	8.74252500
H	3.80729700	-0.88504300	7.43106800
C	4.63272900	-1.95376000	11.05756400
H	4.35466200	0.11613100	11.57785000
C	4.60920400	-2.91488200	10.04468600
H	4.28205300	-3.25175900	7.94035800
H	4.86152000	-2.24451600	12.07922800
H	4.82764700	-3.95490200	10.26667800
C	4.38641300	2.21329300	9.86200200
C	5.74813100	2.16847000	10.20551200
C	3.63457300	3.34572300	10.21699000
C	6.33134300	3.22417800	10.90303700
H	6.34085300	1.30360400	9.92614700
C	4.23212300	4.40317400	10.90030400
H	2.58074300	3.38558400	9.96281400
C	5.58086100	4.34912800	11.25403900
H	7.38485600	3.17101300	11.16272500
H	3.63208700	5.26712300	11.17244800
H	6.04019400	5.17021700	11.79586600

6.4 Crystallographic and Structural Refinement Data

6.4-1 4,10-Dichloro-2,8-*bis*[4-(*n*-hexyl)phenyl]chrysene (120)

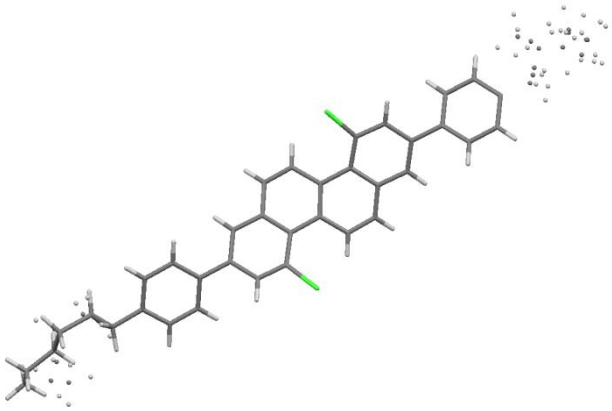

CCDC number	1029714	
UoM identification code	s4067na	
Empirical formula	C42 H42 Cl2	
Formula weight	617.66	
Temperature	100(2) K	
Wavelength	1.54178 Å	
Crystal system	Monoclinic	
Space group	P2(1)/c	
Unit cell dimensions	a = 15.5669(11) Å	α = 90°.
	b = 11.5716(8) Å	β = 96.615(4)°.
	c = 18.0171(14) Å	γ = 90°.
Volume	3223.9(4) $Å^3$	
Z	4	
Density (calculated)	1.273 Mg m^{-3}	
Absorption coefficient	2.020 mm^{-1}	
F(000)	1312	
Crystal size	0.29 x 0.23 x 0.13 mm^3	
Theta range for data collection	2.86 to 72.94°.	
Index ranges	-19<=h<=19, -14<=k<=14, -21<=l<=19	
Reflections collected	27577	
Independent reflections	6250 [R(int) = 0.0604]	
Completeness to theta = 67.00°	98.6 %	

Absorption correction	Semi-empirical from equivalents
Max. and min. transmission	0.7792 and 0.607457
Refinement method	Full-matrix least-squares on F^2
Data / restraints / parameters	6250 / 48 / 436
Goodness-of-fit on F^2	1.074
Final R indices [I>2sigma(I)]	R1 = 0.0611, wR2 = 0.1708
R indices (all data)	R1 = 0.0732, wR2 = 0.1818
Largest diff. peak and hole	0.542 and -0.447 e.$Å^{-3}$

6.4-2 4,10-Dichloro-2,8-*bis*(trifluoromethyl)chrysene (130)

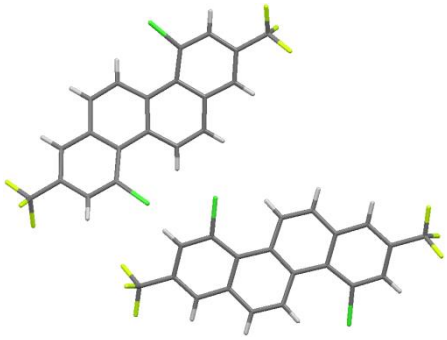

CCDC number	1029715	
UoM identification code	s4084na	
Empirical formula	C20 H8 Cl2 F6	
Formula weight	433.16	
Temperature	100(2) K	
Wavelength	1.5418 Å	
Crystal system	Triclinic	
Space group	P -1	
Unit cell dimensions	a = 8.5128(3) Å	α = 97.590(3)°.
	b = 11.4844(5) Å	β = 96.803(3)°.
	c = 13.1495(5) Å	γ = 103.045(3)°.
Volume	1226.69(9) $Å^3$	
Z	3	
Density (calculated)	1.759 Mg m^{-3}	
Absorption coefficient	4.224 mm^{-1}	
F(000)	648	
Crystal size	0.28 x 0.21 x 0.07 mm^3	
Theta range for data collection	3.43 to 74.63°.	
Index ranges	-10<=h<=10, -13<=k<=14, -15<=l<=16	
Reflections collected	8880	
Independent reflections	4698 [R(int) = 0.0232]	
Completeness to theta = 67.00°	96.3 %	
Absorption correction	Semi-empirical from equivalents	
Max. and min. transmission	1.00000 and 0.66534	
Refinement method	Full-matrix least-squares on F^2	

Data / restraints / parameters	4698 / 0 / 379
Goodness-of-fit on F^2	1.003
Final R indices [I>2sigma(I)]	R1 = 0.0329, wR2 = 0.0842
R indices (all data)	R1 = 0.0364, wR2 = 0.0865
Largest diff. peak and hole	0.489 and -0.262 e.$Å^{-3}$

6.4-3 4,10-Diphenyl-2,8-*bis*[4-(*n*-hexyl)phenyl]chrysene (132)

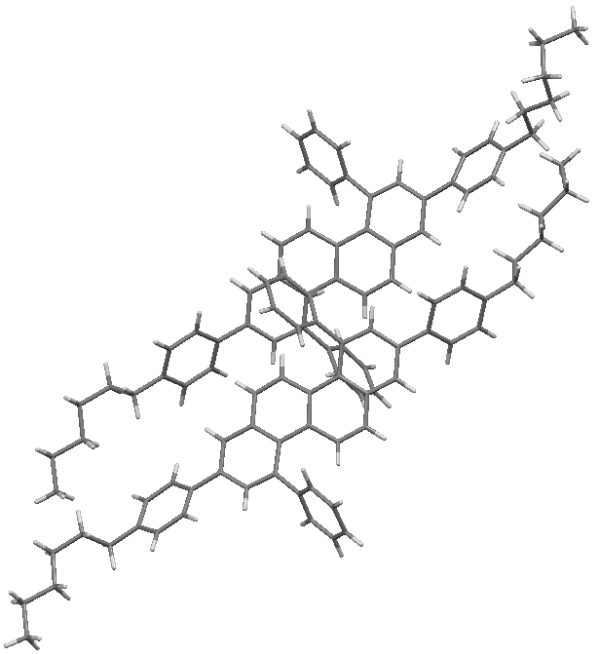

CCDC number	1029713	
UoM identification code	s3937ma	
Empirical formula	C54 H52	
Formula weight	700.96	
Temperature	100(2) K	
Wavelength	1.54178 Å	
Crystal system	Orthorhombic	
Space group	P2(1)2(1)2(1)	
Unit cell dimensions	a = 13.2582(6) Å	α = 90°.
	b = 14.2403(8) Å	β = 90°.
	c = 42.561(2) Å	γ = 90°.
Volume	8035.6(7) $Å^3$	
Z	8	
Density (calculated)	1.159 Mg m^{-3}	
Absorption coefficient	0.487 mm^{-1}	
F(000)	3008	
Crystal size	0.15 x 0.11 x 0.03 mm^3	
Theta range for data collection	3.27 to 70.11°.	
Index ranges	-9<=h<=15, -13<=k<=17, -51<=l<=45	

Reflections collected	23068
Independent reflections	13704 [R(int) = 0.0348]
Completeness to theta = 66.60°	99.2 %
Absorption correction	Semi-empirical from equivalents
Max. and min. transmission	0.9855 and 0.801691
Refinement method	Full-matrix least-squares on F^2
Data / restraints / parameters	13704 / 0 / 977
Goodness-of-fit on F^2	1.008
Final R indices [I>2sigma(I)]	R1 = 0.0458, wR2 = 0.1064
R indices (all data)	R1 = 0.0612, wR2 = 0.1150
Absolute structure parameter	-0.9(10)
Largest diff. peak and hole	0.379 and -0.197 e.$Å^{-3}$